

6738

NATIONAL LIBRARY  
OTTAWA



BIBLIOTHÈQUE NATIONALE  
OTTAWA

NAME OF AUTHOR... SAURENDRA NATH GUHA MAJUMDAR  
TITLE OF THESIS... EXPERIMENTAL AND ANALYTICAL  
... STUDY ... OF ... THE ... BEHAVIOR OF  
... COUPLED SHEAR WALL-FRAME STRUCTURES  
UNIVERSITY... OF ... ALBERTA  
DEGREE FOR WHICH THESIS WAS PRESENTED... P.H.D.  
YEAR THIS DEGREE GRANTED... 1970

Permission is hereby granted to THE NATIONAL LIBRARY  
OF CANADA to microfilm this thesis and to lend or sell copies  
of the film.

The author reserves other publication rights, and  
neither the thesis nor extensive extracts from it may be  
printed or otherwise reproduced without the author's  
written permission.

(Signed)... *S. Guha Majumdar*

PERMANENT ADDRESS:

*Dept. of Civil Engg.,  
University of Alberta,  
Edmonton*

DATED... 15.9... 1970

NL-91 (10-68)

THE UNIVERSITY OF ALBERTA

EXPERIMENTAL AND ANALYTICAL STUDY  
OF THE BEHAVIOR OF COUPLED SHEAR  
WALL-FRAME STRUCTURES

BY



SAURENDRA NATH GUHA MAJUMDAR

A THESIS

SUBMITTED TO THE FACULTY OF GRADUATE STUDIES  
IN PARTIAL FULFILMENT OF THE REQUIREMENTS FOR THE DEGREE  
OF DOCTOR OF PHILOSOPHY

DEPARTMENT OF CIVIL ENGINEERING


EDMONTON, ALBERTA


FALL, 1970

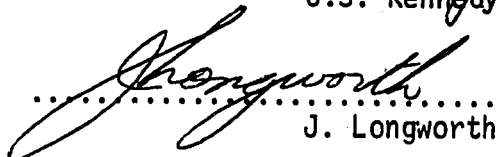
UNIVERSITY OF ALBERTA  
FACULTY OF GRADUATE STUDIES


The undersigned certify that they have read, and recommend to the Faculty of Graduate Studies for acceptance, a thesis, entitled EXPERIMENTAL AND ANALYTICAL STUDY OF THE BEHAVIOR OF COUPLED SHEAR WALL-FRAME STRUCTURES submitted by SAURENDRA NATH GUHA MAJUMDAR in partial fulfilment of the requirements for the degree of Doctor of Philosophy.

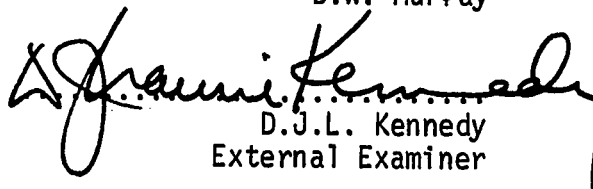
  
.....  
P.F. Adams Supervisor

  
.....  
L.W. Jackson

  
.....  
J.S. Kennedy

  
.....  
J. Longworth

  
.....  
D.W. Murray

  
.....  
D.J.L. Kennedy  
External Examiner

Date 26 Aug 70.....

## ABSTRACT

The object of this dissertation is to develop an approximate second-order analysis to trace the response of a coupled shear wall-frame structure upto its ultimate load. Various aspects of the analysis are checked by comparing the predicted results with the tests performed on specimens designed to simulate portions of a tall structure.

For the analysis, the actual structure is lumped into an equivalent structural model. The model is then analyzed under a constant vertical load and monotonically increasing lateral loads. The method of analysis accounts for the wall-frame interaction forces, the base rotations, the finite width of the shear wall, the inelastic behavior of both wall and frame elements and the secondary moments produced by the axial forces in the columns acting on the deformed structure.

Tests were performed on three, four-story, single-bay, coupled shear wall-frame specimens. Each test specimen consisted of a reinforced concrete shear wall and a steel column stack, connected at four levels by rigidly framed steel beams. The first two specimens were designed to exhibit behavior characteristic of the bottom stories of a tall structure and the third to simulate the behavior of the top stories. The experimental results were compared with the behavior predicted by the second-order elastic-plastic

analysis. The results indicate that the load-carrying capacity of coupled shear wall-frame structures can be closely predicted by this analysis.

A design method has been developed for coupled shear wall-frame structures which is a combination of the present method of analysis and the sway subassemblage technique. The method essentially consists of three steps: a design for gravity load only, an analysis of the lumped structure by the present method and finally a check using the subassemblage method, to ensure that the resistance assigned to the steel bents can indeed be achieved.

## ACKNOWLEDGEMENTS

This study forms part of a general investigation, "Behavior of Multi-Story Structures", currently in progress at the Department of Civil Engineering, University of Alberta. J.G. MacGregor and P.F. Adams are directors of the project. The project receives financial support from the Canadian Steel Industries Construction Council, the National Research Council of Canada and the Defence Research Board.

The author wishes to acknowledge the continuing encouragement and assistance of Dr. P.F. Adams who supervised the work leading to the dissertation. The comments and criticisms of L.W. Jackson, J.S. Kennedy, J. Longworth, D.W. Murray and D.J.L. Kennedy of Carleton University, who acted as the external examiner, are gratefully acknowledged. The author also acknowledges the contributions made by R.P. Nikhed and M. Suko during the development of the analytical portion of the dissertation. The tests could not have been performed without the assistance of the students and staff of the Structural Engineering Laboratory, University of Alberta, Edmonton. Suggestions by J.H. Wynhoven, W.J. Clark and J.H. Davison are acknowledged with thanks. Messrs. H. Panse, L. Burden, D.R. Delicate, G. Graham and D. Chambers assisted with the practical aspects of the test setup.

Miss Helen Wozniuk typed the manuscript with great care. Her co-operation is appreciated.

## TABLE OF CONTENTS

	Page
Title Page	i
Approval Sheet	ii
Abstract	iii
Acknowledgements	v
Table of Contents	vi
List of Tables	x
List of Figures	xi
List of Symbols	xvi
 CHAPTER I INTRODUCTION	 1
CHAPTER II PREVIOUS INVESTIGATIONS	7
2.1 Introduction	7
2.2 Shear wall Structures	8
2.3 Elastic Analysis of Multi-Story Structures	9
2.4 Elastic-Plastic Analysis of Unbraced Planar Frames	10
2.5 Inelastic Analysis of Coupled Structures	13
2.6 Experimental Investigations of Multi-Story Frames	14
2.7 Summary	16

## TABLE OF CONTENTS (continued)

	Page
CHAPTER III    ANALYTICAL MODEL AND METHOD OF ANALYSIS	20
3.1    Introduction	20
3.2    Analytical Model	20
3.3    Uniformly Distributed Loads	23
3.4    Assumptions in the Analysis	24
3.5    Method of Analysis	25
CHAPTER IV    BEHAVIORAL STUDY OF A 24 STORY STRUCTURE	37
4.1    Introduction	37
4.2    Lumping of the 24 Story Building	37
4.3    Comparison Between Approximate and Rigorous Methods of Analysis	38
4.4    The $P\Delta$ Effect	41
4.5    The Effect of Variation of Wall-to-Column Stiffness Ratio	42
4.6    Shear Distribution in the Structure	45
4.7    Design Method	47
CHAPTER V    TEST PROGRAM	61
5.1    Introduction	61
5.2    Test Frames	61
5.3    Material Properties	63
5.4    Loading Sequence and Arrangement	64
5.5    Test Setup	65
5.6    Lateral Bracing System	66
5.7    Instrumentation	66

## TABLE OF CONTENTS (continued)

	Page
CHAPTER VI    TEST RESULTS	80
6.1    Introduction	80
6.2    Test Results - Frame A	80
6.3    Test Results - Frame B	86
6.4    Test Results - Frame C	88
CHAPTER VII   DISCUSSION OF TEST RESULTS	112
7.1    Introduction	112
7.2    Analytical Predictions	112
7.3    Discussion of Results - Frame A	114
7.4    Discussion of Results - Frame B	117
7.5    Discussion of Results - Frame C	119
CHAPTER VIII   SUMMARY, CONCLUSIONS AND RECOMMENDATIONS	124
8.1    Summary	124
8.2    Conclusions	126
8.3    Future Recommendations	127
LIST OF REFERENCES	128
APPENDIX A    DERIVATION OF JOINT ROTATION EQUATIONS	A1
APPENDIX B    FORCED CONVERGENCE EQUATIONS	B1
APPENDIX C    DERIVATIONS OF THE EQUIVALENT $P\Delta$ SHEAR	C1
APPENDIX D    NOMENCLATURE AND PRINTOUT OF THE FORTRAN PROGRAM	D1
D.1    Nomenclature for Fortran Program	D1
D.2    Printout of the Fortran Program	D6

## TABLE OF CONTENTS (continued)

	Page
<b>APPENDIX E    DESIGN EXAMPLE</b>	<b>E1</b>
E.1    Introduction	E1
E.2    Design Steps	E1
<b>APPENDIX F    MATERIAL PROPERTIES</b>	<b>F1</b>
F.1    Introduction	F1
F.2    Wide-Flange Shapes	F1
F.2.1    Residual Stresses	F1
F.2.2    Tensile Test Results	F2
F.3    Concrete	F2
F.4    Reinforcing Steel	F3

## LIST OF TABLES

Table		Page
4.1	Member Sizes of a Typical Bent of the 24 Story Structure	49
4.2	Strengths and Stiffnesses of the Frame Members of the Lumped Model	50
5.1	Member Properties - Test Specimens	69
A.1	Modification of the Elastic Slope-Deflection Equations for Joint Equilibrium	A5
F.1	Mechanical Properties of Structural Steel	F4
F.2	Concrete Strength	F5
F.3	Properties of Reinforcement	F5

## LIST OF FIGURES

Figure		Page
1.1	Free Deflected Shape of Frame and Shear Wall	5
	(a) Free Frame	
	(b) Free Wall	
1.2	Final Shape of Combined Shear Wall-Frame System	5
1.3	First and Second Order Load-Deflection Relationships	6
2.1	Simplified Models for Shear Wall Structures	17
	(a) Bandel's Model	
	(b) Gould's Model	
2.2	Khan's Model	18
2.3	Central Portion of a Two-Story Unit	18
2.4	Test Frame Simulating Multi-Story Structures	19
3.1	Analytical Model	29
3.2	Plan View - Example Building	30
3.3	Equivalent Bent - Example Structure	31
3.4	Analytical Model - Example Structure	32
3.5	Reduction Factor for Plastic Moment Capacity	33
3.6	Moment-Curvature Relationship - Frame Members	34
3.7	Moment-Curvature Relationship - Shear Wall	34
3.8	Deflected Shape of the Shear Wall at Different Stages of the Iteration Process	35
3.9	Shear Wall Subjected to Entire Lateral Load	35
3.10	Deflected Frame System	36

## LIST OF FIGURES (continued)

Figure	Page
3.11 Frame Forces and Moments on Shear Wall	36
4.1 Plan View - 24 Story Building	51
4.2 Elevation - 24 Story Building	52
(a) Typical Bent	
(b) Lumped Model	
4.3 Lumped Model for Clark's Analysis	53
4.4 First and Second Order Load-Deformation Relationships	54
4.5 The $P\Delta$ Effect	55
4.6 Effect of Variation in Wall-to-Column Stiffness Ratio	56
4.7 Moment Distribution over the Shear Wall	57
4.8 Effect of Variation in Wall-to-Column Stiffness and Strength Ratio	58
4.9 Shear Distributions in the Lower Portion of the 24 Story Structure	59
(a) Shear Distribution - First Story	
(b) Shear Distribution - Second Story	
4.10 Shear Distributions in the Upper Portion of the 24 Story Structure	60
(a) Shear Distribution - Top Story	
(b) Shear Distribution - 20th Story	
5.1 Typical Test Specimen	70
5.2 Shear Wall Erection	71
5.3 Typical Beam-to-Wall Joint	71
5.4 Prefabricated Assembly	71

## LIST OF FIGURES (continued)

Figure		Page
5.5	Loading Arrangement	72
5.6	Gravity-Load Simulator	73
5.7	Horizontal Jack Attachment	73
	(a) Front View	
	(b) Location of Strain Gauges in the Dynamometer - Section AA	
	(c) Circuit Diagram	
5.8	Overall View of Test Setup	74
5.9	Side View of Test Setup	74
5.10	Lateral Bracing Locations	75
5.11	Dymec Data Acquisition System	75
5.12	Strain Gauge Locations - Steel Frame	75
5.13	Strain Gauge Locations - Shear Wall	76
5.14	Strain Gauges at a Beam-to-Wall Joint	76
5.15	Rotation Meter Locations	77
5.16	Typical Beam-to-Column Joint	77
5.17	Rotation Meter	78
5.18	Column Base Detail	78
5.19	Transducer and Dial Gauge Locations	79
6.1	Column Base Rotation - Frame A	91
6.2	Load-Deflection Relationships - Frame A	92
6.3	Bending Moment Distributions - Frame A	93
	(a) Load No. 9	
	(b) Load No. 13	

# LIST OF FIGURES (continued)

Figure		Load
6.4	Beam Plastic Hinge - Frame A	94
6.5	Load-Rotation Relationships - Frame A	95
6.6	Plastic Hinge in Top Story Column - Frame A	96
6.7	Plastic Hinge at Column Base - Frame A	96
6.8	Axial Load Distribution in the Column Stack - Frame A	97
6.9	Wall Bending Moment Distributions - Frame A (a) Load No. 9 (b) Load No. 13	98
6.10	Cracking at Wall Base - Frame A	99
6.11	Crushing at Wall Base - Frame A	99
6.12	Frame A after Testing	100
6.13	Load-Deflection Relationships - Frame B	101
6.14	Joint Yielding due to Vertical Load - Frame B	102
6.15	Column Yielding due to Vertical Load - Frame B	102
6.16	Cracking in the Shear Wall After Testing - Frame B	103
6.17	Lateral Buckling - Frame B	103
6.18	Front View of Top Story Column After Lateral Buckling - Frame B	104
6.19	Third Level Beam-to-Column Joint After Testing - Frame B	104
6.20	Plastic Hinge at the Column Base - Frame B	105
6.21	Shear Wall Base Detail - Frame C	105

## LIST OF FIGURES (continued)

Figure		Page
6.22	Load-Deflection Relationships - Frame C	106
6.23	Plastic Hinge in the Top Story Column - Frame C	107
6.24	Plastic Hinge at Third Level Beam - Frame C	107
6.25	Axial Load Distribution in the Column Stack - Frame C	108
6.26	Bottom Story Shear Distribution - Frame C	109
6.27	Top Story Shear Distribution - Frame C	110
6.28	Frame C After Testing	111
7.1	Migration of Plastic Hinge	123
C.1	$P\Delta$ Effect - Multi-Story Structure	C3
E.1	Structure Load-Deflection Relationships - 5th Story	E6
E.2	Structure Load-Deflection Relationships - 24th Story	E7
E.3	Frame Load-Deformation Relationships - 5th Story	E8
E.4	Frame Load-Deformation Relationships - 24th Story	E9

## LIST OF SYMBOLS

### Subscripts and Superscripts

i	Subscript referring to the story number or floor number
1,2 etc	Subscripts referring to the cycle number in the $P\Delta$ iteration process
n	Superscript referring to cycle number in the wall-frame iteration process
bf	Subscript referring to the beam spanning between the column and the roller support; in addition, for moments and rotations, refers to the conditions at the column end of the beam
bw	Subscript referring to the beam spanning between the column and shear wall; in addition, for moments and rotations, refers to the conditions at the column end of the beam
c	Subscript referring to the column
wb	Subscript referring to the beam spanning between the column and the shear wall; in addition, for moments and rotations, refers to the conditions at the wall end of the beam
w	Subscript referring to the shear wall

### Material Properties

$\epsilon$	Strain
$\epsilon_y$	Yield strain
$\epsilon_{st}$	Strain at the onset of strain-hardening
$\sigma$	Stress
$\sigma_y$	Yield stress
$\sigma_u$	Ultimate stress
$E$	Modulus of elasticity (steel)
$E_{st}$	Strain-hardening modulus
$E_c$	Modulus of elasticity (concrete)
$I$	Moment of inertia
$M_p$	Plastic moment capacity
$M_p^*$	Effective plastic moment capacity of a member at the center of the joint, considering the migration of the plastic hinge
$M_{pc}$	Plastic moment capacity reduced for axial load
$M_{ult}$	Ultimate moment capacity of shear wall under combined axial load and flexure
$\phi_p$	Curvature corresponding to $M_p$ assuming ideally elastic behavior ( $\phi_p = M_p/EI$ )
$\phi_{pc}$	Curvature corresponding to $M_{pc}$ assuming ideally elastic behavior ( $\phi_{pc} = M_{pc}/EI$ )
$\phi_{ult}$	Curvature corresponding to $M_{ult}$ in the shear wall ( $\phi_{ult} = M_{ult}/E_c I$ )

### Member Properties

$d$	Depth of beam
$D$	Width of shear wall
$h$	Story height
$L$	Length of beam
$K$	Stiffness ( $EI/L$ ) or $EI/h$ of an individual member in the actual structure
$K_E$	Equivalent stiffness of a member in the lumped model
$K_r$	Wall-to-column stiffness ratio
$M_P$	Plastic moment capacity of an individual member in the actual structure
$M_{PE}$	Equivalent plastic moment capacity of a member in the lumped model
$M_r$	Wall-to-column plastic moment capacity ratio

### Forces and Deformations

$F$	Applied lateral force on the wall
$H$	Applied lateral force on the structure
$H'$	Additional lateral force to be applied to simulate the $P\Delta$ effect on the structure
$M$	Moment developed at the end of a member
$P$	Total vertical load
$P_c$	Vertical load on the column stack
$P_w$	Vertical load on the shear wall
$R$	End reaction of beam

$V$	Story shear
$V'$	Extra story shear due to the $P\Delta$ effect
$w$	Uniformly distributed load per unit length
$\alpha$	Reduction factor for the plastic moment capacity of beams to simulate the uniformly distributed load
$\beta$	Ratio of frame shear to the total applied shear (including the $P\Delta$ shear)
$\epsilon$	Convergence limit for the iteration process
$\Delta$	Lateral deflection of the structure
$\Delta'$	Lateral deflection of the structure, after applying the forced convergence formula
$\theta$	Rotation of the frame or wall joint
$\theta'$	Joint rotation after applying the forced convergence formula
$\delta$	Vertical deflection of the beam-to-wall connection
$\delta'$	Vertical deflection of the beam-to-wall connection after applying the forced convergence formula
$\rho$	Sway rotation; the ratio of the relative deflection of the story to the story height or chord rotation for the beams

## CHAPTER I

### INTRODUCTION

With the introduction of structural steel shapes in the later part of the nineteenth century, a large number of framed multi-story buildings were constructed (1). The lateral loads were assumed to be transferred through the floor system to massive end walls and finally to the foundation. The introduction of diagonal bracing in the early twenties provided a more effective and economical means of resisting lateral loads. The diagonal bracing members in combination with the beams and columns made up a vertical truss system which replaced the massive walls and transmitted the lateral forces to the foundation.

Modern buildings are often constructed with rigidly connected steel bents framing spacious interior areas. The elevator cores and stairwells form stiff interior shear walls. The interior walls, acting in combination with the rigidly framed bents, provide stability against translatory movements caused by wind and earthquake loadings, thus serving both the structural and non-structural function of the building. A structural system consisting of coupled shear walls and rigid frames appears to be economical for buildings in the 20-40 story range. Above this limit, diagonal bracing or other framing systems are generally used (2).

The increasing number of coupled shear wall-frame structures has emphasized the need for a knowledge of the behavior of this type of system. It has been common in the past to design the frame to resist the vertical loads acting on the structure and the shear walls to resist the lateral forces (3). The above procedure is acceptable for low buildings, but for tall structures the interaction between the shear wall and the frame is significant (21). If the frame alone resisted the lateral forces, it would deflect in a shear mode as shown in Fig. 1.1a, while the free shear wall would be subjected to the cantilever type of deformation shown in Fig. 1.1b. Since the two elements are connected at each floor level, interaction forces will be developed in the structure and the final deflected shape will be as shown in Fig. 1.2. The distribution of lateral load between the shear wall and the frame must be determined before a rational design procedure can be formulated.

The response of coupled shear wall-frame structures in the elastic range has been predicted by various methods. Many of the methods are applicable for regular structures with uniform member properties throughout the height of the structure. Since the structure under consideration is highly indeterminate, methods which account for the inelastic action of the structure are necessary to assess the complete behavior of the system. A number of elastic-plastic solutions for large unbraced planar frames have been reported, however, similar results for coupled shear wall-frame structures are limited.

The traditional methods of analysis may lead to a set of ill-conditioned equations with the accompanying difficulties in solution because of the large difference in the stiffnesses of the various structural elements.

The object of this dissertation is to develop an approximate method of analysis to trace the response of the coupled shear wall-frame structure up to the ultimate load and to verify the applicability of the analysis by comparing the results with those of experiments performed on carefully chosen specimens. Computer methods are indispensable for the elastic-plastic analysis of large structures, since the structure must be analyzed in several stages of deterioration to obtain the complete response. In order to reduce the computations to a reasonable limit, the structure will be simplified to an equivalent structural model. With the approximate analysis programmed for the digital computer, the behavior of shear wall-frame structures can be traced as shown in Fig. 1.3. The lateral load at the top level of the structure,  $H$ , is plotted versus the top level deflection,  $\Delta$ . In tall buildings, the axial load plays a dominant role and produces additional overturning moments commonly referred to as  $P\Delta$  moments; where  $P$  is the axial load and  $\Delta$  is the deflection due to sidesway. The effect of these secondary moments is to reduce the capacity of the structure to resist lateral loads as shown in Fig. 1.3. The present method of analysis takes into account these 'secondary' moments, and thus will be termed a second-order analysis as opposed to

the first-order analysis which neglect these effects.

The analytical and experimental research work performed on coupled shear wall-frame structures and planar frames is discussed in Chapter II of this dissertation. In Chapter III, the method of analysis is described and the assumptions on which it is based are discussed. The method of lumping the structure into an analytical model is also presented. The behavior of a 24 story structure is studied under various conditions in Chapter IV. This study forms the basis for the design of the experimental program. In addition, a design example is included in Appendix E.

Three, four-story, one-bay structures were designed to exhibit behavior similar to that of portions of a tall building. The design was based on the computer program developed for the analysis of coupled shear wall-frame structures. The first two specimens were designed to exhibit behavior characteristic of the bottom stories of a tall structure and the last to simulate the behavior of the top stories. The specimen description, test arrangement, loading scheme, and instrumentation are presented in Chapter V. Chapter VI is devoted to the description of the results of the tests on the three specimens. In Chapter VII, comparisons are made between the theoretical predictions and the observed response of the specimens. The summary, conclusions and recommendations are included in Chapter VIII.

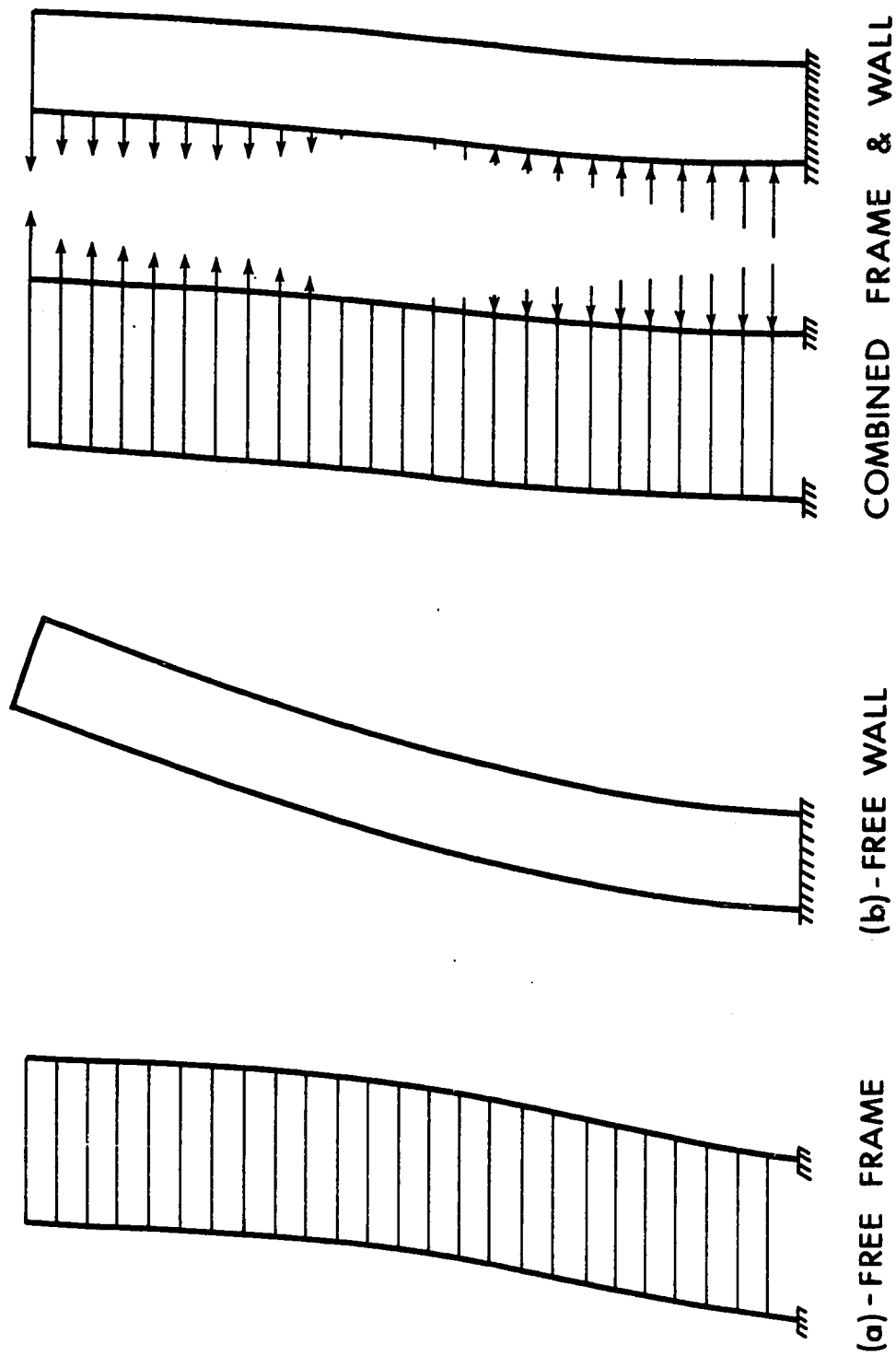


FIG. 1.1 FREE DEFLECTED SHAPE OF FRAME AND SHEAR WALL

WALL-FRAME SYSTEM

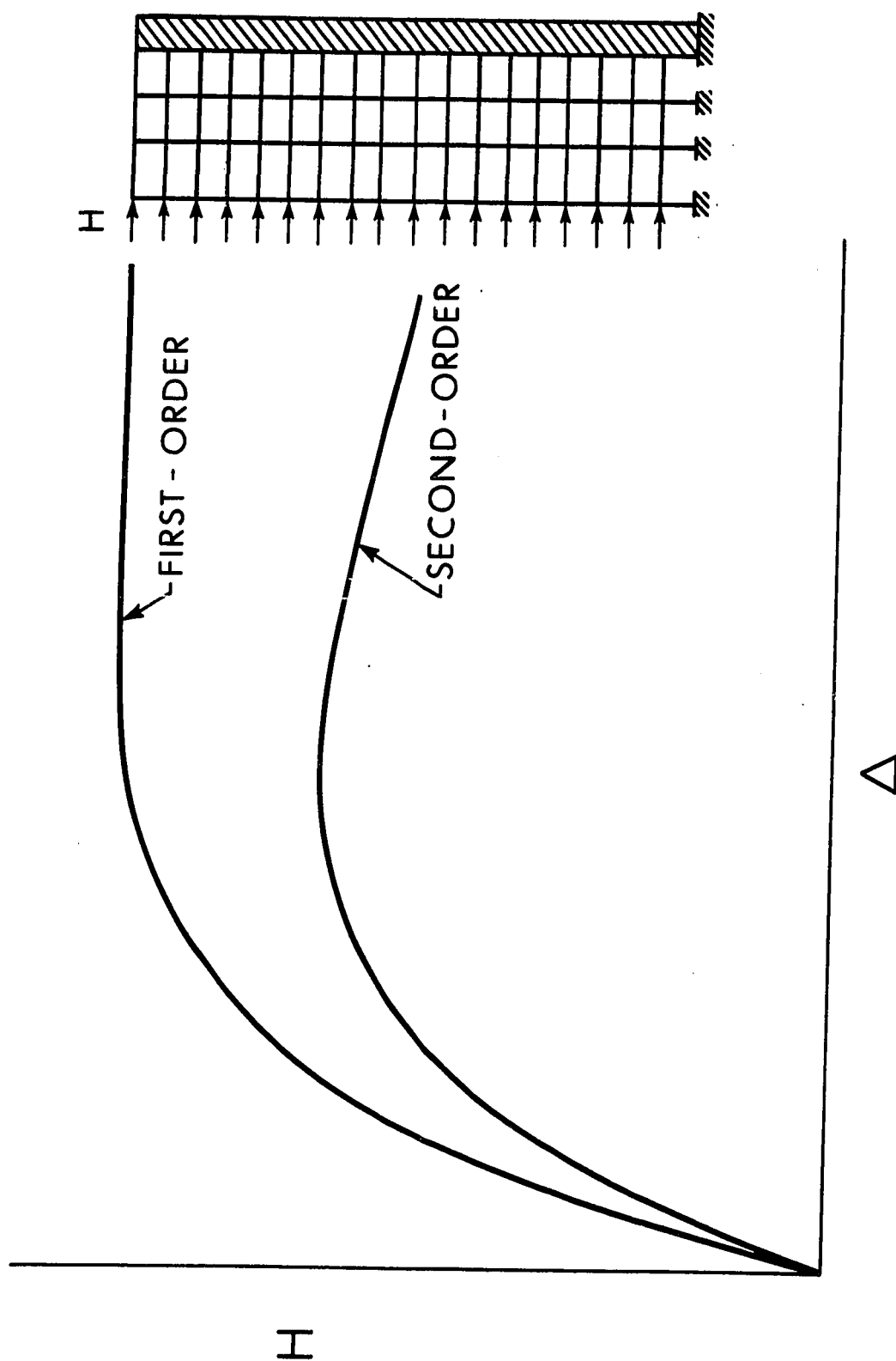


FIG. 1.3 FIRST AND SECOND ORDER LOAD-DEFLECTION RELATIONSHIPS

## CHAPTER II

### PREVIOUS INVESTIGATIONS

#### 2.1 Introduction

In order to investigate the problems discussed in Chapter I, it is necessary to develop a technique to predict the load-deflection relationship for coupled shear wall-frame structures up to the ultimate load.

This chapter first presents a brief summary of the methods of analysis for coupled shear walls; this leads naturally to a discussion of similar solutions for coupled shear wall-frame structures. The analysis of large framed structures, which include shear walls, are also presented and the possibility of utilizing these methods for the present problem are considered.

The above investigations consider the response of the structure in the elastic range; the current state of knowledge regarding elastic-plastic analysis of unbraced frames and coupled shear wall-frame structures is next reviewed. In addition, the experimental work performed on specimens simulating large structures is briefly summarized.

The development of the basic approach for the present problem is discussed with reference to this review.

## 2.2 Shear Wall Structures

Coupled shear wall structures generally consist of two or more shear walls connected by beams or slabs, while coupled shear wall-frame structures consist of conventional beam and column elements which act together with stiff shear walls. The important aspect of the design of these structures is the proportioning of the lateral loads between the shear walls or between the frame and the shear wall. Coull and Smith (4) have presented an excellent review of the methods available to analyze structures containing shear walls.

Coupled shear walls have been analyzed by replacing the discrete connecting beams by a continuous lamina of equivalent stiffness (5,6,7). However, in order to obtain a closed form solution, constant structural properties have been assumed throughout the height of the structure. Coull and Puri (8) have taken into account the shear deformation of the shear walls. Recently, a finite element technique (9) has been used which takes into account the distortion of the shear walls and the stress concentrations at the beam-to-wall junctions.

The above work has been extended to provide closed form solutions for coupled shear wall-frame structures. Cardan (10) has developed expressions for the lateral stiffness of various types of beam and column arrangements. The main assumptions in this approach are that the properties of the wall are constant throughout the height and that the forces acting on the wall are continuously distributed

over the height of the building. A differential equation, expressing the equilibrium of the shear wall is formulated with the rotation as the unknown parameter.

The energy method has been used by Bandel (11), who replaces the shear wall by an equivalent truss as shown in Fig. 2.1a. The deformed shape of the wall is expressed as a power series and simultaneous equations are developed from the minimization of the total potential energy of the system.

Gould (12) utilized the finite difference technique, where the frame is replaced by rotational and translational springs linked by rigid bars as shown in Fig. 2.1b. In the analysis, it is assumed constant story height and shear wall stiffness. The lateral resistance of a particular floor is determined from the properties of the members in each floor and their relationship with adjacent floors. The lateral deformations of the wall are represented by finite difference equations, one for each story.

Recently, coupled shear wall-frame bents have been analyzed by Oakberg and Weaver (13) by applying the finite element technique. The finite element model can accommodate rectangular openings and piers. The method takes into account the effects of shearing and local deformations. Several other elastic analyses (14-18) have also been reported for analyzing shear wall-frame structures.

### 2.3 Elastic Analysis of Multi-Story Structures

Clough, Wilson and King (19) have developed a method of

analysis for a building consisting of several parallel rigid frames. All the bents in the building are analyzed simultaneously by assuming that the bents are connected by inextensible links. This is equivalent to assuming that the floor diaphragms are inextensible.

This method has been extended (20) to bents composed of shear walls acting with frames. The axial deformations of the columns and shear walls have been considered, although the secondary moments due to the  $P\Delta$  effect are neglected. A three-dimensional analysis can also be performed, on the assumption that under lateral load each floor level of the building can translate but not rotate. The lateral stiffnesses of each frame (in both directions of the building) are evaluated and summed to obtain the total building stiffness.

An iterative method has been used by Khan and Sbarounis (21), in which the building is lumped into an analytical model consisting of a shear wall system and a frame system as shown in Fig. 2.2. The method accounts for the variation of wall and frame properties. The effects of base rotation, plastic rotation of the wall and secondary deflections of the frame have also been discussed. Influence curves are developed to estimate the distribution of shear between the wall and the frame for a wide range of structural proportions.

#### 2.4 Elastic-Plastic Analysis of Unbraced Planar Frames

An excellent review of the previous work on the elastic-plastic analysis of unbraced frames is reported in References 22 and 23.

In a multi-story structure, where the axial loads and the secondary deflections play an important role, the second-order elastic-plastic analysis (23-27) yields close correlation with the true behavior. Modern high speed computers are particularly suitable for elastic-plastic analysis, since the structure must be analyzed in several stages of deterioration, in order to obtain the complete response. The second-order effects that may be taken into account are the axial shortening of the columns, the reduction in column stiffness due to the axial load, the curvature shortening of the members and the secondary, or  $P\Delta$ , moments as defined in Chapter I. Inelastic action is normally represented by point plastic hinges with the influence of strain-hardening neglected. A second-order elastic analysis is performed on the original structure. When the plastic moment capacity is achieved at a particular location, a hinge is assumed to be inserted in the structure. The stiffness is then modified to take into account the new configuration of the frame which is then re-analyzed under the next increment of load.

The earliest computerized analysis for unbraced planar frames subjected to static, proportional loads, was developed by Jennings and Majid (24). Matrix techniques have been used with the displacement vector as the unknown. If during any stage of loading, plastic hinges form in the structure, the number of unknowns is increased by the number of hinges. Each time a new hinge is formed, the determinant of the stiffness matrix, before and after hinge formation, is calculated. When the determinant passes from a positive value to a zero or a negative value, the maximum capacity of the structure has been attained. Davies (25) has extended this analysis to consider the effects of variable repeated loading,

strain-hardening and hinge reversals based on the bending deformations of the structure.

A similar method, developed by Parikh (26), utilizes the slope-deflection equations, including the axial load effects. By satisfying the moment and shear equilibrium equations, a set of simultaneous equations is generated. The axial load effect is taken into account by a series of iterations. The equations are solved by the Gauss-Seidel Iteration method in order to use the available memory locations of the computer more efficiently. However, the exact order of hinge formation during a given load increment is not known.

The second-order elastic-plastic analysis presented by Korn and Galambos (23) combines the features of the two analyses described above. The formulation technique is similar to Parikh's, although the equations are solved by matrix techniques. The plastic hinges are detected in sequence, however, similar to the procedure used by Jennings and Majid (24).

In the Subassembly Method (27), isolated parts of a multi-story frame can be analyzed as independent units. The points of inflection in the columns are assumed to occur at mid-height, so that two imaginary slices through the structure isolate one floor level with its attached columns as shown in Fig. 2.3. Four subassemblies, each consisting of a column restrained by the adjacent beams are ob-

tained from this model. An inelastic analysis is performed on each subassembly and the response of the complete story is obtained by summing the responses of each subassembly. In a coupled shear wall-frame structure, however, the behavior of a portion of shear wall can not be isolated, since the deflections and rotations of each part of the wall depend on the deformation of the wall as a whole.

## 2.5 Inelastic Analysis of Coupled Structures

Several elastic analyses of coupled structures have been described in Sections 2.2 and 2.3 of this chapter. However, none of these analyses attempt to analyze the structure in the inelastic range. Clark (28) has developed a method of analysis, which predicts the response of reinforced concrete shear wall-frame structures up to the ultimate load. The approach is similar to Parikh's analysis. The analysis is performed on a planar bent consisting of rigid frames and shear walls. The slope-deflection equations are modified to take into account the finite width of the shear walls.

The entire building is analyzed as a two-dimensional bent; consisting of the rigid frames and walls, linked together by rigid bars. The example structures presented are symmetrical, with the shear wall placed at the center of the bent. A system of ill-conditioned equations may be generated, if the stiffness ratio of the shear wall to the column is high. Hence, this approach is not suitable for all types of coupled shear wall-frame structures and needs further investigation.

## 2.6 Experimental Investigations of Multi-Story Frames

In addition to the development of an analytical procedure, this dissertation reports the results of experiments on specimens simulating portions of an entire structure. Extensive experimental work has been performed in the process of developing rational and economical design methods for multi-story braced and unbraced steel frames. An excellent review of the large-scale tests on steel frames has been reported in References 22 and 31.

The results of tests on three, three-story, two-bay frames have been reported by Yura (29). These tests were performed to verify the plastic design method for braced frames. The geometry of the frame was the same for all test specimens, however, the loading conditions varied, including full gravity load, checkerboard gravity load and checkerboard gravity with lateral load. Yarimci (30) reported the results of full-size tests on three-story unbraced steel frames. Two basic failure mechanisms were exhibited by these specimens; the sway mechanism and the combined mechanism. It was observed that unbraced frames are likely to fail by overall instability before the formation of collapse mechanism.

Arnold, Adams and Lu (31) have tested a single-story frame under non-proportional loading. The frame is shown in Fig. 2.4, and was designed to exhibit behavior similar to that of the lower stories of a multi-story frame. The main objective of the test was to study the effect of axial load and the influence of strain-hardening on the

response of unbraced structures as an aid to the development of a rational design procedure for such structures. A second-order elastic-plastic analysis has been applied to predict the response of the portal frame. In addition, the strain-hardening effect has been included in the analysis in a rational manner. The test results were predicted closely by the analysis.

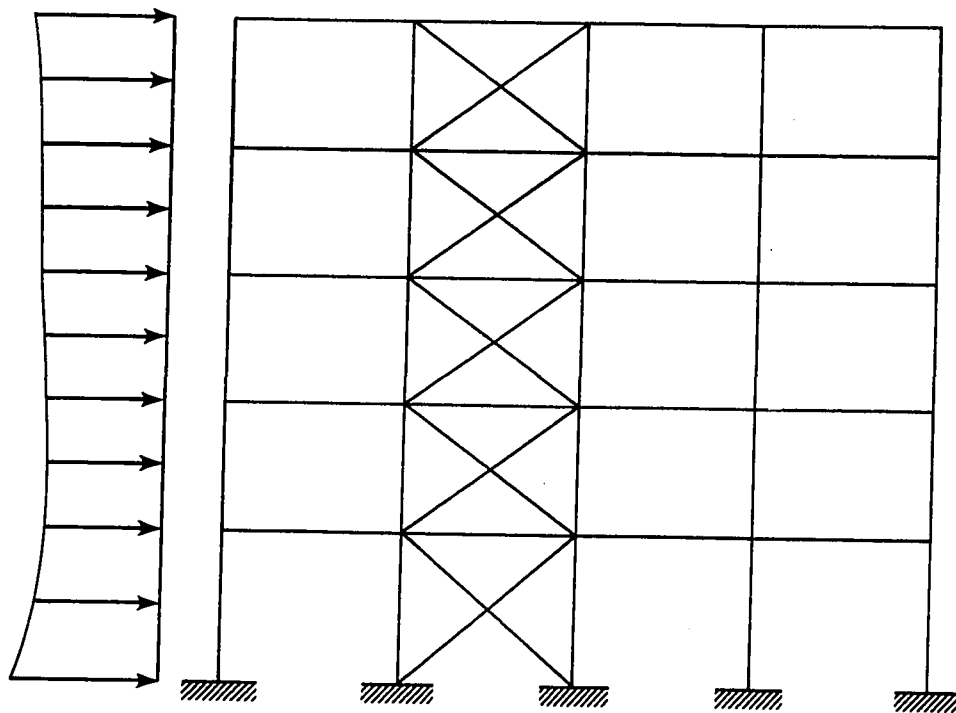
The single-story, single-bay frame shown in Fig. 2.4, was also subjected to static cyclic loading (32), which simulated the effects of earthquake motions on frame response. A single-story, single-bay frame and a three-story, single-bay frame were tested by Carpenter and Lu (33) to study the behavior of steel frames subjected to cyclic loading. The test frames were typical of current aseismic design practice and simulated portions of an eight-story prototype frame. Each frame was subjected to 50 cycles of increasing amplitudes of horizontal displacement. It was observed that the presence of residual  $P\Delta$  moments has a significant effect on frame behavior.

Nikhed (34) has tested a reinforced concrete four-story, single-bay coupled shear wall-frame structure. The vertical load in the column and shear wall were applied initially and held constant during the test. Next, the lateral load was incremented. The response of the test frame was closely predicted by a second-order inelastic analysis.

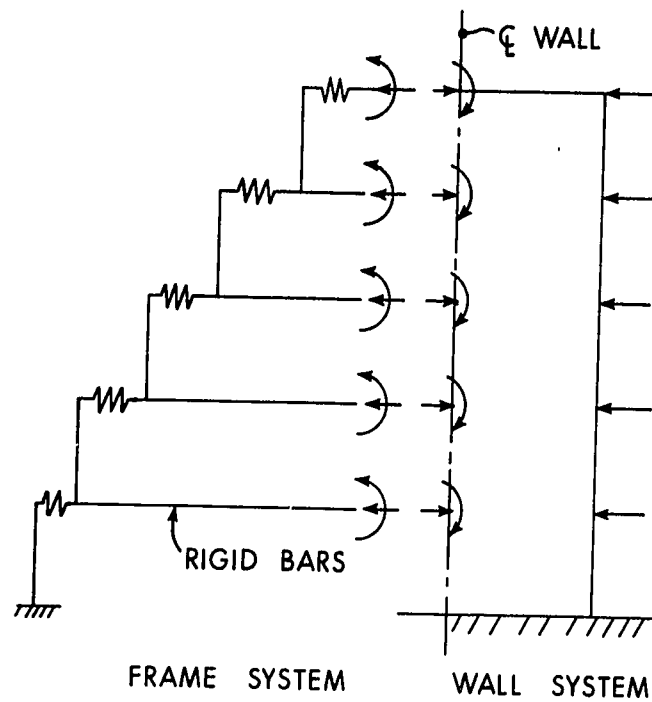
## 2.7 Summary

At this point, it is now possible to discuss the adequacy of the present state of knowledge for the structures under consideration. Except for Clark (28), no other analysis predicts the complete load-deflection history of coupled shear wall-frame structures. However, Clark's analysis does not include the possible base rotations of the columns and shear walls and for structures having even moderately stiff shear walls the analysis involves a set of ill-conditioned equations, which in turn may produce misleading results.

The force-fitting method developed by Khan and Sbarounis (21) does not induce ill-conditioning, since the iterative solution treats the stiff shear wall element separately from the rigid frames. Hence, this approach is utilized in the present analysis, so that the ill-conditioning effect is eliminated. As mentioned in Section 2.4, Parikh's (26) elastic-plastic method of analysis makes more efficient use of computer storage capacity compared to other available methods. Hence, it was decided to combine the better features of the above two analyses (21,26), to develop an elastic-plastic analysis for coupled shear wall-frame structures. The development of an analysis and design procedure must be based on experimental evidence. Until now, only one large-scale test on this type of structure has been reported (34). Hence, a test program was initiated in order to investigate those aspects of behavior for which analytical techniques are inadequate.



(a) BANDEL'S MODEL



(b) GOULD'S MODEL

FIG. 2.1 SIMPLIFIED MODELS FOR SHEAR WALL STRUCTURES

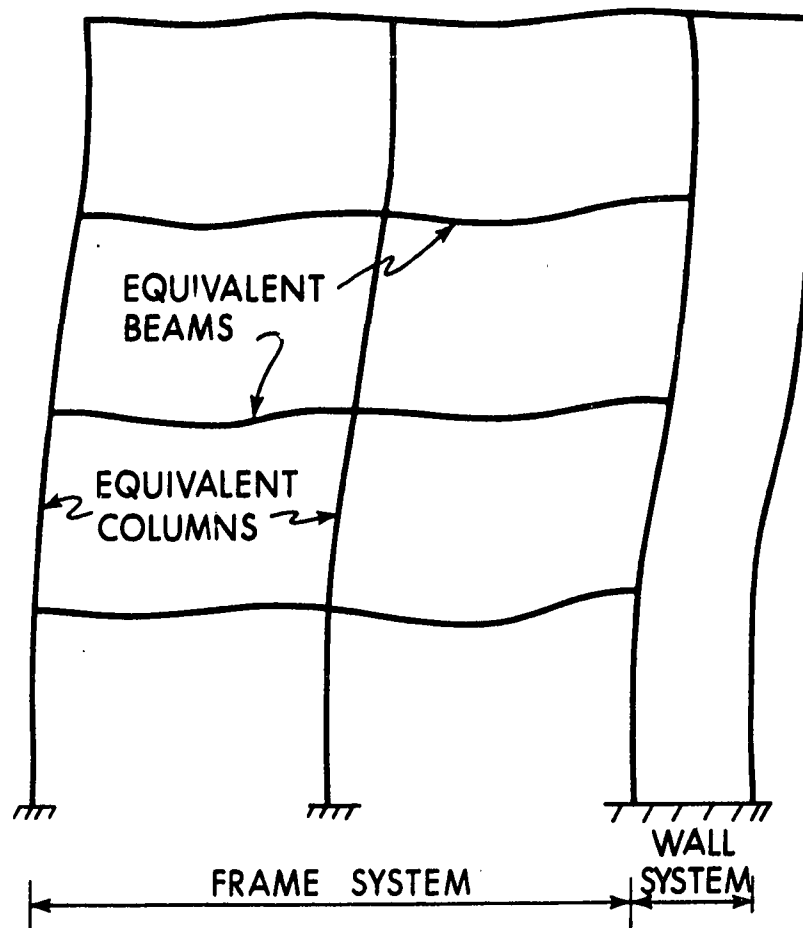


FIG. 2.2 KHAN'S MODEL

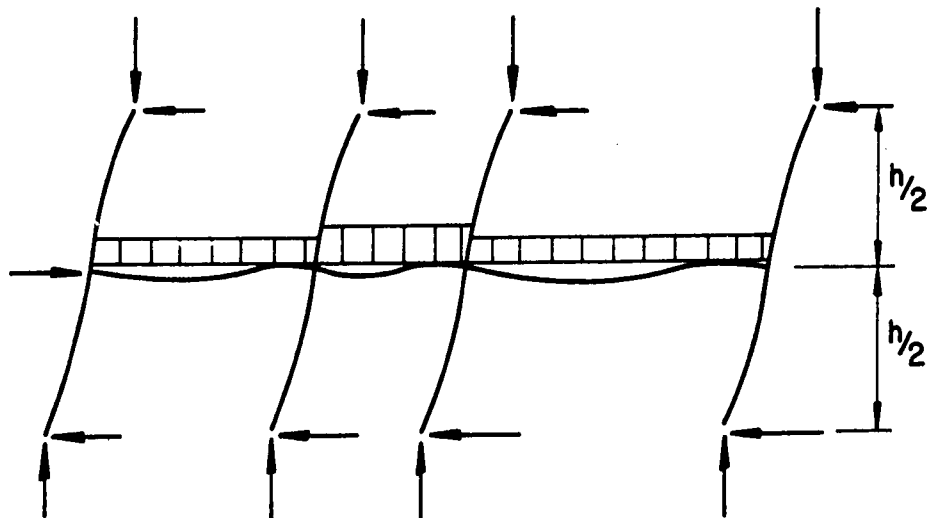


FIG. 2.3 CENTRAL PORTION OF A TWO-STORY UNIT

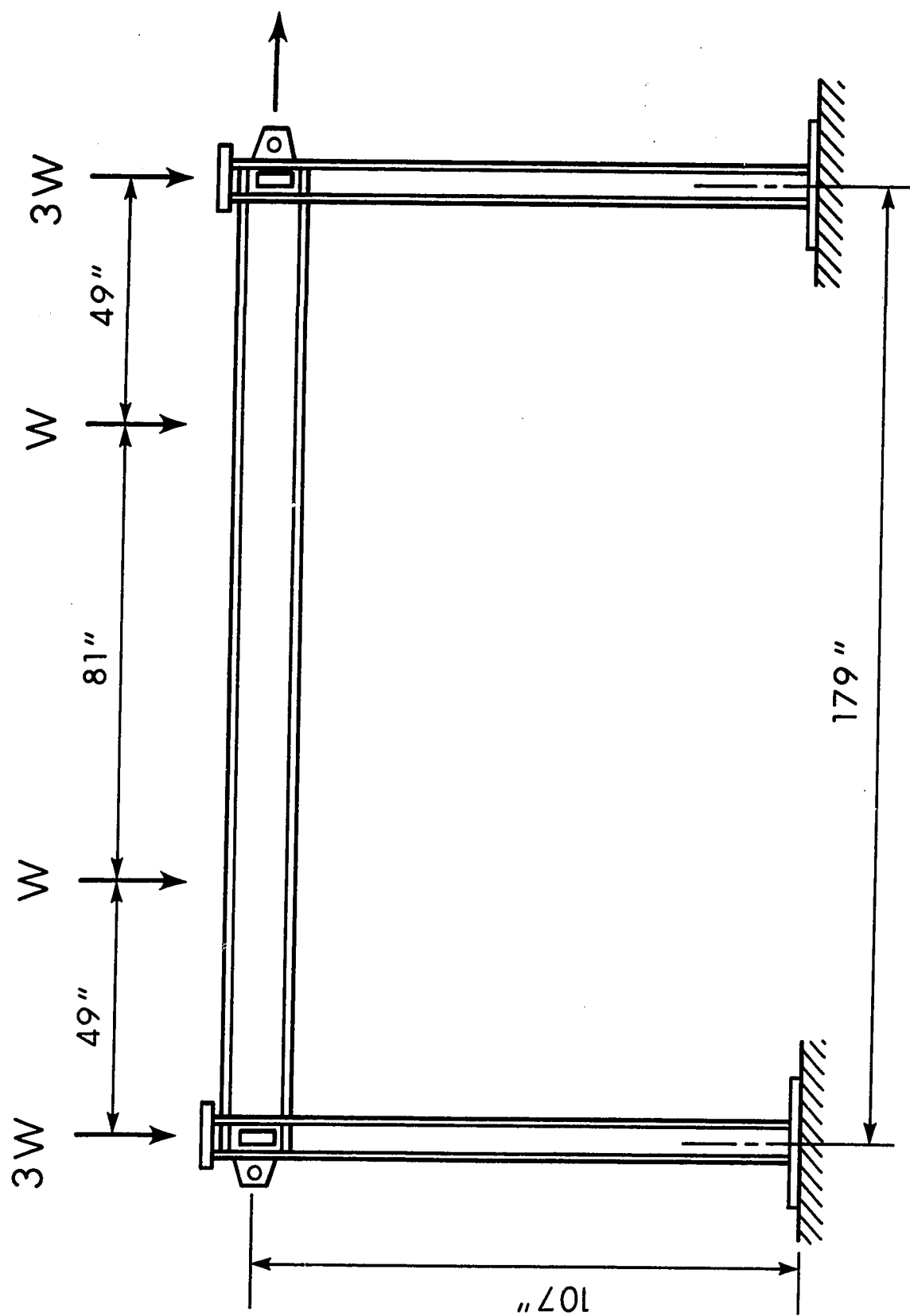


FIG. 2.4 TEST FRAME SIMULATING MULTI-STORY STRUCTURES

## CHAPTER III

### ANALYTICAL MODEL AND METHOD OF ANALYSIS

#### 3.1 Introduction

The basic approach to the analysis in this dissertation follows from the review in Chapter II. For a large structure, an elastic-plastic analysis results in an excessive number of computations. One way to simplify the analysis is to replace the actual structure by a substitute structural model. This technique has been used by several authors (35-37) to analyze planar multi-story frames.

In the present dissertation, an analytical model, similar to that used by Khan and Sbarounis (21), has been developed to represent the actual structure. The model is then subjected to a second-order elastic-plastic analysis. The lumping of the actual structure into the model is described in the initial part of this chapter. The assumptions in the analysis are then discussed and the method of analysis is presented.

#### 3.2 Analytical Model

The actual coupled shear wall-frame building is lumped into the analytical model shown in Fig. 3.1. The model is analyzed to determine forces and deformations under the loads that would be applied to the actual structure. The analytical model consists of the

Frame System and the Shear Wall System. In Fig. 3.1, the beam  $b_i f_i$  represent beams in the actual structure which span between two adjacent columns; the beam  $b_i w_i$  represents the beams in the actual structure linking the shear wall to the columns. The subscript  $i$  denotes the floor level; the numbering system starts at the base of the structure. The equivalent column in each story of the analytical model is assigned a strength and stiffness equal to the sum of the strengths and stiffnesses of all the columns in a particular story of the actual structure. In the model, the shear wall system has a strength and stiffness which is equal to the sum of the strengths and stiffnesses of the individual walls.

In the analysis of the model, joints  $b_i$  and  $f_i$  are subjected to equal rotations in order to simulate the deformed shape of the beam in the actual structure. For the beam  $b_i f_i$ , the following relations are satisfied at each floor:

$$KE_{bfi} = 2 \cdot \sum K_{bfi} \quad (3.1)$$

$$MPE_{bfi} = 2 \cdot \sum MP_{bfi} \quad (3.2)$$

where  $KE_{bfi}$ ,  $MPE_{bfi}$  are the stiffness and plastic moment capacity of the beams spanning between the column and the roller support and  $K_{bfi}$  and  $MP_{bfi}$  are the stiffness and plastic moment capacity of the individual beams in the actual structure. For the beam  $w_i b_i$ , the

following relations are satisfied at each floor:

$$KE_{wbi} = \sum K_{wbi} \quad (3.3)$$

$$MPE_{wbi} = \sum MP_{wbi} \quad (3.4)$$

where  $KE_{wbi}$  and  $MPE_{wbi}$  are the stiffness and plastic moment capacity of the beam connecting the column to the shear wall and  $K_{wbi}$  and  $MP_{wbi}$  are the stiffness and plastic moment capacity of the individual beams in the actual structure. If necessary, the rotational springs at the wall and column bases can be adjusted to simulate the flexibility of the foundation.

Coupled shear wall-frame structures may have bents consisting of various combinations of shear walls and frames. The plan view of a building with two exterior shear walls and seven interior frame bents is shown in Fig. 3.2. Assuming the floor diaphragms to be rigid, this building can be simplified to the system shown in Fig. 3.3. It is assumed that the floor diaphragms do not offer rotational restraint to the shear wall. In Fig. 3.3,  $K_c$  and  $K_b$  are the stiffnesses ( $EI/L$ ) and  $M_{pc}$  and  $M_p$  are the plastic moment capacities of each individual column (reduced for axial load) and beam respectively in a particular story of the building. The analytical model representing the building is shown in Fig. 3.4 with the members having the strengths and stiffnesses as given by Equations (3.1) to (3.4).

### 3.3 Uniformly Distributed Loads

The beams in the analytical model are not subjected to transverse loads. Hence the hinging pattern in the model does not directly correspond to that in the actual structure. For example, if uniformly distributed loads acted on the beams, plastic hinges would form earlier than predicted by the model, at the leeward end of the member. On the other hand, plastic hinges would form later than predicted at the windward end or in the interior of the beam. Although these two effects should be compensating to some extent, the approximate method would tend to overestimate the ultimate load by ignoring the additional flexibility (and resulting secondary moments) of the actual structure caused by the earlier hinge formation in the leeward side of the beam.

In order to simulate the influence of the uniformly distributed loads, the plastic moment capacities of the beam in the analytical model are reduced (34). In Fig. 3.5,  $\alpha$ , the reduction factor is plotted versus  $wL^2/M_p$  where  $w$  represents the uniformly distributed load and  $M_p$  is the plastic moment capacity of the beam. The lower solid line represents the condition corresponding to a single hinge at the leeward end of the beam. On further increase in the wind moment, a second hinge will form either at the windward end or between the ends of the beam and is represented by the dashed curve in Fig. 3.5. If the value of  $\alpha$  is taken corresponding to the single hinge configuration, the results obtained by the analysis of the lumped frame will be too conservative since the second hinge is forced

to form at the first hinging load. On the other hand, if the dashed curve is used, the result will be unconservative since the first hinging load is increased. The reduction factor used in the analysis has been taken as the mean curve, shown by the broken line in Fig.

3.5. Several structures have been analyzed (34) using the above modification. The ultimate load carrying capacity given by the model corresponds closely to that obtained from an analysis of the actual structure.

#### 3.4 Assumptions in the Analysis

In the present analysis, it is assumed that the behavior of a shear wall-rigid frame building can be represented by the analytical model described in the previous sections. Each floor of the building is assumed to form a diaphragm of infinite rigidity. Torsional effects, due to asymmetry of load or structural layout, have not been considered.

In the analysis of the model, it is assumed that lateral-buckling, lateral-torsional buckling and local buckling of the members are prevented. The effects of axial shortening and shear deformation of the members and the effect of axial load on the stiffness of the columns have been neglected. It is assumed that idealized plastic hinges will form only at the ends of the members.

The individual members are assumed to have elastic-plastic moment-curvature ( $M-\phi$ ) relationships as shown in Fig. 3.6. In this figure,  $M_{pc}$  is the plastic moment capacity of the member, reduced for

axial load (in the columns) while  $\phi_{pc}$  represents the curvature corresponding to  $M_{pc}$ , assuming ideally elastic behavior. The moment-curvature relationship for the shear wall is shown in Fig. 3.7. The relationship is formulated in a piecewise linear fashion by specifying moment and curvature co-ordinates. The moment,  $M$ , is non-dimensionalized as  $M/M_{ult}$  and the curvature,  $\phi$ , is non-dimensionalized as  $\phi/\phi_{ult}$ , where  $\phi_{ult} = M_{ult}/E_c I$ .

For each vertical member, the value of  $M_{pc}$  is read as input data and is based on an estimate of the axial loads in the members at the ultimate load condition. Thus the influence of changes in axial loads during the loading process is neglected; this is consistent with the development of the simplified model. If these changes do influence the behavior of the structure, bounds on the ultimate strength can be obtained by using the  $M_{pc}$  values consistent with the different distributions of axial loads, and performing several analyses.

### 3.5 Method of Analysis

The loading is assumed to be applied statically. The structure is analyzed under constant vertical loads and monotonically increasing lateral loads. The basic solution procedure is shown schematically in Fig. 3.8. To analyze the model for a given lateral load level, the loads are first applied to the shear wall and the free deflected shape is computed as shown by the dashed curve in Fig. 3.8. The deflection at the  $i$ th level is  $\Delta_{wi}^{(1)}$  where the superscript represents the number of the iteration cycle. The frame is then forced into a corresponding configu-

ration and the negative shears developed are applied at each floor level to the shear wall. The relative deflection,  $\Delta_{wi}^{(2)}$  is computed as shown by the solid curve in Fig. 3.8. The frame is then forced into a new position characterized by a deflection  $\Delta_{wi}^{(3)}$  as shown by the broken line. The deflections  $\Delta_{wi}^{(3)}$  are functions of the deflections  $\Delta_{wi}^{(1)}$  and  $\Delta_{wi}^{(2)}$  and are computed by a forcing procedure (21). The negative shears in the frame are again computed and applied to the shear wall; the process is repeated until the total shears developed are in equilibrium with the applied lateral loads.

The  $P\Delta$  effect is included at each stage of the process. The secondary moments in each story are computed from a knowledge of the deflected shape and the vertical loads. The corresponding shears are then added to each floor level and the additional deflections computed. The process is continued until the deflected shapes converge. In order to obtain the complete load-deflection history of the structure up to the ultimate load, the lateral loads are increased and the above process is repeated. At each stage of loading, the inelastic action of the frame and the shear wall is accounted for by using the appropriate moment-curvature relationships in the computation of the deflection and resulting forces.

The method of analysis is summarized in the following steps:

- (a) The vertical loads acting on the structure and the initial lateral loads are selected.
- (b) The lateral loads are applied to the shear wall. The deformations of the shear wall are computed by applying moment-area principles.

The corresponding rotations, lateral displacements and vertical displacements are represented by  $\theta_{wi}^{(1)}$ ,  $\Delta_{wi}^{(1)}$  and  $\delta_{wi}^{(1)}$  as shown in Fig. 3.9. The initial subscript w refers to the shear wall, while i is the floor under consideration and the superscript represents the initial iteration cycle.

(c) The frame system is then forced into the deflected shape of the shear wall as shown in Fig. 3.10. Moment-equilibrium equations, relating the joint rotation to the deformation of adjacent joints and the member properties, are generated using the slope-deflection equations. The detailed derivation of these equations are given in Appendix A. The solution of this set of simultaneous equations by the Gauss-Seidel Iteration Technique yields the joint rotations; from these the moments and shears are computed. The forces developed by the frame at level i of the shear wall are shown schematically in Fig. 3.11 where  $F_i$ ,  $R_{wbi}$ ,  $M_{wbi}$  represent the axial force in the beam, and the vertical shear and moment at the junction, respectively. The subscript, wb, refers to the beam spanning between the column and wall.

(d) The net out-of-balance forces are applied to the wall and the resulting deflections,  $\Delta_{wi}^{(2)}$ , rotations,  $\theta_{wi}^{(2)}$  and vertical displacements,  $\delta_{wi}^{(2)}$ , are computed as described in Step (b).

(e) In order to speed convergence, the frame is not forced into the deformation mode defined by  $\Delta_{wi}^{(2)}$ , etc. Instead the frame is forced into the position defined by the forced-convergence equations (B.1), (B.2) and (B.3) in Appendix B. Next steps (c) to (e) are repeated. For any cycle (after the initial cycle), the forcing equations (B.1),

(B.2), and (B.3) are replaced by equations (B.4), (B.5), and (B.6), given in Appendix B. Convergence tests are performed at the end of Step (d) and must satisfy condition (B.7), for rotations, and (B.8) for deflections as given in Appendix B.

(f) If the system has not converged as defined above, the Steps from (d) to (f) are repeated.

(g) On the other hand, if the system has converged, the  $P\Delta$  effect is included. The structure is reanalyzed under the applied lateral loads plus the increased story shears due to the  $P\Delta$  effect. The derivation of the additional forces due to the  $P\Delta$  effect is contained in Appendix C.

(h) At the end of each load increment, the deflected shape of the structure is known as well as the distribution of forces and moments. The moments at the ends of the members are checked to see that plastic hinging has not occurred. If hinges have formed, the moment-equilibrium equations at each beam-to-column joint are modified. The revised equations for various hinge patterns are included in Appendix A. In order to determine the complete load-deflection curve for the structure, the lateral load is incremented and Steps (b) to (h) are repeated.

A Fortran Program has been developed to perform the analysis. The nomenclatures and a printout of the program have been included in Appendix D. Using the computer program, several structures have been analyzed (34,38) and the results compared with those obtained by other methods. The lumping technique and the iteration solution produced results that compared closely with those reported in the literature (17,21,28).

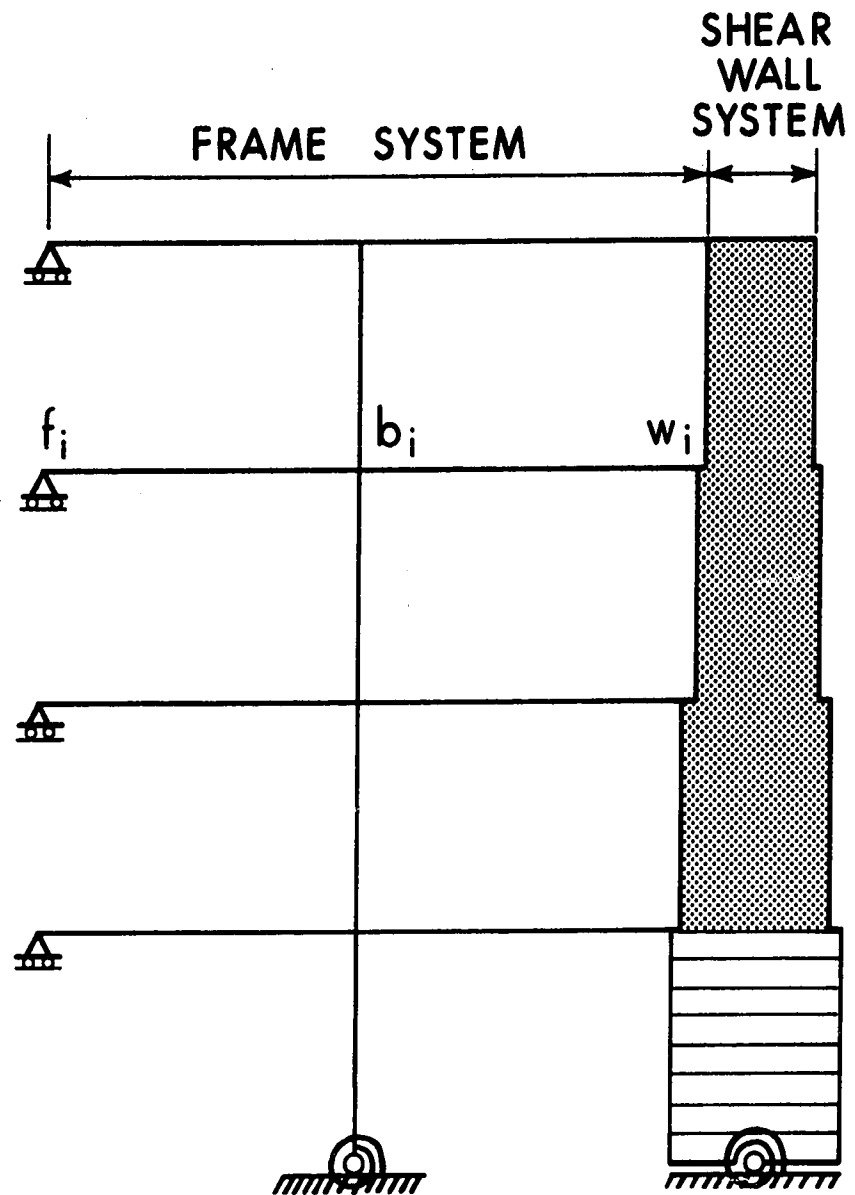


FIG.3.1 ANALYTICAL MODEL

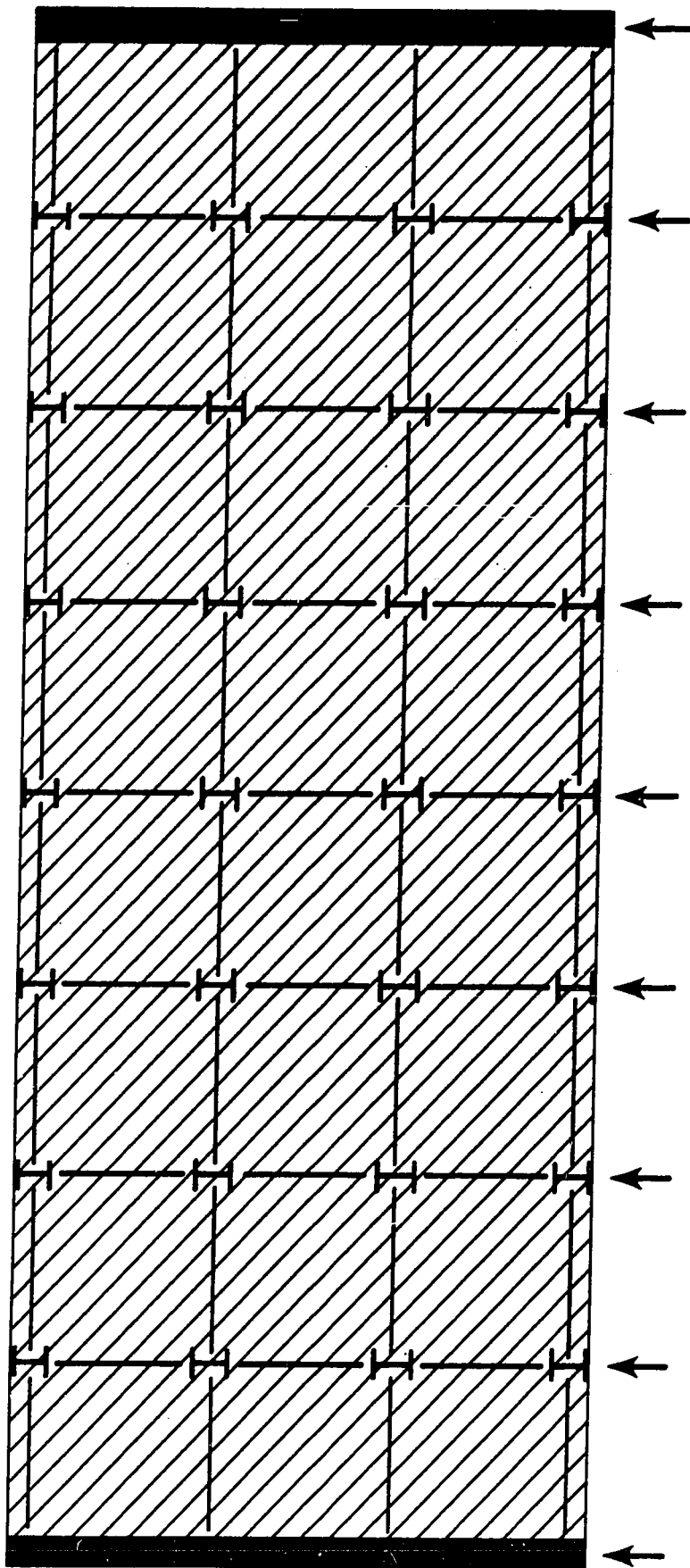


FIG. 3.2 PLAN VIEW - EXAMPLE BUILDING

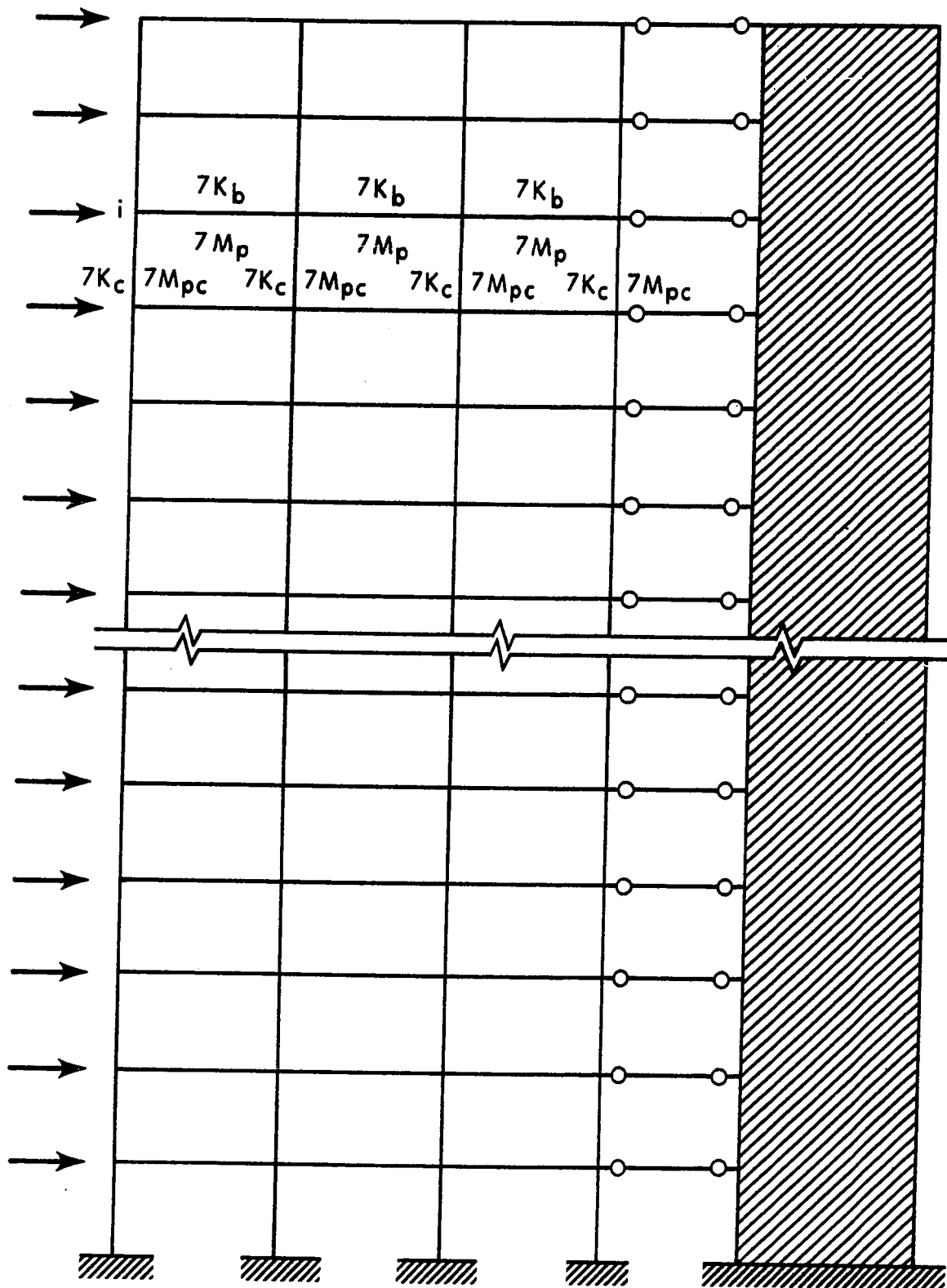


FIG. 3.3 EQUIVALENT BENT - EXAMPLE STRUCTURE

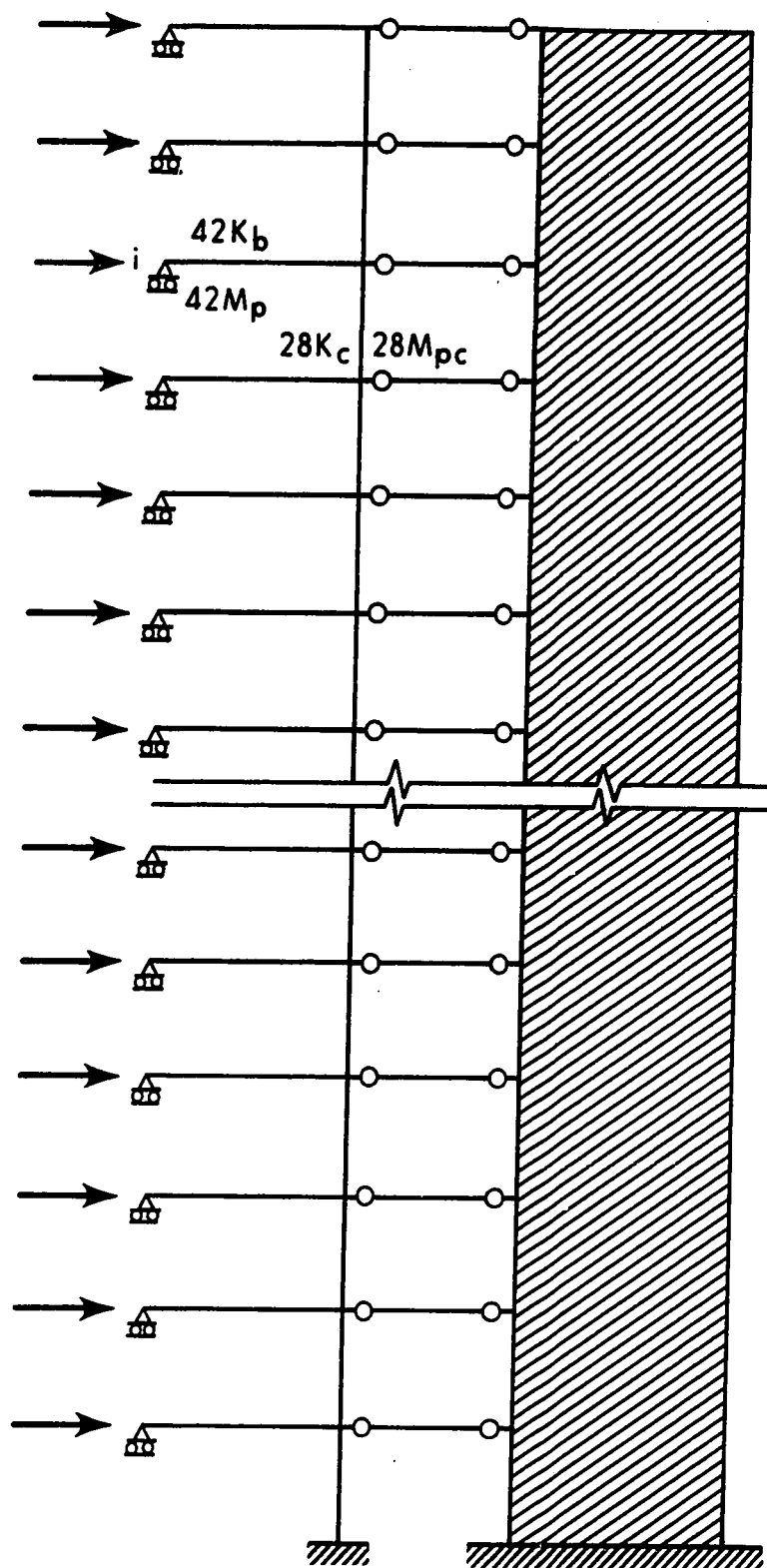


FIG. 3.4 ANALYTICAL MODEL - EXAMPLE STRUCTURE

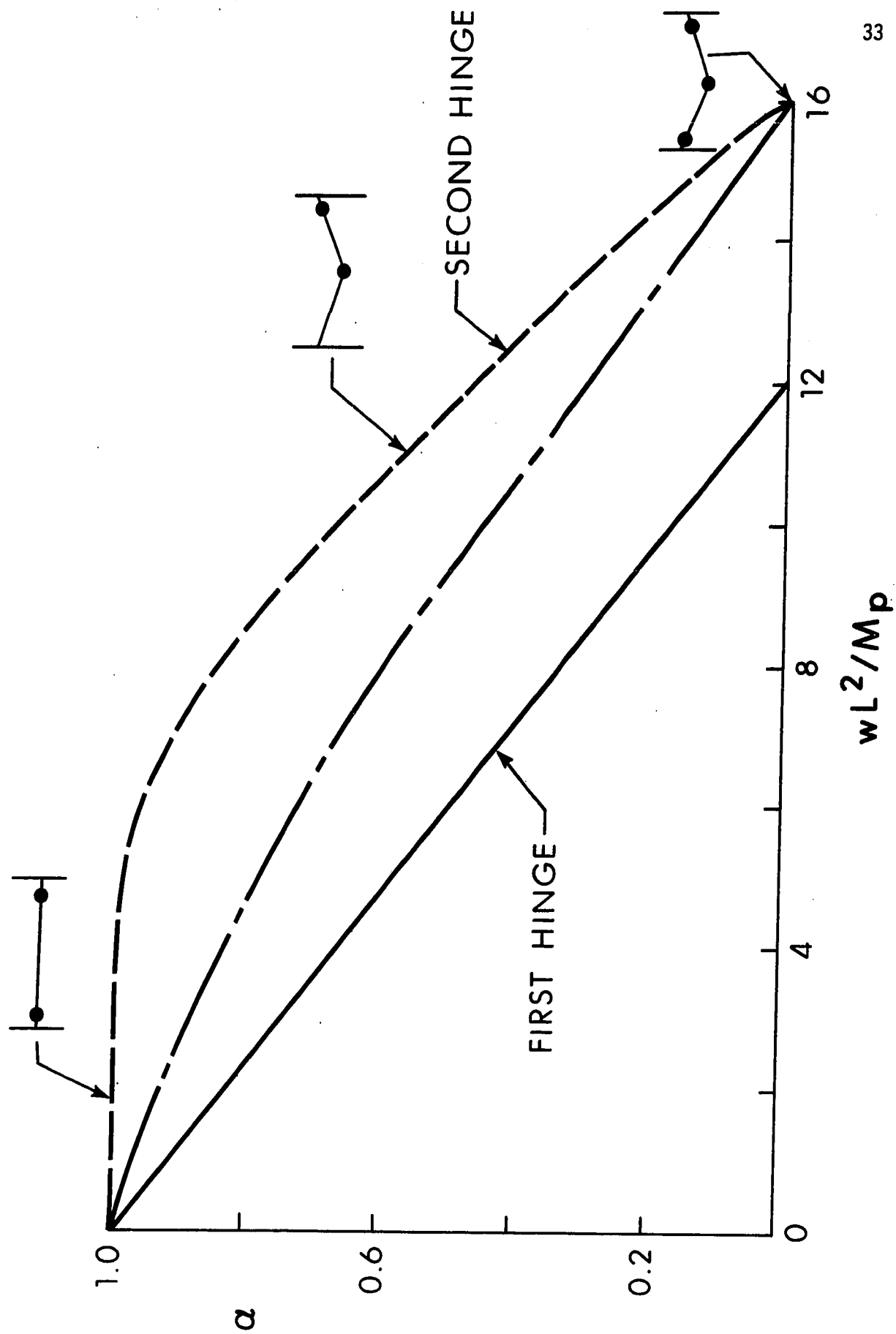


FIG. 3.5 REDUCTION FACTOR FOR PLASTIC MOMENT CAPACITY

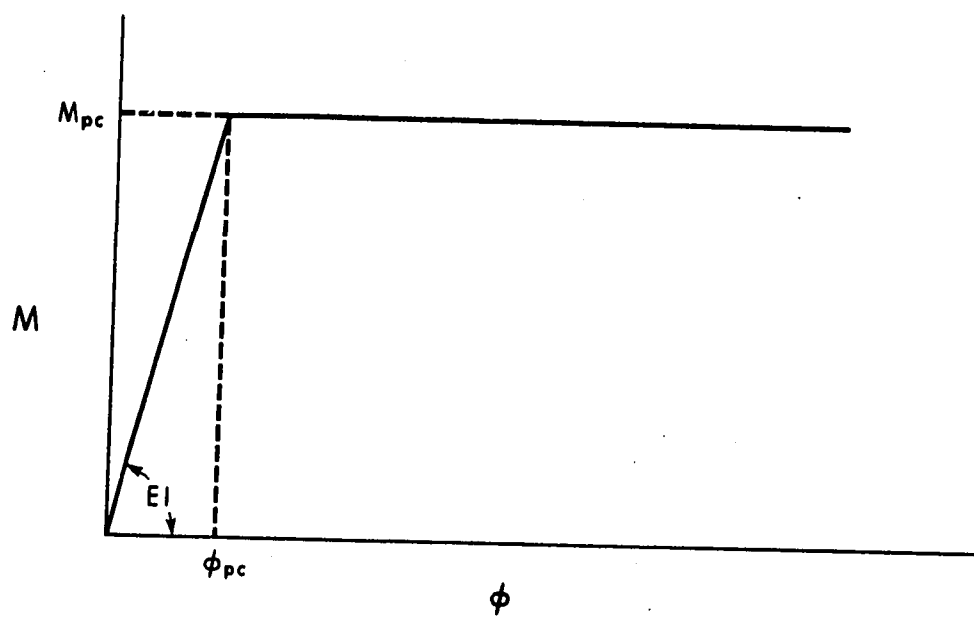


FIG. 3.6 MOMENT-CURVATURE RELATIONSHIP - FRAME MEMBERS

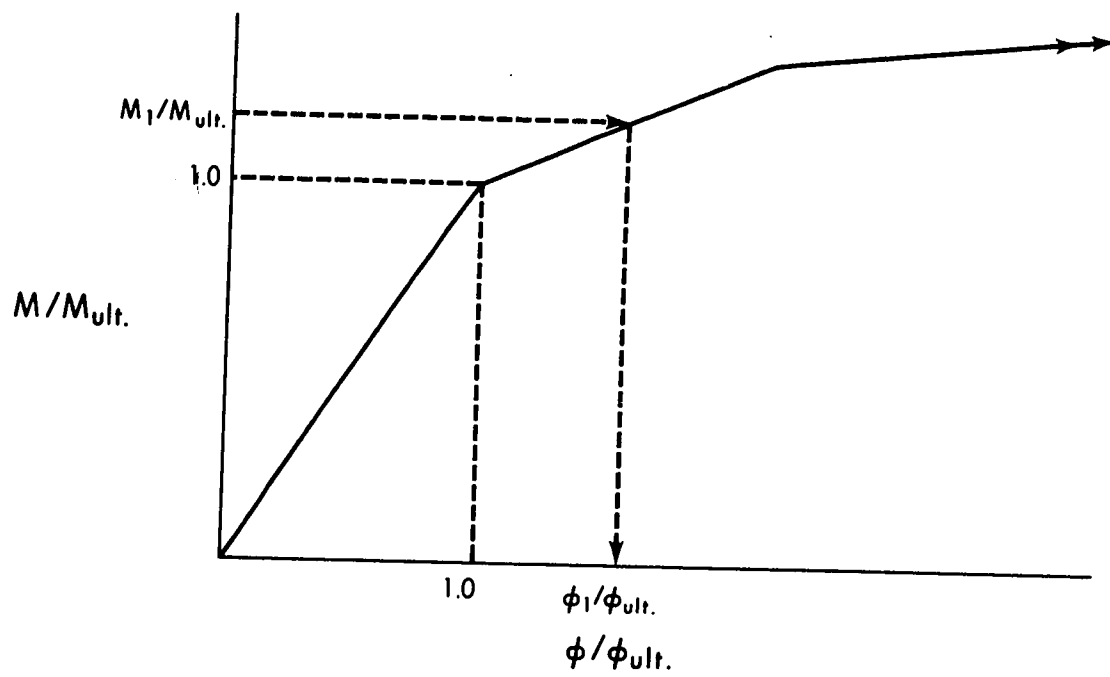
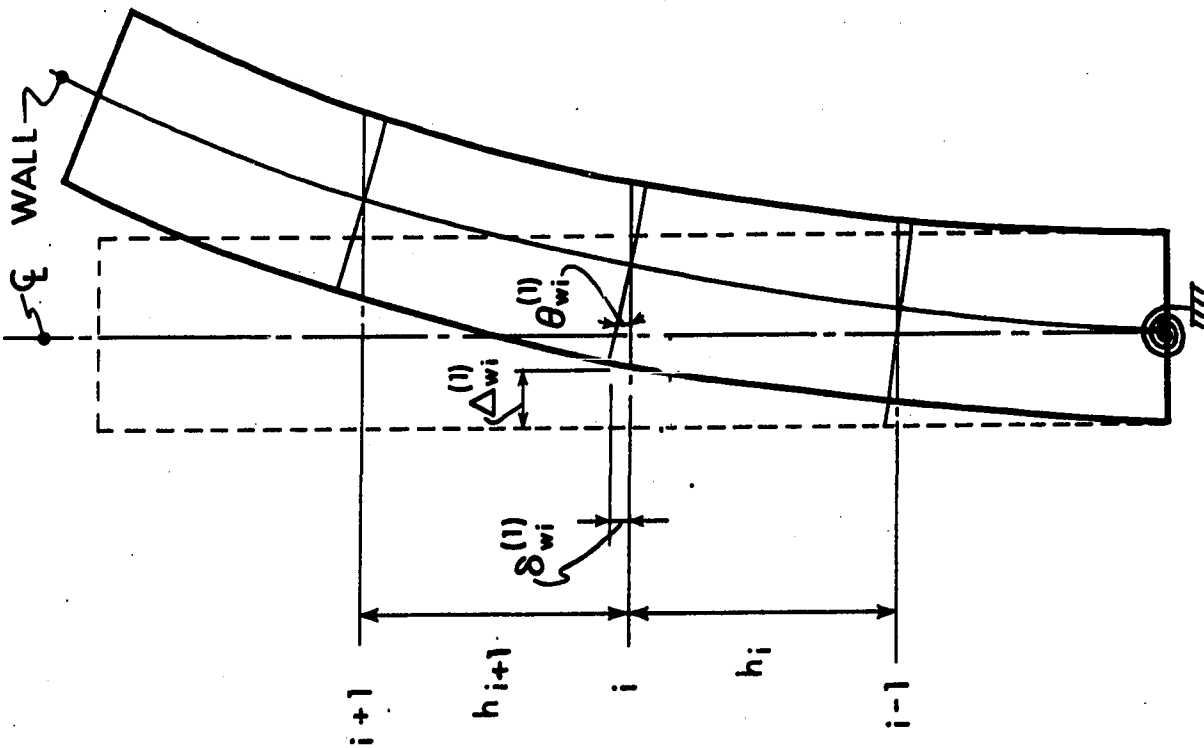


FIG. 3.7 MOMENT-CURVATURE RELATIONSHIP - SHEAR WALL



35

FIG. 3.9 SHEAR WALL SUBJECTED TO  
ENTIRE LATERAL LOAD

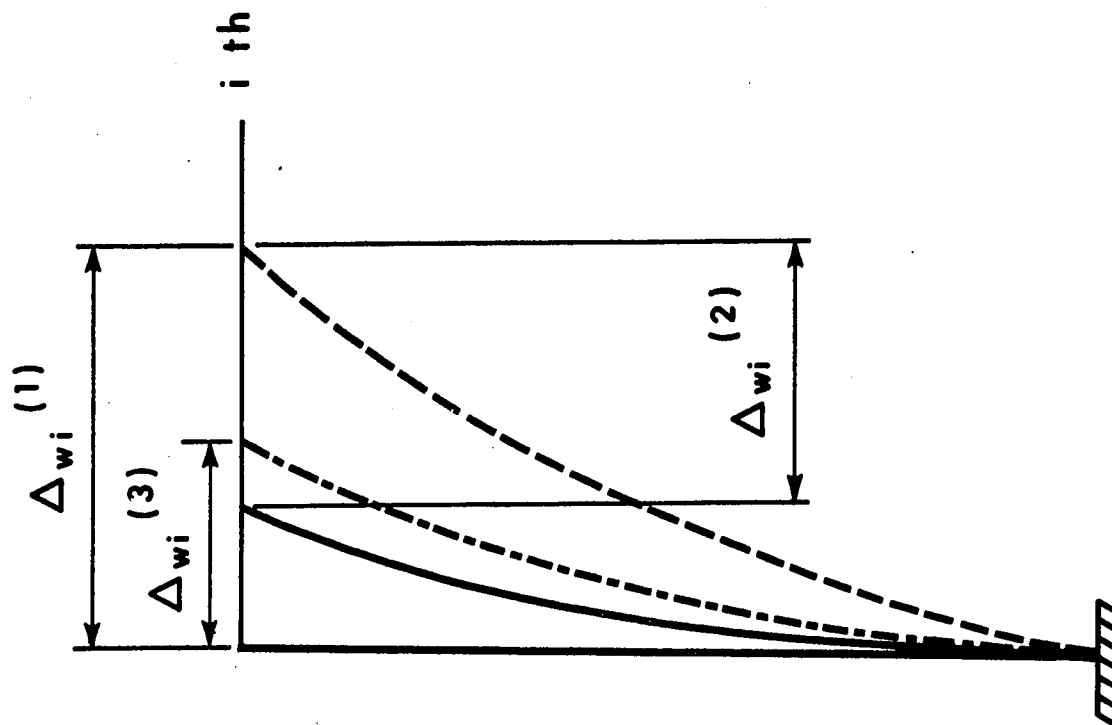


FIG. 3.8 DEFLECTED SHAPE OF THE SHEAR WALL AT DIFFERENT  
STAGES OF THE ITERATION PROCESS



## CHAPTER IV

### BEHAVIORAL STUDY OF A 24 STORY STRUCTURE

#### 4.1 Introduction

A 24 story coupled shear wall-frame structure has been analyzed by the procedure described in the previous chapter. Different aspects of the behavior of the structure are discussed in this chapter. The plan view of the 24 story building is shown in Fig. 4.1. The building consists of four 24-ft. bays and one 30-ft. center bay in the long direction. It is assumed that each floor of the building acts as a diaphragm of infinite (in-plane) rigidity. The lateral load is applied to the long side of the structure and resisted by the combined action of six frames and a single shear wall. A typical bent is shown in Fig. 4.2a. The bent has been designed plastically, assuming that diagonal bracing is present (39) in the 28-ft. bay. The member sizes (A36 steel) determined by the above procedure are listed in Table 4.1.

#### 4.2 Lumping of the 24 Story Building

The 24 story building is lumped into the analytical model shown in Fig. 4.2b; the frame system is linked to the shear wall, since the flexural restraint offered to the wall through the slab is neglected. The span of the beam in the lumped model is 20-ft.; the aver-

age for the three spans of the bent in Fig. 4.2a. The stiffness of the column in the lumped model is the sum of the stiffnesses of all the columns in the story. The reduced plastic moment capacity of each column is calculated on the basis of axial loads given in Table 6.13 of Reference 39, adjusted to account for the plan area attributed to each column. The plastic moment capacity of the column in the lumped model is the sum of the reduced plastic moment capacities of the individual columns. The stiffness and strength of the rigidly framed beam is twice the sums of the stiffnesses and strengths of all the beams in the story, as given by Equations (3.1) and (3.2). As discussed in the previous chapter, the plastic moment capacity of the beam has been reduced to account for the presence of the uniformly distributed load. Table 4.2 lists the strengths and stiffnesses of the frame members of the lumped model. The factored vertical loads on the building, included in this table, have been taken from Table 6.13 of Reference 39, and adjusted to account for the different plan areas of the bents.

#### 4.3 Comparison Between Approximate and Rigorous Methods of Analysis

The structure has been analyzed by the rigorous method presented in Reference 28 and also by the present approximate procedure. The results of the two analyses are compared for a structure having a  $K_r$  value of 5, where  $K_r$  represents the ratio of the shear wall-to-column stiffness of the bottom story of the structure. The ratio of the ultimate moment capacity of the shear wall to the plastic moment

capacity of the column,  $M_r$ , is taken as 5. In order to analyze the building by the method of Reference 28, the building is lumped into a single frame linked to a shear wall as shown in Fig. 4.3. The six frames of the original building (Fig. 4.1) have been lumped into a single bent, and linked to the shear wall. Since axial deformations of the beams are neglected in the analysis, this arrangement is equivalent to enforcing equal lateral deflections on each of the frames and the shear wall, at each floor level. The stiffnesses and strengths of the members in the frame of Fig. 4.3 are six times those of the members in Table 4.1. The uniformly distributed load on the girders of the actual structure is given in Table 6.9 of Reference 39. For this comparison, the values of  $K_r$  and  $M_r$  are constant throughout the height of the building. The slope of the strain-hardening branch of the moment-curvature relationship for the shear wall in the approximate analysis is 1 in 300.

The responses of the structure as predicted by the two analyses are very similar. Both first and second order elastic-plastic analyses have been performed. Figure 4.4 plots the lateral force at the top of the structure,  $H$ , versus  $\Delta/H_t$ , the ratio of the top level deflection to the total height of the structure. In Fig. 4.4, the dashed curves represent the results of the lumped analysis, while the solid curves represent the results predicted by the rigorous analysis of Reference 28.

The two curves shown in Fig. 4.4a are predicted by a first-order elastic-plastic analysis. The uniformly distributed load was removed

from the beams for the rigorous analysis in order to completely eliminate the  $P\Delta$  effect. This structure is a 'weak beam-strong column' type and hence the hinges form mainly in the beams. The first hinge in the structure is detected at point 'a' as shown in Fig. 4.4a. Up to point 'b', the approximate analysis predicts slightly higher load capacities than does the more rigorous solution, the maximum difference in load being 3% in this region. Beyond point 'a', the approximate analysis detects more hinges in the structure than does the rigorous analysis and slightly underestimates the load beyond point 'b'.

The structure continues to resist lateral load beyond point 'c', until wall hinging is predicted at a lateral load (H) of 52.0 kips by both analyses. Finally, at a lateral load of 56.0 kips, a mechanism condition is reached due to the formation of column hinges.

In Fig. 4.4b, the two curves represent the second-order elastic-plastic load-deformation relationships for the structure. The effect of the uniformly distributed load acting on the beams is included in the rigorous analysis and the moment capacities of the beams in the lumped model have been reduced to compensate for this effect. The analyses take into account the  $P\Delta$  effect and the reduction in the plastic moment capacities of the column due to the presence of the axial loads.

The approximate analysis predicts the first hinge at the

9th level beam at point 'd' as shown in the lower dashed curve in Fig. 4.4. The strength of the structure is overestimated up to point 'e' and the difference in response in this region, (between the two analyses) is larger than that shown by the upper two curves. This is due to the formation of plastic hinges in the center span of the unlumped model; the actual structure accordingly deteriorates more rapidly because of the additional  $P\Delta$  effect. The approximate analysis underestimates the ultimate load by about 7%.

#### 4.4 The $P\Delta$ Effect

The effect of the  $P\Delta$  moments on the response of the 24 story structure is demonstrated in Fig. 4.5 using the approximate analysis. Two structures have been analyzed with  $K_r$  ratios of 50 and 500. The value of  $K_r$  in this case corresponds to the bottom story of the structure. Since the wall is continued throughout the height of the structure, the value of  $K_r$  is increased toward the top. The value of  $M_r$  is 5 in the bottom story of the structure and the same ultimate moment capacity is continued throughout the complete height of the wall.

In Fig. 4.5, the top level lateral force,  $H$ , has been plotted versus the top story sway rotation,  $\rho$ . The solid curves represent the second-order elastic-plastic analysis of the structure; the dashed curves represent the response, neglecting the effects of  $P\Delta$  moments. The structure having  $K_r$  equal to 50, showed a reduction of about 32% in its ultimate load capacity due to  $P\Delta$  effect. The first hinge in the

structure forms in the frame at the stages indicated by the solid circles, while wall hinging is initiated at stages indicated by the open circles. In the structure having  $K_r$  equal to 500, the  $P\Delta$  effect caused a 28% reduction of the ultimate load. The stiff shear wall in this structure attracts a larger proportion of the bending moment and hence the first hinge forms in the shear wall, as shown by the reversed positions of the solid and open circles. The  $P\Delta$  effect caused significant reduction in the ultimate load-carrying capacity of these structures. In this case, the structure with  $K_r$  value of 500 suffered a smaller reduction in ultimate load-carrying capacity.

#### 4.5 The Effect of Variation of Wall-to-Column Stiffness Ratio

The effect of a variation in the ratio of wall-to-column stiffness,  $K_r$ , is shown in Fig. 4.6. The graph plots the top level lateral force,  $H$ , versus the top story sway rotation,  $\rho$ . The response of structures having  $K_r$  ratios of 50, 100, 500, 1000, 3000 and 10,000 have been plotted in Fig. 4.6. For all structures, the ratio of wall-to-column moment capacity,  $M_r$ , has been held constant at 5. The solid circles indicate the loading stage at which the first hinge occurs in the frame, while the open circles represent the initiation of hinging in the shear wall.

In structures having  $K_r$  ratios of 50 and 100, hinging occurs in the frame system before inelastic action in the shear wall. The structure undergoes large inelastic deformations with a gradual deterioration in stiffness. Once hinging is initiated in the wall, the

structure approaches a mechanism condition. The difference between the loads corresponding to hinging in the shear wall and in the frame, decreases with an increase in the  $K_r$  value of the structure.

This behavior changes at a  $K_r$  value of approximately 160. In this case, hinging in the frame and inelastic action in the shear wall begin simultaneously. Hence, for structures having  $K_r$  values of 500, 1000, 3000 and 10,000 inelastic action occurs in the shear wall before the first plastic hinge forms in the frame system, as indicated in Fig. 4.6. The deterioration in stiffness is more rapid for deformations beyond this stage. For the 24 story structure, the ultimate load-carrying capacity increased with the increase in the stiffness of the shear wall.

The moment distributions over the shear wall for structures having  $K_r$  ratios of 50, 500 and 1000, are shown in Fig. 4.7. The story number,  $N$ , is plotted versus the bending moment,  $M$ , in Fig. 4.7. The plot corresponds to a top story sway rotation of approximately 0.0003 for each of the structures. The point of contraflexure in the wall moves towards the top and the shear wall attracts greater bending moments, as the  $K_r$  ratio increases.

In most practical structures the ratio of the wall-to-column moment capacities,  $M_r$ , will increase with an increase in the stiffness ratio  $K_r$ . The solid curves in Fig. 4.8 are the load-deformation curves for structures having  $K_r$  values of 50, 500, 3000 and 10,000

and  $M_r$  values of 5, 10, 20, 30 respectively. Figure 4.8 is a plot of the top level lateral force,  $H$ , versus the top story sway rotation,  $\rho$ . As before, the solid and open circles represent the initiation of hinging in the frame and wall respectively. An increase in the value of  $M_r$  did not essentially change the behavior of these structures. For the structures with  $K_r$  ratios of 500, 3000 and 10,000, the shear wall initiated the inelastic action of the structure and hinges in the beams of the frame system developed at a later stage. Hence this behavior is similar to the behavior of the corresponding structures discussed with reference to Fig. 4.6. However, the ultimate load-carrying capacity of the structure with a constant value of  $K_r$  increased significantly with the increase in the value of  $M_r$ . In order to illustrate this increase the response of the structure with a  $K_r$  value of 3000 and an  $M_r$  value of 5 has been replotted as the broken curve in Fig. 4.8. The ultimate load-carrying capacity of this structure is increased by approximately three times, due to an increase in  $M_r$  from 5 to 20.

In many cases, the ultimate load-carrying capacity of the structure was marked by hinging in the shear wall in the lower part of the structure. It may be economical to strengthen only the bottom part of the shear wall. The dashed curve in Fig. 4.8 is the response of the structure having  $K_r$  equal to 500. The bottom four stories of the shear wall have a constant moment of inertia corresponding to an  $M_r$  ratio of 10, while the rest of the stories have a

constant moment of inertia corresponding to an  $M_r$  ratio of 5. The ultimate load is increased by approximately 50% in this case compared to the structure with a uniform  $M_r$  ratio of 5.

#### 4.6 Shear Distribution in the Structure

In the lower stories of a coupled shear wall-frame structure, the applied lateral forces are resisted almost entirely by the shear wall. However, in the top stories, the frames are forced over by the rotations of the much stiffer wall elements and must resist shears that are many times greater than those due to the applied loads. The distribution of resisting shears in the various stories is dependent on the relative strength and stiffness of the shear walls and frames.

The distribution of shear for the lower portion of a structure having  $K_r$  equal to 50 and  $M_r$  equal to 5, is shown in Fig. 4.9. In this figure, the shear at a particular story,  $V$ , has been plotted versus  $\rho$ , the sway rotation of the story considered. Figure 4.9a represents the shear distribution for the bottom story, while Fig. 4.9b represents the distribution for the second story. The frame carries approximately 5% of the total shear in the bottom story, at point 'a', where the first hinge forms in the frame. However, the above percentage increases as the inelastic action progresses and finally at the ultimate load, the frame resists approximately 7% of the total shear in the bottom story. The shear distribution of the second-story is similar, although the second story sway rotations are much larger than bottom story sway rotations. Approximately 13%

of the total second story shear is carried by the frame at point 'b' where the inelastic action is initiated in the frame. This increases to 18% at the ultimate load stage. Thus, the relative shear resisted by the frame increases for the higher stories.

The shear distribution in the upper portion of the structure is shown in Fig. 4.10. This figure is a plot of the shear force,  $V$ , versus the sway rotation,  $\rho$ . The shear distribution for the top story is shown in Fig. 4.10a, while the distribution for the 20th story is shown in Fig. 4.10b. In the top story, the shear wall develops negative shears due to the 'whipping action', which is characteristic of a coupled shear wall-frame structure. In order to maintain equilibrium, the frame system develops shears at the top story, which are approximately nine times the applied shears at point 'a'. The percentage of total shear resisted by the frame increases, until hinges form in the top story beams. At this stage, the frame system is unable to resist the additional shears and hence the extra applied shear is carried by the shear wall. The 'whipping action' is much smaller in the 20th story as shown in Fig. 4.10b and in fact the wall shear actually reverses in sense during the progress of loading.

In summary, two types of behavior exist in a coupled shear wall-frame structure. The columns in the bottom stories of a tall structure are subjected to high axial loads. These columns may be forced to deform inelastically through a significant range before the structure is able to attain its ultimate load. In the top stories,

the shear resisted by the frame is much higher than the applied shear. This action leads to early hinging in the frame and corresponding reductions in stiffness and strength.

#### 4.7 Design Method

A plastic design method (40) for structures consisting of coupled steel frames and reinforced concrete shear walls has been developed on the basis of the method of analysis described in Chapter III combined with the subassembly method for unbraced frames (27,39). The three steps involved in the design procedure are described below:

(a) The structure is designed for gravity load using a load factor of 1.70. It is assumed here that the shear walls have a certain minimum stiffness so that the capacities of the columns are not reduced by sway effects. Preliminary member sizes are determined from this design.

(b) The entire structure is then lumped into the analytical model shown in Fig. 3.1. The model is analyzed by the method described in Chapter III. The analysis includes the effects of hinging in the frame, inelastic action in the wall and the  $P\Delta$  effect.

The ultimate load obtained from the above analysis must be greater than the factored load (load factor = 1.30). However, if the above condition is not satisfied, the strengths and stiffnesses of the member elements of the structure are modified. In addition, the structure must meet the prescribed limits on working load deflections.

(c) The steel rigid frames should be able to resist that portion of the shear assigned to them from the analysis in Step (b). The sway subassemblage technique (27,39) has been applied to determine the lateral shear versus the sway deformation behavior of particular stories of the structure.

A safe design of a story will result if the total resisting shear developed by the frame bents in Step (c) is greater than that assigned to it from Step (b). However, if the above condition is not met, the member sizes of the story are revised until satisfactory.

The 24 story structure analyzed in this chapter, has been designed by the above procedure. The details are given in Appendix E.

TABLE 4.1 MEMBER SIZES OF A TYPICAL BENT OF THE 24 STORY STRUCTURE

Story or Floor No.	Col. A	Col. B	Col. C	Col. D	Beam AB	Beam BC	Beam CD
1	14WF314	14WF314	14WF398	14WF398	14WF34	12B16.5	20I65.4
2	14WF314	14WF314	14WF398	14WF398	14WF34	12B16.5	20I65.4
3	14WF287	14WF287	14WF370	14WF370	14WF34	12B16.5	20I65.4
4	14WF287	14WF287	14WF370	14WF370	14WF34	12B16.5	20I65.4
5	14WF264	14WF264	14WF314	14WF342	14WF34	12B16.5	18WF60
6	14WF264	14WF264	14WF314	14WF342	14WF34	12B16.5	18WF60
7	14WF228	14WF228	14WF287	14WF287	14WF34	12B16.5	18WF60
8	14WF228	14WF228	14WF287	14WF287	14WF34	12B16.5	18WF60
9	14WF202	14WF202	14WF246	14WF246	14WF34	12B16.5	18WF55
10	14WF202	14WF202	14WF246	14WF246	14WF34	12B16.5	18WF55
11	14WF176	14WF176	14WF219	14WF219	14WF34	12B16.5	18WF55
12	14WF176	14WF176	14WF219	14WF219	14WF34	12B16.5	18WF55
13	14WF150	14WF142	14WF184	14WF193	14WF34	12B16.5	18WF55
14	14WF150	14WF142	14WF185	14WF193	14WF34	12B16.5	18WF55
15	14WF127	14WF127	14WF158	14WF158	14WF34	12B16.5	18WF55
16	14WF127	14WF127	14WF158	14WF158	14WF34	12B16.5	18WF55
17	14WF111	14WF111	14WF136	14WF136	14WF34	12B16.5	18WF55
18	14WF111	14WF111	14WF136	14WF136	14WF34	12B16.5	18WF55
19	14WF78	14WF78	14WF111	14WF111	14WF34	12B16.5	18WF55
20	14WF78	14WF78	14WF111	14WF111	14WF34	12B16.5	18WF55
21	12WF58	12WF58	12WF79	12WF79	14WF34	12B16.5	18WF55
22	12WF58	12WF58	12WF79	12WF79	14WF34	12B16.5	18WF55
23	12WF40	12WF40	12WF58	12WF58	14WF34	12B16.5	18WF55
24	12WF40	12WF40	12WF58	12WF58	14B26	12JR11.8	16WF45

TABLE 4.2 STRENGTHS AND STIFFNESSES OF THE FRAME  
MEMBERS IN THE LUMPED MODEL

Story or Floor	Moment of Inertia (in <sup>4</sup> )		Plastic Mom. Capacity (in kips)		Vertical Load (kips)
	Column	Beam	Column	Beam	
1	124956	16195	382113	44580	52166
2	124956	16195	397581	44580	49966
3	112392	16195	350555	44580	47764
4	112392	16195	364805	44580	45563
5	95192	14601	310593	33880	43362
6	95192	14601	321883	33880	41162
7	82248	14601	255765	33880	38956
8	82248	14601	268630	33880	36760
9	69216	13795	214140	28100	34560
10	69216	13795	226851	28100	32358
11	59376	13795	187249	28100	30156
12	59376	13795	199368	28100	27956
13	48816	13795	155138	28100	25756
14	48816	13795	166651	28100	23554
15	40176	13795	132878	28100	21352
16	40176	13795	145461	28100	19150
17	34308	13795	122127	28100	16950
18	34308	13795	133857	28100	14750
19	25404	13795	94290	28100	12548
20	25404	13795	105857	28100	10348
21	13668	13795	63640	28100	8148
22	13668	13795	79898	28100	5988
23	9432	13795	53341	28100	3948
24	9432	9352	59467	22140	1546

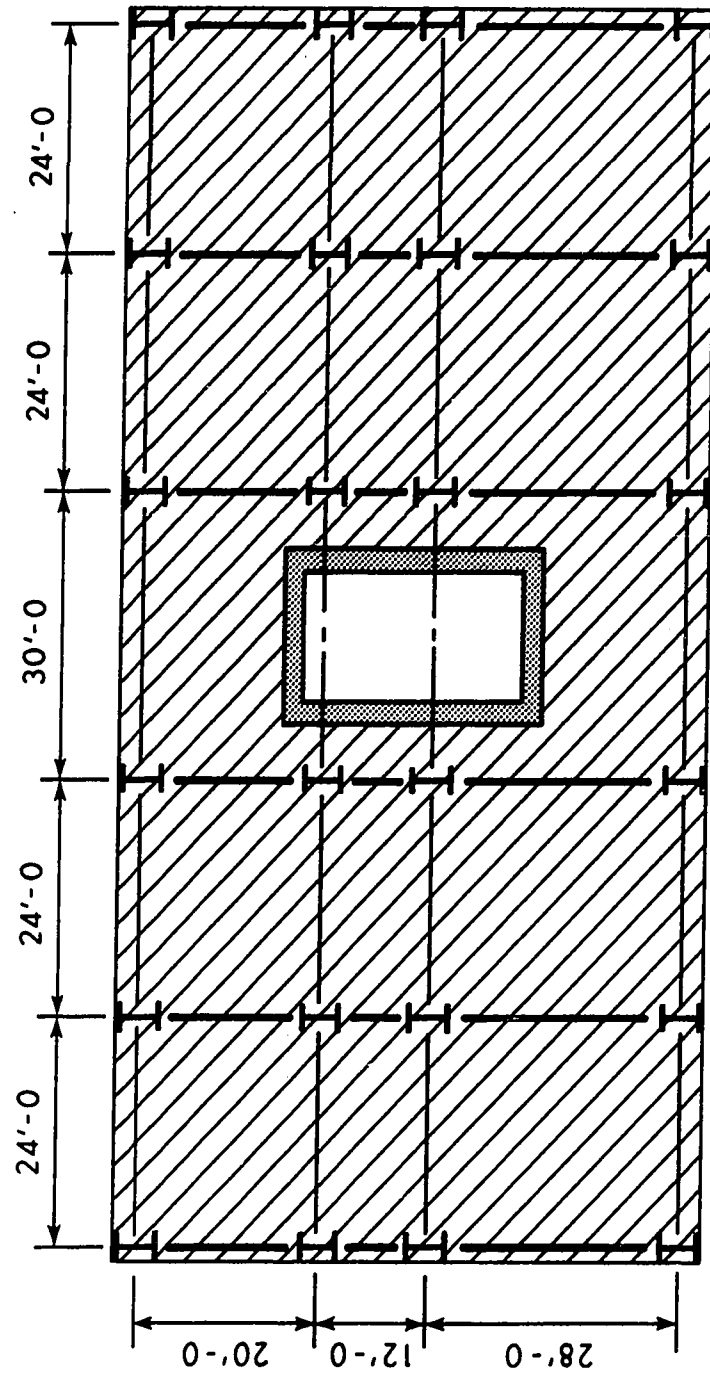


FIG. 4.1 PLAN VIEW - 24 STORY BUILDING

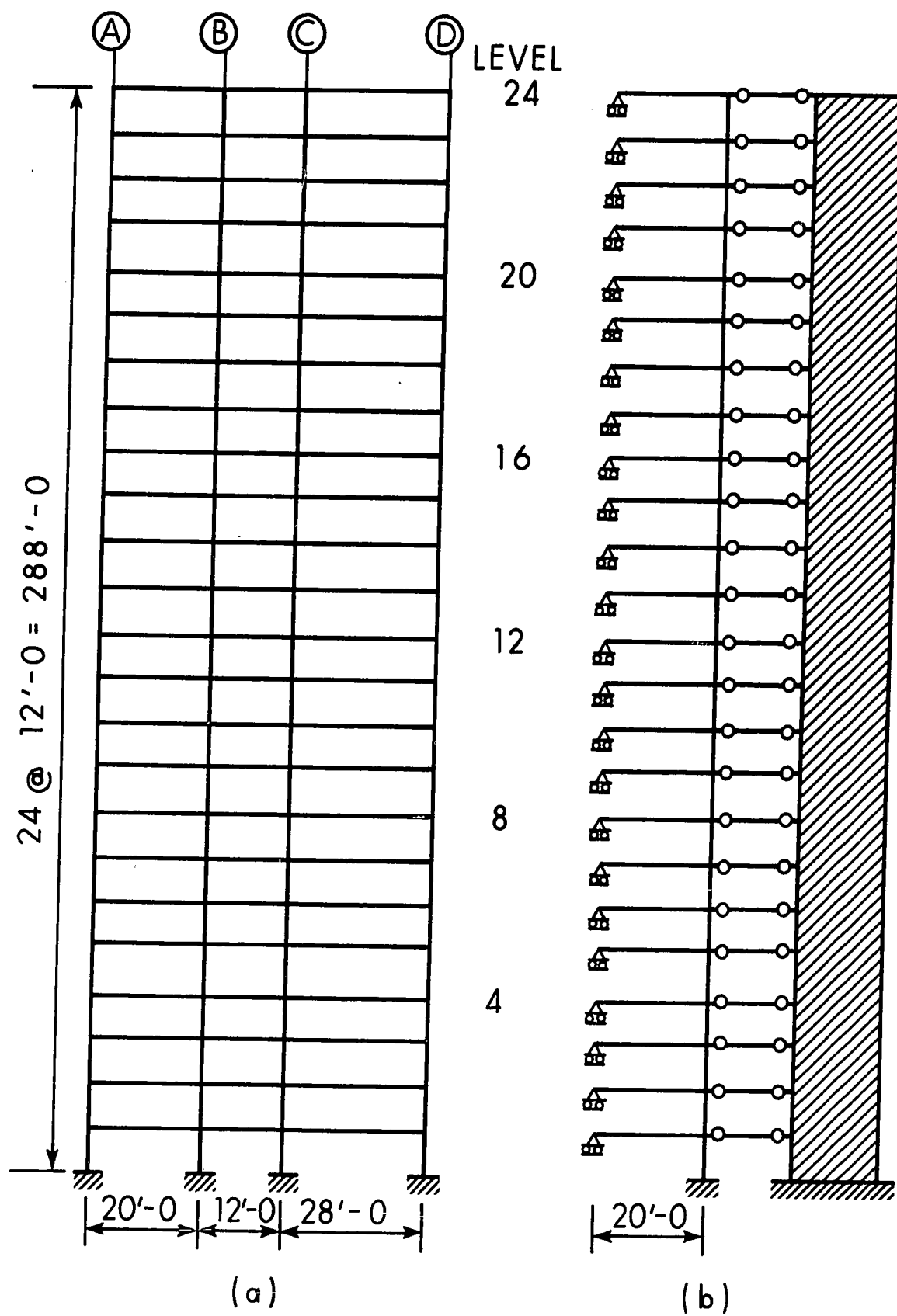


FIG. 4.2 ELEVATION - 24 STORY BUILDING

(a) TYPICAL BENT ; (b) LUMPED MODEL

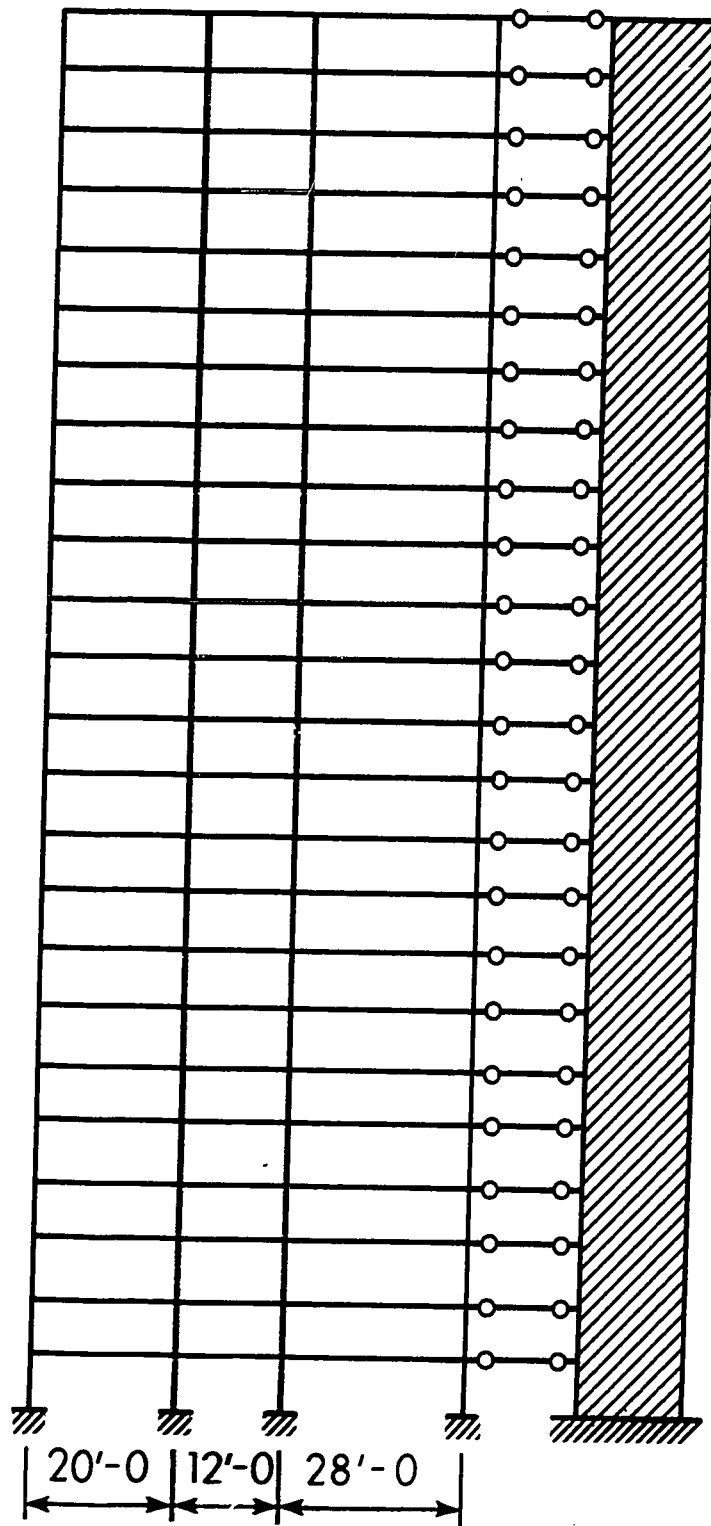


FIG. 4.3 LUMPED MODEL FOR CLARK'S ANALYSIS

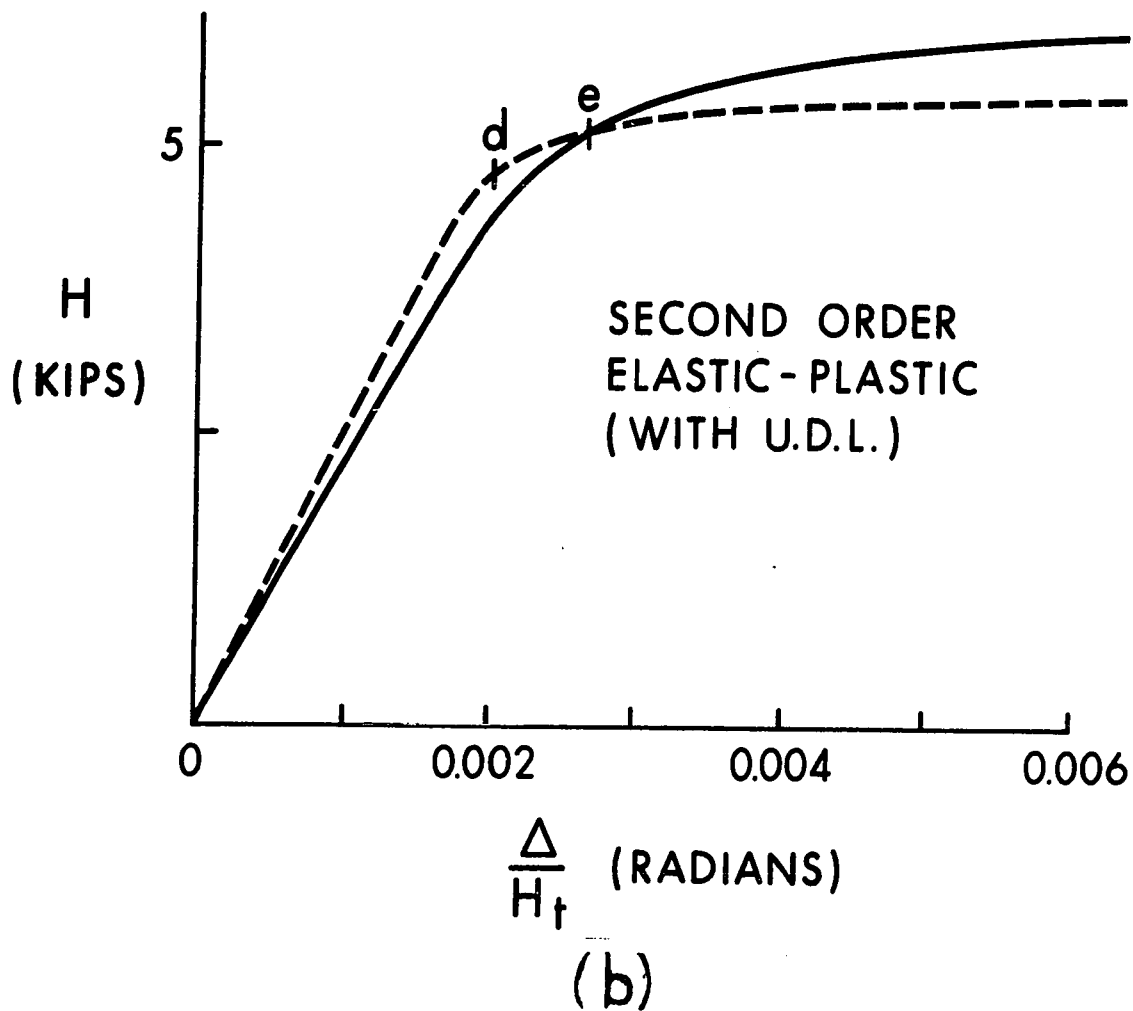
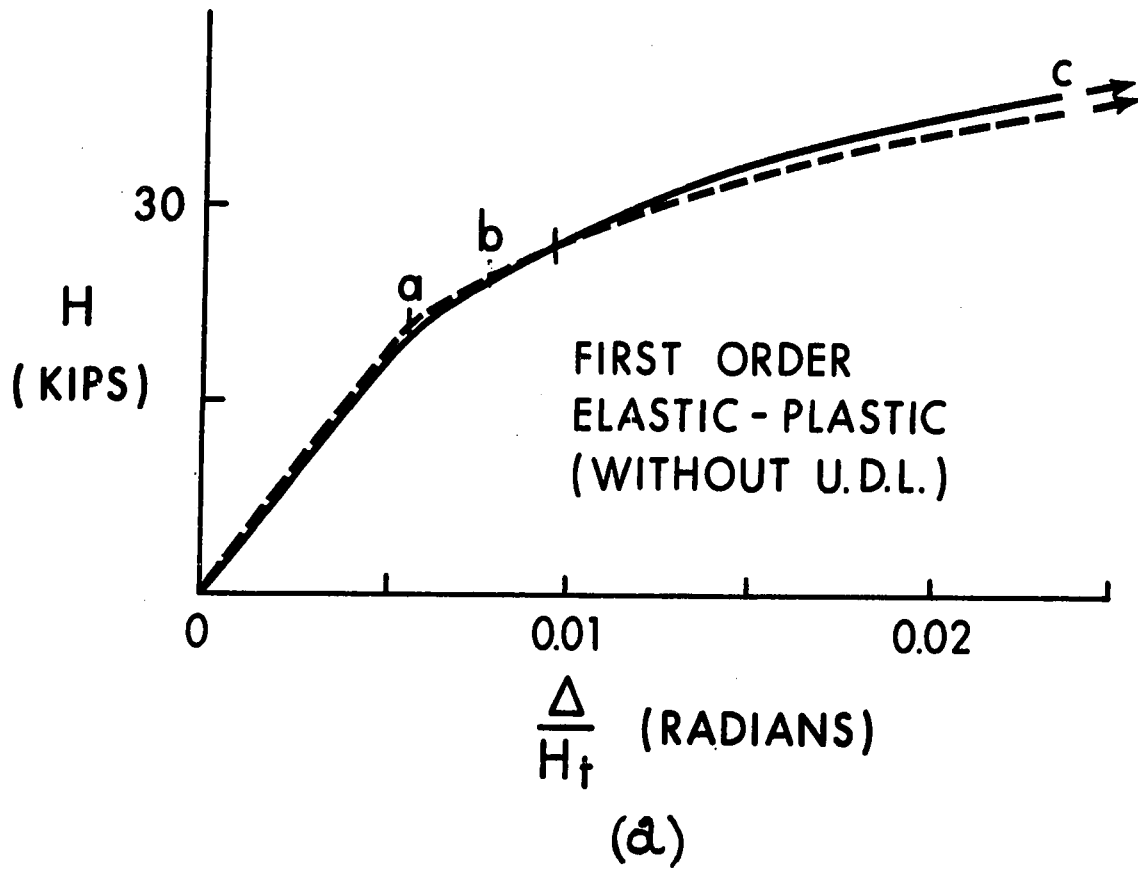
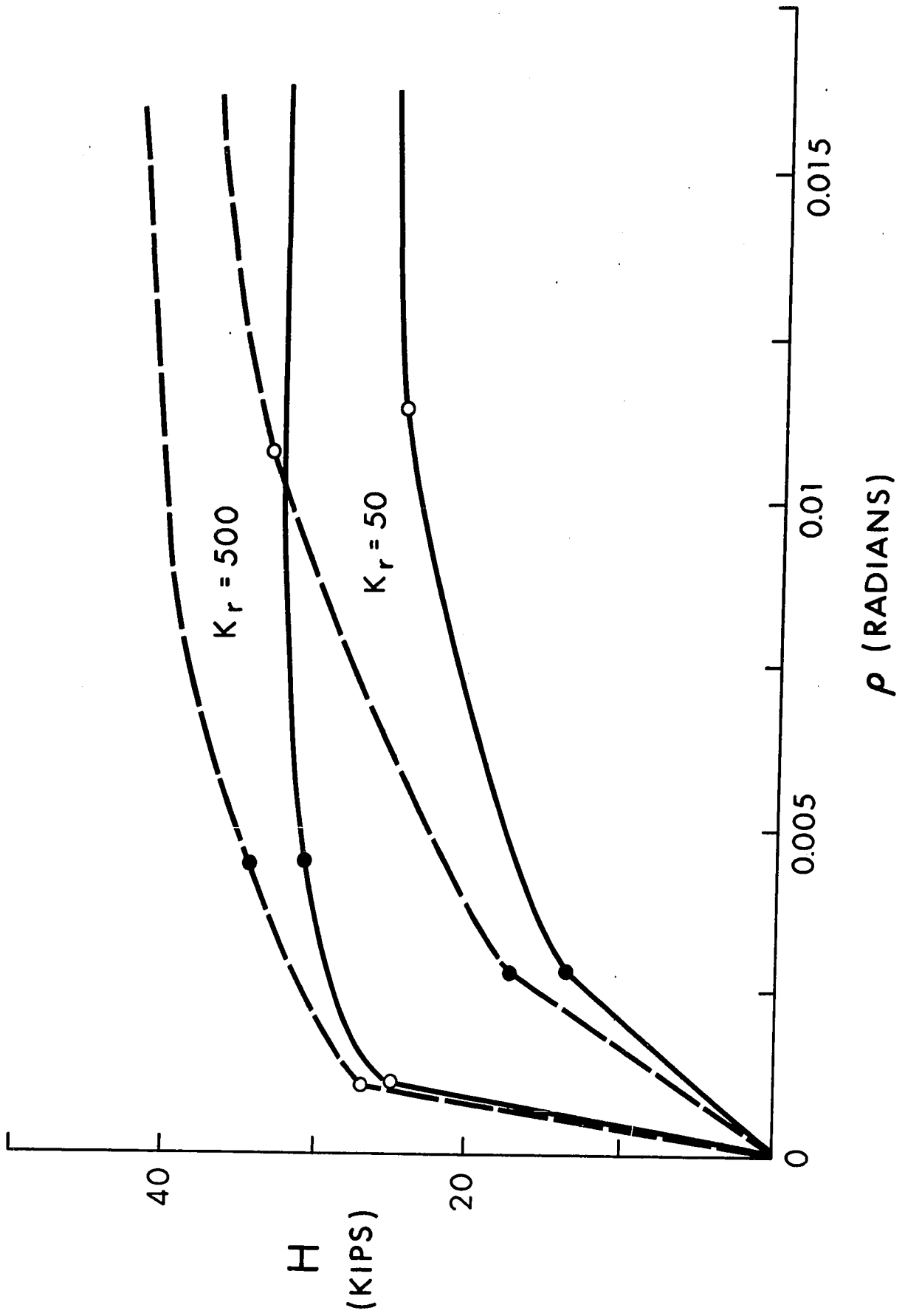


FIG. 4.4 FIRST AND SECOND ORDER LOAD-DEFORMATION RELATIONSHIPS

FIG. 4.5 THE  $P_{\Delta}$  EFFECT

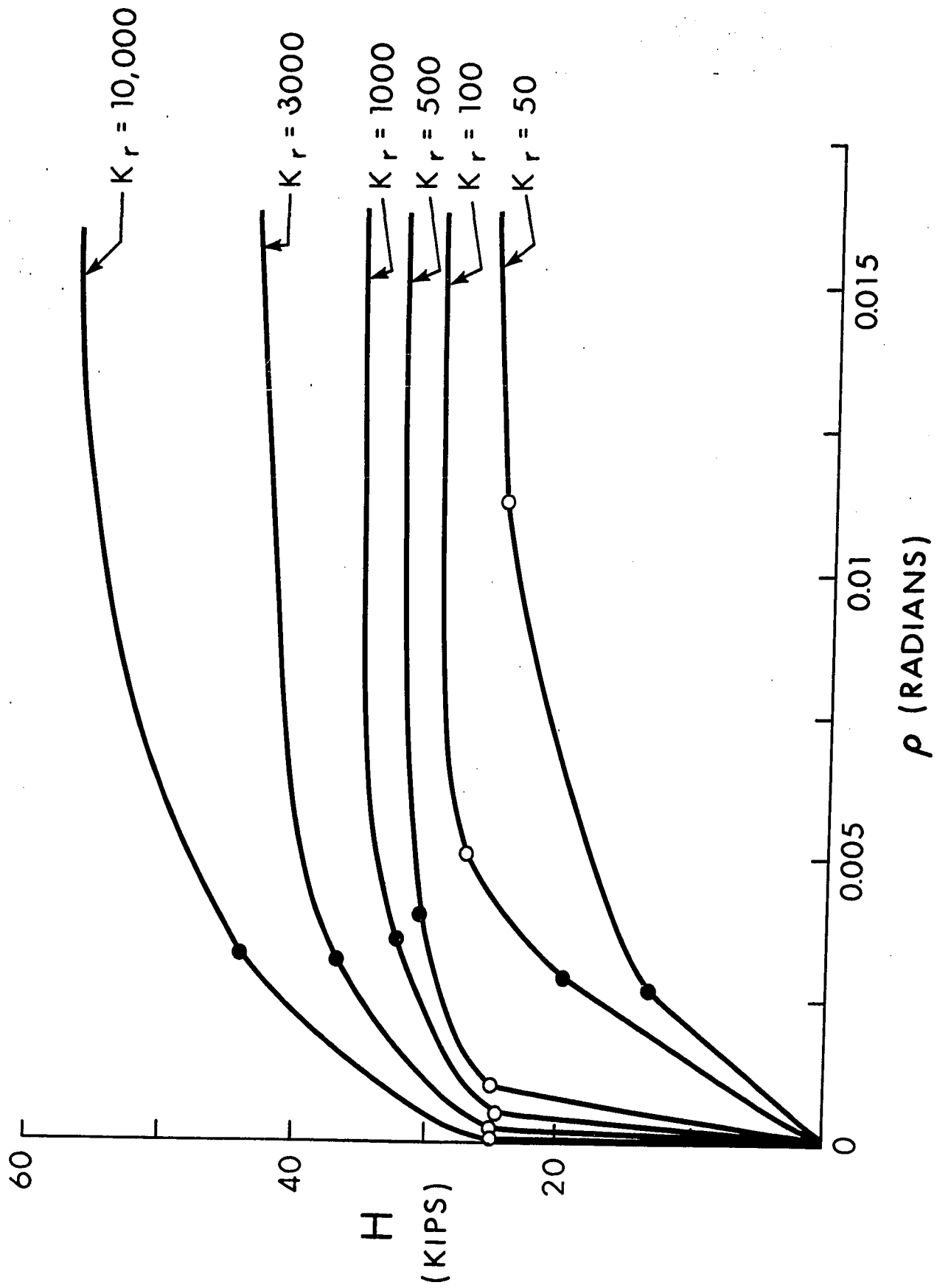


FIG. 4.6 EFFECT OF VARIATION IN WALL-TO-COLUMN STIFFNESS RATIO

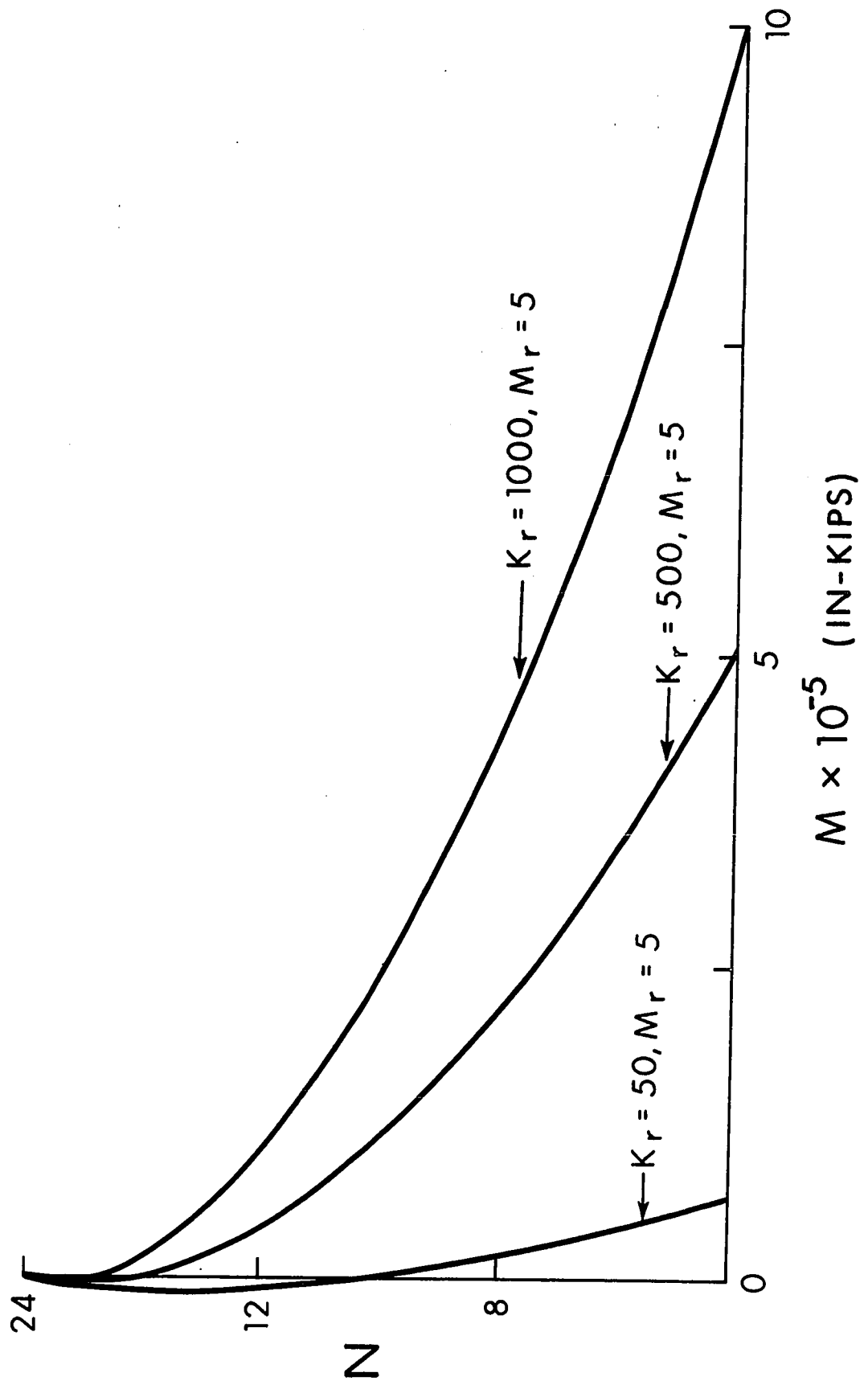


FIG. 4.7 MOMENT DISTRIBUTION OVER THE SHEAR WALL

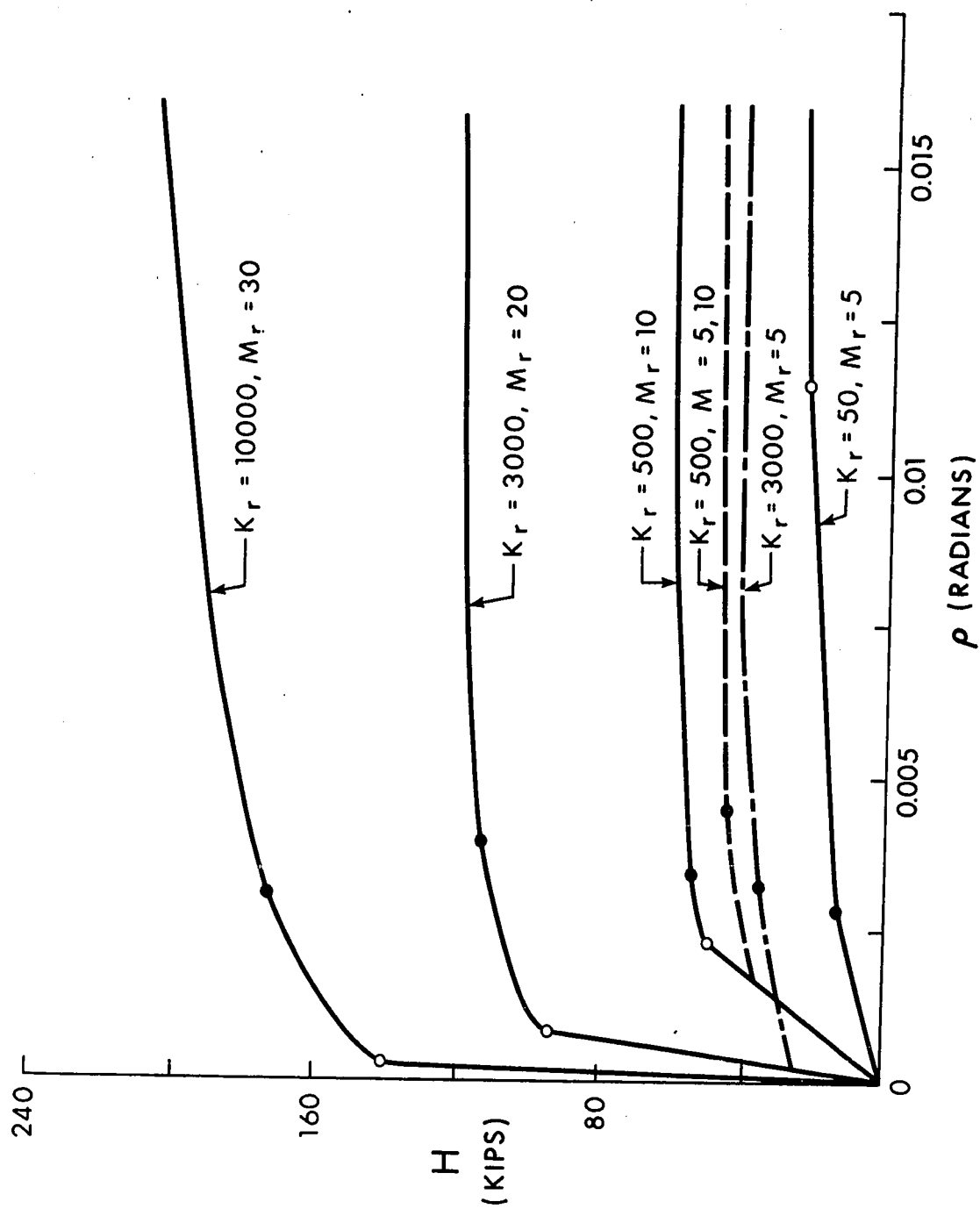
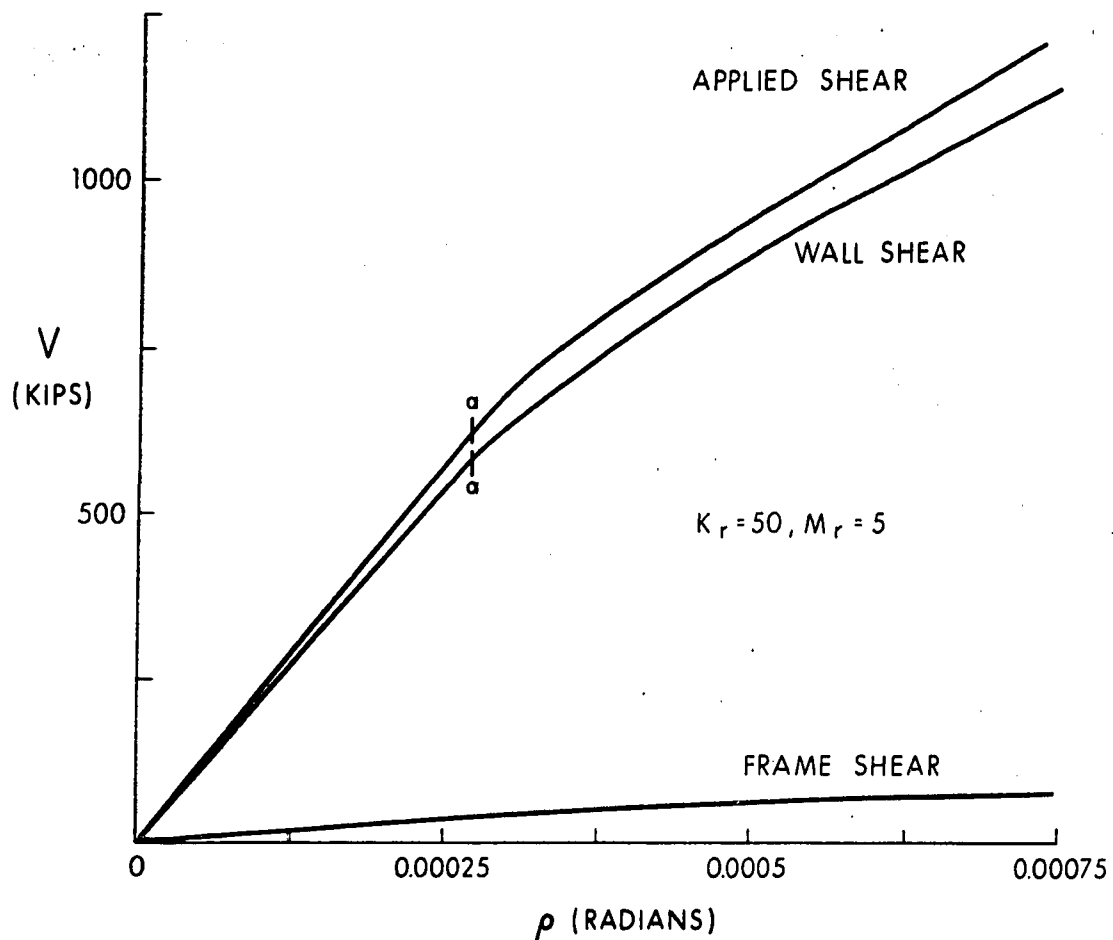
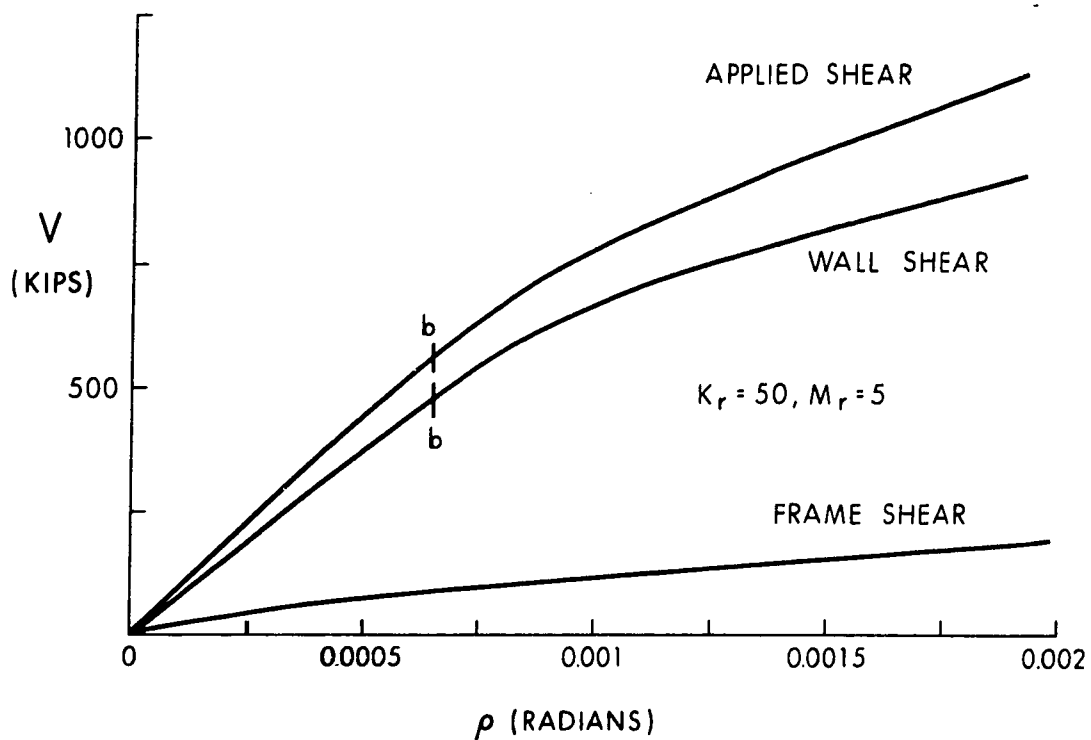


FIG. 4.8 EFFECT OF VARIATION IN WALL-TO-COLUMN STIFFNESS AND STRENGTH RATIO

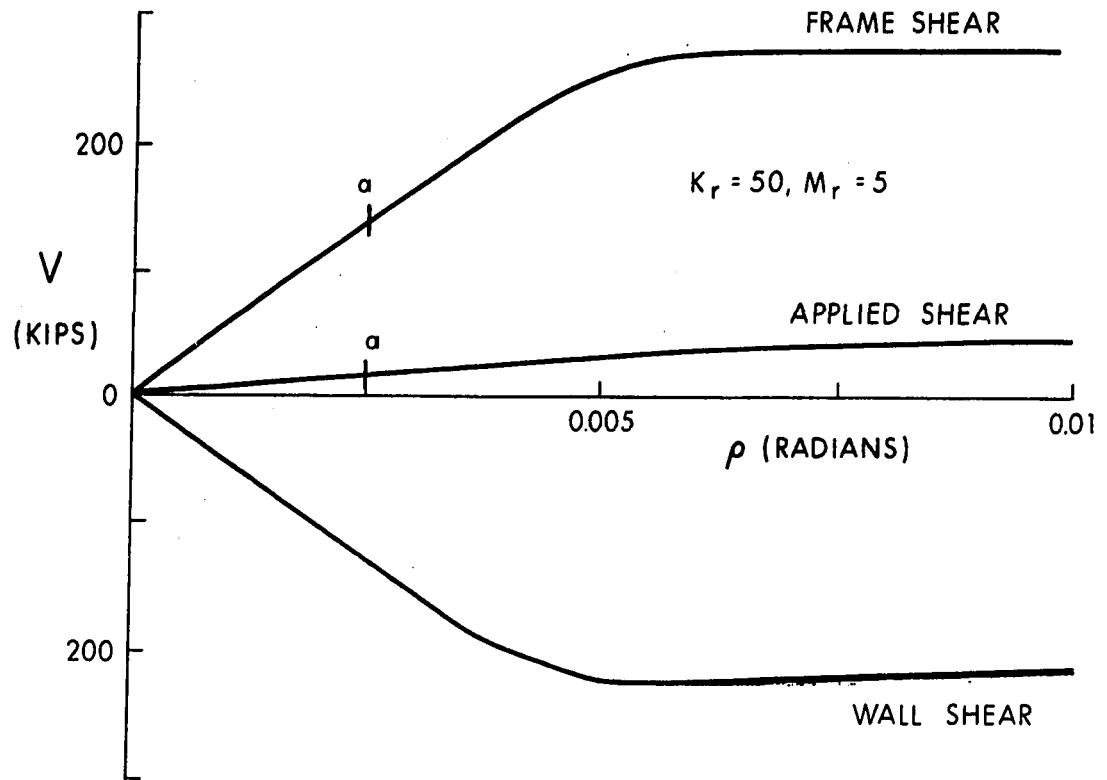


(a) SHEAR DISTRIBUTION - FIRST STORY

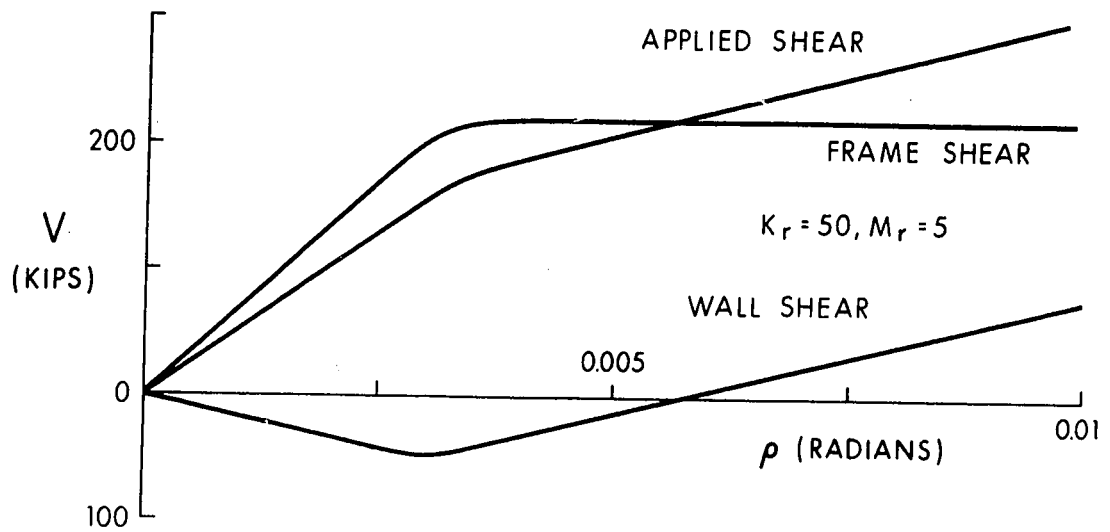


(b) SHEAR DISTRIBUTION - SECOND STORY

FIG. 4.9 SHEAR DISTRIBUTIONS IN THE LOWER PORTION OF THE 24 STORY STRUCTURE



(a) SHEAR DISTRIBUTION - TOP STORY



(b) SHEAR DISTRIBUTION - 20th STORY

FIG. 4.10 SHEAR DISTRIBUTIONS IN THE UPPER PORTION OF

THE 24 STORY STRUCTURE

## CHAPTER V

### TEST PROGRAM

#### 5.1 Introduction

Behavioral studies of a typical coupled shear wall-frame structure have isolated two distinct areas which require experimental investigation. Based on the discussion contained in the previous chapter, three test frames were designed. Frames A and B were designed to simulate the behavior of the bottom stories of a large structure while Frame C was designed to simulate the behavior of the top stories of the structure. The models used are the simplest from the testing point of view, yet retain the elements of behavior characteristic of the larger structure; no attempt was made to match the boundary and loading conditions.

#### 5.2 Test Frames

A schematic diagram of a typical test specimen is shown in Fig. 5.1. The specimen consists of a single shear wall and column stack. Girders at four levels are rigidly connected to the columns and to plates set into the wall. The tops of the column and the wall are bolted to the laboratory floor. A typical cross-section through the shear wall is shown in the inset to Fig. 5.1. The longitudinal reinforcement is designed to provide

the required strength and stiffness; the ties are selected from shear considerations.

The dimensions and the strengths and stiffnesses of the members used in the three test specimens are listed in Table 5.1. In Table 5.1, the moment of inertia,  $I$ , and the plastic moment capacities,  $M_p$  (girder),  $M_{pc}$  (reduced for axial load in the column), or  $M_{ult}$  (in the wall) are given for the members as well as the modulus of elasticity,  $E_c$ , for the wall sections. For the girders and columns, the weak axis slenderness ratio,  $L/r_y$ , between points of lateral support, is also listed. The value of the axial load in the column is represented by  $P_c$  and that in the wall by  $P_w$ .

The structural steel test frames were fabricated of wide-flange shapes, large enough so that standard fabrication procedures could be employed. The shear walls were cast horizontally, cured for 28 days, then lifted into place. The erection of the shear wall is shown in Fig. 5.2. The steel frame was then erected adjacent to the shear wall. The alignment of the test specimen was checked by transit and the steel frame clamped to the shear wall and braced in position. The four beam-to-column joints and the column base plate connection were then welded.

The beam-to-wall joints were designed to develop moments 15% greater than the plastic moment capacities of the beams to allow for the possibility of strain-hardening. A sectional view of a typical beam-to-wall joint is shown in Fig. 5.3. The moment capacity

is developed by the force in the reinforcing bars, acting through the distance between the tension and compression bars, as shown in Fig. 5.3. The bars were plug welded to steel plates which were inset flush with the outer surfaces of the wall. The beam face was butt-welded to one plate.

The reinforcing bars were continued through the wall and butt-welded to a second plate set flush with the opposite face of the wall. The hydraulic jacks were attached to lugs in the second plate as shown in Fig. 5.3. The prefabricated assembly is shown in Fig. 5.4.

### 5.3 Material Properties

The structural shapes used in the test program were of CSA-G40.12 steel, which is similar to ASTM-A36 but has a specified minimum yield stress of 44 ksi (41). The shapes used in the frames are the 4M13, 5WF18.9, and 5WF16 sections. All shapes were cold-straightened by rotarizing except for the 5WF16 section, which is used for the columns in Frame A. Measurements on the cross-sections were made with micrometers and vernier calipers. The dimensions were within 1% of the values given in the CISC Manual (42). Residual strains and material properties were measured on specimens cut from pieces taken from the same heats as the members used to fabricate the test frames. The results of the residual strain measurements and of the tensile tests are given in Appendix F. Compression and split tensile tests were performed on standard concrete

cylinders at the time of testing of the structure. The test results of the concrete cylinders are listed in Appendix F, as well as the results of tension tests on specimens of the reinforcing steel.

#### 5.4 Loading Sequence and Arrangement

The test frames were subjected to non-proportional loading. The vertical loads were applied initially to the tops of the column and shear wall. These loads were maintained at constant values, while the lateral loads at each floor level were incremented.

The loading arrangement is shown in Fig. 5.5. The vertical load was applied by hydraulic tension jacks and transmitted to the laboratory floor through gravity-load simulators, bolted to the floor. The hydraulic pressure in the ram was provided by an air-driven pump and regulated by adjustment of the air and hydraulic line pressures at the control panel.

As shown in Fig. 5.5, a tie rod connects the top end of the tension jack to a cross beam. Strain gauges were mounted on each tie rod to act as load cells. The assemblies were calibrated so that the vertical loads could be determined. The cross beam framed into the distributing beam which spans between the top of the column and the shear wall. The proportion of the total vertical load applied to the column or shear wall can be adjusted by varying the position of the cross beam.

In testing frames subjected to both gravity and lateral loads, the line of action of the applied load must remain vertical

as the structure sways. For ordinary loading systems, restraining horizontal load components will develop if the jack is attached to a fixed support at one end and to the structure at the other end. The gravity-load simulator (43), used in this test program maintained a vertical line of action for the hydraulic jacks. The tension jack and the gravity-load simulator, during the test, are shown in Fig. 5.6.

The tests were performed by adjusting the hydraulic pressure in the horizontal jacks so that the structure deformed in a sidesway mode. The four horizontal jacks were controlled by a separate pump console which allowed the load in each jack to be adjusted independently. Each hydraulic jack is of 20 kip capacity with a 20 inch stroke. The arrangement of the horizontal jack with the accompanying dynamometer is shown in Fig. 5.7a. One end of the jack is connected to the shear wall and the reaction is taken by the auxiliary supporting structure at the other end. A precalibrated load-cell is attached to the piston of the jack as shown in the figure. Figure 5.7b is a section through the load-cell shaft showing the strain gauge arrangement. The electrical connection diagram is shown in Fig. 5.7c. In the above figures, gauges 1 and 4 are attached in the direction of load while gauges 2 and 3 are placed transversely.

### 5.5 Test Setup

An overall view of the test setup is shown in Fig. 5.8 where the whitewashed steel frame is seen connected to the reinforced

shear wall. The tension jack, gravity-load simulator, tie rod and the distributing beam can also be seen in this photograph. Figure 5.9 shows a side view of the test setup. The specimen is centrally located between two auxiliary frames. Platforms are placed in alternate levels to facilitate the testing operation. The articulated lateral bracing mechanisms span between the specimen and the auxiliary frames. The rotation meters, for measuring member end rotations, can be seen hanging at each joint.

#### 5.6 Lateral Bracing System

The purpose of the lateral bracing system is to prevent out-of-plane movement of the specimen. The lateral bracing system, used in this test program, is based on Watt's straight-line mechanism (44), and prevents out-of-plane movement at the braced points while allowing the specimen to deform in its own plane.

The lateral bracing points in the specimen, for Frames A and C, are shown in Fig. 5.10. However, for Frame B, the mid-height brace in each column was omitted. The unbraced slenderness ratios for Frames A and C are well within the limits of plastically designed structures, however, the column slenderness ratio,  $L/r_y$ , was 64 for Frame B; the accepted limit is 54 (45).

#### 5.7 Instrumentation

The test specimens were instrumented to determine the axial forces, bending moments, shear forces, deflections and rotations at

various locations. The voltage readings from the various input devices were directly read on a seven-track tape in the DYMEC DATA ACQUISITION SYSTEM which is shown in Fig. 5.11.

For each member in the steel frame, strain readings are taken on two cross-sections as shown in Fig. 5.12. In order to minimize errors arising from any twisting action, four SR-4 strain gauges were mounted at each cross-section of the steel frame as shown in the inset to Fig. 5.12. The strains at these cross-sections remained within the elastic range during the test; thus the axial force and the bending moment at the strain gauge locations can be determined. Since the deflections at these location are also measured for the columns, the secondary moments can be determined and the end moments acting on the column segments can be estimated.

The shear wall is also instrumented with SR-4 gauges as shown in Fig. 5.13 where the short vertical lines represent the locations of the SR-4 strain gauges. The gauges are placed on either side of the beam connections. Figure 5.14 shows a shear wall joint before casting with eight strain gauges in place on the reinforcement. The strain values are read into a computer program together with the material characteristics of the concrete and the reinforcing steel to determine the axial force and bending moment at each gauged section.

The rotations of members were measured adjacent to each joint. In Fig. 5.15, the twenty-three locations are shown, at

which rotations were measured. The top beam-to-column joint with the adjacent rotation meters is shown in Fig. 5.16. The figure also shows the arrangement of the transducers, lateral bracing and the roller supporting the distributing beam at this joint. The rotation meter consists of a thin strip of metal from which a weight is suspended (43) as shown in Fig. 5.17. The bending strains induced in the strip of metal are recorded and used as a measure of the rotation. The rotation meters were calibrated in order to determine the relationship between the voltage and rotation.

A typical detail of the column base is shown in Fig. 5.18. Rotation of the column and wall base plates were measured to predict the degree of fixity at the base. This was subsequently incorporated into the analysis of the structure.

The lateral deflections of the column and the axial shortening of the column and wall were measured by displacement transducers (7DC DT). The lateral deflections were measured at each beam-to-column joint and at the quarter points of each column. In addition, pairs of dial gauges were used to measure the lateral deformation of the flange tips at mid-height of each column, to determine the twisting motion of these points. Figure 5.19 shows schematically the location of transducers and dial gauges. The transducers and dial gauges were attached to a free standing column at one end and attached to the column of the test frame at the other end.

TABLE 5.1 MEMBER PROPERTIES - TEST SPECIMENS

SPECIMEN	GIRDER				COLUMN					SHEAR WALL (BASE)		
	SECTION	I (IN <sup>4</sup> )	M <sub>p</sub> (IN KIPS)	L/r <sub>y</sub>	SECTION	I (IN <sup>4</sup> )	P <sub>c</sub> (KIPS)	M <sub>pc</sub> (IN KIPS)	L/r <sub>y</sub>	P <sub>w</sub> (KIPS)	E <sub>c</sub> I (IN <sup>2</sup> KIPS)	M <sub>ult</sub> (IN KIPS)
A	4M13	10.4	244	80	5WF16	21.3	125	152	24	72	1.98×10 <sup>7</sup>	2980
B	4M13	10.4	244	80	4M13	10.4	110	87	64	50	1.98×10 <sup>7</sup>	2980
C	5WF18.9	23.8	444	62	5WF18.9	23.8	70	362	25	40	1.32×10 <sup>7</sup>	2000

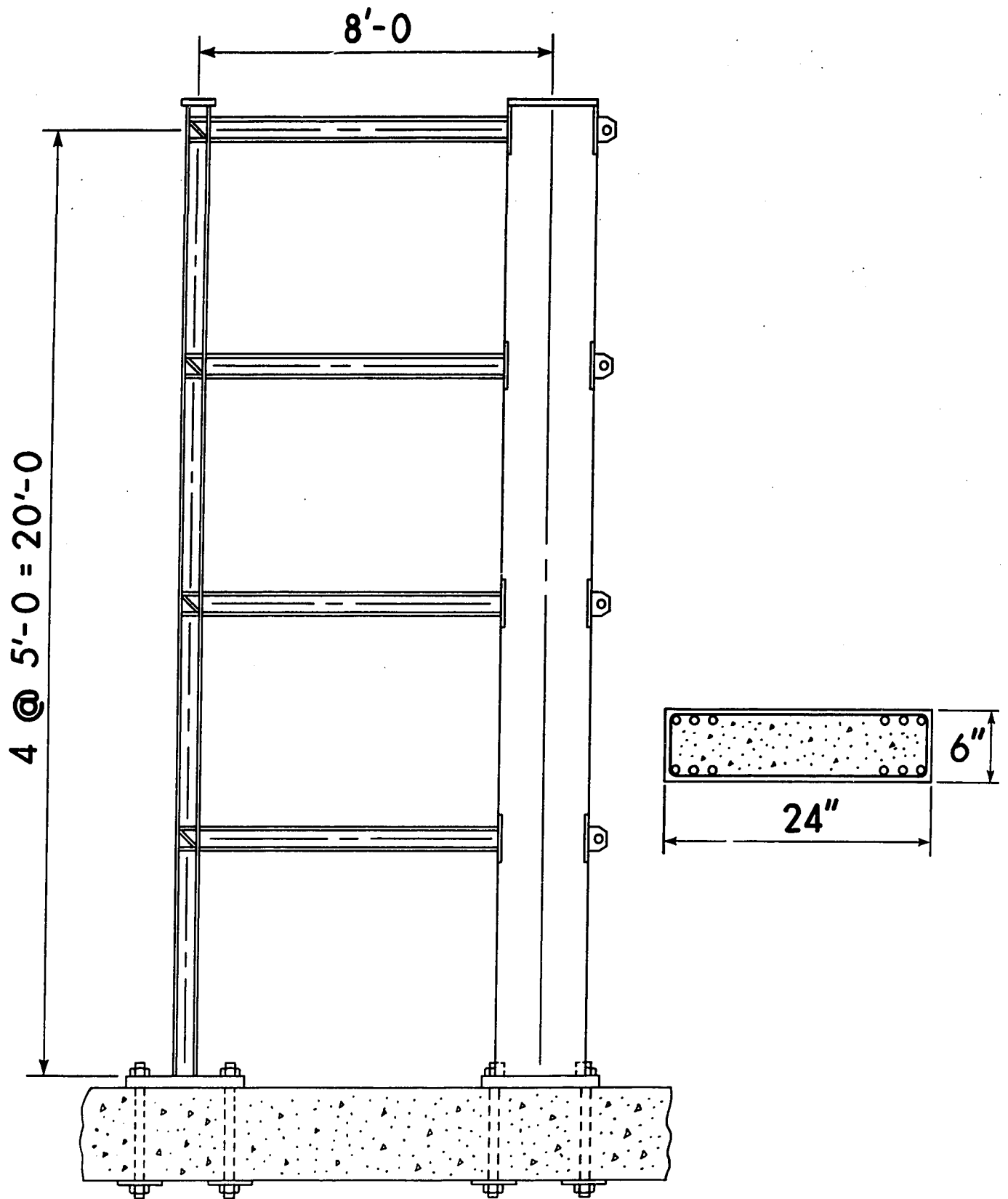


FIG. 5.1 TYPICAL TEST SPECIMEN

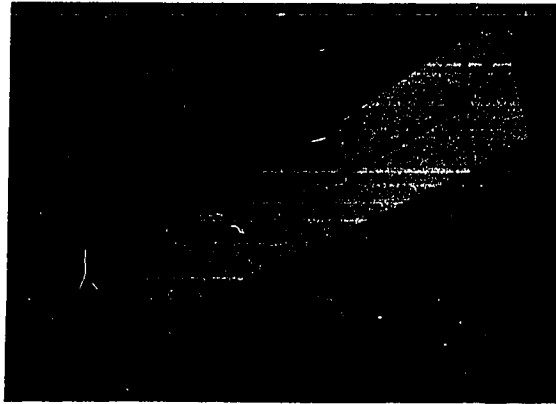


FIG. 5.2 SHEAR WALL ERECTION

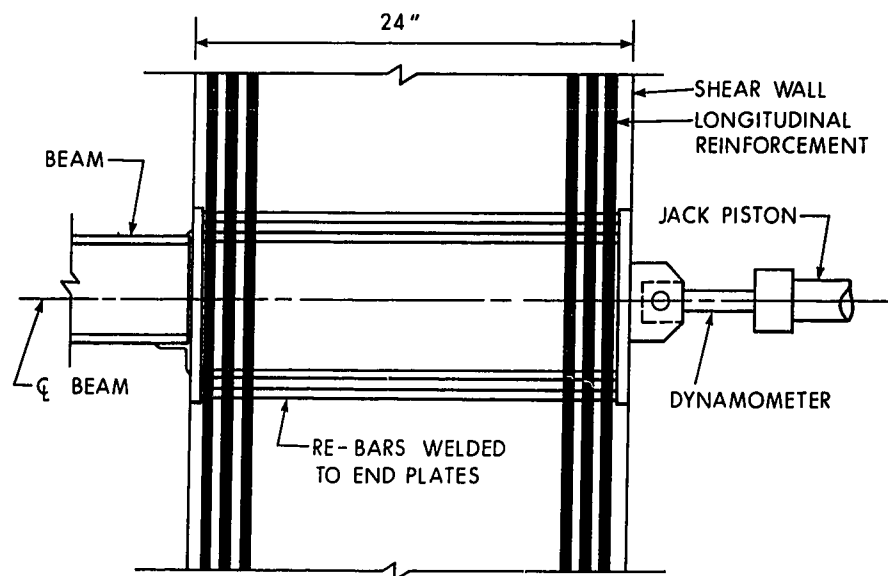


FIG. 5.3 TYPICAL BEAM-TO-WALL JOINT

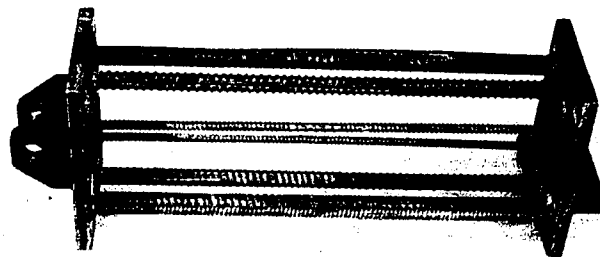


FIG. 5.4 PREFABRICATED ASSEMBLY

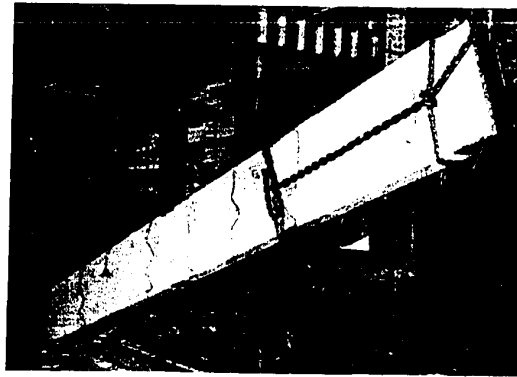


FIG. 5.2 SHEAR WALL ERECTION

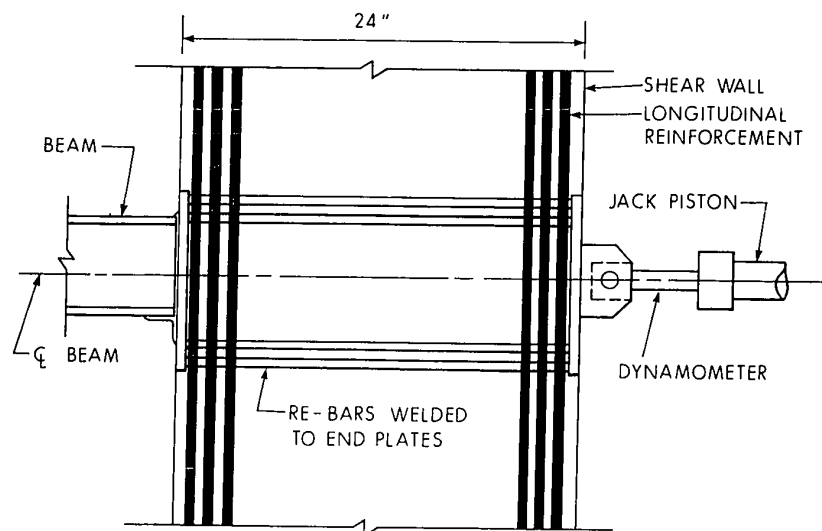


FIG. 5.3 TYPICAL BEAM-TO-WALL JOINT

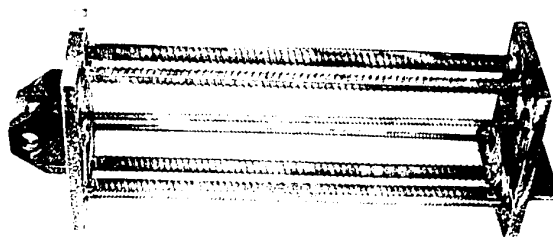


FIG. 5.4 PREFABRICATED ASSEMBLY

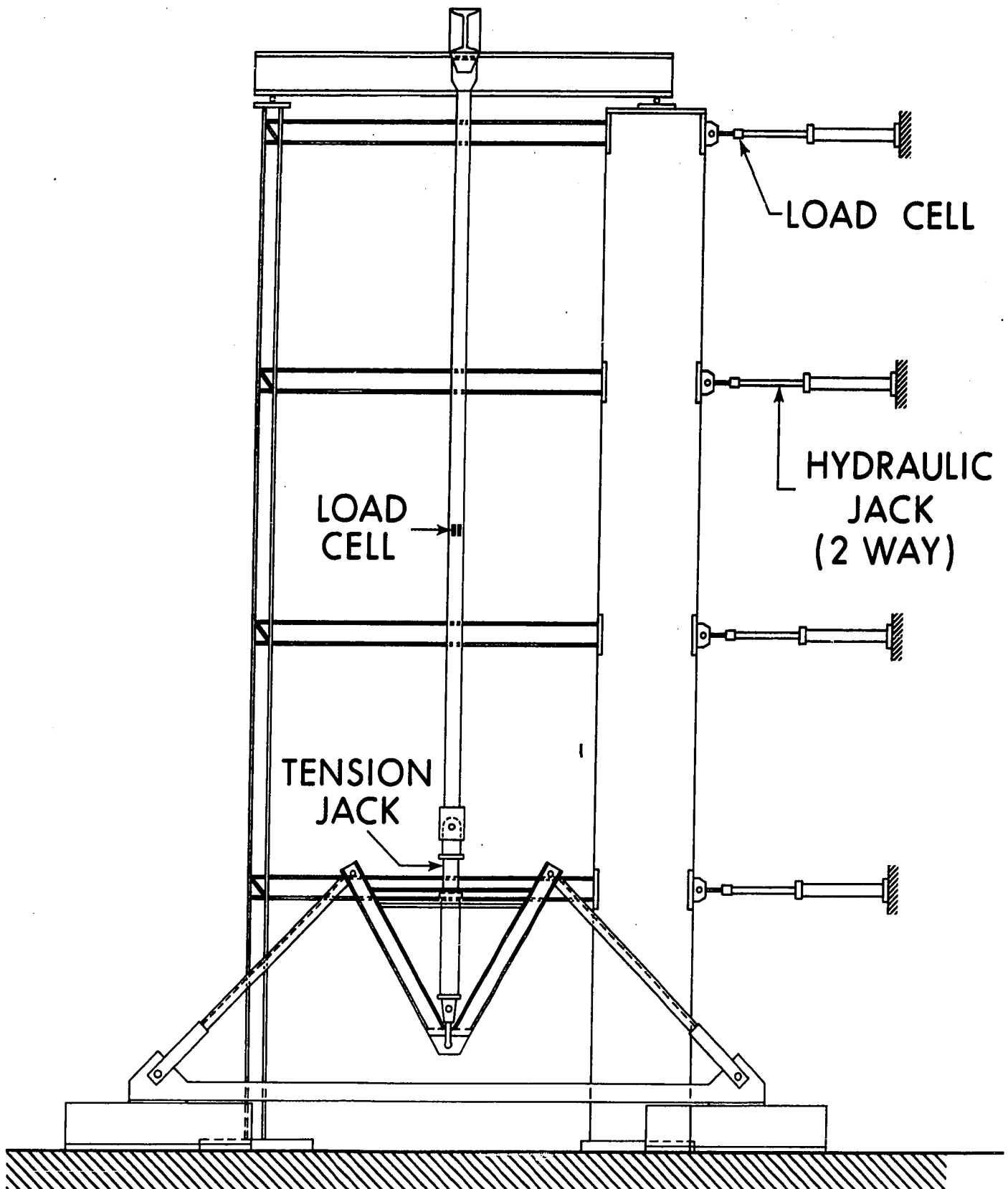


FIG. 5.5 LOADING ARRANGEMENT

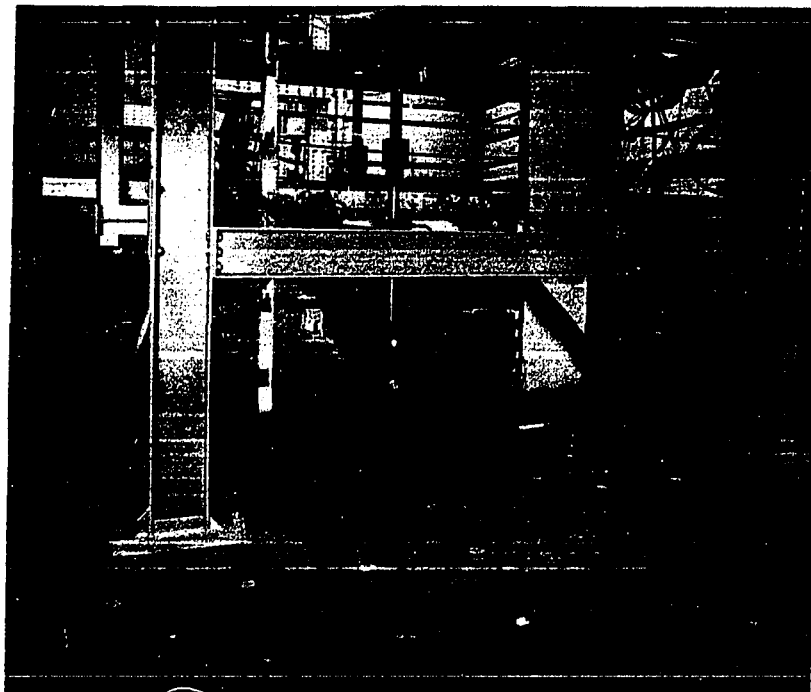


FIG. 5.6 GRAVITY-LOAD SIMULATOR

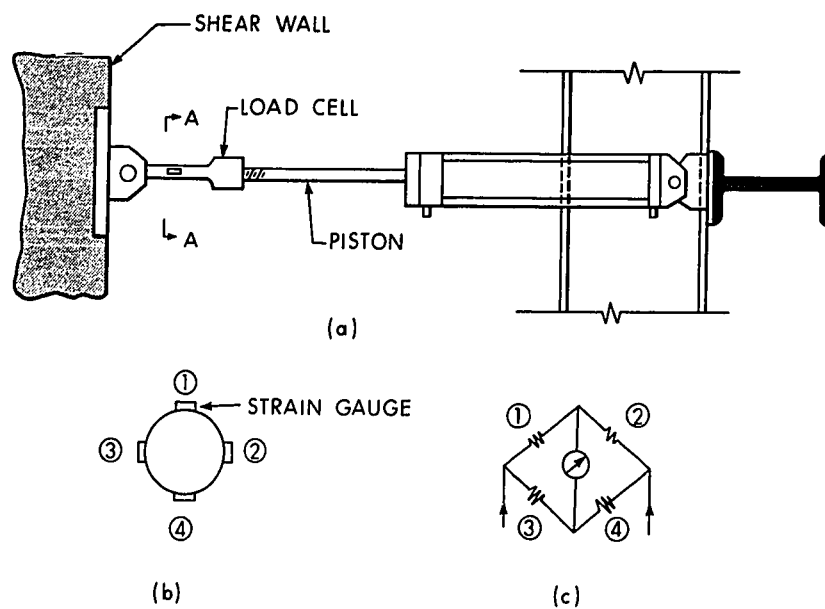


FIG. 5.7 HORIZONTAL JACK ATTACHMENT

- (a) FRONT VIEW;
- (b) LOCATION OF STRAIN GAUGES IN THE DYNAMOMETER - SECTION AA;
- (c) CIRCUIT DIAGRAM

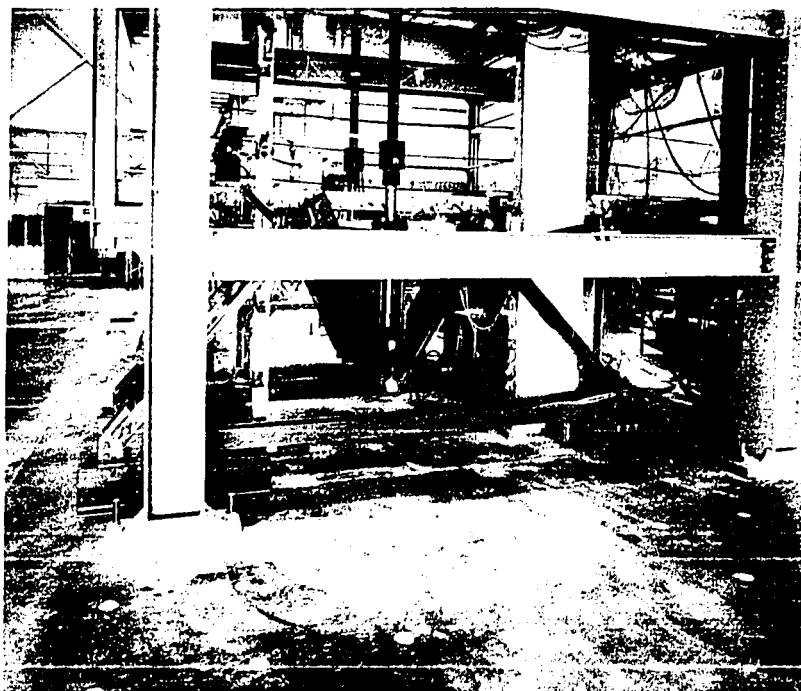


FIG. 5.6 GRAVITY-LOAD SIMULATOR

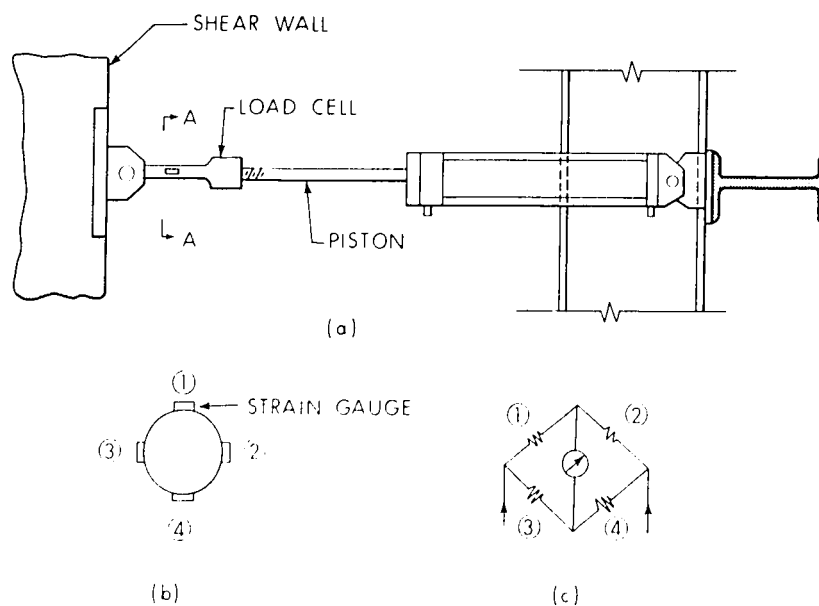


FIG. 5.7 HORIZONTAL JACK ATTACHMENT

- (a) FRONT VIEW;  
 (b) LOCATION OF STRAIN GAUGES IN THE DYNAMOMETER - SECTION AA;  
 (c) CIRCUIT DIAGRAM

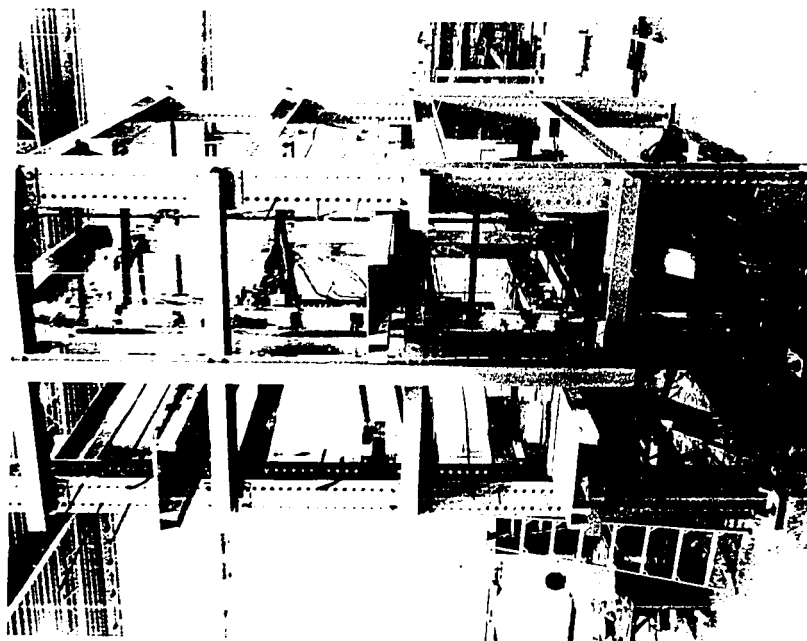


FIG. 5.9 SIDEVIEW OF TEST SETUP

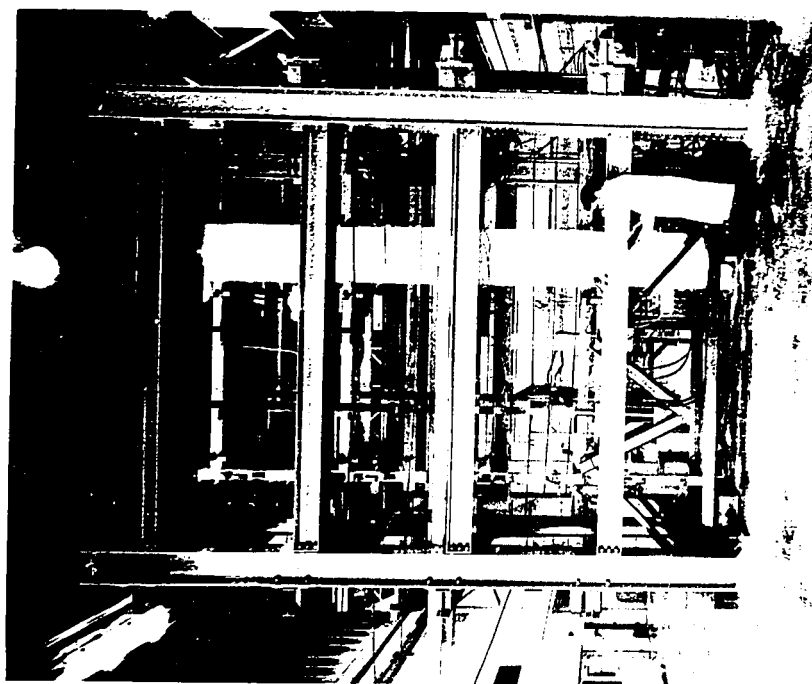


FIG. 5.8 OVERALL VIEW OF TEST SETUP

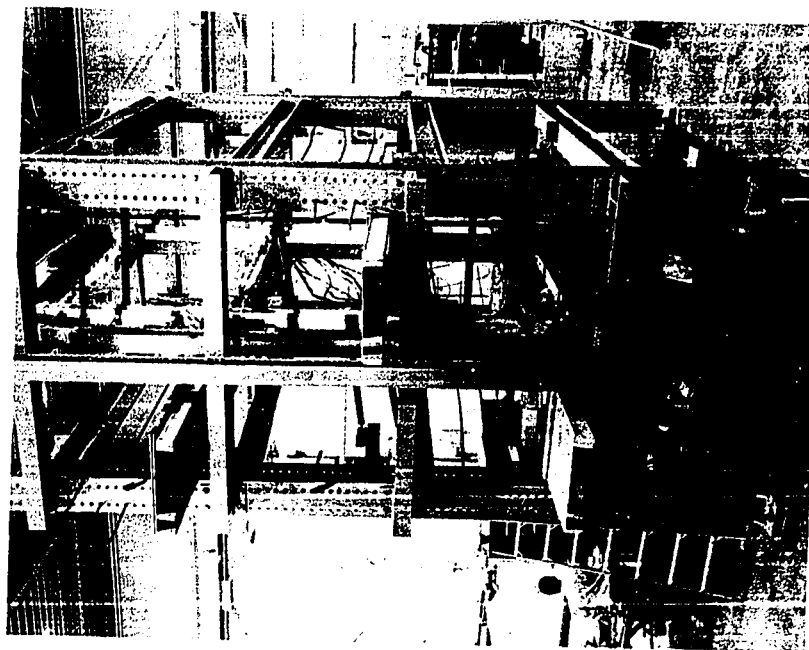


FIG. 5.9 SIDEVIEW OF TEST SETUP

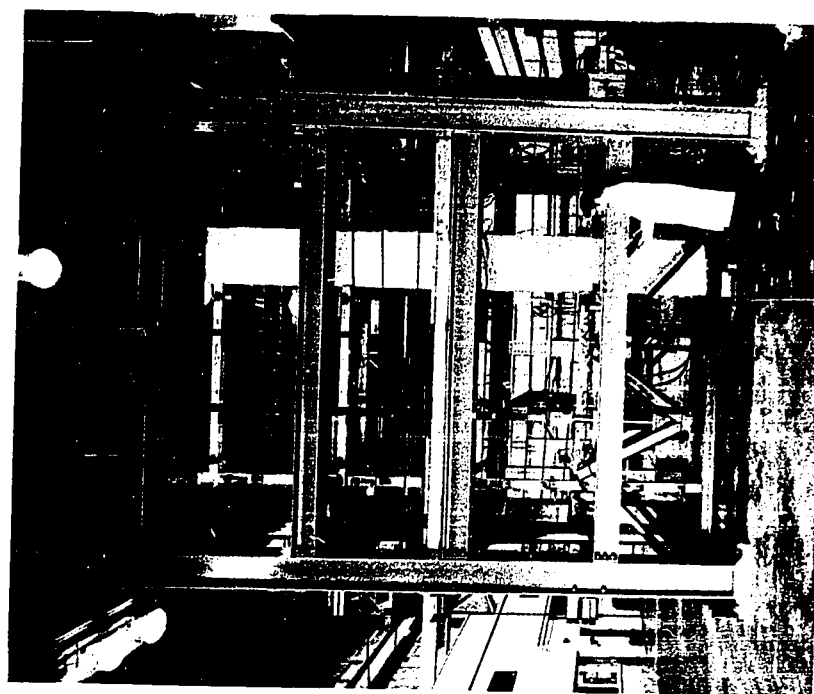


FIG. 5.8 OVERALL VIEW OF TEST SETUP

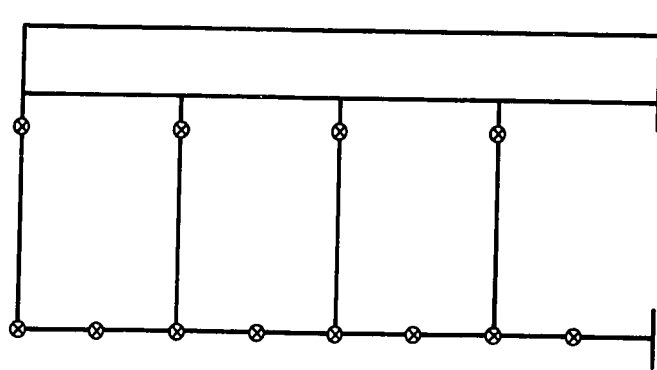


FIG. 5.10 LATERAL BRACING LOCATIONS

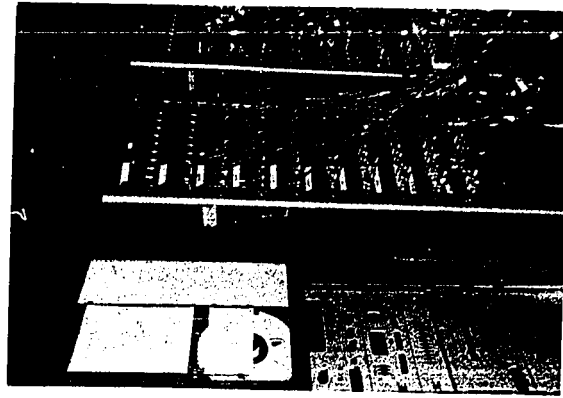


FIG. 5.11 DYMEC DATA ACQUISITION SYSTEM

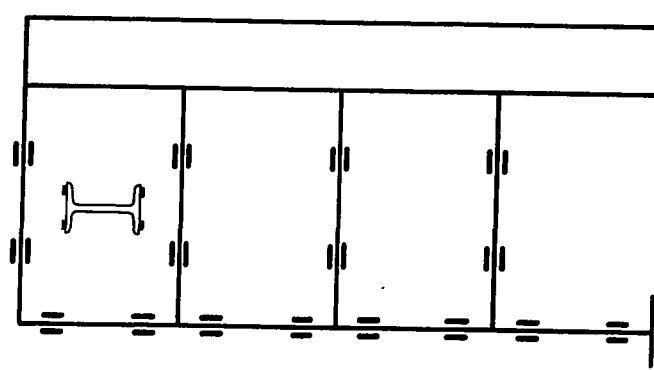


FIG. 5.12 STRAIN GAUGE LOCATIONS - STEEL FRAME

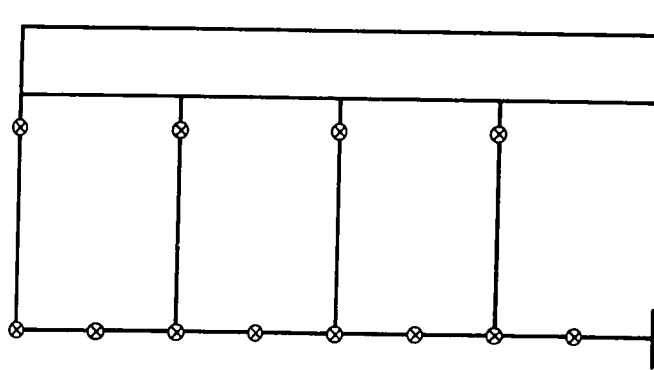


FIG. 5.10 LATERAL BRACING LOCATIONS

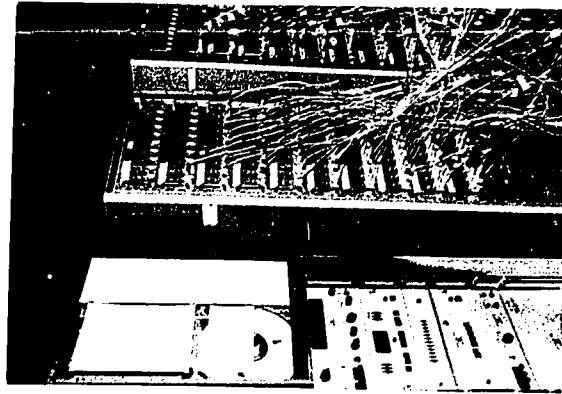


FIG. 5.11 DYMEC DATA ACQUISITION SYSTEM

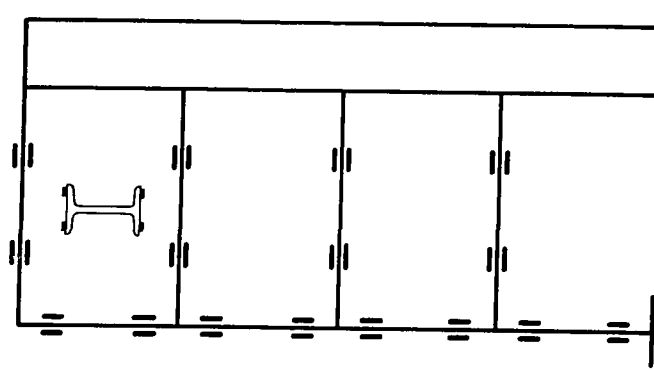


FIG. 5.12 STRAIN GAUGE LOCATIONS - STEEL FRAME

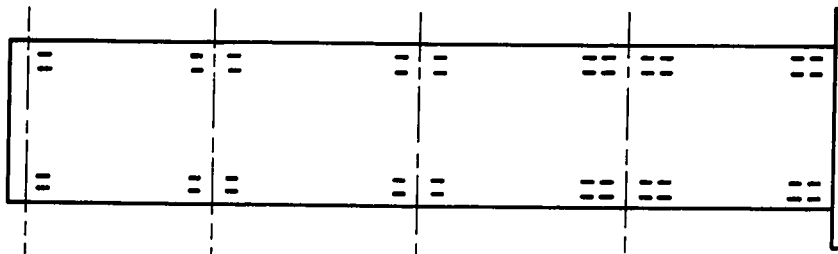


FIG. 5.13 STRAIN GAUGE LOCATIONS - SHEAR WALL

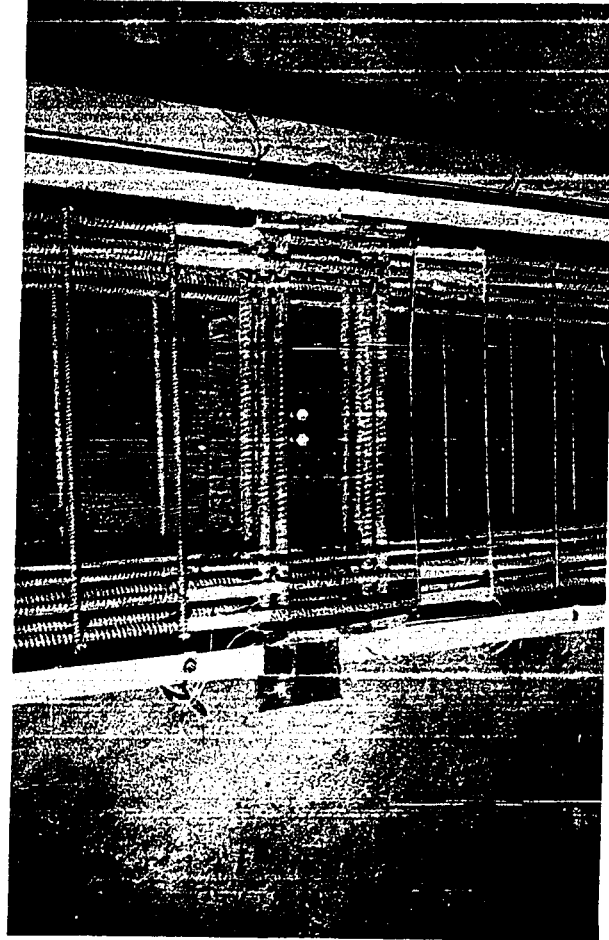


FIG. 5.14 STRAIN GAUGES AT A BEAM-TO-WALL JOINT

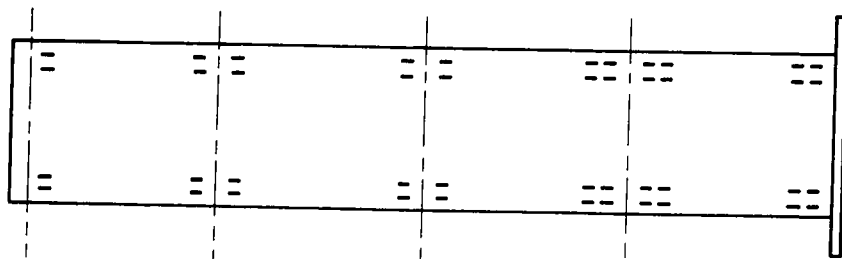


FIG. 5.13 STRAIN GAUGE LOCATIONS - SHEAR WALL



FIG. 5.14 STRAIN GAUGES AT A BEAM-TO-WALL JOINT

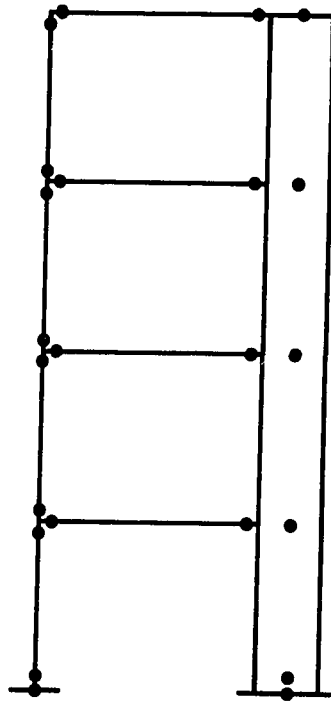


FIG. 5.15 ROTATION METER LOCATIONS

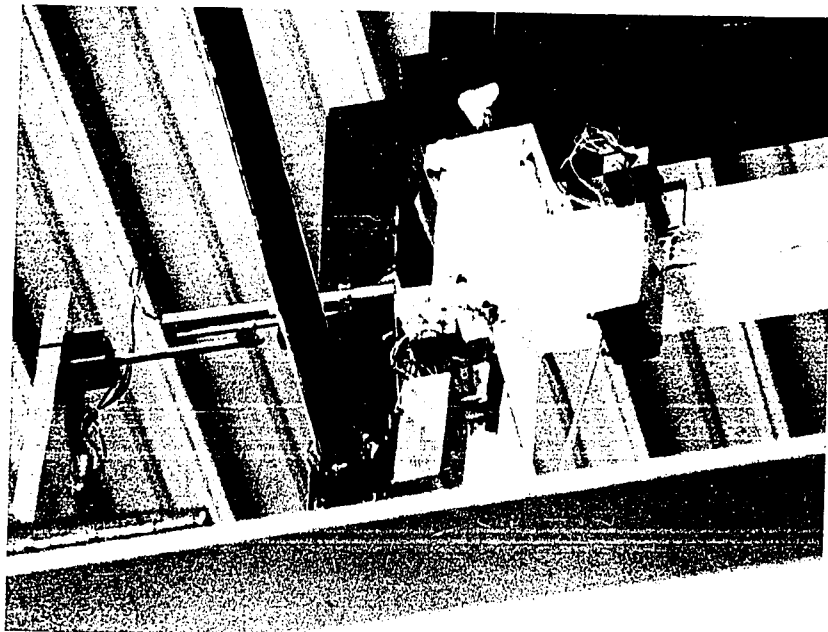


FIG. 5.16 TYPICAL BEAM-TO-COLUMN JOINT

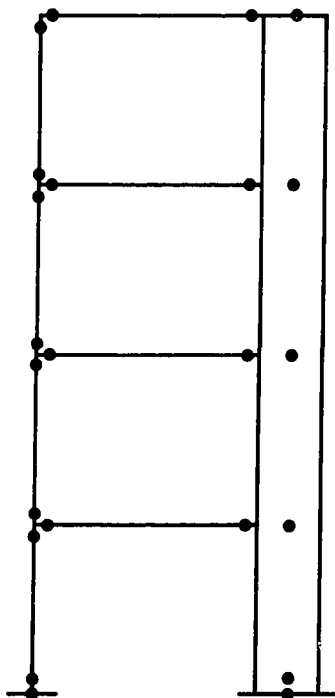


FIG. 5.15 ROTATION METER LOCATIONS

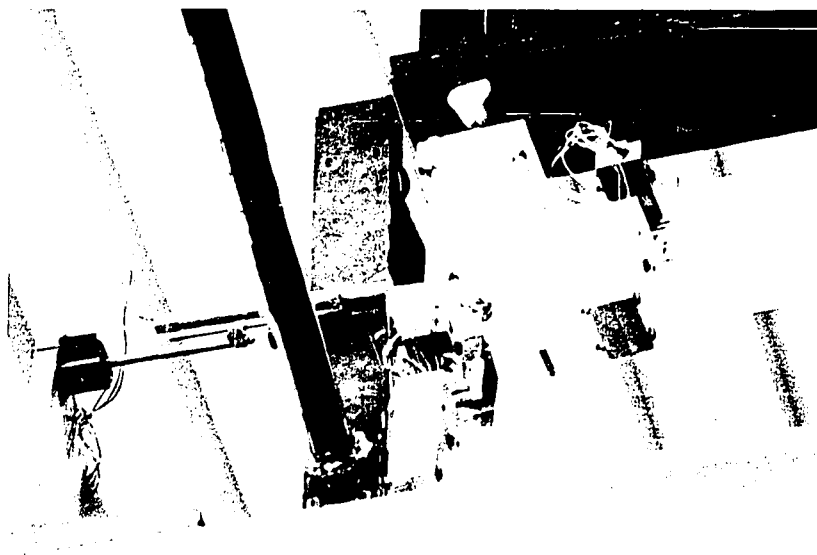


FIG. 5.16 TYPICAL BEAM-TO-COLUMN JOINT

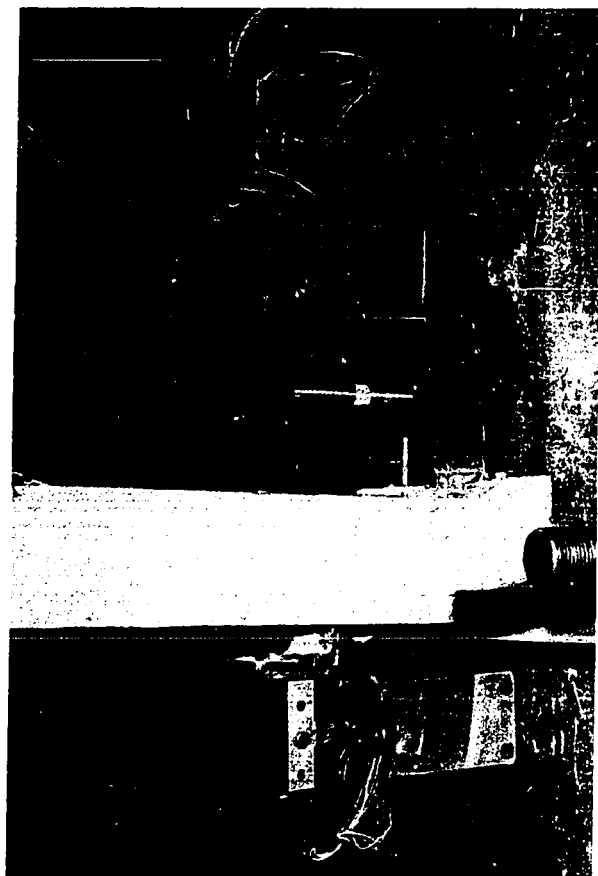


FIG. 5.18 COLUMN BASE DETAIL

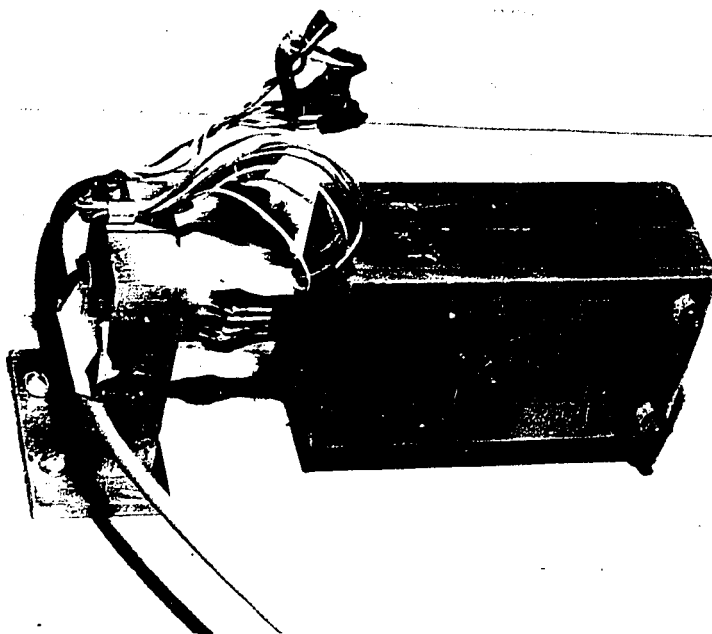


FIG. 5.17 ROTATION METER

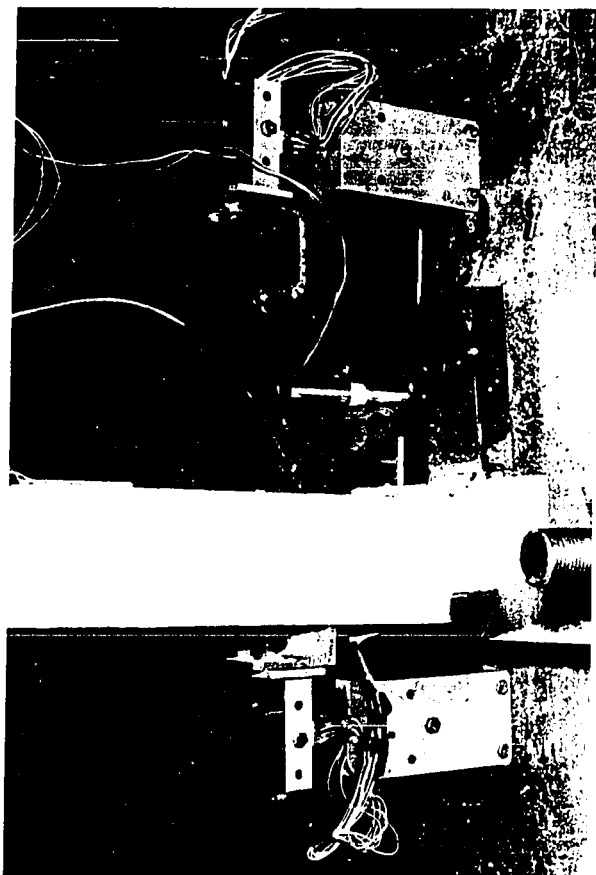


FIG. 5.18 COLUMN BASE DETAIL

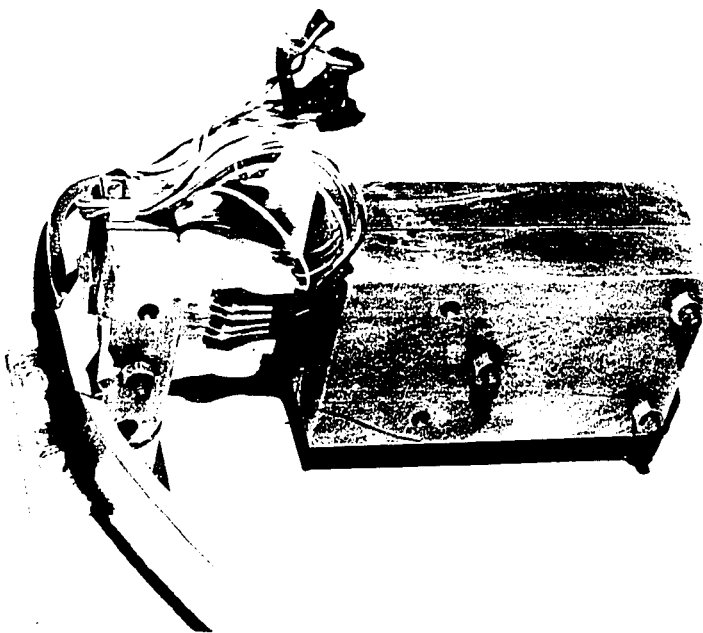


FIG. 5.17 ROTATION METER

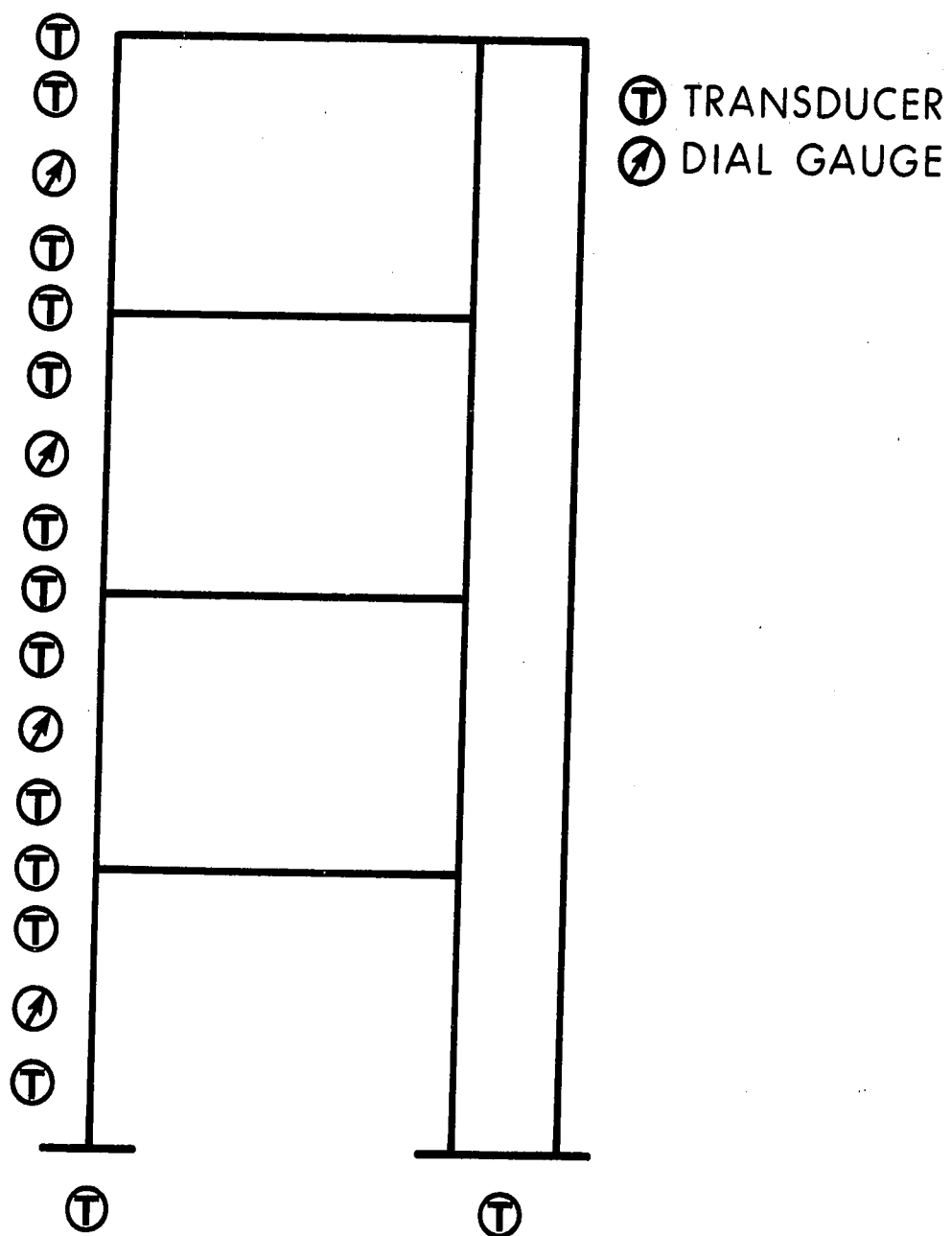


FIG. 5.19 TRANSDUCER AND DIAL GAUGE LOCATIONS

## CHAPTER VI

### TEST RESULTS

#### 6.1 Introduction

The results of tests on three coupled shear wall-frame specimens are reported in this chapter. The frames were subjected to non-proportional loading; the vertical loads were applied initially and held constant, while the horizontal loads were gradually increased. In the elastic range, the test was performed by incrementing the horizontal loads, however, the lateral deflection of the top story was used as a reference value as the structure was deformed in the inelastic range. After each load increment, voltage readings from the strain gauges, dynamometers and rotation meters were recorded on a seven-track tape and the extent of yielding of the steel members was sketched along with the cracking patterns in the shear wall.

#### 6.2 Test Results - Frame A

This frame was designed to simulate the behavior of the bottom portion of a tall building. Lateral bracing mechanisms were attached at each beam-to-column joint and at mid-height of each column length. The columns of the frame were subjected to high axial loads as expected in the bottom stories of a tall structure.

The base plates of the column and shear wall were bolted

to the laboratory floor and the base plate rotations were observed during the test. Figure 6.1 is a plot of the column base moment,  $M_b$ , versus the rotation of the column base plate,  $\theta_b$ . The solid circles with the adjacent numbers, represent stages during the test at which data was recorded. The moment-rotation curve, approximated by the three dashed lines shown in Fig. 6.1, has been incorporated into the theoretical analysis. Similarly, the moment-rotation relationship for the shear wall base has been approximated by two straight lines and incorporated in the analysis.

The horizontal load,  $H$ , versus the top level sway deflection,  $\Delta$ , is plotted in Fig. 6.2. The experimental results are shown by full lines joining the solid circles. The numbers adjacent to each circle represent stages at which data was recorded. The dashed curve represents the response of the frame predicted by a second-order elastic-plastic analysis, while the broken curve represents the predicted behavior neglecting the  $P\Delta$  effect. This system of identification is also used in the subsequent figures unless mentioned otherwise.

The total vertical load applied to Frame A was 197 kips. This load was applied in four increments with total loads of 120 kips, 168 kips and 178 kips. The application of vertical load did not cause yielding in the structure. The horizontal loads were then incremented, while the vertical load was maintained constant; the maximum variation in the vertical load was 3% during the testing period.

The horizontal loads were incremented in a proportional manner. Equal loads were applied at all floor levels.

At load No. 9, yielding was observed at two locations in the column, as shown in the observed hinge configuration in the inset to Fig. 6.2. In this case, the solid circles represent the locations of the observed hinges and the adjacent numbers correspond to the stages at which yielding was first observed. Yielding in the column occurred almost entirely in the compression flange due to the cumulative strains induced by the axial loads and bending moments. Up to Load No. 10, the horizontal load increments were used to control the progress of the test. Beyond this load, the test was performed by regulating the top level sway deflections. At Load No. 13, the structure reached its maximum strength; beyond this point the deformations were accompanied by decreases in lateral load.

The structure was unloaded at Load No. 15 and the test terminated. The structure was later subjected to static cyclic reversals of load. The response of the structure under cyclic loading is beyond the scope of this dissertation.

Strains were measured at two cross-sections in each member of the steel frame. These sections remained elastic during the test. The axial loads and bending moments in the members were computed from the strain distribution across the cross-section. The bending moment diagrams at Load Nos. 9 and 13 are shown in Fig. 6.3. The solid lines represent the experimentally obtained bending moment diagrams,

plotted on the tension side of the member, and the dashed lines represent those obtained from a second-order elastic-plastic analysis. The numbers in the figure are the moments in inch kips, computed from strain gauge readings.

Figure 6.3a is the bending moment diagram at Load No. 9, where first yielding was observed in the structure. At this point, yielding was observed in the compression flange at the base of the bottom story column and the top of the fourth story column. The column base moment at this load is lower than the plastic moment capacity of the member; and at this stage the yield lines had not completely penetrated through the cross-section. The moment distribution at the ultimate load (Load No. 13) is shown in Fig. 6.3b. At this point, all the hinges shown in the inset to Fig. 6.2 have formed.

The actual position of the hinging region in the second level beam-to-column joint for Frame A is shown in Fig. 6.4. At this joint, the beam hinge formed first and hence extensive yielding did not occur in the column. The compression flange yielded at Load No. 12. The hinge locations have shifted away from the stiff strong connection area and, as the structure deforms further, will spread along the beam. The yielding in the compression flange extended approximately 8 inches from the face of the column flange with more severe yielding on one side of the flange. At other beam hinge locations, yielding was fairly uniform across the flange width.

At the hinge locations, the members rotated inelastically without observed local or lateral deformations. The lateral load,  $H$ , versus the top story column end rotation,  $\theta$ , is plotted in Fig. 6.5. The solid circles are the experimental points and the numbers adjacent to the solid circles are the load numbers corresponding to Fig. 6.2. The dashed curve is obtained from a second-order elastic-plastic analysis. The extent of yielding in the compression flange of the column at the fourth level beam-to-column joint is shown in Fig. 6.6. At Load No. 9, the whitewash flaked off in a diagonal line as shown in the figure. Beyond this point, the yielded zone extended along the length of the column as the structure deformed laterally; the final length of the hinging region was approximately 9 inches. The second hinge, which formed at the same load, occurred at the base of the column, as shown in Fig. 6.7. As before, extensive yielding occurred in the compression flange, although no yielding was observed in the tension flange.

The application of lateral load causes a variation in the axial loads developed throughout the structure. The axial load distribution in the column stack is shown in Fig. 6.8. In this figure, the story number,  $N$ , has been plotted versus the axial load in the column,  $P_c$ . The encircled numbers in the figure correspond to load numbers in Fig. 6.2. The axial loads are computed from the strain measurements at two locations in each column segment. In Fig. 6.8, the axial load in a story is the average of the axial loads at these two locations. The dashed line represents the reaction of

the distributing beam at the top of the column. The solid lines represent the axial load distribution corresponding to Load Nos. 6, 9 and 13. First yielding in the structure was observed at Load No. 9, while the ultimate load was attained at Load No. 13. The axial loads in the column varied considerably in all stories because of the upward shear forces from the beams. The variation of axial load and its effect on the behavior of the structure will be discussed in the next chapter with reference to Fig. 6.8.

The bending moment distributions in the shear wall at Load Nos. 9 and 13 are shown in Fig. 6.9. The solid lines represent the experimentally obtained bending moments, while the dashed lines represent the results of a second-order elastic-plastic analysis. Cracking occurred mainly in the bottom two stories of the wall. The high moment gradients in the bottom stories of the wall are typical for the lower stories of this type of structure. At Load No. 9, cracks were observed in the tension zone at the bottom story. As additional lateral load was applied, the neutral axis shifted towards the compressive edge of the wall and the cracks increased in length and width. Figure 6.10 shows the crack pattern in the lower half of the bottom story shear wall. The cracks are inclined due to the presence of relatively high horizontal shears in this region. The horizontal line, extending over the depth of the wall, is a shrinkage crack. The widest inclined crack starts about 6 inches above the base plate and the crack opening can be seen clearly in the

figure; the concrete spalled off in this region. The side view of the shear wall base at the end of the test is shown in Fig. 6.11.

The front view of the test specimen at the end of the test is shown in Fig. 6.12. The structure exhibits a considerable amount of residual deformation.

### 6.3 Test Results - Frame B

The second test specimen was also designed to simulate the behavior of the bottom stories of a tall structure, but the lateral brace at mid-height of each column was not used. As in Frame A, the axial loads applied to the column stack were high. The moment-rotation relationships obtained for the bases of the column and shear wall were similar to those obtained for Frame A and the results have been incorporated in the analysis. In Fig. 6.13, the top level lateral load,  $H$ , versus the top level lateral deflection,  $\Delta$ , has been plotted. The predicted and observed hinge patterns are shown in the inset to Fig. 6.13. Hinges formed primarily in the columns.

The full vertical load in the structure was applied in three equal increments. As the last increment of vertical load was applied, the column stack yielded at scattered locations in the upper two stories. The frame, as fabricated, was out of plumb laterally by 1/4" between the top two girders; the axial load acting through this distance appeared to be responsible for yielding. This caused the top column length to bow out slightly before the lateral load was applied.

The yielding of the third level beam-to-column joint, under vertical load only, is shown in Fig. 6.14. Yielding at this location is probably caused by residual stresses due to fabrication of the joint. Figure 6.15 shows the typical yielding in the interior flange of the fourth story column stack. The yielding in this case is mainly influenced by the axial load and the resulting bowing of the column, as whitewash flaked off only on one side of the flange in the yielded region.

Lateral loads were applied proportionally to the structure. At approximately Load No. 6, the connection at the third level beam-to-wall joint showed signs of slip. The structure was unloaded at Load No. 8 and the connection rewelded. The structure was then reloaded and behaved much as expected. Severe cracking occurred in the bottom story of the shear wall beyond Load No. 13. The crack pattern of the bottom story shear wall at Load No. 14 is shown in Fig. 6.16. The horizontal lines are initial shrinkage cracks. As before, inclined cracks are caused by the combined effects of the horizontal shear and bending moment. As the structure deformed slightly beyond Load No. 14, yielding spread along the top story column and the column buckled suddenly between points of lateral bracing. The test was terminated at this stage.

The end view of the top two stories of the buckled specimen is shown in Fig. 6.17. Buckling in the top story occurred between the lateral bracing points at the top two floor levels. In the top story, the wide flange section yielded completely for three-quarters

of the column length. The deformation of the top story column is shown in Fig. 6.18. The figure shows the complete yielding of the cross-section. Extensive yielding occurred at other beam-to-column joints. Figure 6.19 shows the hinging at the third level beam-to-column joint at the end of the test. The plastic hinge at the base of the column is shown in Fig. 6.20.

#### 6.4 Test Results - Frame C

This frame was designed to simulate the upper portion of a tall structure. In this case, the shears imposed on the columns may be much greater than the applied shears and consequently the shears in the wall are reversed. In order to simulate this action, the base of the shear wall was pinned mechanically in Frame C. The shear wall base detail is shown in Fig. 6.21. The load is transferred to the laboratory floor through a 2 inch diameter high strength steel pin. Friction is almost eliminated by bearings. The shear wall is cast with a plate at the bottom, to receive the longitudinal reinforcement. The wall is erected and bolted to the top plate of the mechanical hinge as shown in the figure. The moment-rotation characteristic at the base was observed during the test and incorporated in the analysis. The lateral bracing arrangement was similar to Frame A.

Frame C was subjected to constant vertical loads and monotonically increasing lateral loads, as were the other two frames. However, the magnitude of the lateral load applied at the top level

was half of that in the other levels. The lateral load,  $H$ , versus the top level lateral deflection,  $\Delta$ , is plotted in Fig. 6.22. The predicted and observed hinge patterns are shown in the inset to Fig. 6.22.

The full vertical load was applied in two increments. Yielding did not occur at this stage. At Load No. 8, the first hinge was detected at the base of the column. Up to Load No. 9, the lateral load was incremented by monitoring the hydraulic pressure in the jacks. Beyond this point, the test was performed by limiting the top level sway. The ultimate load was reached at Load No. 17. The applied loads were reduced at this stage and the specimen unloaded.

At the end of the test, three hinges had formed in the columns and seven hinges in the beams as shown in the observed hinge configuration in the inset to Fig. 6.22. The plastic hinge in the top of the column at the fourth level beam-to-column joint is shown in Fig. 6.23. Yielding in the compression flange of the column was first observed at Load No. 13 and the length of the hinge had extended to approximately 12 inches at the end of the test. The hinging area in the third level beam at the beam-to-column joint is shown in Fig. 6.24. Yielding extended about 12 inches from the face of the column at the end of the test. Although the hinges were subjected to considerable inelastic rotation, local or lateral buckling did not occur during the test. The extent of yielding at other hinge locations was similar, but less severe.

The variation of the axial load over the column stack of Frame C is plotted in Fig. 6.25. In this figure, the story number,  $N$ , has been plotted versus the axial load in the column stack,  $P_c$ . The solid lines represent the axial load distribution corresponding to Load Nos. 2, 6, 10 and 17. At Load No. 2, full vertical load has been applied to the structure. The structure has swayed in the negative sense since the axial shortening of the column stack is greater than that of the shear wall. In general, the application of lateral load caused a reduction in the column load, since the column is located in the windward end of the specimen. The variation of the axial load and its effect on the behavior of the structure will be discussed in the next chapter with reference to Fig. 6.25.

The shear distribution in the bottom story, throughout the test is shown in Fig. 6.26. In this figure, the shear,  $V$ , has been plotted against the top level sway deflection,  $\Delta$ . In this case the shear wall carries the bulk of the applied shear. Similarly, the shear distribution at the top story of Frame C is shown in Fig. 6.27. This figure plots the top story shear,  $V$ , versus the top level sway deflection,  $\Delta$ . In this case, the resisting shears developed by the column exceeded the applied shear force and the shear force in the wall acts to load the column.

The attainment of ultimate load (Load No. 17) was marked by hinging in the columns and beams, but no appreciable damage to the wall. Figure 6.28 shows the overall view of Frame C after testing.

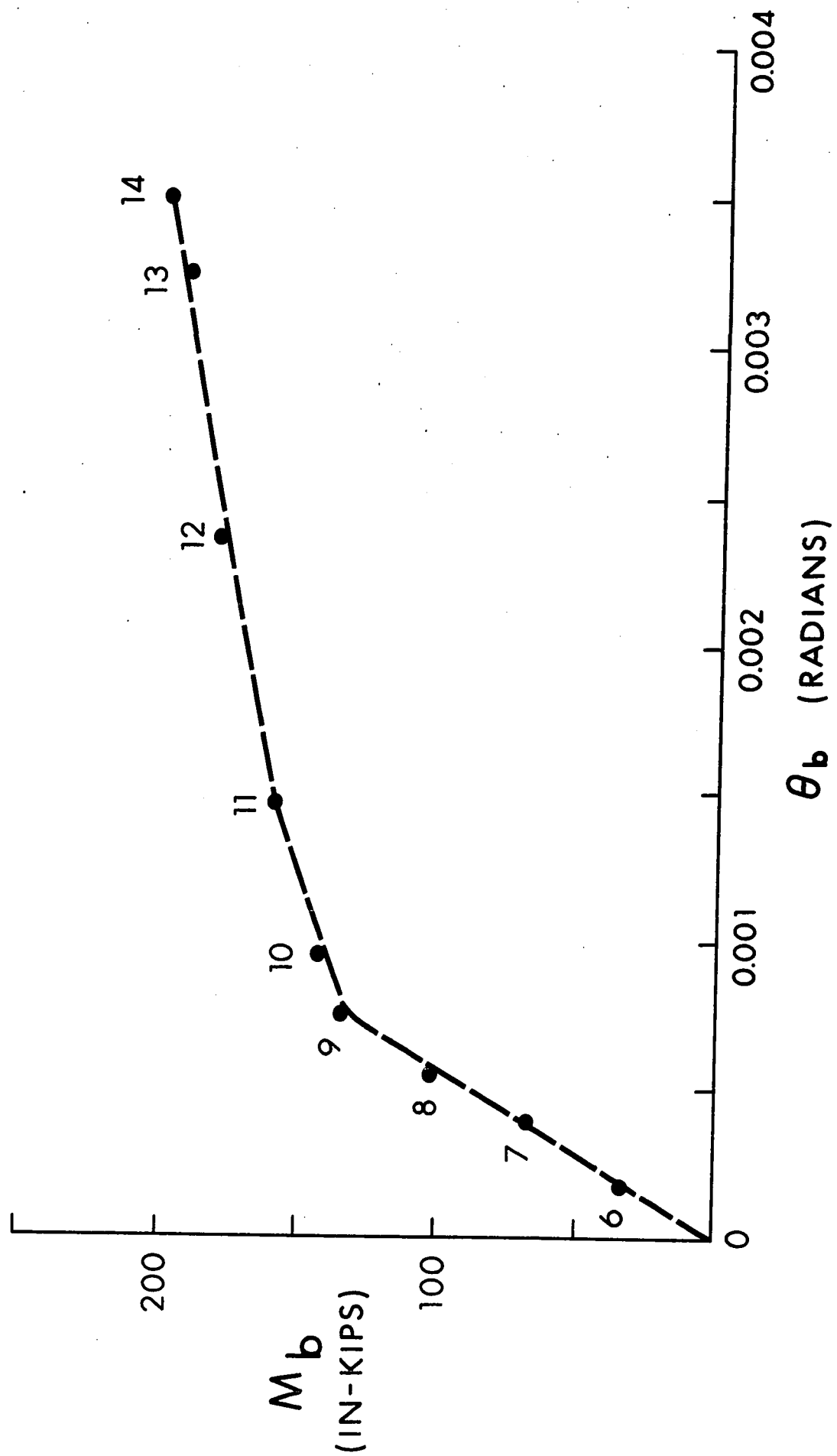


FIG. 6.1 COLUMN BASE ROTATION - FRAME A

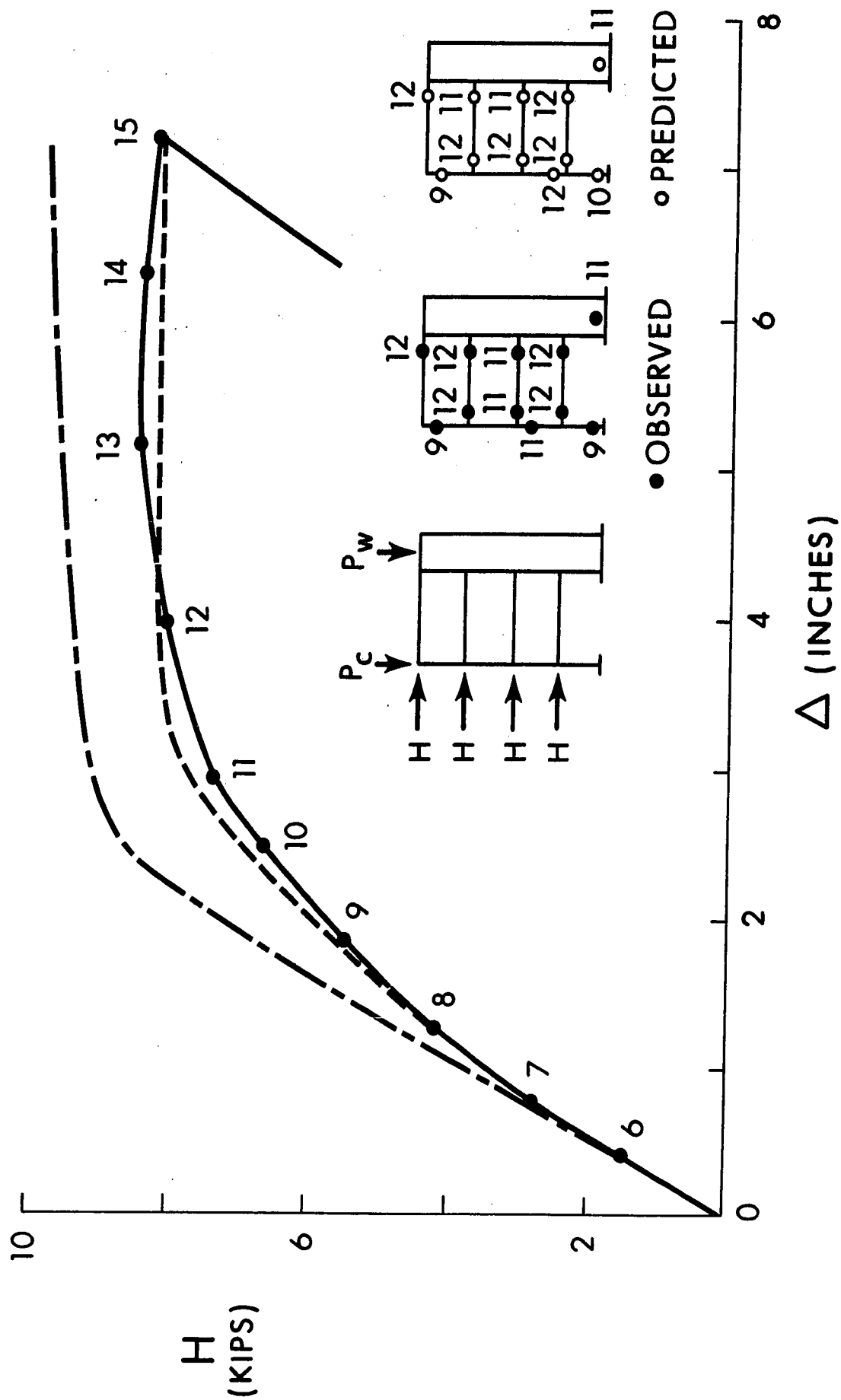


FIG. 6.2 LOAD-DEFLECTION RELATIONSHIPS - FRAME A

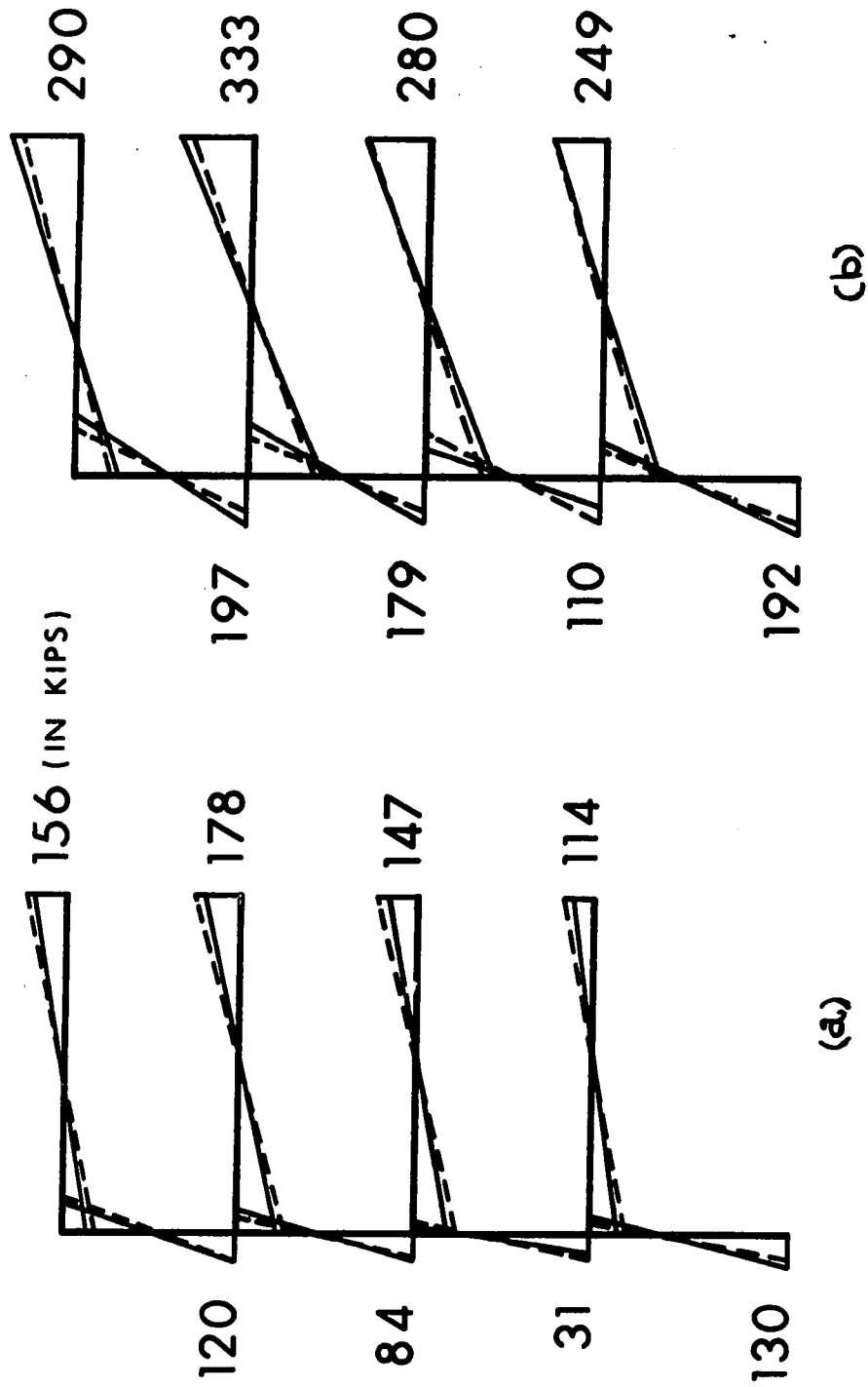


FIG. 6.3 BENDING MOMENT DISTRIBUTIONS - FRAME A

(a) LOAD NO. 9

(b) LOAD NO. 13



FIG. 6.4 BEAM PLASTIC HINGE - FRAME A



FIG. 6.4 BEAM PLASTIC HINGE - FRAME A

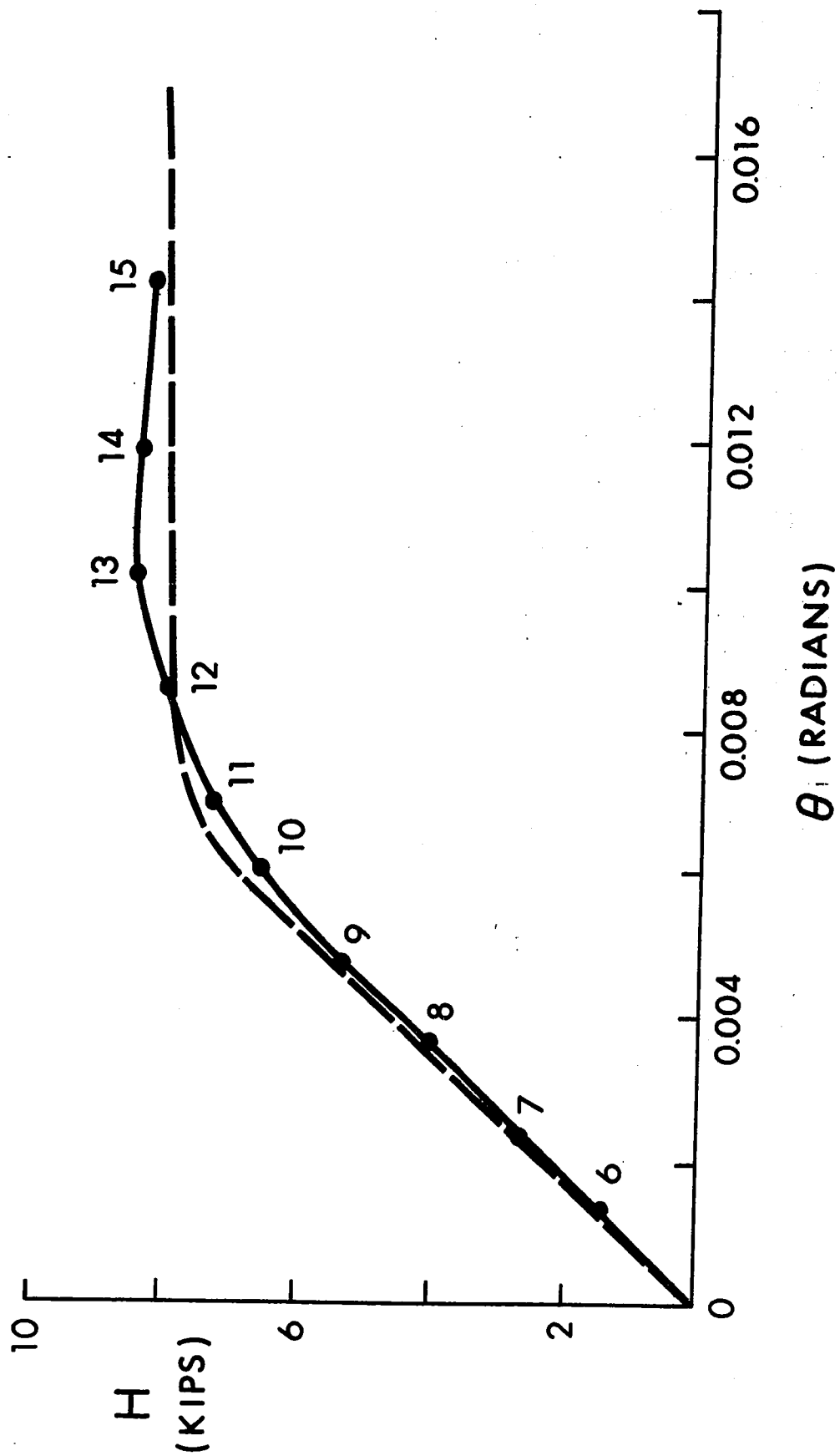


FIG. 6.5 LOAD-ROTATION RELATIONSHIPS - FRAME A

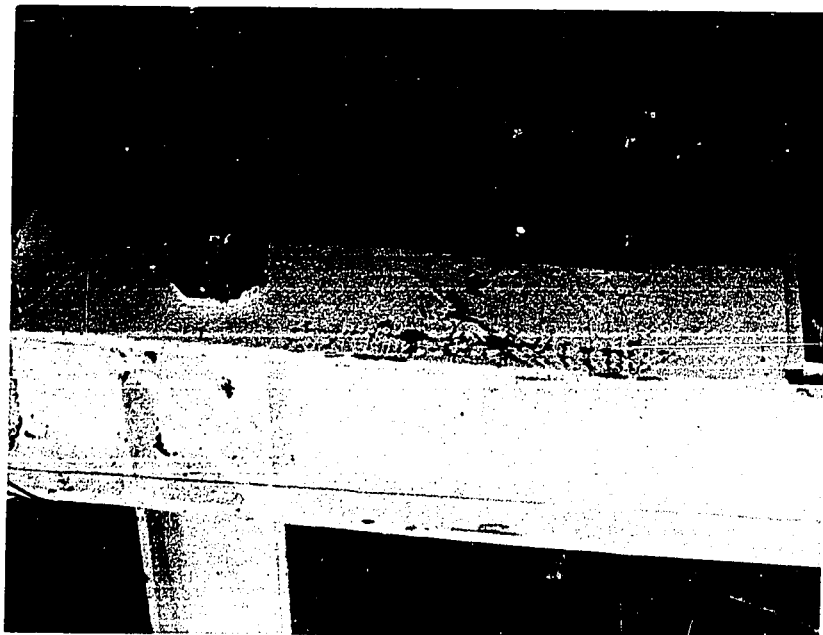


FIG. 6.6 PLASTIC HINGE IN TOP STORY COLUMN - FRAME A

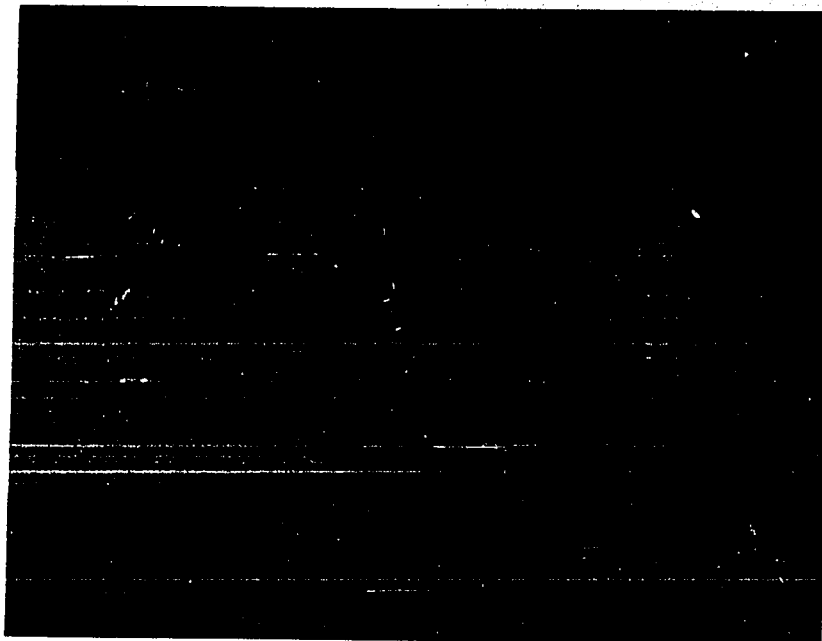


FIG. 6.7 PLASTIC HINGE AT COLUMN BASE - FRAME A

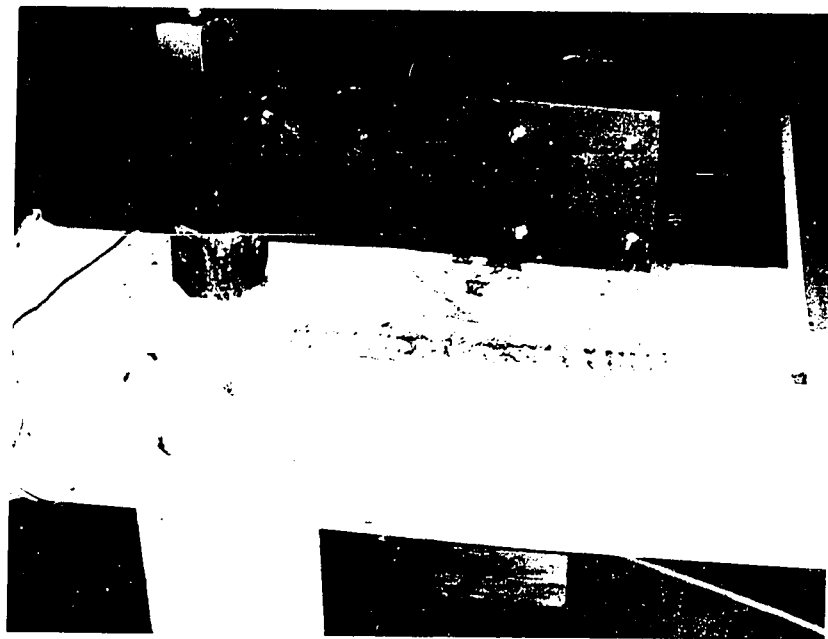


FIG. 6.6 PLASTIC HINGE IN TOP STORY COLUMN - FRAME A

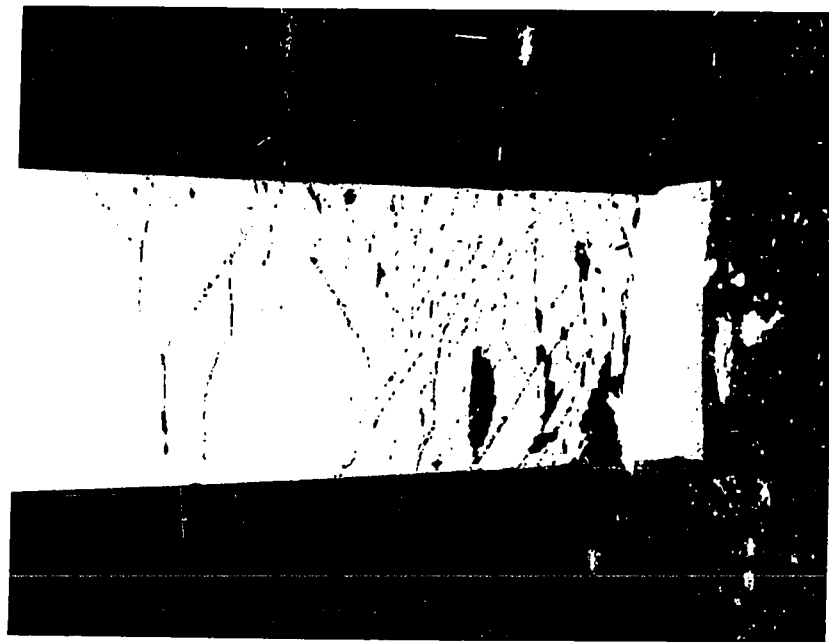


FIG. 6.7 PLASTIC HINGE AT COLUMN BASE - FRAME A

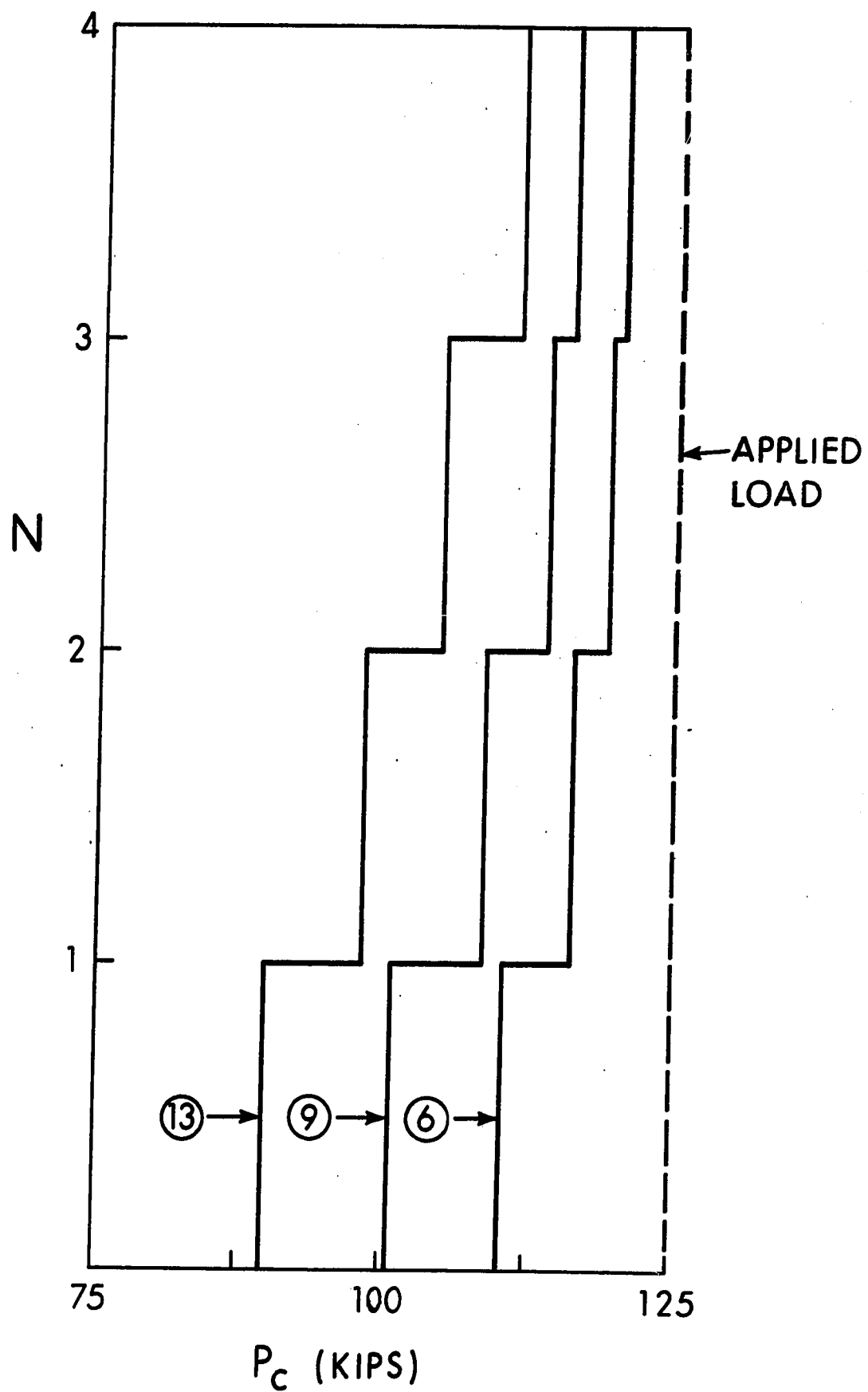


FIG. 6.8 AXIAL LOAD DISTRIBUTION IN THE COLUMN STACK - FRAME A

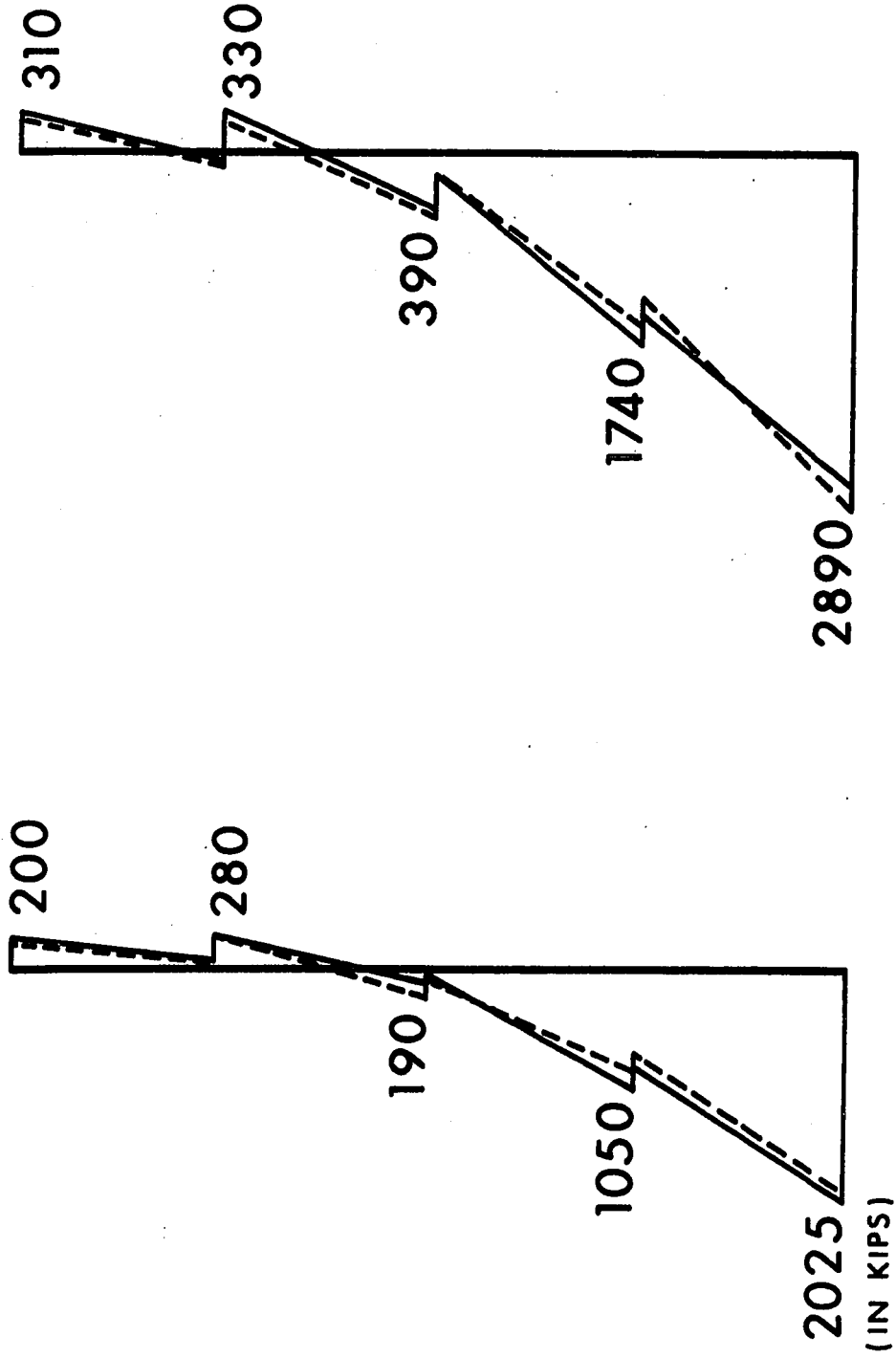


FIG. 6.9 WALL BENDING MOMENT DISTRIBUTIONS - FRAME A

(a) LOAD NO. 9

(b) LOAD NO. 13

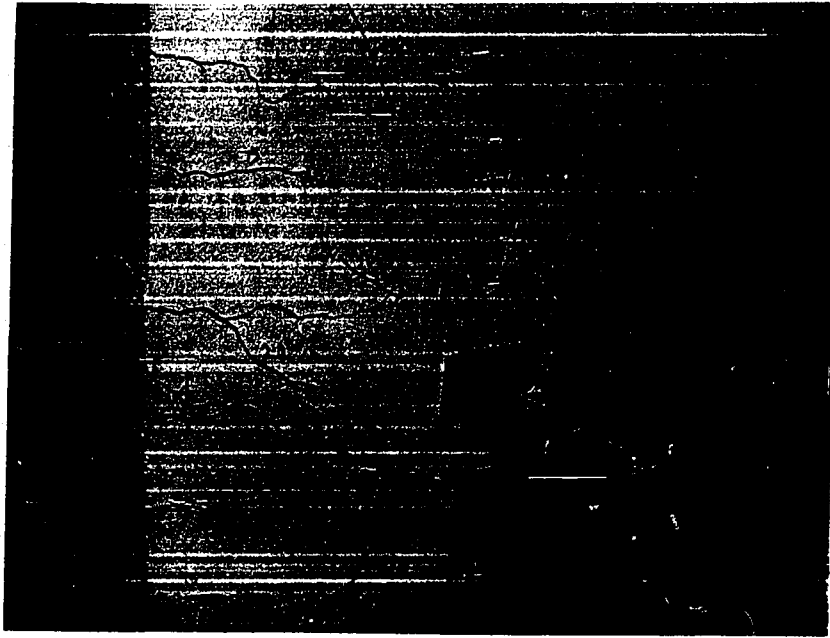


FIG. 6.10 CRACKING AT WALL BASE - FRAME A

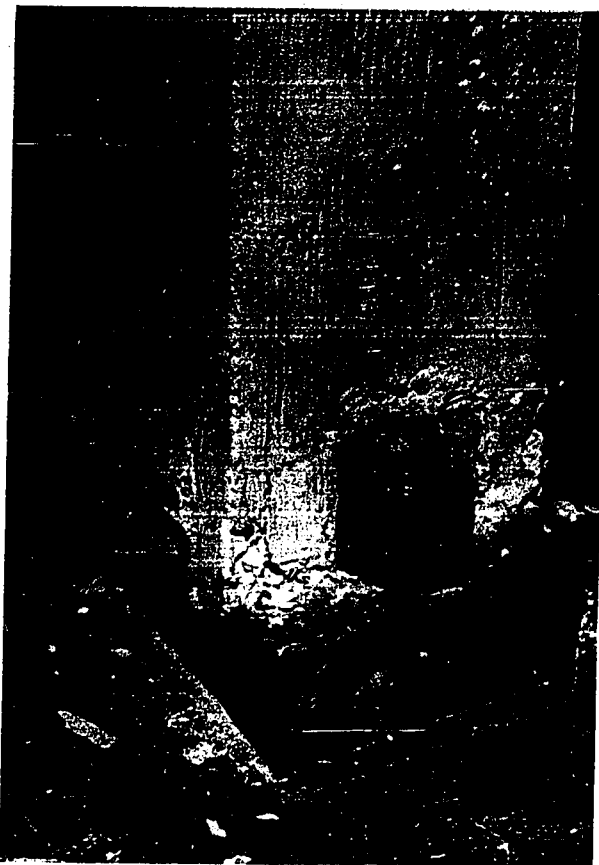


FIG. 6.11 CRUSHING AT WALL BASE - FRAME A

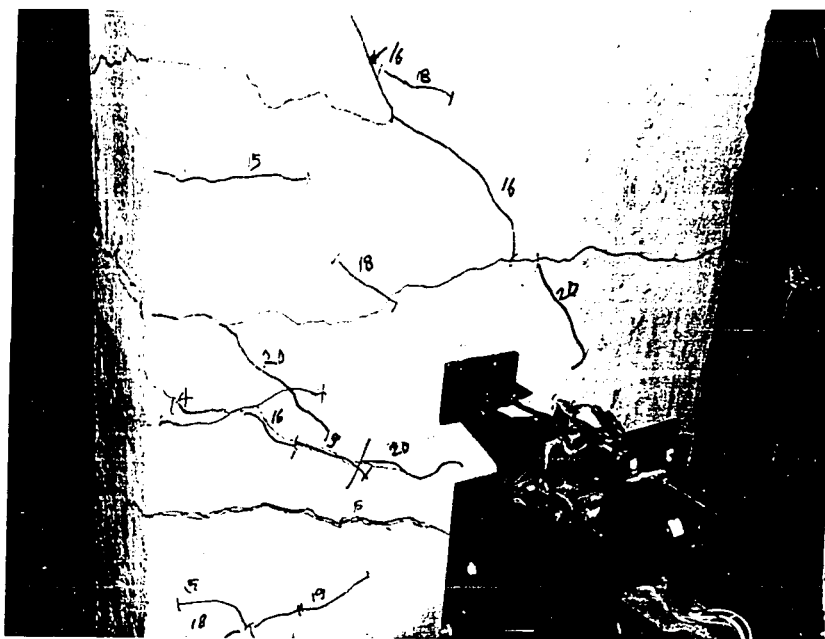


FIG. 6.10 CRACKING AT WALL BASE - FRAME A



FIG. 6.11 CRUSHING AT WALL BASE - FRAME A

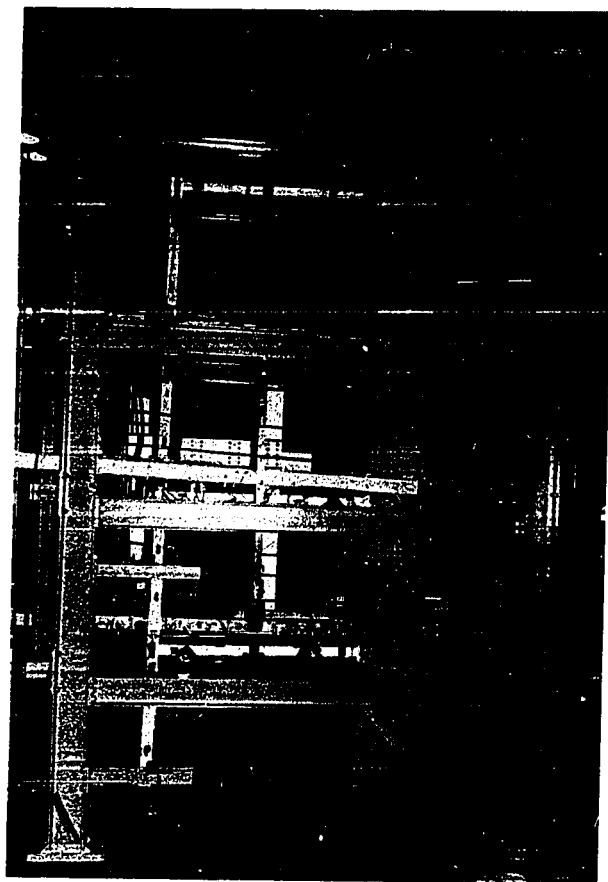


FIG. 6.12 FRAME A AFTER TESTING

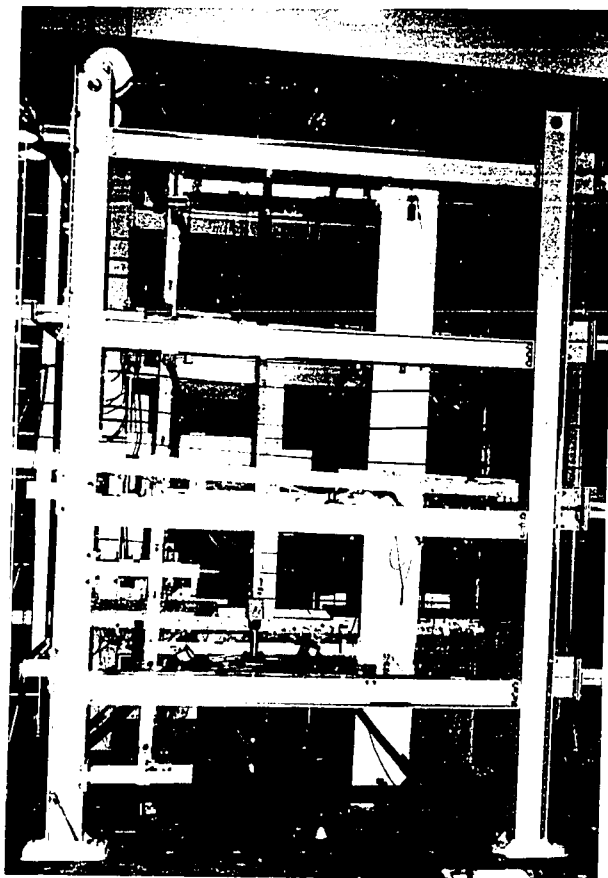


FIG. 6.12 FRAME A AFTER TESTING

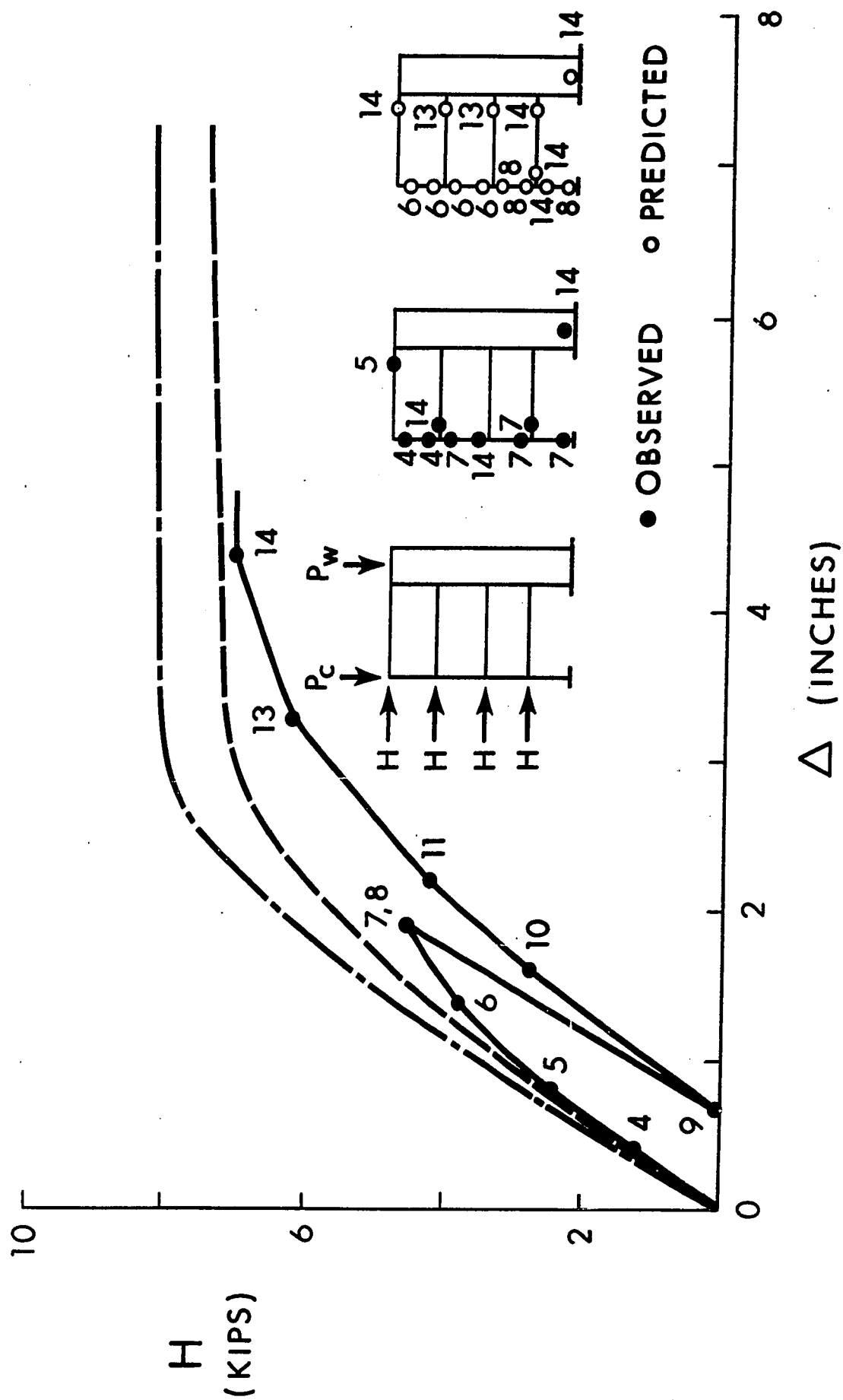


FIG. 6.13 LOAD-DEFLECTION RELATIONSHIPS - FRAME B

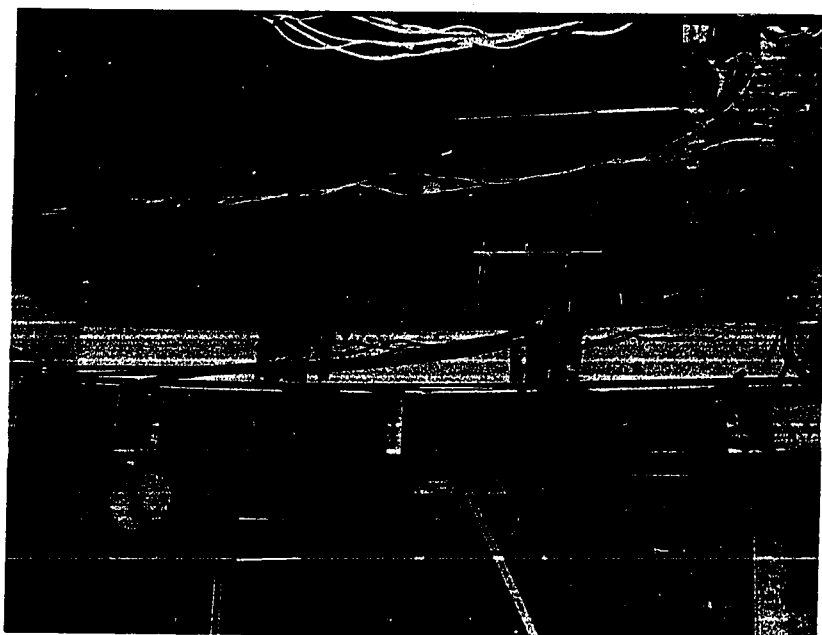


FIG. 6.15 COLUMN YIELDING DUE TO  
VERTICAL LOAD - FRAME B

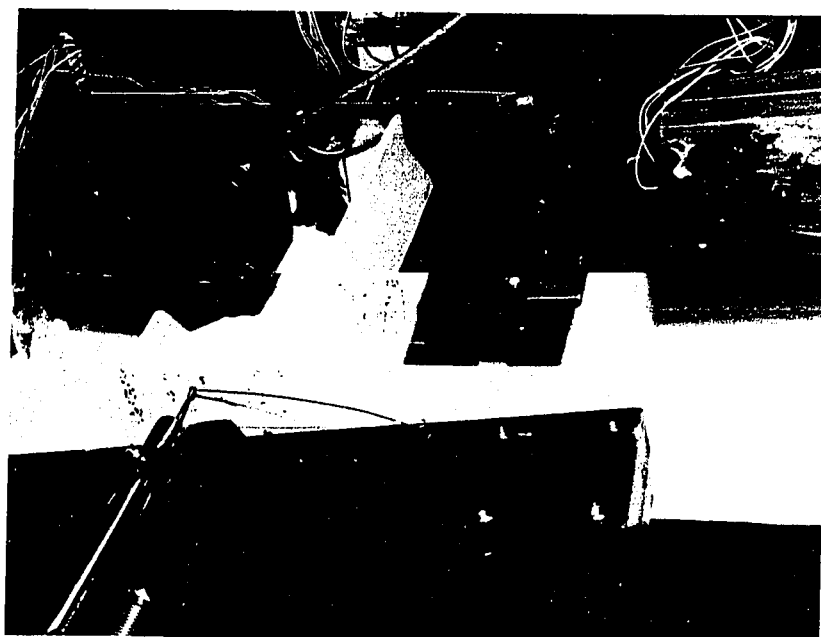


FIG. 6.14 JOINT YIELDING DUE TO  
VERTICAL LOAD - FRAME B

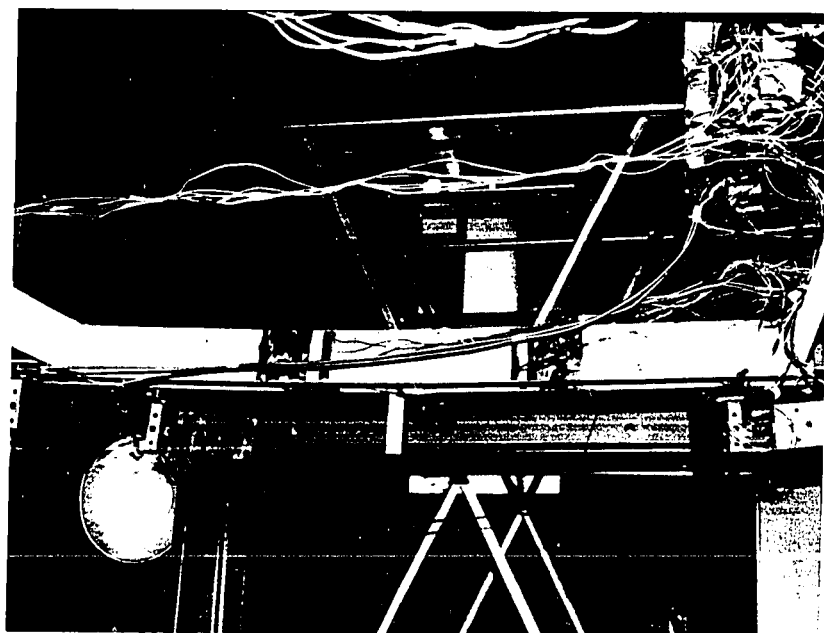


FIG. 6.15 COLUMN YIELDING DUE TO  
VERTICAL LOAD - FRAME B



FIG. 6.14 JOINT YIELDING DUE TO  
VERTICAL LOAD - FRAME B

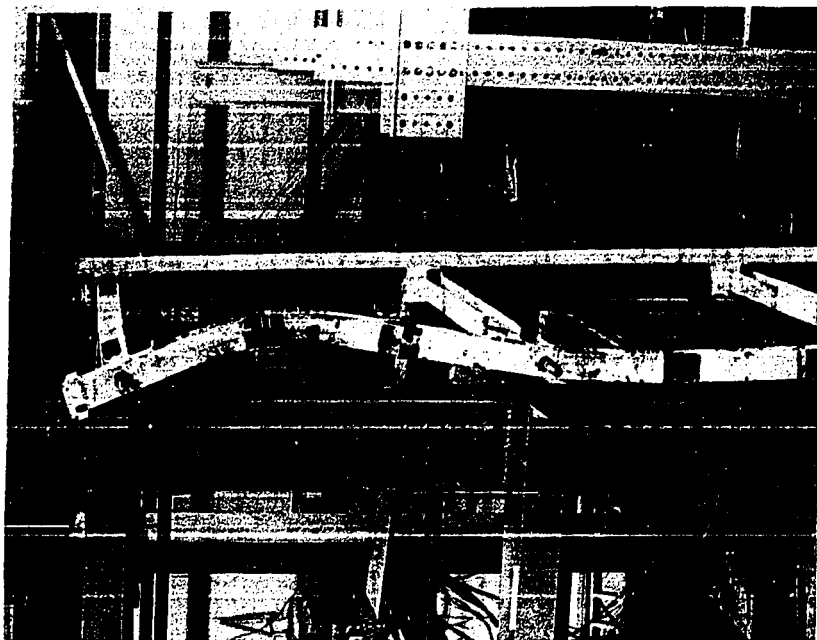


FIG. 6.17 LATERAL BUCKLING - FRAME B

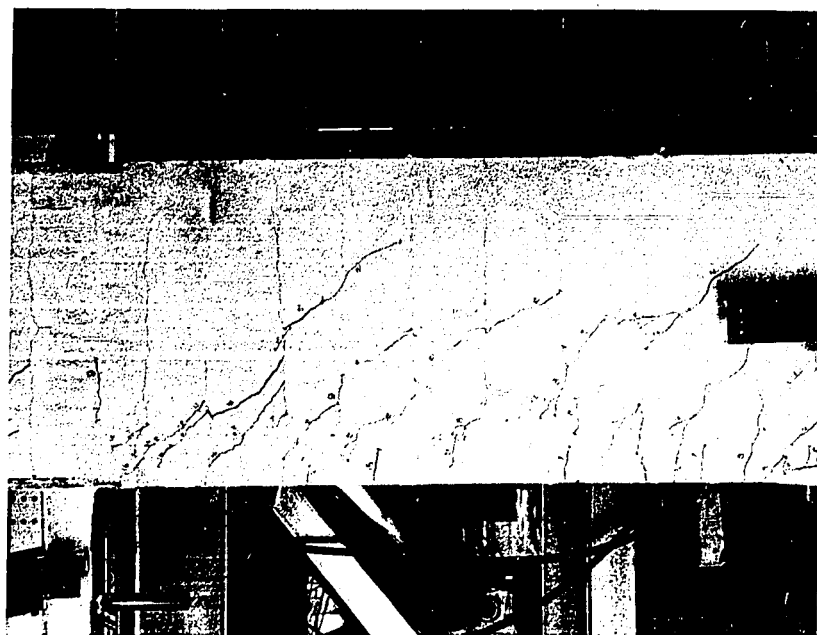


FIG. 6.16 CRACKING IN THE SHEAR WALL  
AFTER TESTING - FRAME B

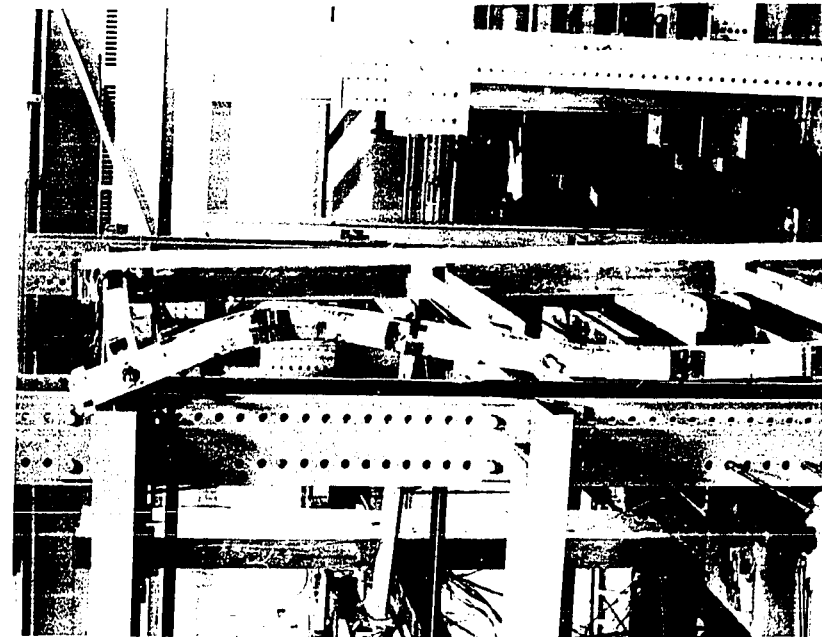


FIG. 6.17 LATERAL BUCKLING - FRAME B

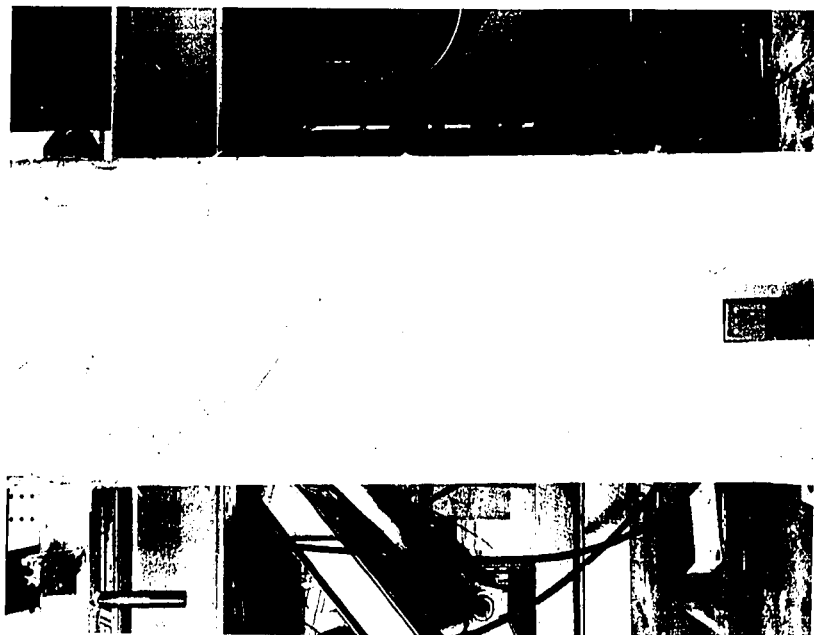


FIG. 6.16 CRACKING IN THE SHEAR WALL  
AFTER TESTING - FRAME B

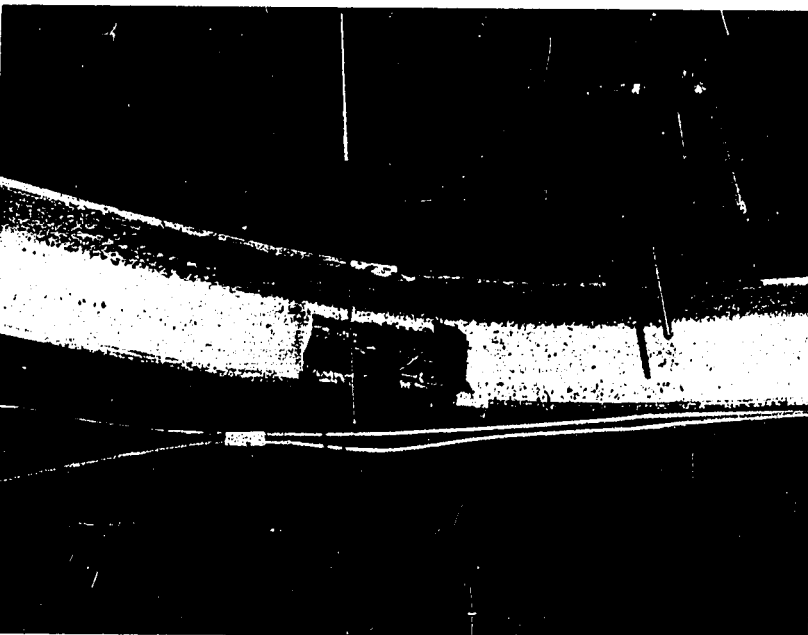


FIG. 6.18 FRONT VIEW OF TOP STORY COLUMN AFTER  
LATERAL BUCKLING - FRAME B

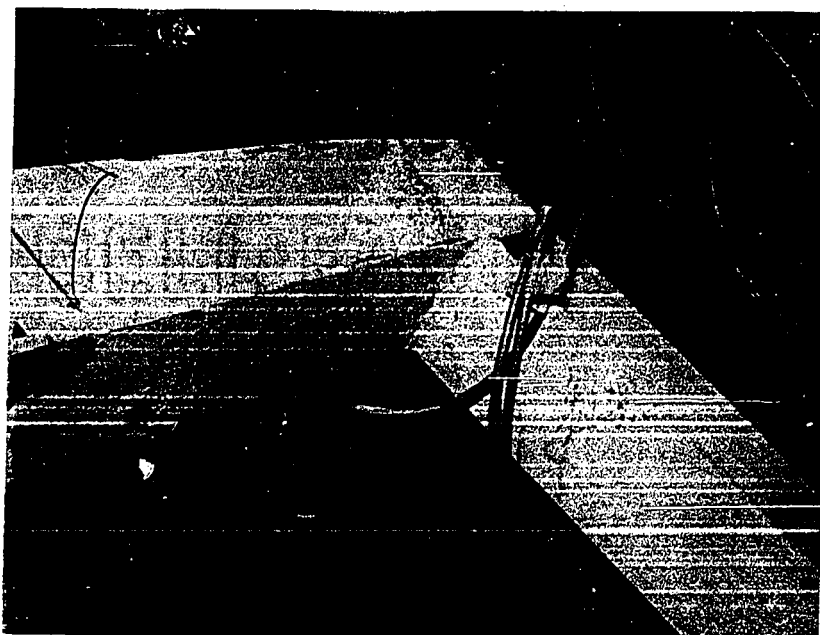


FIG. 6.19 THIRD LEVEL BEAM-TO-COLUMN JOINT  
AFTER TESTING - FRAME B

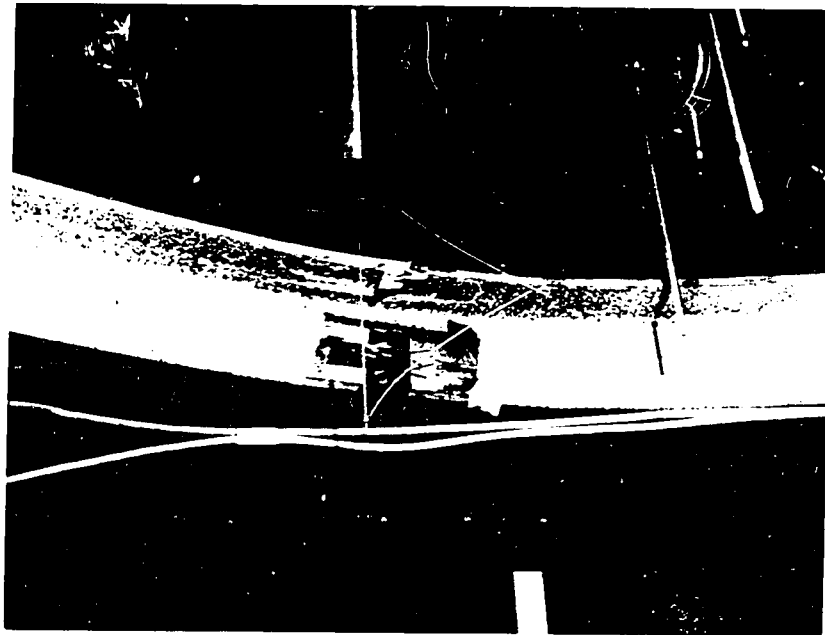


FIG. 6.18 FRONT VIEW OF TOP STORY COLUMN AFTER  
LATERAL BUCKLING - FRAME B

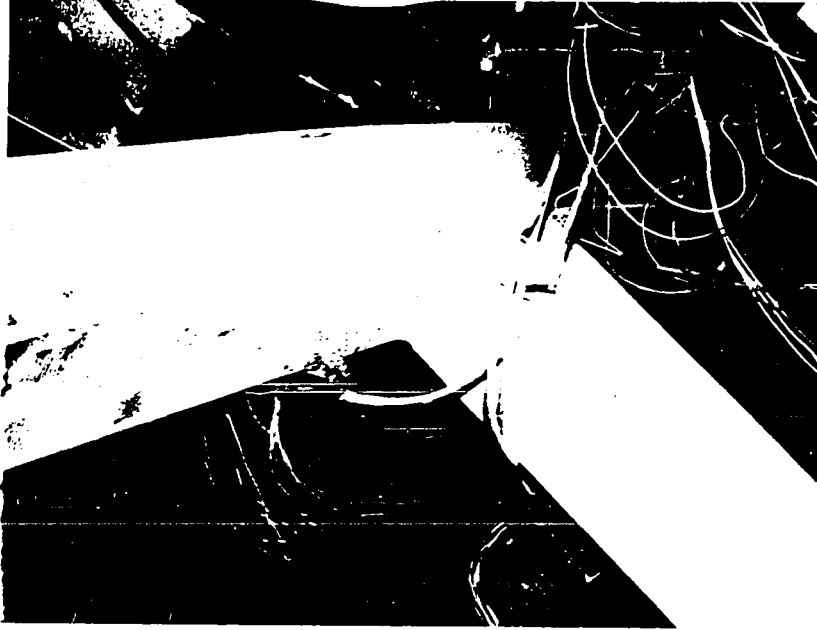


FIG. 6.19 THIRD LEVEL BEAM-TO-COLUMN JOINT  
AFTER TESTING - FRAME B

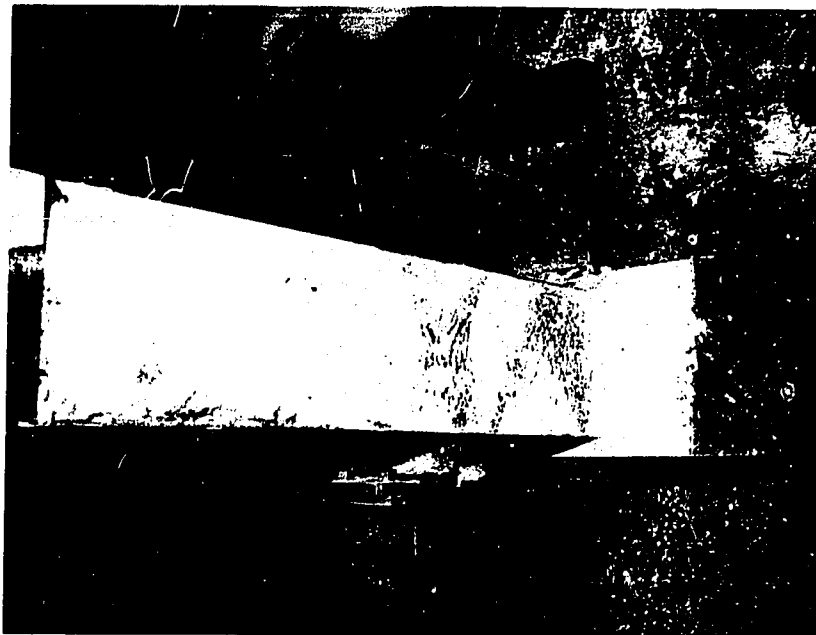


FIG. 6.20 PLASTIC HINGE AT THE COLUMN BASE - FRAME B



FIG. 6.21 SHEAR WALL BASE DETAIL - FRAME C

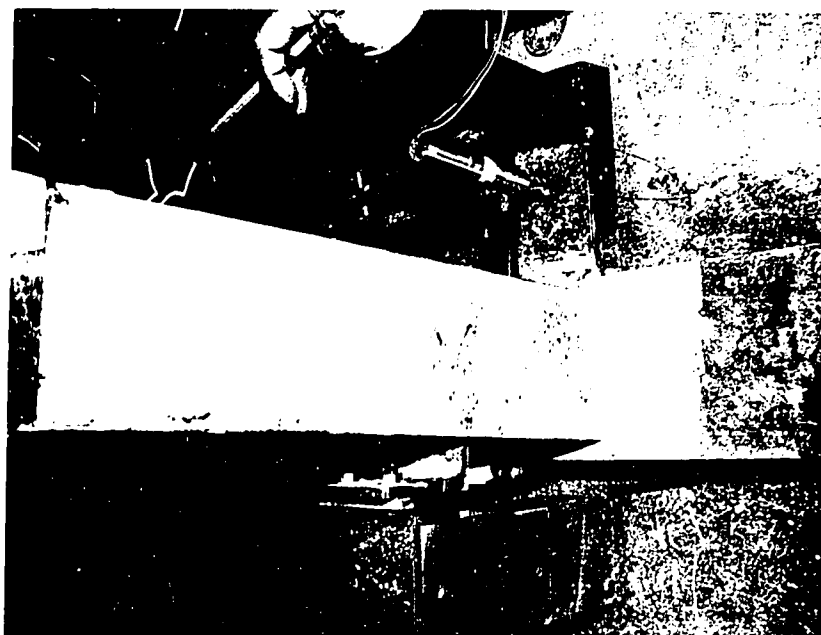


FIG. 6.20 PLASTIC HINGE AT THE COLUMN BASE - FRAME B



FIG. 6.21 SHEAR WALL BASE DETAIL - FRAME C

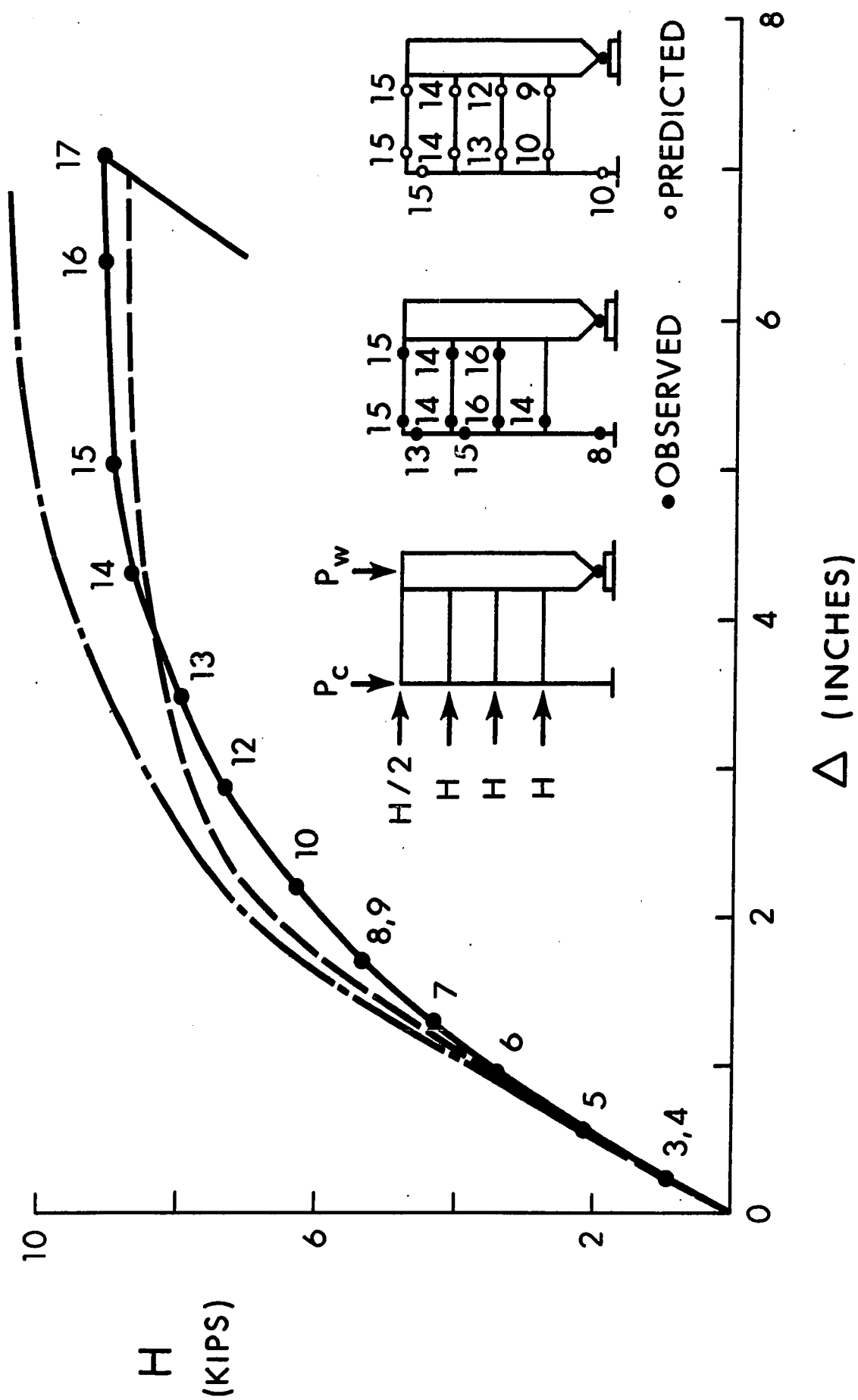


FIG. 6.22 LOAD-DEFLECTION RELATIONSHIPS - FRAME C



FIG. 6.23 PLASTIC HINGE IN THE TOP STORY COLUMN - FRAME C



FIG. 6.24 PLASTIC HINGE AT THIRD LEVEL BEAM - FRAME C



FIG. 6.23 PLASTIC HINGE IN THE TOP STORY COLUMN - FRAME C



FIG. 6.24 PLASTIC HINGE AT THIRD LEVEL BEAM - FRAME C

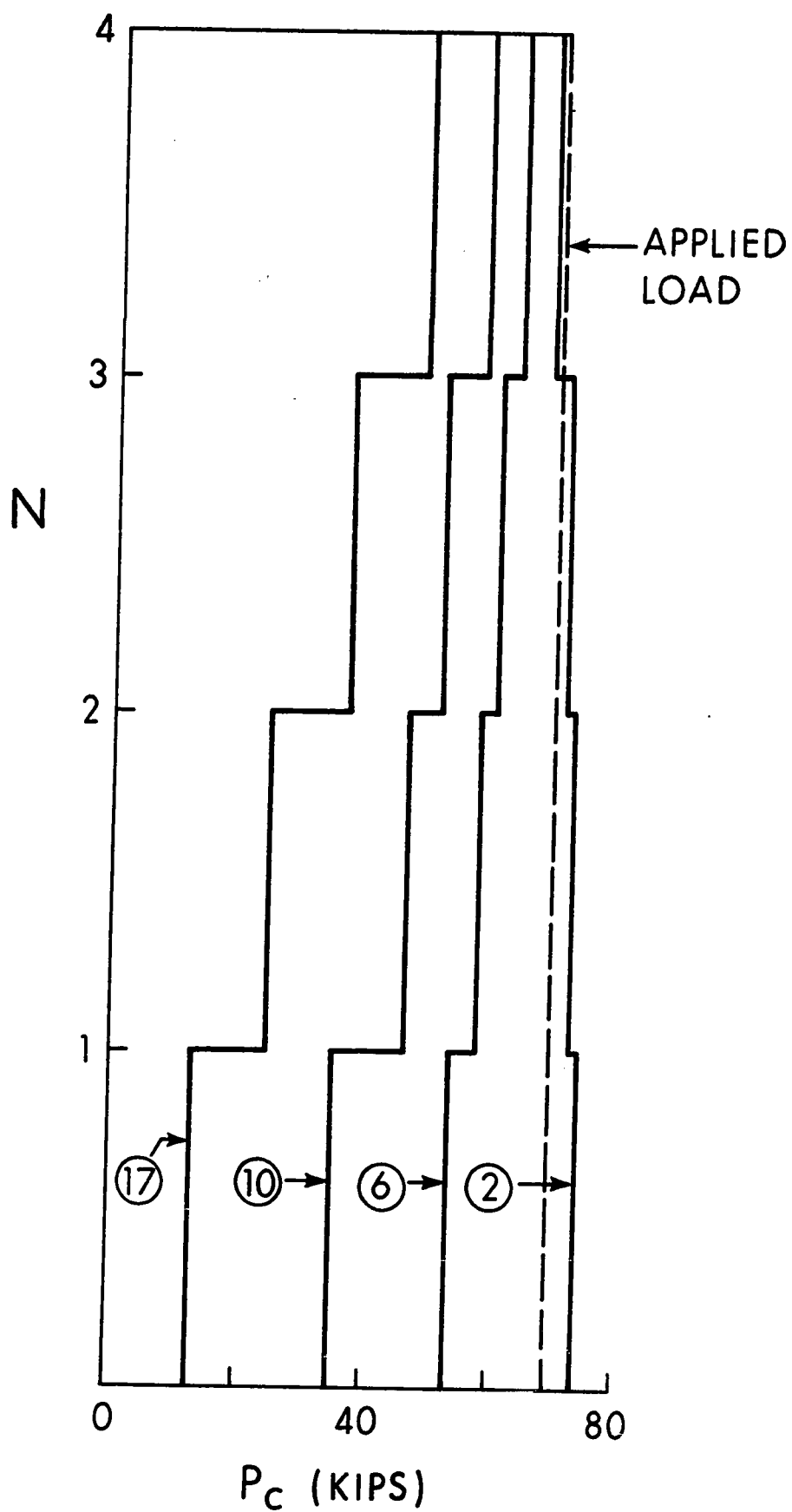


FIG. 6.25 AXIAL LOAD DISTRIBUTION IN THE COLUMN STACK - FRAME C

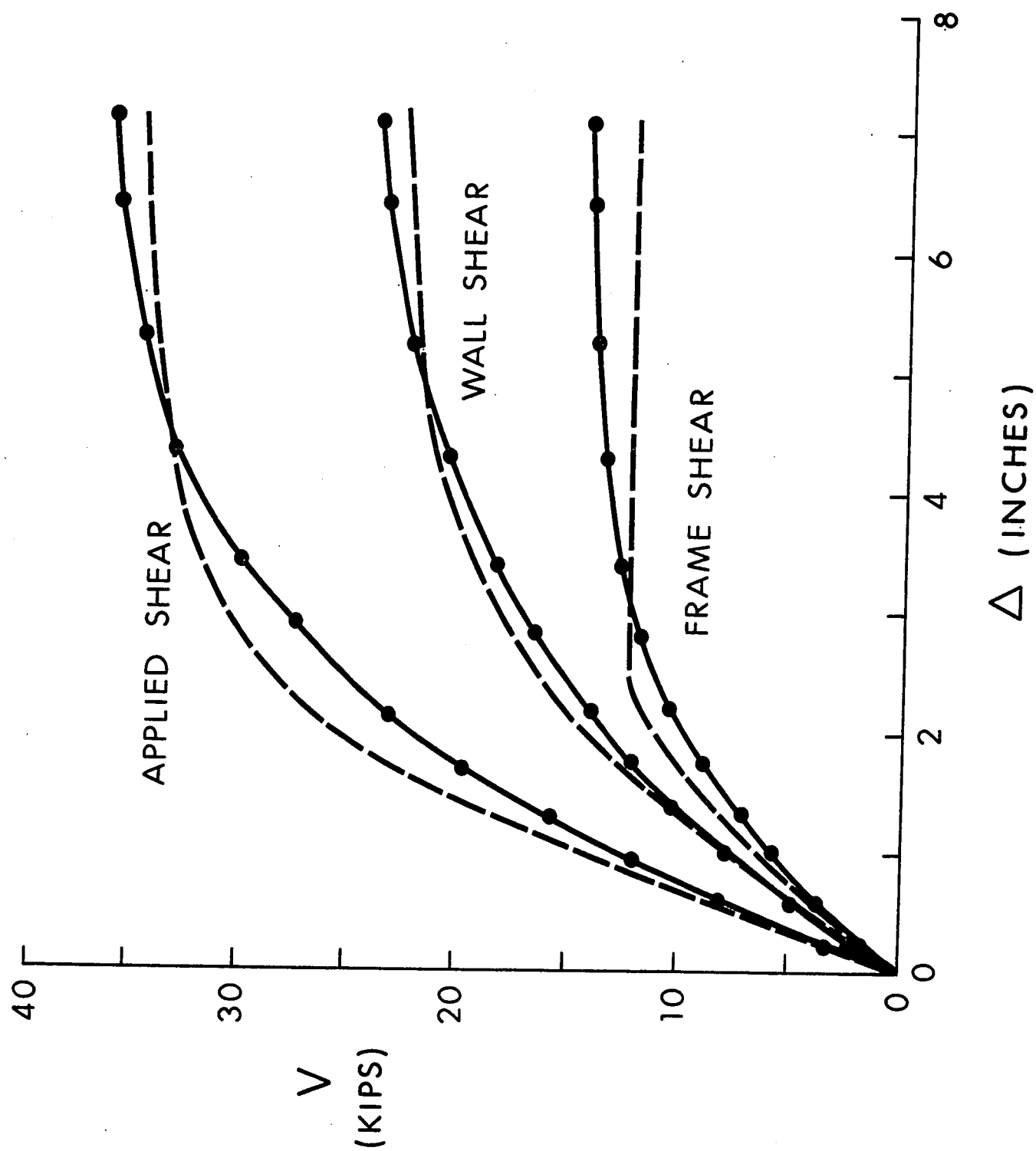


FIG. 6.26 BOTTOM STORY SHEAR DISTRIBUTION - FRAME C

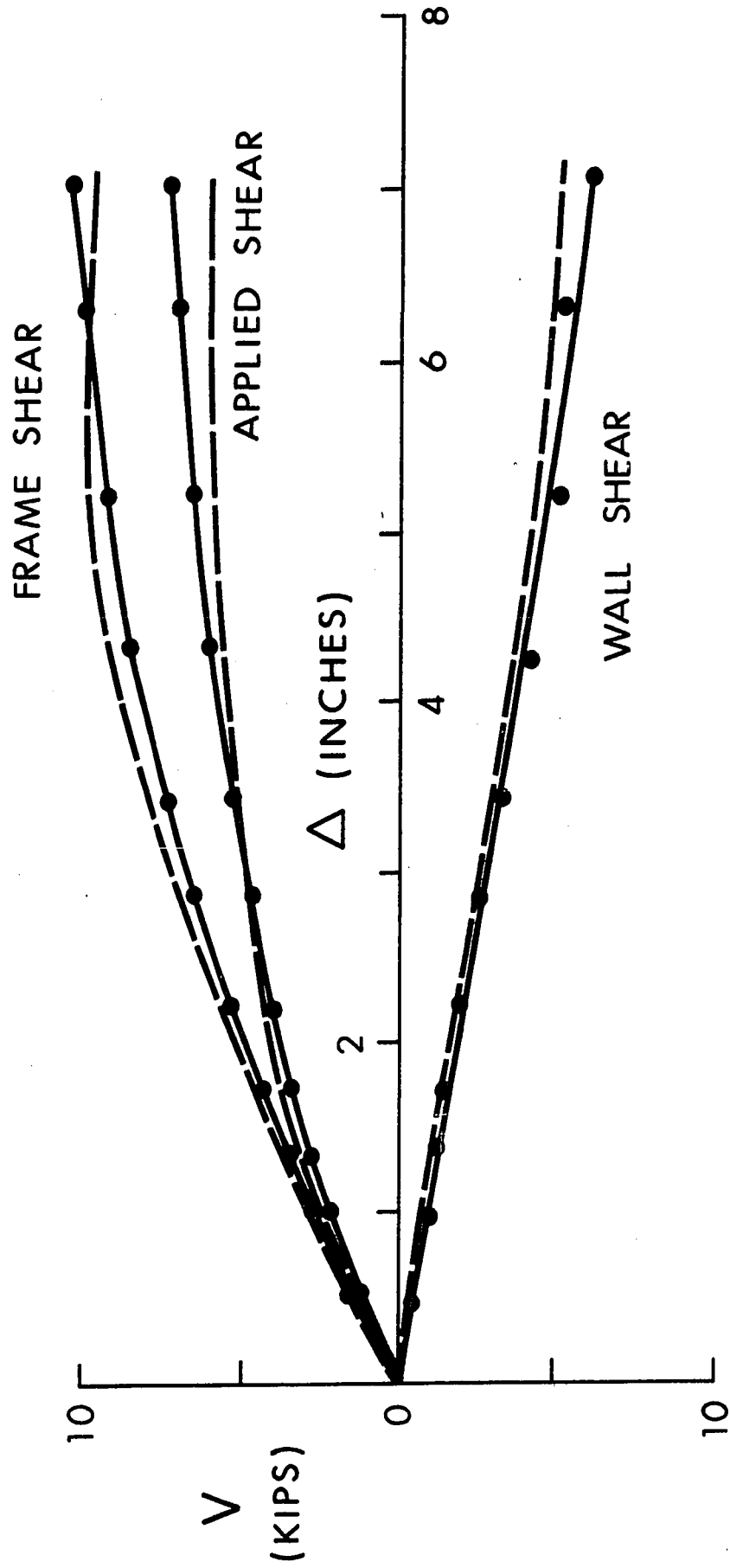


FIG. 6.27 TOP STORY SHEAR DISTRIBUTION - FRAME C

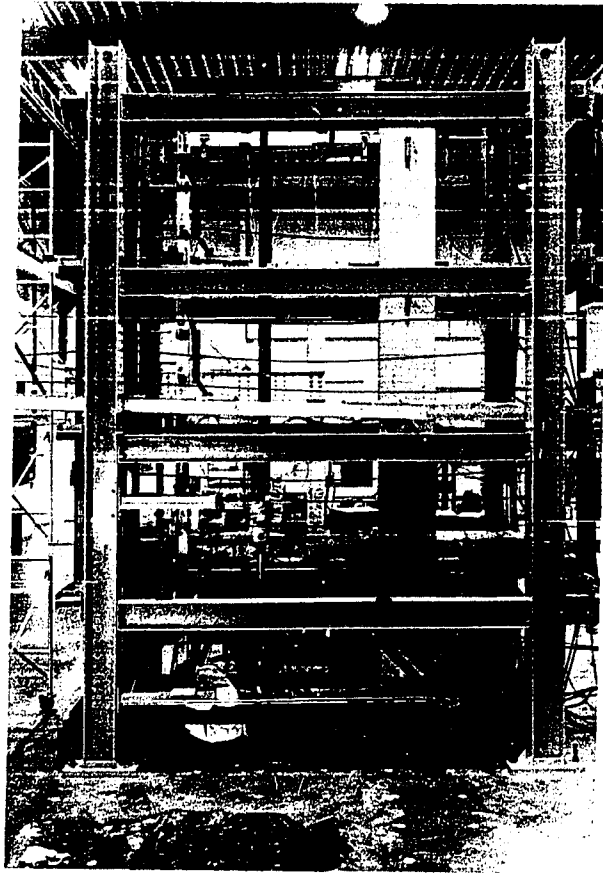


FIG. 6.28 FRAME C AFTER TESTING

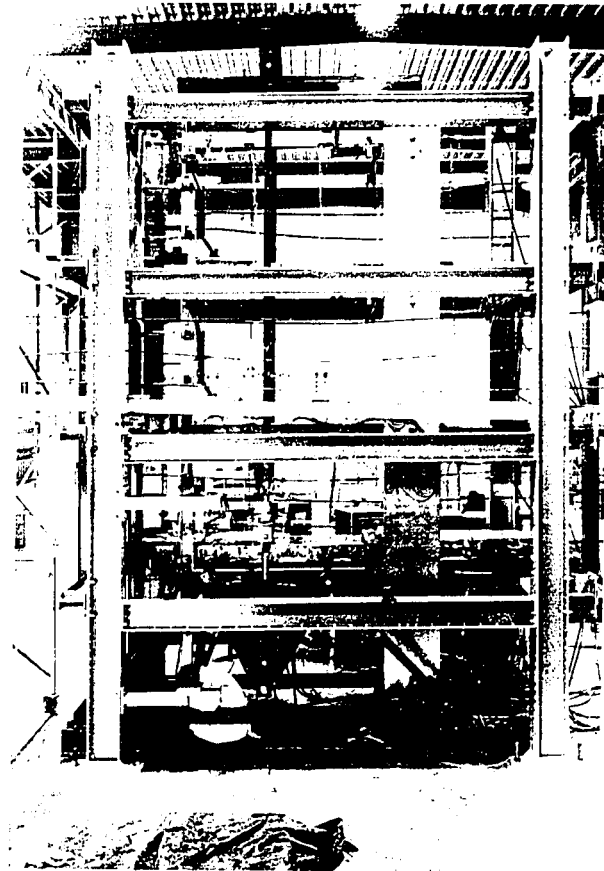


FIG. 6.28 FRAME C AFTER TESTING

## CHAPTER VII

### DISCUSSION OF TEST RESULTS

#### 7.1 Introduction

The results of tests on three coupled shear wall-frame test specimens have been presented in the previous chapter. The specimens were analyzed by a computer program based on the method of analysis described in Chapter III. This chapter compares the behavior of the test frames with the analytical predictions.

#### 7.2 Analytical Predictions

The response of each test specimen has been predicted by a second-order inelastic analysis, which considers the in-plane behavior of the structure. The effects of axial shortening and shear deformation of the members and the effect of axial load on the stiffnesses of the columns have been neglected. The moment-curvature relationships for the steel members are assumed to be elastic-plastic and since the influence of the uniformly distributed loads on the beam hinging patterns has been neglected the idealized plastic hinges will form at the ends of the members only. A bilinear moment-curvature relationship has been assumed for the shear wall, the slope of the strain-hardening branch being 1 in 300. As in planar steel frames (30,31), it will be shown here that a second-order in-

elastic analysis reliably predicted the response of the coupled shear wall -frame structures tested.

The responses of the test specimens were initially predicted by assuming the bases of the column and wall to be fixed. However, the bases rotated during the test as shown by the moment-rotation curve for the column base plotted in Fig. 6.1. The moment-rotation curves for the bases of the column and shear wall were approximated by straight lines and the computer program was modified to take the resulting flexibilities into account at the appropriate stages of loading.

The analysis assumes that hinges form at the geometric centers of the joints. Since the joints of a rigid frame are stiffer and stronger than the adjacent members, the hinges are forced away from the joint areas (31,46). This effectively strengthens the member in which the hinge forms. Hence, the effect of the shifts in hinge locations is to increase the ultimate load of the structure. This increase in strength has been incorporated into the analysis by assuming the plastic moment capacity at the geometric center of the joint is increased as shown in Fig. 7.1 to a value,  $M_p^*$

$$M_p^* = M_p \frac{\frac{L}{2}}{\frac{L}{2} - d} \quad (7.1)$$

where  $M_p$  is the plastic moment capacity of the section, and  $L$  is the center to center span of the member. This implies that a plastic

hinge will form in the member only when the plastic moment capacity has been achieved at a distance,  $d$ , equal to the depth of the member, from the joint center.

Another assumption in the analysis is that the beam-to-wall joints are rigid. In fact, these joints have some flexibility and this effect has been included in the analysis by increasing the effective lengths of the beams by an amount equal to half the beam depth (47). This modification slightly reduces the stiffness of the structure and hence the load-carrying capacity. In summary, the predicted responses include the  $P\Delta$  effect, the base rotations, the shift of the plastic hinge locations and the beam-to-wall joint flexibilities.

### 7.3 Discussion of Results - Frame A

The response of Frame A is plotted in Fig. 6.2. The broken curve in the figure represents the predicted behavior neglecting the  $P\Delta$  effect, while the dashed curve represents the predicted behavior including this effect. The full lines joining the solid circles represent the test results. As shown in Fig. 6.2, the  $P\Delta$  effect significantly influences the response of Frame A, reducing the predicted ultimate load by approximately 17%.

The response predicted by the second-order inelastic analysis agrees closely with the observed response of Frame A as illustrated in Fig. 6.2. In the analysis, the base of the shear wall developed its ultimate moment capacity at approximately Load No. 11. A mechanism

formed at Load No. 12; beyond this stage the load-deflection curve is essentially horizontal. For deflections beyond Load No. 12, the analysis underestimated the strength of the structure. The ultimate strength is 5% higher than predicted, possibly due to the influence of strain-hardening.

The predicted and observed hinge patterns for Frame A are shown in the inset to Fig. 6.2. The numbers adjacent to the open circles correspond to the Load Numbers at which the hinges formed (or were predicted). The first plastic hinge was predicted to form at the top of the fourth story column at Load No. 9; this corresponds to the observed behavior of the frame. As additional deformation is imposed, more hinges form in the girders and columns. Finally, the wall reaches its ultimate moment capacity at Load No. 11. Although the detailed sequence of hinge formation, as predicted by the analysis, was not followed, the trends are very similar.

The dashed curves in Fig. 6.3 represent the predicted bending moment diagrams for the frame members. The solid lines represent the bending moment diagram computed from strain gauge readings. The correlation between the predicted and observed bending moments is within 3% in all cases. Generally, the beam moments are slightly overestimated. The out of balance moments at the joints are within 5% of the beam moments, for all cases. The bending moment diagram at the ultimate load is shown in Fig. 6.3b; the theoretical predictions correspond to the observed sway deflection at Load No. 13. At this stage the theory underestimates the actual hinge moments, since it neglects the influence of strain-hardening.

The member ends at plastic hinge locations rotated significantly (without any evident local buckling) as shown in the load-rotation curve in Fig. 6.5. The dashed curve represents the predicted joint rotations at the top of the top story column. The predicted and observed values are in good agreement, however, larger discrepancies occurred at other hinge locations. Hinge reversals were not observed at any of the plastic hinge locations.

The axial load distributions in the column stack at Load Numbers 6, 9 and 13 are shown in Fig. 6.8. The column is located on the 'windward' side of the specimen. For this structure, the application of lateral load causes the axial load to decrease in the column stack and increase in the shear wall.

Due to the application of the lateral load, the beams of Frame A deform in a double-curvature mode. Thus, the reaction from the beam reduces the applied axial load in the column stack, with the maximum reduction in the bottom story. The first lateral load is applied on the structure at Load No. 6. At this stage, the net axial load is less than the applied axial load over the column stack as shown in Fig. 6.8. At the bottom story, the difference between these loads is approximately 10%. With the application of additional lateral loads, the net axial load in the column decreases further as shown in the axial load distributions at Load Nos. 9 and 13 in Fig. 6.8. At the ultimate load (Load No. 13), the net axial load is approximately 28% less than the applied load at the top of

the column. In an actual building, this change in axial load will depend on the arrangements of columns and shear walls in different bents of the structure.

The predicted bending moment distributions in the shear wall for Load Nos. 9 and 13 are shown by the dashed lines in Fig. 6.9. The agreement between the predicted and observed values is within 10% compared with 3% of the steel frame. This is to be expected, partly because of the variability of the material. At the beam-to-wall joints the out of balance moments are within 5% of the beam moments, in all cases.

In summary, the results of the test of Frame A showed good agreement with the results predicted by the modified second-order inelastic analysis. For this structure, the  $P\Delta$  effect influenced the ultimate load significantly.

#### 7.4 Discussion of Results - Frame B

The behavior of Frame B has also been compared with the theoretical predictions. As mentioned in the previous chapter, scattered yielding was observed in the top two column segments due to the application of vertical loads; hence the lateral loads were applied to a partly yielded structure. The idealized moment-curvature relationship (Fig. 3.6) used in this analysis is not directly applicable to the columns of Frame B, since yielding occurred along the column length before the application of lateral loads. Thus the stiffness of the structure is reduced considerably. This effect has been included in the theoretical analysis by reducing the stiffness (26) of the affected columns to correspond with the re-

maintaining elastic core of the cross-section.

The responses of Frame B (with and without the  $P\Delta$  effect) are shown by the dashed and broken curves respectively in Fig. 6.13. In this case, the predicted ultimate load was reduced by approximately 12% due to the  $P\Delta$  effect. Up to Load No. 6, the agreement between the observed and predicted responses is satisfactory. However, beyond this point, the connection at the third level beam-to-wall joint showed signs of slipping. The lateral load was removed at Load No. 7 and the joint repaired. After reloading, the structure behaved as expected, with the shapes of the predicted and observed load-deflection curves agreeing closely.

As additional lateral loads were applied, the bending moments caused yielding to spread from the beam-to-column joints along the height of the column. The out-of-plane and torsional movements were measured at mid-height of each column. These increased gradually as expected, until the structure had achieved its ultimate load (Load No. 14). At this stage, the column suddenly buckled about its weak axis, between points of lateral restraint.

Inelastic action was mainly concentrated in the column. The predicted and observed hinge patterns are shown in the inset to Fig. 6.13. The difference between the predicted and observed hinge patterns is apparently due to additional girder flexibility caused by slippage at the beam-to-wall joints. Hinges did not form at these locations, even though predicted.

Frame B simulated the behavior of the bottom portion of a tall structure and attained approximately the ultimate load predicted by the modified analysis. However, a distinct lack of ductility was exhibited by Frame B, since the structure failed prematurely due to lateral buckling of the column. For Frame B, the mid-height brace in each column was omitted and the column slenderness ratio was 64, above the accepted limit of 54 (45). This column would be acceptable according to the proposed design rules for braced frames (45), with a slight reduction in moment capacity. The influence of the spacing of lateral bracing on the behavior of a multi-story structure is therefore dramatically illustrated by the difference in behavior of Frames A and B.

#### 7.5 Discussion of Results - Frame C

Frame C exhibited behavior characteristic of the upper portion of a tall structure. In Fig. 6.22, the broken curve is the predicted response without the  $P\Delta$  effect and the dashed curve includes this effect. Although the applied axial load is much smaller in Frame C, as compared to Frames A and B, the  $P\Delta$  effect reduced the ultimate load by approximately 16%. This high reduction can be partly attributed to the hinged base condition of the shear wall. The second-order theory overestimates the stiffness of the structure in the intermediate stages of loading. The theory underestimates the ultimate strength by approximately 4%. As in Frame A, this is possibly due

to the neglect of strain-hardening in the analysis.

The observed and predicted hinge configurations are shown in the inset to Fig. 6.22 and a reasonable correlation exists between the two. The first yielding in the structure was observed at the base of the column, although the predicted first hinge is at the first level beam-to-wall joint. As in Frame A, the final plastic hinge patterns are almost identical, although the detailed sequence of hinge formation is not followed.

The axial load distributions in the column stack of Frame C is shown in Fig. 6.25 for four stages of loading. At Load No. 2, the structure is subjected to axial load only. At this stage, the axial load in the column increased towards the bottom on account of the axial shortening effect. At this stage, the difference between the applied and developed axial load is approximately 5% in the bottom story. As more and more lateral load is applied, the net axial load in the column decreases as shown in the axial load distributions for Load Numbers 6, 10 and 17 in Fig. 6.22. At the ultimate load (Load No. 17), the axial load in the bottom story varied significantly from the applied reaction at the top of the column.

The above behavior corresponds to the pulling of the test specimen, which means that the column stack is located on the windward side of the structure while the shear wall is located on the leeward side. However, if the structure was pushed in the opposite direction, the axial loads in the column stack would increase and

hence yielding would occur earlier, this would accentuate the possibility of local buckling, lateral buckling or lateral-torsional buckling in the column stack.

The lateral shear distribution in the 24 story structure ( $K_r = 50$ ,  $M_r = 5$ ) has been studied in detail in Chapter IV. The design of Frame C is based on the shear distribution of the upper portion of this structure. In the top story of this structure, the frame system develops shears which are many times greater than the applied shears. In order to balance the applied shears, the wall develops shears which act in the opposite direction. In the lower stories, the 'whipping action' diminishes and at the 19th story, the shears in the frame and wall act in the same direction. In the lower portion of the structure, the shear wall carries the bulk of the shear, for example at the bottom story the wall carries 95% of the total applied shear. The shear distributions for the bottom and top stories of Frame C are shown in Fig. 6.26 and 6.27 respectively. These distributions are similar to those for the corresponding stories of the 24 story structure.

At the bottom story of Frame C, the shear wall carries approximately 51% of the total applied shear as shown in Fig. 6.26. The dashed curves in this figure correspond to the second-order analysis. In this analysis, the frame resists additional shears until hinges form in the first level beam and column base. Beyond this point, the additional applied shears are carried by the shear

wall alone. However, the observed response of the frame shows an increase in shear even after the formation of the above hinges. This is possibly due to the effect of strain-hardening at the plastic hinge locations.

In the top story of Frame C, the analytical response agreed closely with the observed response as shown in Fig. 6.27. The frame resists a shear equal to 1.5 times the applied shear in the top story of Frame C, at the ultimate load. In this case, the shear force in the wall acts to load the column. As mentioned before, this 'whipping action' will be even more pronounced in a taller structure, depending on the relative stiffnesses and strengths of the shear wall, column and beam. The high shears in the upper portion of the structure may lead to early hinging. This in turn leads to earlier deterioration of the structure, which accentuates the  $P\Delta$  effect. Hence, a rational analysis and design procedure should consider the interaction of the frame and shear wall up to the ultimate load.

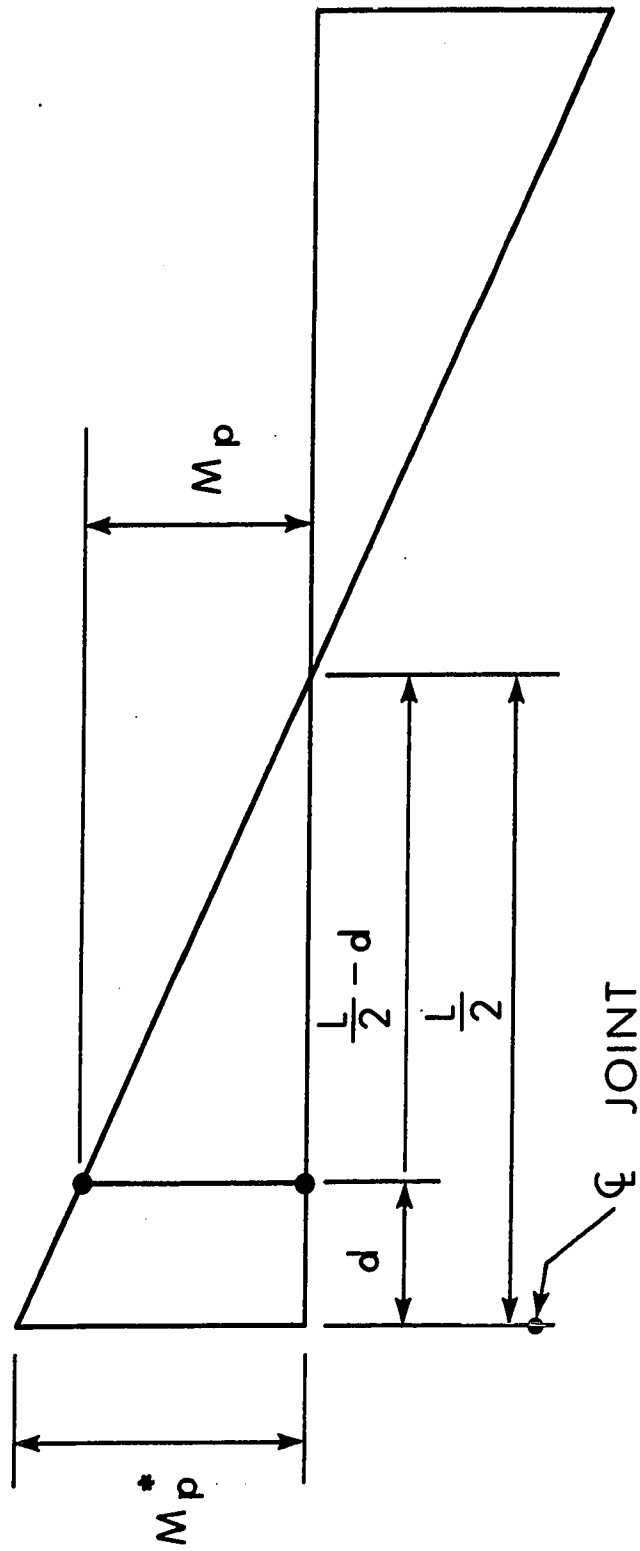


FIG. 7.1 MIGRATION OF PLASTIC HINGE

## CHAPTER VIII

## SUMMARY, CONCLUSIONS AND RECOMMENDATIONS

8.1 Summary

This dissertation has presented a second-order analysis for coupled shear wall-frame structures which traces the response of the structure up to the ultimate load. Based on the behavioral study of a 24 story structure, a program of large-scale tests was initiated. The applicability and rationality of the present method of analysis is assessed by comparing the theoretical predictions with the results of experiments on carefully chosen specimens.

For the analysis, the actual structure is first lumped into an analytical model. The structure is then analyzed under a constant vertical load and monotonically increasing lateral loads. The analysis takes into account the formation of plastic hinges in the frame, the inelastic action of the shear wall and the secondary moments caused by the  $P\Delta$  effect. In the inelastic range, the slope-deflection equations are modified to consider members at different stages of plastic hinge formation. The analysis considers the inelastic action of the shear wall by modifying the stiffness of the yielded segments of the wall so as to be consistent with the assumed moment-curvature relationship. The  $P\Delta$  effect has been simulated at each loading stage by analyzing the structure under an additional

equivalent lateral force. A Fortran Program has been developed to perform the analysis. Using the program, several structures have been analyzed; the results in the inelastic range, compared closely with those reported in the literature.

The behavior of a 24 story structure has been studied in detail. Based on this study, three test specimens were designed to simulate the action of portions of a taller structure and to investigate the aspects of behavior for which analytical techniques are inadequate.

The specimens consist of a single shear wall and column stack rigidly connected at four levels by girders. Frame A was designed to simulate the behavior of the bottom stories of a tall structure, with heavily loaded columns subjected to significant inelastic deformation. Frame B also simulated the behavior of this portion of the structure, but the columns were not adequately braced. Finally, Frame C was designed to exhibit the 'whipping action' characteristic of the top stories of a coupled shear wall-frame structure. The response predicted by the second-order elastic-plastic analysis agreed closely with the observed response. Frame B reached the predicted ultimate load, but exhibited a distinct lack of ductility. The frame failed suddenly when the column stack buckled about its weak axis.

All three tests were planned as a part of a program to develop design procedures for coupled structures. The facets of behavior discussed, with the exception of the lateral column buckling,

have been included in the design method (40) described in Chapter IV (Appendix E).

## 8.2 Conclusions

The analysis presented in the early portion of this dissertation adequately predicts the response of a coupled shear wall-frame structure. The ill-conditioning problem, which may arise because of the large difference in stiffness between the various structural elements, is eliminated by the iterative solution procedure. The behavioral study of the 24 story structure, indicated that the distribution of lateral load between the shear wall and the frame system is complex and depends on the interaction among the various elements. The  $P\Delta$  effect, combined with the inelastic action of the wall and frame caused a significant reduction in the load-carrying capacity of the structure. The load-carrying capacity of a given structure increased with increases in the wall-to-column stiffness and/or strength ratios. The results of tests on specimens designed to simulate the behavior of portions of the structure can be adequately predicted by the second-order elastic-plastic analysis.

Two types of behavior exist in different portions of a coupled shear wall-frame structure. First, the bottom story columns are subjected to high axial loads. Before the structure attains its ultimate load, these columns may be forced to deform significantly in the inelastic range. Second, in the top stories of a tall structure, the frame system develops shears which are many times greater than the

applied shears. Consequently, early hinging and a corresponding reduction in stiffness and local-carrying capacity may result from this action. The design method presented herein is able to account for both types of behavior.

### 8.3 Future Recommendations

The present second-order inelastic analysis closely predicted the response of coupled shear wall-frame structures. However, several aspects of behavior require further investigation.

It has been observed (28) that the neglect of axial shortening may lead to an underestimate of the sway deflections without altering the ultimate load appreciably. Also, the shear deformation of the wall may be significant, particularly in the lower portions (17). The present analysis should be extended to include these effects. In order to understand the behavior of the structure fully, the unloading branch of the load-deflection curve should also be determined.

Additional large-scale tests are indicated; the specimens should be specifically designed to investigate the influence of transverse beam loads and to further explore the implications of the column lateral bracing spacing. An extension of the testing program should also investigate the behavior of structures unsymmetrical in plan.

## LIST OF REFERENCES

1. Beedle et al, "Structural Steel Design," The Ronald Press Company, New York, 1964.
2. Khan, F.R., "Current Trends in Concrete High-Rise Buildings," Tall Buildings, Proceedings of a Symposium held at the University of Southampton, Pergamon Press, April, 1966.
3. Benjamin, J.R., "Statically Indeterminate Structures," McGraw-Hill Book Co. Inc., New York, 1959.
4. Coull, A., and Smith, B.S., "Analysis of Shear Wall Structures (A Review of Previous Research)," Tall Buildings, Proceedings of a Symposium held at the University of Southampton, Pergamon Press, April, 1966.
5. Beck, Hubert, "Contribution to the Analysis of Coupled Shear Walls," ACI Journal, Proceedings V. 59, August 1962.
6. Rosman, Riko, "Approximate Analysis of Shear Walls Subjected to Lateral Loads," ACI Journal, Proceedings, V. 61, June, 1964.
7. Coull, A., and Choudhury, J.R., "Analysis of Coupled Shear Walls," ACI Journal, Proceedings V. 64, September, 1967.
8. Coull, A., and Puri, R.D., "Analysis of Pierced Shear Walls," Proceedings ASCE, V. 94, ST1, January, 1968.
9. Girijavallabhan, C.V., "Analysis of Shear Walls with Openings," Proceedings ASCE, V. 95, ST10, October, 1969.

10. Cardan, B., "Concrete Shear Walls Combined with Rigid Frames in Multi-Story Buildings Subject to Lateral Loads," ACI Journal, Proceedings V. 58, September, 1961.
11. Bandel, H., "Frames Combined with Shear Trusses under Lateral Loads," Proceedings ASCE, V. 88, ST6, December, 1962.
12. Gould, P.L., "Interaction of Shear Wall-Frame Systems in Multi-story Buildings," ACI Journal, Proceedings V. 62, January, 1962.
13. Oakberg, R.G., and Weaver, W.W., "Analysis of Frames with Shear Walls by Finite Elements," Proceedings of the Symposium on Applications of Finite Element Method in Civil Engineering, Vanderbilt University, Nashville, Tennessee, November, 1969.
14. Rosenbleuth, E., and Holtz, J., "Elastic Analysis of Shear Walls in Tall Buildings," ACI Journal, Proceedings V. 31, June, 1960.
15. Rosman, R., "Laterally Loaded Systems Consisting of Walls and Frames," Tall Buildings, Proceedings of a Symposium held at the University of Southampton, Pergamon Press, April, 1966.
16. Parme, A.L., "Design of Combined Frames and Shear Walls," P.C.A. Advanced Engineering Bulletin No. 14, 1965.
17. Goldberg, J.E., "Analysis of Multistory Buildings Considering Shear Wall and Floor Deformation," Tall Buildings, Proceedings of a Symposium held at the University of Southampton, Pergamon Press, April, 1966.

18. Tezcan, S.S., "Analysis and Design of Shear Wall Structures," Tall Buildings, Proceedings of a Symposium held at the University of Southampton, Pergamon Press, April, 1966.
19. Clough, R.W., Wilson, E.L., and King, I.P., "Large Capacity Multi-Story Frame Analysis Programs," Proceedings ASCE, V. 89, ST4, August, 1963.
20. Clough, R.W., King, I.P., and Wilson, E.L., "Structural Analysis of Multi-Story Buildings," Proceedings ASCE, V. 90, ST3, June, 1964.
21. Khan, F.R., and Sbarounis, J.A., "Interaction of Shear Wall with Frames in Concrete Structures under Lateral Loads," Proceedings ASCE, V. 90, ST3, June, 1964.
22. Beedle, L.S., Lu, L.W., and Lim, L.C., "Recent Developments in Plastic Design Practice," Proceedings ASCE, V. 95, ST9, September, 1969.
23. Korn, A., and Galambos, T.V., "Behavior of Elastic-Plastic Frames," Proceedings ASCE, V. 94, ST5, May, 1968.
24. Jennings, A., and Majid, K., "An Elastic-Plastic Analysis by Computer for Framed Structures Loaded up to Collapse," The Structural Engineer, Vol. 43, No. 12, 1965.
25. Davies, J.M., "The Stability of Plane Frameworks under Static and Repeated Loading," Ph.D. Thesis, Victoria University of Manchester, 1965.

26. Parikh, B.P., "Elastic-Plastic Analysis and Design of Unbraced Multi-Story Steel Frames," Fritz Engineering Laboratory Report No. 273.44, Lehigh University, 1966.
27. Daniels, J.H., and Lu, L.W., "The Subassemblage Method of Designing Unbraced Multistory Frames," Fritz Engineering Laboratory Report No. 273.37, Lehigh University, February, 1966.
28. Clark, W.J., and MacGregor, J.G., "Analysis of Reinforced Concrete Shear Wall-Frame Structures," Structural Engineering Report No. 16, University of Alberta, Edmonton, November, 1968.
29. Yura, J.A., "The Strength of Braced Multistory Steel Frames," Fritz Engineering Laboratory Report No. 273.28, Lehigh University, September, 1965.
30. Yarimci, E., "Incremental Inelastic Analysis of Framed Structures and Some Experimental Verifications," Fritz Engineering Laboratory Report No. 273.45, Lehigh University, May, 1966.
31. Arnold, P., Adams, P.F., and Lu, L.W., "Strength and Behavior of an Inelastic Hybrid Frame," Proceedings ASCE, V. 94, ST1, January, 1968.
32. Arnold, P., Adams, P.F., and Lu, L.W., "The Effect of Instability on the Cyclical Behavior of a Frame," International Symposium on the Effects of Repeated Loading of Materials and Structural Elements, Mexico City, September, 1966.

33. Carpenter, L.D., and Lu, L.W., "Behavior of Steel Frames Subjected to Repeated and Reversed Loads," Final Report, 8th Congress of the International Association for Bridge and Structural Engineering, New York, September, 1968.
34. Nikhed, R.P., MacGregor, J.G., and Adams, P.F., "Studies of Reinforced Concrete Shear Wall-Frame Structures," Structural Engineering Report No. 25, University of Alberta, Edmonton, June, 1970.
35. Kloucek, C.V., "Distribution of Deformation," Orbis Ltd., Prague, 1949.
36. Lightfoot, E., "Substitute Frames in the Analysis of Rigid-Jointed Structure - Part I and II, "Civil Engineering and Public Works Review, December, 1957 and January, 1958.
37. Frischmann, W.W., Prabhu, S.S., and Toppler, J.F., "Multi-Story Frames and Interconnected Shear Walls Subjected to Lateral Loads," Part I and II, Concrete and Constructional Engineering, June and July, 1963,
38. Majumdar, S.N.G., Nikhed, R.P., MacGregor, J.G. and Adams, P.F., "Approximate Analysis of Frame-Shear Wall Structures," Structural Engineering Report No. 14, University of Alberta, Edmonton, May, 1968.
39. "Plastic Design of Multi-Story Frames (Lecture Notes)," Fritz Engineering Laboratory Report No. 273.20, Lehigh, University, 1965.

40. Adams, P.F. and MacGregor, J.G., "Plastic Design of Coupled Frame-Shear Wall Structures," Proceedings ASCE, Vol. 96, ST9, September, 1970.
41. "General Information on Structural Steel," Publication No. 2074, Canadian Institute of Steel Construction, Toronto, Ontario, March, 1970.
42. "Handbook of Steel Construction", Canadian Institute of Steel Construction, Toronto, Ontario, 1967.
43. Yarimci, E., Yura, J.A., and Lu, L.W., "Techniques for Testing Structures Permitted to Sway," Experimental Mechanics, Society for Experimental Stress Analysis, Vol. 7, No. 8, August, 1967, pp. 76-84.
44. Dunkerly, S., and Morley, A., "Mechanism," Longmans Green and Co., London, 1928, p. 120.
45. "Plastic Design of Braced Multi-Story Frames," American Iron and Steel Institute, New York, 1968.
46. Lay, M.G., and Galambos, T.V., "The Experimental Behavior of Restrained Columns," Bulletin No. 110, Welding Research Council, New York, November, 1966.
47. Michael, D., "The Effect of Local Wall Deformations on the Elastic Interaction of Cross Walls Coupled by Beams," Tall Buildings, Proceedings of a Symposium held at the University of Southampton, Pergamon Press, April, 1966.
48. Huber, A.W., and Beedle, L.S., "Residual Stress and the Compressive Strength of Steel," Welding Journal, 33(12), Research Supplement 589-S to 614 S, December, 1954.

49. Delicate, D.J.R., "Cold Work Effects on Material Properties of Steel," Civ. Eng. 459 Report, University of Alberta, Edmonton, May, 1970.
50. Adams, P.F., Lay, M.G., and Galambos, T.V., "Experiments on High Strength Steel Members," Welding Research Council, Bulletin No. 110, November 1965.

## APPENDIX A

## DERIVATION OF JOINT ROTATION EQUATIONS

The frame system has been forced into the deformed shape of the wall shown in Fig. 3.10. Applying the slope-deflection equations, the moment  $M_{bwi}$  at the end  $b_i$  of the right beam is given by:

$$M_{bwi} = KE_{wbi}(4\theta_i + 2\theta_{wbi} - 6\rho_{wbi}) \quad (A.1)$$

where  $KE_{wbi} = EI/L$  is the stiffness of the right beam ( $b_iw_i$ ) and  $\rho_{wbi}$  is the vertical chord rotation of the right beam connecting the column to the wall. Also in the above equation,  $\theta_i$  is the rotation of the frame joint and  $\theta_{wbi}$  is the rotation at the wall end of the right beam, in the  $i$ th story.

Considering the left beam  $b_if_i$  and applying the slope-deflection equation; assuming that the joint rotations at the two ends  $b_i$  and  $f_i$  are equal, the moment  $M_{bfi}$ , at the end  $f_i$  is given by:

$$M_{bfi} = 6 \cdot KE_{bfi} \cdot \theta_i \quad (A.2)$$

The column  $b_i b_{i+1}$  between the  $i$  th and the  $i+1$  th story had a stiffness of  $KE_{ci+1}$  and the chord rotation of this column is  $\rho_{ci+1}$ . The moment,  $M_{ci+1}$ , at the bottom end  $b_i$  of the column  $b_i b_{i+1}$  is given by

$$M_{ci+1} = KE_{ci} (4\theta_i + 2\theta_{i+1} - 6\rho_{ci+1}) \quad (A.3)$$

where  $\theta_{i+1}$  is the rotation of the frame joint at the  $i+1$  th level.

The moment,  $M_{ci}$ , at the top end,  $b_i$ , of the column  $b_i b_{i-1}$  is given by:

$$M_{ci} = KE_{ci} (4\theta_i + 2\theta_{i-1} - 6\rho_{ci}) \quad (A.4)$$

where  $KE_{ci} = EI/L$  is the stiffness of the column  $b_i b_{i-1}$  and  $\rho_{ci}$  is the chord rotation of the column.  $\theta_{i-1}$  is the rotation of the frame joint at the  $i-1$  th level.

Equating the sum of the joint moments to zero

$$M_{bwi} + M_{bfi} + M_{ci} + M_{ci+1} = 0 \quad (A.5)$$

and substituting the values of the end moments from the above equations the joint equilibrium equation becomes:

$$KE_{wbi} (4\theta_i + 2\theta_{wbi} - 6\rho_{wbi}) + 6KE_{bfi} \theta_i +$$

$$KE_{ci} (4\theta_i + 2\theta_{i-1} - 6\rho_{ci}) + KE_{c\ i+1}$$

$$(4\theta_i + 2\theta_{i+1} - 6\rho_{c\ i+1}) = 0 \quad (A.6)$$

and after simplification

$$\theta_i = \{KE_{wbi} (6\rho_{wbi} - 2\theta_{wbi}) + KE_{ci} (6\rho_{ci} - 2\theta_{i-1})$$

$$+ KE_{c\ i+1} (6\rho_{c\ i+1} - 2\theta_{i+1})\} / \{4KE_{wbi} + 4KE_{ci} +$$

$$4KE_{c\ i+1} + 6KE_{bfi}\} \quad (A.7)$$

Equation (A.7) can be written in the following simplified form

$$\theta_i = \frac{A + B + C + D}{A + B + C + D} \quad (A.8)$$

Where in the numerator,

$$A = KE_{wbi} (6\rho_{wbi} - 2\theta_{wbi})$$

$$B = KE_{ci} (6\rho_{ci} - 2\theta_{i-1})$$

$$C = KE_{c \ i+1} (6\rho_{c \ i+1} - 2\theta_{i+1})$$

and

$$D = 0$$

And in the denominator,

$$A' = 4KE_{wbi}$$

$$B' = 4KE_{ci}$$

$$C' = 4KE_{c \ i+1}$$

and

$$D' = 6KE_{bfi}$$

Equations (A.7) and (A.8) are valid for the elastic analysis only. When a plastic hinge forms at any one of the potential hinge locations, the joint rotation equation must be modified. Table A.1 lists the substitutions to be made in Eqn. (A.8) for the formation of hinges in the various members, so that the joint rotation equation will conform to the particular hinge pattern considered.

In Table A.1,  $MPE_{bfi}$ ,  $MPE_{wbi}$  are the plastic moment capacities of the beams  $b_i f_i$  and  $b_i w_i$ , and  $MPE_{ci}$  is the plastic moment capacity (reduced for axial load) of the column.

TABLE A.1  
MODIFICATION OF ELASTIC SLOPE-DEFLECTION  
EQUATIONS FOR JOINT EQUILIBRIUM

Member	Hinge Location	Substitution to be Made In Equation (A.8)
$b_i w_i$	$w_i$	$A = 3KE_{wbi} - \rho_{wbi} - MPE_{wbi}/2$
		$A' = 3KE_{wbi}$
	$b_i$ or $b_i, w_i$	$A = MPE_{wbi}$ $A' = 0$
$b_i b_{i-1}$	$b_{i-1}$	$B = 3KE_{ci} \cdot \rho_{ci} - MPE_{ci}/2$
		$B' = 3KE_{ci}$
	$b_i$ or $b_i b_{i-1}$	$B = MPE_{ci}$ $B' = 0$

TABLE A.1 (continued)

Member	Hinge Location	Substitution to be Made In Equation (A.8)
$b_i b_{i+1}$	$b_{i+1}$	$C = 3KE_{C\ i+1} \cdot \rho_{C\ i+1} - MPE_{C\ i+1}/2$ $C' = 3KE_{C\ i+1}$
	$b_i$ or $b_{i+1}$	$C = MPE_{C\ i+1}$ $C' = 0$
	$f_i$	$D = MPE_{bfi}/2$ $D' = 3KE_{bfi}$
$b_i f_i$	$b_i$ or $b_i f_i$	$D = MPE_{bfi}$ $D' = 0$

## APPENDIX B

## FORCED CONVERGENCE EQUATIONS

The forced convergence equations and the convergence tests in Step (e) in the method of analysis are given in this appendix. The convergence equations for the rotations and deflections of the frame and the vertical displacement of the end of the wall beam; which define the position of the frame after the initial cycle, are given below:

$$\theta_{wi}'(2) = \frac{\theta_{wi}^{(1)} \cdot \theta_{wi}^{(1)}}{\theta_{wi}^{(1)} - \theta_{wi}^{(2)}} \quad (B.1)$$

$$\Delta_{wi}'(2) = \frac{\Delta_{wi}^{(1)} \cdot \Delta_{wi}^{(1)}}{\Delta_{wi}^{(1)} - \Delta_{wi}^{(2)}} \quad (B.2)$$

and 
$$\delta_{wi}'(2) = \theta_{wi}'(2) \cdot D_{wi}/2 \quad (B.3)$$

In the above equations,  $\theta_{wi}^{(1)}$ ,  $\Delta_{wi}^{(1)}$  and  $\delta_{wi}^{(1)}$  represent the rotations, lateral displacements and vertical displacements of beam-to-wall joints corresponding to the initial application of lateral loads to the shear wall as shown in Fig. 3.9. The deformations of the wall obtained by applying the net out-of-balance forces are then:  $\theta_{wi}^{(2)}$ ,  $\Delta_{wi}^{(2)}$  and  $\delta_{wi}^{(2)}$ . The final position of the frame

is defined by the deformations  $\theta_{wi}'(2)$ ,  $\Delta_{wi}'(2)$ ,  $\delta_{wi}'(2)$ . In the above quantities, the superscript represents the cycle number. In equation (B.3),  $D_{wi}$  is the width of the shear wall at the  $i$ th floor.

The above forcing equations, modified for cycles other than the initial cycle, are given below:

$$\theta_{wi}'(n) = \frac{\theta_{wi}'(1) \cdot \theta_{wi}'(n-1)}{\theta_{wi}'(n-1) - \theta_{wi}'(n)} \quad (B.4)$$

$$\Delta_{wi}'(n) = \frac{\Delta_{wi}'(1) \cdot \Delta_{wi}'(n-1)}{\Delta_{wi}'(n-1) - \Delta_{wi}'(n)} \quad (B.5)$$

and

$$\delta_{wi}'(n) = \theta_{wi}'(n) \cdot D_{wi}/2 \quad (B.6)$$

where  $n$  denotes the cycle in progress.

At the end of Step (d) in Chapter III, convergence tests were performed. These tests must satisfy the following conditions; for rotations:

$$\frac{\theta_{wi}'(n) - \theta_{wi}'(n-1)}{\theta_{wi}'(n)} < \epsilon' \quad (B.7)$$

and for deflections:

$$\frac{\Delta_{wi}'(n) - \Delta_{wi}'(n-1)}{\Delta_{wi}'(n)} < \epsilon' \quad (B.8)$$

In equations (B.7) and (B.8),  $\epsilon'$  is the specified convergence limit, which is normally set at 0.01.

## APPENDIX C

DERIVATIONS OF THE EQUIVALENT  $P\Delta$  SHEAR

The  $P\Delta$  effect plays a dominant role in the behavior of tall structures. The vertical load on the structure,  $P$ , acting through a sidesway displacement,  $\Delta$ , produces an additional overturning moment commonly known as the  $P\Delta$  moment. In this analysis the  $P\Delta$  effect has been taken into account by analyzing the structure under an equivalent lateral force. In Fig. C.1a,  $H_i$  is the applied lateral load at the  $i$ th floor. Due to this applied force system, a lateral deflection  $\Delta_{1i}$  is produced.

The story moment between the  $i$ th and  $i-1$ th floor due to the  $P\Delta$  effect is obtained by taking moments about the  $i$ th floor of all the axial loads above this level. Similarly, by taking moments at each level, the other story moments are obtained. The extra shear due to the  $P\Delta$  effect,  $V_i'$ , is given by:

$$V_i' = \frac{\sum_{j=i}^n P_j (\Delta_{1j} - \Delta_{1j-1})}{h_i} \quad (C.1)$$

where  $h_i$  is the story height at the  $i$ th story and  $P_j$  is the total vertical load on the structure at the  $j$ th story.

The additional lateral load,  $H_{1i}'$ , simulating the  $P\Delta$  effect

can then be determined and is given by:

$$\begin{aligned}
 H_{1i}' &= V_i' - V_{i+1}' \\
 &= \frac{\sum_{i=1}^n P_i (\Delta_{1i} - \Delta_{1i-1})}{h_i} - \frac{\sum_{i+1}^n P_{i+1} (\Delta_{1i+1} - \Delta_{1i})}{h_{i+1}} \quad (C.2)
 \end{aligned}$$

The structure is now reanalyzed under the lateral force system,  $H_i + H_{1i}'$  (without considering vertical loads). In Fig. C.1b,  $\Delta_{2i}$  is the lateral deflection corresponding to the new lateral force system. If these deflections do not agree (within a specified convergence limit), the additional horizontal force,  $H_{2i}'$ , due to the  $P\Delta$  effect for the next cycle is given by

$$H_{2i}' = \frac{\sum_{i=1}^n P_i (\Delta_{2i} - \Delta_{2i-1})}{h_i} - \frac{\sum_{i+1}^n P_{i+1} (\Delta_{2i+1} - \Delta_{2i})}{h_{i+1}} \quad (C.3)$$

The structure is again analyzed under the lateral force system  $H_i + H_{2i}'$ . The process is continued until the changes in lateral deflections are within the convergence limit.

The total vertical load at each floor level has been read into the program. In the present method of simulating the  $P\Delta$  effect, a constant vertical load has been used throughout the analysis. In the actual structure, the girder shears will introduce tension in one column and compression in the other. This will not change the total vertical load or the gross  $P\Delta$  effect.

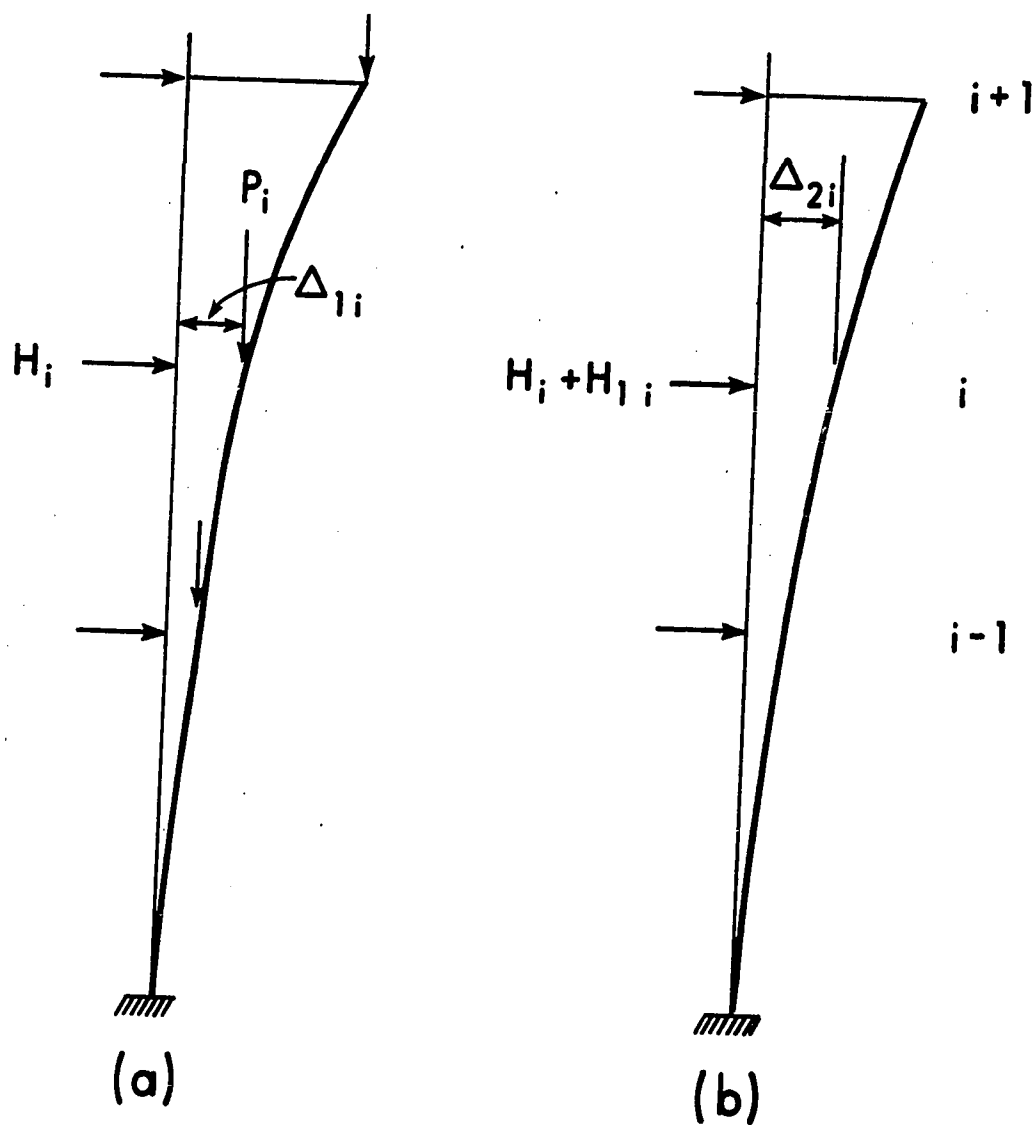


FIG. C.1  $P\Delta$  EFFECT - MULTI-STORY STRUCTURE

## APPENDIX D

## NOMENCLATURE AND PRINTOUT OF THE FORTRAN PROGRAM

D.1 Nomenclature for the Fortran Program

BAKA	A subroutine subprogram
BMOM	Bottom moment in a segment of the shear wall (kip-in)
BMOMF	Bottom moment in the bottom of the lowest segment in a story (kip-in)
CON	Convergence limit for the deflection and rotation
CDEFF	Floor level deflection of shear wall after applying convergence formula
CROTF	Floor level rotation of shear wall after applying convergence formula
DEF	Deflection of wall at a section (in)
DEFF	Deflection of the wall at the floor level (in)
DMBF	Moment at the column end of the left hand beam computed in the previous loading condition (kip-in)
DMBW	Moment at the column end of the right hand beam computed in the previous loading condition (kip-in)
DMCB	Moment at the bottom end of column in a particular story computed in the previous loading condition (kip-in)
DMCT	Moment at the top end of a column in a particular story computed in the previous loading condition (kip-in)
DMFB	Moment at the left end of the left hand beam computed in the previous loading condition (kip-in)

DMWB	Moment at the wall end of the right hand beam computed in the previous loading condition (kip-in)
DW	Width of shear wall (in)
EF	Youngs modulus of elasticity of the frame (kip/in <sup>2</sup> )
EW	Youngs modulus of elasticity of the wall (kip/in <sup>2</sup> )
F	Applied force on the wall from frame analysis (kip)
FD	Horizontal design load acting at floor level (kip)
FRAME	A subroutine subprogram
FOC	Frame force at the floor level (kip)
FW	Final force on wall at each floor level (kip)
HBF	Length of left hand beam (in)
HBW	Length of right hand beam (in)
HLI	Percentage of original horizontal load to be increased in the elastic range
HLIR	Percentage of original horizontal load to be increased in the inelastic range
HS	Story height (in)
HSF	Height of floor level from base (in)
IK,IX	Dummy constants
IVL	Dummy constants for stopping the program if the deformation exceeds certain specified limit
KB	Spring constant at the base of the shear wall (kip-in/rad)
KC	Spring constant at the base of the column (kip-in/rad)
L	Product of number of story and number of segments in a story

MAX	Maximum no. of cycle to be performed for any iteration process
MI	Moment of inertia of shear wall ( $\text{in}^4$ )
MIBF	Moment of inertia of left hand beam ( $\text{in}^4$ )
MIBW	Moment of inertia of right hand beam ( $\text{in}^4$ )
MIC	Moment of inertia of column ( $\text{in}^4$ )
MII	Moment of the segment of the shear wall ( $\text{in}^4$ )
MM	No. of problems to be solved
MMCB	Moment at the bottom of a column in a story (kip-in)
MMCT	Moment at the top of a column in a story (kip-in)
MMMM	Counter for iteration with the effect of axial load
MOMB	Moment at the base of the shear wall (kip-in)
MOMBF	Moment at the column end of the left hand beam in the cycle under consideration (kip-in)
MOMBW	Moment at the column end of the right hand beam in the cycle under consideration (kip-in)
MOMFB	Moment at the left end of the left hand beam in the cycle under consideration (kip-in)
MOMP	Moment in a story due to axial load (kip-in)
MOMW	Total moment at floor level on the shear wall due to end moment and shear from the right hand beam (kip-in)
MOMWB	Moment at the right end of the right hand beam in the cycle under consideration (kip-in)
MPC	Plastic moment capacity of column in a particular story (kip-in)

MPF	Plastic moment capacity of the left hand beam (kip-in)
MPSW	Plastic moment capacity of the shear wall (kip-in)
MPW	Plastic moment capacity of the right hand beam (kip-in)
ND	Number of division in a story
NI	Number of times horizontal load to be incremented
NM	Length of a segment of a wall in a story (in)
NNMM	Segment height from base of wall (in)
NS	Number of stories
PPS	Total axial load in a structure at a floor level (kips)
PS	Vertical load on column (kips)
PSW	Vertical load in wall (kips)
ROB	Sway rotation of right hand beam
ROFA	A subroutine subprogram
ROS	Story rotation of frame (rad)
RMWP	Ratio of moment to plastic moment capacity of wall
RPWP	Ratio of curvature to curvature corresponding to RMWP
ROT	Rotation of wall in a segment (rad)
ROTF	Rotation of wall at the floor level (rad)
ROTFF	Joint rotation of frame (rad)
ROTO	Joint rotation at the base of column (rad)
SBF	Stiffness of left hand beam (kip-in)
SBW	Stiffness of right hand beam (kip-in)
SC	Stiffness of column (kip-in)
SHEARR	Shear at the ends of left hand beam (kip)

SHEARW	Shear at the ends of right hand beam (kip)
SHEC	Shear in column in a story (kip)
SR	A subroutine subprogram
SR 1	A subroutine subprogram
SR 3	A subroutine subprogram
SSB	Slope of the second branch of shear wall moment- curvature diagram
TMOMF	Top moment in the top of the topmost segment in a story (kip-in)
TMOM	Top moment in a segment of the shear wall (kip-in)
VDEF	Vertical uplift of the beam connected with the wall (in)

D.2 Printout of the Fortran Program

```

C
  DIMENSION F(99,30),HSF(30),DW(30),FOC(30),SHEAR(30),ROTF(99,30),
  1ROTFF(99,30),ROTO(99),SHEC(30),FD(30),FW(30),SHEARW(30),PS(30),
  2SHEARR(30),CPHI(300),D(300),D1(300),H(99,30),DELTA(99,30),
  3FA(30),PPS(30),CROTF(99,30),CDEFF(99,30),PPD(30),ZM(300),
  4 DEFF(99,30),HBF(30),HBW(30),HS(30),SBF(30),SC(30),SBW(30),
  5F11(30),TMOM(300),BMOM(300),TMOMF(30),BMOMF(30),DMFB(30),
  6DMBF(30),DMBW(30),DMWB(30),CSHEC(30),DMCB(30),DMCT(30)
  REAL NNM(300),NNMM(300),MIA(300),MII(300),MMCT(30),MMCB(30),
  1KB,KC,MOMW(30),MOMWB(30),MOMBW(30),MOMBF(30),MOMFB(30)
  2,MPF(30),MPW(30),MPC(30),MPS(300)
20 FORMAT(1H1)
21 FORMAT(1HK)
22 FORMAT(1H )
  READ(5,130) MM
130 FORMAT(1X,I2)
  DO 400 JJ=1,MM

C
C   INPUT STATEMENTS FOR DATA BY SUBROUTINE SR.
C
  CALL SR (L,NS,ND,EW,KC,KB,FD,NI,HS,DW,PS,MPF,NNM,
  1 MPW,MPC,SC,SBW,SBF,IVL,PPD,HBF,HBW,
  2 RMWP,RPWP,MAX,CON,HLI,HLIR,HSF,F,MII,MPS,NNMM,MIA,PPS,ALPHA)
  NL=JJ-1
  KP=0
  SSB=(RMWP-1.0)/(RPWP-1.0)
  DO 302 NJ=1,NI

C
C   SHEAR WALL ANALYSIS BEGINS.
C
  IK=0
  IX=0
  MMMM=1
  DO 131 K=1,NS
    H(NJ,K)=F(1,K)
131 CONTINUE
132 CALL BAKA (IK,IX,MMMM,L,NS,ND,EW,KC,KB,HS,DW,PS,NNM,MPF,MPW,
  1MPC,SC,SBW,SBF,HBW,MAX,CON,HSF,F,MII,NNMM,TMOM,BMOM,MOMW,ROTB,TMOM
  2F,BMOMF,ROTF,DEFF,ROTFF,ROTO,ITER,NJ,DMCB,DMCT,DMBF,DMFB,DMBW,
  3DMWB,MMCB,MMCT,MOMBW,MOMWB,FOC,SHEC,CSHEC,SHEARW,NCYCLE,SHEAR,CDEF
  4F,CROTF,ZM,MIA)
  IF(IX.EQ.1)GO TO 245
  IF(IK.EQ.1)GO TO 272
233 IF(PPS(1).LE.0.0)GO TO 260
  IF(MMMM.EQ.1.AND.NJ.EQ.1)GO TO 235
  IF(MMMM.EQ.1)GO TO 256
  DO 234 N=1,NS
    IF(ABS((CDEFF(MMMM,N)-CDEFF(MMMM-1,N))/CDEFF(MMMM,N)).GE.CON.OR
  1. ABS((CROTF(MMMM,N)-CROTF(MMMM-1,N))/CROTF(MMMM,N)).GE.CON)GO
  2TO 251
234 CONTINUE
  GO TO 260

```

```

C
C   OUTPUT STATEMENTS FOR RESULTS OF FRAME ANALYSIS BY SUBROUTINE ROFA
C   (WITHOUT THE EFFECT OF AXIAL LOADS)
C
235 WRITE(6,240)
240 FORMAT(/45X,'RESULT WITHOUT THE EFFECT OF AXIAL LOAD'//)
    CALL ROFA (ROTFF,SHEC,FOC,MMCB,MMCT,ROTO,NS,NCYCLE,ITER,MMMM)
    DO 242 N=1,NS
        MOMFB(N)=SBF(N)*6.0*ROTFF(ITER,N)
        MOMBF(N)= MOMFB(N)
        SHEARR(N)=2.0*MOMFB(N)/HBF(N)
        WRITE(6,241) N,MOMBW(N),MOMWB(N),MOMBF(N),MOMFB(N),SHEARW(N),SHEAR
1R(N)
241 FORMAT(13X,I3,1X,4F19.2,5X,F10.2,7X,F10.2/)
242 CONTINUE
    WRITE(6,21)
    DO 244 K=1,NS
        F11(K)=F(1,K)-FOC(K)
        F(1,K)=F11(K)
244 CONTINUE
    IX=1
    GO TO 132
245 WRITE(6,22)
C
C   OUTPUT STATEMENTS FOR RESULTS OF SHEAR WALL ANALYSIS BY SUBROUTINE
C   SR3 (WITHOUT THE EFFECT OF AXIAL LOADS)
C
    CALL SR3 (BMOMF,TMOMF,ROTB,NS,F11,FOC,SHEAR,ROTF,DEFF,CROTF,CDEFF,
1MMMM)
    IX=0
    WRITE(6,21)
C
C   ADDITIONAL HORIZONTAL LOAD TO SIMULATE P-DELTA EFFECT
C
251 IF(MMMM .EQ. MAX) GO TO 254
256 PPS(NS+1)=0.0
    HS(NS+1)=5000.0
    CDEFF(MMMM,NS+1)=CDEFF(MMMM,NS)
    F(1,1)=H(NJ,1)+ALPHA*(PPS(1)*CDEFF(MMMM,1)/HS(1)-PPS(2)*(CDEFF(MMM
1M,2)-CDEFF(MMMM,1))/HS(2))
    IF(NS .EQ. 1) GO TO 253
    DO 252 N=2,NS
        F(1,N)=H(NJ,N)+ALPHA*(PPS(N)*(CDEFF(MMMM,N)-CDEFF(MMMM,N-1))/HS(N)
1-PPS(N+1)*(CDEFF(MMMM,N+1)-CDEFF(MMMM,N))/HS(N+1))
252 CONTINUE
253 MMMM=MMMM+1
    GO TO 132
C
C   OUTPUT STATEMENTS FOR RESULTS OF FRAME ANALYSIS BY SUBROUTINE ROFA
C
254 WRITE(6,255)
255 FORMAT(10X,'CONVERGENCE (CALCULATION OF THE EFFECT OF AXIAL LOAD)
1WAS NOT ENOUGH'//)
260 CALL ROFA (ROTFF,SHEC,FOC,MMCB,MMCT,ROTO,NS,NCYCLE,ITER,4MMM)
    DO 270 N=1,NS
        IF(NJ .EQ. 1) GO TO 261
        IF(ABS(DMFB(N)) .GE. MPF(N)) GO TO 262
261 MOMFB(N)=SBF(N)*6.0*ROTFF(ITER,N)
    GO TO 263

```

```

262 MOMFB(N)=DMFB(N)
263 MOMB(N)=MOMFB(N)
264 SHEARR(N)=2.0*MOMFB(N)/HBF(N)
    WRITE(6,241)N,MOMBW(N),MOMWB(N),MOMB(N),MOMFB(N),SHEARW(N),SHEARR
    1(N)
270 CONTINUE
    DO 271 K=1,NS
        DELTA(NJ,K)=CDEFF(MMMM,K)
        F11(K)=F(1,K)-FUC(K)
        F(1,K)=F11(K)
271 CONTINUE
    IK=1
    GO TO 132
272 WRITE(6,21)

C
C   OUTPUT STATEMENTS FOR RESULTS OF SHEAR WALL ANALYSIS BY
C   SUBROUTINE SR3
C
    CALL SR3 (BMOMF,TMCMF,ROTB,NS,F11,FOC,SHEAR,ROTF,DEFF,CROTF,CDEFF,
    1MMMM)
    WRITE(6,21)

C
C   DETECTION OF HINGES IN SHEAR WALL.
C
    IF(NL .NE. JJ) GO TO 273
    IF(ABS(DELTA(NJ,NS)) .GT. STUPD) GO TO 960
273 SSB=(RMWP-1.0)/(RPWP-1.0)
    DO 284 J = 1,L
        D(J)=(TMOM(J)+BMOM(J))/(2.0*MPS(J))
        D1(J)=D(J)*MPS(J)
        IF(ABS(D(J)) .LT. 1.0) GO TO 284
        IF(NL .NE. JJ) GO TO 274
        CPHI(J)=(D(J)-1.0)/SSB + 1.0
        MII(J)=D(J) * MIA(J) / CPHI(J)
274 KP=KP+1
        IF(KP .GE. 2) GO TO 281
275 WRITE(6,280)
280 FORMAT(45X,37HDETECTION OF HINGES IN THE SHEAR WALL///)
281 WRITE(6,282)J,D(J),D1(J)
282 FORMAT(5X,20HHINGE IN SECTION NO.,I3,2X,51H RATIO OF MOMENT IN WALL
    1 TO PLASTIC MOMENT CAPACITY=,F5.2,2X,15HMOMENT IN WALL=,F14.2/)
    WRITE(6,283) MII(J),MIA(J)
283 FORMAT (5X,'REDUCED MOMENT OF INERTIA =',F13.2,3X,'INITIAL MOMENT
    1 OF INERTIA =',F13.2//)
284 CONTINUE
    WRITE(6,21)

C
C   DETECTION OF HINGES ON FRAME BY SUBROUTINE SR1.
C
    CALL SR1 (DMFB,DMBF,DMBW,DMWB,DMCT,DMCB,MOMFB,MOMB,N,MOMBW,MOM
    1WB,MMCT,MMCB,NS,M3,MPF,MPW,MPC)
    IK=0
    IF(NL .EQ. JJ) GO TO 285
    IF(KP .GE. 1 .OR. M3 .GE. 1) GO TO 295

C
C   HORIZONTAL LOAD IS INCREMENTED
C
285 IF(NJ .EQ. NI) GO TO 960
    WRITE(6,21)

```

```

        WRITE(6,291)
291  FORMAT(50X,'HORIZONTAL LOAD INCREMENTED'//)
        WRITE(6,292)
292  FORMAT(10X,'FLOOR NO.',5X,'HORIZONTAL LOAD(K)',5X,'VERTICAL LOAD(
      1K)')//)
        DO 294 K=1,NS
          F(1,K)=H(NJ,K)+HLI*FD(K)
          IF(IVL .LE. 0) GO TO 296
          PPS(K)=PPS(K)+HLI*PPD(K)
296  WRITE(6,293) K,F(1,K),PPS(K)
293  FORMAT(13X,I3,11X,F8.2,16X,F8.2//)
294  CONTINUE
        KP=0
        GO TO 302

C
C  HORIZONTAL LOAD IS DECREMENTED
C
C  COMPUTE SECTION HEIGHT FROM BASE IN INCH
C
295  IF(NJ .EQ. NI) GO TO 960
        STOPD=30.0*ABS(DELTA(NJ,NS))
        WRITE(6,300)
300  FORMAT(1HK,15X,'HORIZONTAL LOAD DECREMENTED TO MAKE THE FRAME ELAS
      TIC SO THAT HORIZONTAL LOAD CAN BE INCREMENTED SLOWLY'//)
        WRITE(6,292)
        DO 301 K=1,NS
          F(1,K)=H(NJ,K)-HLI*FD(K)+HLIR*FD(K)
          IF(IVL .LE. 0) GO TO 303
          PPS(K)=PPS(K)-HLI*PPD(K)+HLIR*PPD(K)
303  DMFB(K)=0.0
        DMBF(K)=0.0
        DMWB(K)=0.0
        DMBW(K)=0.0
        DMCT(K)=0.0
        DMCB(K)=0.0
        WRITE(6,293) K,F(1,K),PPS(K)
301  CONTINUE
        HLI=HLIR
        NL=JJ
        KP=0
302  CONTINUE

C
C  OUTPUT THE ROTATION AND DEFLECTION OF EACH HORIZONTAL LOAD
C
960  DO 907 N=1,NS
        WRITE(6,915) N
915  FORMAT(48X,'LOAD-DEFLECTION DATA FOR FLOOR NO. ',I3//)
        WRITE(6,905)
905  FORMAT(10X,'HORIZONTAL LOAD(KIP)',5X,'DEFLECTION(IN)')//)
        DO 906 K = 1,NJ
          WRITE(6,908) H(K,N),DELTA(K,N)
908  FORMAT(16X,F8.2,11X,E13.6//)
906  CONTINUE
907  CONTINUE
400  CONTINUE
        STOP
        END

```

C  
C  
C  
C  
C  
C

SUBROUTINE SR READS IN DATA - COMPUTES CO-ORDINATES OF EACH FLOOR FROM THE BASE AND THE STIFFNESS OF MEMBERS - ALSO ALL THE INPUT QUANTITIES ARE PRINTED OUT

```

SUBROUTINE SR (L,NS,ND,  EW,KC,KB,FD,NI,HS,DW,PS,      MPF,NNM,
1 MPW,MPC,      SC,SBW,SBF,IVL,PPD,      HBF,HBW,
2  RMWP,RPWP,MAX,CON,HLI,HLIR,HSF,F,MII,MPS,NNMM,MIA,PPS,ALPHA)
  DIMENSION FD(30),HS(30),DW(30 ),PS(30),      SC(30),
1 SBF(30),SBW(30),      HBF(30),
2 HBW(30),HSF(30),F(99,30),PSW(30),PPS(30),PPD(30)
  REAL MI(30),MPF(30),MPW(30),MPC(30),MPSW(30),MIC(30),MIBF(30),
1 MIBW(30),NM(30),NNM(300),MII(300),MPS(300),NNMM(300),MIA(300),
2 KB,KC
  READ(5,200)KB,KC,EF,EW,NS,ND,MAX,CON,HLI,NI,HLIR
200 FORMAT(1X,2E18.5,2F7.0,3I3,2F5.2,I3,F5.2)
  READ(5,470) RMWP,RPWP,ALPHA,IVL
470 FORMAT(1X,2F7.2,F5.2,I3)
  DO 202 K=1,NS
    READ(5,204)FD(K),HS(K),HBF(K),HBW(K),DW(K),MI(K),MIC(K),
1 MIBF(K),MIBW(K)
204 FORMAT(1X,F5.2,4F7.2,4F11.2)
  202 CONTINUE
  DO 102 K=1,NS
    READ(5,101)PS(K) ,PSW(K)
101 FORMAT(1X,2F8.2)
  102 CONTINUE
  DO 205 K = 1,NS
    READ(5,500)      MPF(K),MPW(K),MPC(K),MPSW(K)
500 FORMAT( 17X ,3F14.2,F21.2)
  205 CONTINUE

```

C  
C  
C  
C  
C

ALL FORCE UNITS ARE IN KIPS AND ALL LENGTH UNITS ARE IN INCHES UNLESS STATED OTHERWISE.

```

L=NS*ND
NDN=0
K=1-ND
CB=0.0
DO 22 J=1,NS
  NM(J)=HS(J)/FLOAT(ND)
  HSF(J)=CB+HS(J)
  CB=HSF(J)
  SBW(J)=EF*MIBW(J)/HBW(J)
  SBF(J)=EF*MIBF(J)/HBF(J)
  SC(J)=EF*MIC(J)/HS(J)
  F(1,J)=FD(J)
  PPS(J)=PS(J)+PSW(J)
  PPD(J)=PPS(J)
  K=K+ND
  NDN=NDN+ND
DO 23 N=K,NDN
  NNM(N)=NM(J)
  MII(N)=MI(J)

```

```

      MIA(N)=MI(J)
      MPS(N) = MPSW(J)
23  CONTINUE
22  CONTINUE

C
C   COMPUTE SECTION HEIGHT FROM BASE IN INCH
C
      BC=0.0
      DO 25 K=1,L
      NNMM(K)=BC+NNM(K)
      BC=NNMM(K)
25  CONTINUE
      WRITE(6,324)
324  FORMAT(1H1)

C
C   OUTPUT STATEMENTS FOR DATA OF FRAME AND SHEAR WALL.
C
      WRITE(6,51)
51  FORMAT(50X,29HDATA FOR SHEAR WALL AND FRAME//)
      WRITE(6,351) NS
351  FORMAT(10X,56HNUMBER OF STORIES =
1      ,I3/)
      WRITE(6,352)ND
352  FORMAT(10X,56HNUMBER OF DIVISION TO BE MADE IN A STORY =
1      ,I3/)
      WRITE(6,355) EW
355  FORMAT(10X,53HMODULUS OF ELASTICITY FOR WALL =
1      ,F9.2/)
      WRITE(6,356) EF
356  FORMAT(10X,53HMODULUS OF ELASTICITY FOR FRAME =
1      ,F9.2/)
      WRITE(6,354) KC
354  FORMAT(10X,43HSPRING CONSTANT AT BASE OF FRAME = ,E19.5/)
      WRITE(6,353) KB
353  FORMAT(10X,43HSPRING CONSTANT AT BASE OF WALL = ,E19.5/)
      WRITE(6,510) CON
510  FORMAT(10X,'CONVERGENCE LIMIT',24X,'=',F20.5/)
      WRITE(6,501) ALPHA
501  FORMAT(10X,'ALPHA',36X,'=',F20.3//)
      WRITE(6,364)
364  FORMAT(1HK)
      WRITE(6,357)
357  FORMAT(10X,10HFLOOR NO./,2X,10HFORCE(KIP),3X,17HMOMENT OF INERTIA,
13X,16HSTORY HEIGHT(IN),3X,14HWALL WIDTH(IN),3X,15HAXIAL LOAD(KIP),
23X,15HAXIAL LOAD(KIP))
      WRITE(6,358)
358  FORMAT(10X,9HSTORY NO.,18X,13HOF WALL (IN4),43X,9HON COLUMN,10X,7H
2ON WALL//)
      DO 10 N=1,NS
      WRITE(6,359)N,FD(N),MI(N),HS(N),DW(N),PS(N),PSW(N)
359  FORMAT(13X,I3,6X,F8.2,7X,F12.2,9X,F8.2,11X,F7.2,9X,F8.2,9X,F8.2/)
10  CONTINUE
      WRITE(6,366)
366  FORMAT(1HK)
      WRITE(6,360)
360  FORMAT(10X,10HFLOOR NO./,2X,14HLENGTH OF BEAM,3X,14HLENGTH OF BEAM
1,3X,17HMOMENT OF INERTIA,3X,17HMOMENT OF INERTIA,3X,17HMOMENT OF I
2NERTIA)
      WRITE(6,361)

```

```

361  FORMAT(10X,9HSTORY NO.,4X,13HON ROLLER(IN),3X,14HCONNECTED WITH,4X
1,14HOF COLUMN(IN4),5X,17HOF BEAM ON ROLLER,3X,17HOF BEAM CONNECTED
2)
WRITE(6,362)
362  FJRMAT(42X,8HWALL(IN),32X,5H(IN4),10X,14HWITH WALL(IN4)//)
DO 71 J=1,NS
WRITE(6,363)J,HBF(J),HBW(J),MIC(J),MIBF(J),MIBW(J)
363  FORMAT(13X,I3,8X,F8.2,9X,F8.2,9X,F11.2,9X,F11.2,9X,F11.2/)
71  CONTINUE
WRITE(6,411)
411  FORMAT(1HK,30X,'PLASTIC MOMENT CAPACITY OF BEAMS, COLUMNS AND WALL
1'//)
WRITE(6,399)
399  FORMAT(10X,10HFLOOR NO./,2X,
1 15HPLASTIC MOMENT,2X,15HPLASTIC MOMENT,2X,15HPLASTIC MO
3MENT, 5X,15HPLASTIC MOMENT)
WRITE(6,406)
406  FORMAT(10X,9HSTORY NO.,3X,
1 15HCAPACITY OF THE,2X,15HCAPACITY OF THE,2X,15HCAPACITY OF T
2HE, 5X,15HCAPACITY OF THE)
WRITE(6,407)
407  FORMAT(22X, 15HBEAM
2ON ROLLER,2X,15HWALL SIDE BEAM,2X,15HCOLUMN (KIP-IN), 5X,15HWALL
3 (KIP-IN).)
WRITE(6,408)
408  FORMAT(26X, 8H(KIP-IN)
1), 7X,8H(KIP-IN)//)
DO 410 K= 1,NS
WRITE(6,409) K, MPF(K),MPW(K),MPC(K),MPSW(K)
409  FORMAT(13X,I3, 6X, F14.2,3X,F14.2,3X,F14.2,2X,E18
1.8/)
410  CONTINUE
WRITE(6,385)
385  FORMAT(1HK,45X,39HSTIFFNESSES (EI/L) OF BEAMS AND COLUMNS//)
WRITE(6,365)
365  FORMAT(10X,10HFLOOR NO./,4X,19HSTIFFNESS OF COLUMN,4X,17HSTIFFNESS
1 OF BEAM,4X,17HSTIFFNESS OF BEAM)
WRITE(6,367)
367  FORMAT(10X,9HSTORY NO.,10X,8H(KIP-IN),11X,15HCONNECTED WITH,5X,17
1HON ROLLER(KIP-IN))
WRITE(6,368)
368  FORMAT(49X,12HWALL(KIP-IN)//)
DO 72 J=1,NS
WRITE(6,369)J,SC(J),SBW(J),SBF(J)
369  FORMAT(13X,I3,9X,F15.2,7X,F15.2,6X,F15.2//)
72  CONTINUE
WRITE(6,481)
481  FORMAT(1HK,40X,53HMOMENT CURVATURE RELATIONSHIP OF THE SHEAR
1 WALL//)
WRITE(6,482)
482  FORMAT(10X,9HPOINT NO.,5X,19HRATIO OF MOMENT IN,5X,18HRATIO OF CU
1RVATURE)
WRITE(6,483)
483  FORMAT(24X,19HWALL TO THE PLASTIC,5X,18HIN WALL TO THE)
WRITE(6,484)
484  FORMAT(24X,19HMOMENT CAPACITY OF,5X,18HCURVATURE OF THE)
WRITE(6,485)
485  FORMAT(29X,9HTHE WALL.,10X,18HWALL AT YIELD PT.//)
WRITE(6,488)
RETURN
END

```

C  
C  
C  
C  
C  
C  
C  
C  
C  
C

SUBROUTINE BAKA COMPUTES THE DISTRIBUTION OF LATERAL LOAD BETWEEN THE FRAME AND SHEAR WALL. MOMENTS AND DEFORMATIONS AT EACH SEGMENT OF THE WALL ARE COMPUTED. THE CONVERGENCE FORMULA IS APPLIED ( EXCEPT THE FIRST CYCLE ) FOR DEFLECTION AND ROTATION. THE DEFORMATIONS COMPUTED BY THE CONVERGENCE FORMULA ARE ENFORCED ON THE FRAME SYSTEM. THE JOINT ROTATION OF THE FRAME ARE COMPUTED IN SUBROUTINE FRAME.

SUBROUTINE BAKA (IK,IX,MPMM,L,NS,ND,EW,KC,KB,HS,DW,PS,NNM,MPF,MPW,1MPC,SC,SBW,SBF,HBW,MAX,CON,HSF,F,MII,NNMM,TMOM,BMOM,MOMW,ROTB,TMOM2F,BMOMF,ROTF,DEFF,ROTF,ROTO,ITER,NJ,DMCB,DMCT,DMBF,DMFB,DMBW,3DMWB,MMCB,MMCT,MOMBW,MOMWB,FOC,SHEC,CSHEC,SHEARW,NCYCLE,SHEAR,CDEF4F,CROTF)

DIMENSION BMOM(300),BMOMF(30),CSHEC(30),CDEFF(99,30),CROTF(99,301),DEF(300),DEFF(99,30),DMCB(30),DMCT(30),DMBW(30),DMWB(30),DW(30),2DMFB(30),DMBF(30),F(99,30),FOC(30),HSF(30),HS(30),HBW(30),PS(30),3ROT(300),ROTF(99,30),ROS(30),ROB(30),ROTF(99,30),ROTO(99),SC(30)4,SBW(30),SBF(30),SHEC(30),SHEARW(30),SHEAR(30),TMOM(300),TMOMF(30)5,VDEF(30)

REAL KB,KC,MOMB,MOMW(30),MII(300),MPC(30),MOMP(30),MPW(30),1MPF(30),MMCB(30),MMCT(30),MOMBW(30),MOMWB(30),NNMM(300),NNM(300)

132 DO 232 M=1,MAX

C  
C  
C

MOMENTS AT VARIOUS SECTIONS (KIP-IN).

MOMB=0.0

NDN=0

K=1-ND

DO 135 N=1,NS

MOMB=MOMB+F(M,N)\*HSF(N)

K=K+ND

NDN=NDN+ND

DO 134 J=K,NDN

RS=0.0

DO 133 I=N,NS

133 RS=RS+F(M,I)\*(HSF(I)-NNMM(J))

TMOM(J)=RS

134 CONTINUE

135 CONTINUE

IF( (IK.EQ.1.OR. IX.EQ.1) GO TO 140

IF(M.EQ.1) GO TO 145

140 DO 142 N=1,NS

MOMB=MOMB+MOMW(N)

RS=0.0

DO 141 I=N,NS

RS=RS+MOMW(I)

141 CONTINUE

MOMW(N)=RS

142 CONTINUE

NDN=0

K=1-ND

DO 144 I=1,NS

K=K+ND

NDN=NDN+ND

DO 143 J=K,NDN

```

      TMCM(J)=TMOM(J)+MOMW(I)
      BMOM(J)=TMOM(J)+SHEAR(I)*NNM(J)
143  CONTINUE
144  CONTINUE
      GO TO 150
145  BMCM(1)=MOMB
      IF(L .EQ. 1) GO TO 150
      DO 146 J=2,L
146  BMCM(J)=TMOM(J-1)

C
C      DEFLECTIONS AT VARIOUS SECTIONS (IN)
C
150  A = (TMCM(1)+MOMB)*NNM(1)/(2.0*EW*MII(1))
      ROTB=MOMB/KB
      ROT(1)=ROTB+A
      DEF(1)=ROTB*NNM(1)+A*NNM(1)/2.0
      IF(L .EQ. 1) GO TO 152
      DO 151 J=2,L
      B=(TMOM(J)+BMOM(J))*NNM(J)/(2.0*EW*MII(J))
      ROT(J) = ROT(J-1) + B
      DEF(J)=DEF(J-1)+ROT(J-1)*NNM(J)+B*NNM(J)/2.0
151  CONTINUE

C
C      MOMENTS, ROTATIONS AND DEFLECTIONS AT EVERY FLOOR LEVEL
C
152  DO 153 N=1,NS
      I=N*ND
      K=I+1-ND
      TMCMF(N)=TMOM(I)
      BMOMF(N)=BMOM(K)
      ROTF(M,N)=ROT(I)
      DEFF(M,N)=DEF(I)
153  CONTINUE
      IF(IX .EQ. 1) RETURN
      IF(IK .EQ. 1) RETURN
      IF(M .EQ. 1) GO TO 155
      DO 154 N=1,NS
      ROTF(M,N)=ROTF(1,N)*ROTF(M-1,N)/(ROTF(M-1,N)-ROTF(M,N))
      DEFF(M,N)=DEFF(1,N)*DEFF(M-1,N)/(DEFF(M-1,N)-DEFF(M,N))
154  CONTINUE
155  ROS(1)=DEFF(M,1)/HS(1)
      IF(NS .EQ. 1) GO TO 161
      DO 160 I=2,NS
      ROS(I)=(DEFF(M,I)-DEFF(M,I-1))/HS(I)
160  CONTINUE
161  DO 162 N=1,NS
      VDEF(N)=-ROTF(M,N)*DW(N)/2.0
      ROB(N)=VDEF(N)/HBW(N)
162  CONTINUE

C
C      COMPUTE MOMENT, SHEAR AND FORCE ON FRAME BY SUBROUTINE FRAME
C
      CALL FRAME (MAX,ROTF,ROTO,SC,ROS,KC,SBW,SBF,ROB,ROTF,NS,ITER,MMM
1, M, DMCB,DMCT,DMBW,DMWB,DMBF,DMFB,MPC,MPP,MPW,NJ,CON)
      IF(NJ .EQ. 1) GO TO 180
      IF(ABS(DMCB(1)) .GE. MPC(1)) GO TO 181
180  MMCB(1)=-KC*ROTO(ITER)
      GO TO 182
181  MMCB(1)=DMCB(1)

```

```

182 IF(NJ .EQ. 1) GO TO 183
    IF(ABS(DMCT(1)) .GE. MPC(1)) GO TO 184
    IF(ABS(DMCB(1)) .GE. MPC(1)) GO TO 185
183 MMCT(1)=SC(1)*(4.0*ROTFF(ITER,1)+2.0*ROTO(ITER)-6.0*ROS(1))
    GO TO 192
184 MMCT(1)=DMCT(1)
    GO TO 192
185 MMCT(1)=SC(1)*(3.0*ROTFF(ITER,1)-3.0*ROS(1))+0.5*DMCB(1)
192 SHEC(1)=(MMCT(1)+MMCB(1))/HS(1)
194 IF(NS .EQ. 1) GO TO 210
    DO 205 K=2,NS
        IF (NJ .EQ. 1) GO TO 195
        IF(ABS(DMCB(K)) .GE. MPC(K)) GO TO 196
        IF(ABS(DMCT(K)) .GE. MPC(K)) GO TO 197
195 MMCB(K)=SC(K)*(4.0*ROTFF(ITER,K-1)+2.0*ROTFF(ITER,K)-6.0*ROS(K))
    GO TO 198
196 MMCB(K)=DMCB(K)
    GO TO 198
197 MMCB(K)=SC(K)*(3.0*ROTFF(ITER,K-1)-3.0*ROS(K))+0.5*DMCT(K)
198 IF(NJ .EQ. 1) GO TO 199
    IF(ABS(DMCT(K)) .GE. MPC(K)) GO TO 200
    IF(ABS(DMCB(K)) .GE. MPC(K)) GO TO 201
199 MMCT(K)=SC(K)*(4.0*ROTFF(ITER,K)+2.0*ROTFF(ITER,K-1)-6.0*ROS(K))
    GO TO 202
200 MMCT(K)=DMCT(K)
    GO TO 202
201 MMCT(K)=SC(K)*(3.0*ROTFF(ITER,K)-3.0*ROS(K))+0.5*DMCB(K)
202 SHEC(K)=(MMCT(K)+MMCB(K))/HS(K)
204 FOC(K-1)=SHEC(K)-SHEC(K-1)
205 CONTINUE
210 FOC(NS)=-SHEC(NS)
    SHEAR(1)=0.0
    DO 219 K=1,NS
        IF(NJ .EQ. 1) GO TO 211
        IF(ABS(DMBW(K)) .GE. MPW(K)) GO TO 212
        IF(ABS(DMWB(K)) .GE. MPW(K)) GO TO 213
211 MOMBW(K)=SBW(K)*(4.0*ROTFF(ITER,K)+2.0*ROTF(M,K)-6.0*ROB(K))
    GO TO 214
212 MOMBW(K)=DMBW(K)
    GO TO 214
213 MOMBW(K)=SBW(K)*(3.0*ROTFF(ITER,K)-3.0*ROB(K))+0.5*DMWB(K)
214 IF(NJ .EQ. 1) GO TO 215
    IF(ABS(DMWB(K)) .GE. MPW(K)) GO TO 216
    IF(ABS(DMBW(K)) .GE. MPW(K)) GO TO 217
215 MOMWB(K)=SBW(K)*(2.0*ROTFF(ITER,K)+4.0*ROTF(M,K)-6.0*ROB(K))
    GO TO 218
216 MOMWB(K)=DMWB(K)
    GO TO 218
217 MOMWB(K)=SBW(K)*(3.0*ROTF(M,K)-3.0*ROB(K))+0.5*DMBW(K)
218 SHEARW(K)=(MOMBW(K)+MOMWB(K))/HBW(K)
    MOMW(K)=-MOMWB(K)-SHEARW(K)*DW(K)/2.0
    F(M+1,K)=-FOC(K)
    SHEAR(1)=SHEAR(1)+F(M+1,K)
219 CONTINUE
    IF(NS .EQ. 1) GO TO 227
    DO 226 K=2,NS
        SHEAR(K)=SHEAR(K-1)-F(M+1,K-1)
226 CONTINUE
227 IF(M .EQ. 1) GO TO 232

```

```

      IF(M .EQ. MAX) GO TO 221
      DO 220 N=1,NS
      IF(ABS((DEFF(M,N)-DEFF(M-1,N))/DEFF(M,N)) .GE. CON .OR. ABS((ROTF(
1M,N)-ROTF(M-1,N))/ROTF(M,N)) .GE. CON) GO TO 232
220 CONTINUE
      GO TO 223
221 WRITE(6,222) MMMM
222 FORMAT(10X,'CYCLE NO.=',I3,7X,'CONVERGENCE (CALCULATION ON WALL) W
      IAS NOT ENOUGH'/)
223 NCYCLE=M
      SHEAR(1)=0.0
      DO 224 N=1,NS
      CDEFF(MMMM,N)=DEFF(NCYCLE,N)
      CROTF(MMMM,N)=ROTF(NCYCLE,N)
      IF(MMMM .EQ. 1) CSHEC(N)=SHEC(N)
      SHEAR(1)=SHEAR(1)+F(1,N)
224 CONTINUE
      IF(NS .EQ. 1) GO TO 230
      DO 225 K=2,NS
      SHEAR(K)=SHEAR(K-1)-F(1,K-1)
225 CONTINUE
230 DO 231 K=1,NS
      SHEAR(K)=SHEAR(K)+SHEC(K)
231 CONTINUE
      RETURN
232 CONTINUE
      RETURN
      END

```

C  
C  
C  
C  
C  
C  
C

IN SUBROUTINE FRAME, THE JOINT ROTATIONS OF THE FRAME FOR A  
SWAYED POSITION (ENFORCED BY THE WALL ) ARE COMPUTED.  
THIS IS PERFORMED BY GAUSS-SEIDEL ITERATION METHOD. IF A HINGE  
FORMS IN THE STRUCTURE THE JOINT ROTATION EQUATION IS MODIFIED.

```

SUBROUTINE FRAME (MAX, ROTFF, ROTO, SC, ROS, KC, SBW, SBF, ROB, ROTF, NS, ITH
1R, MMH, M, DMCB, DMCT, DMBW, DMWB, DMBF, DMFB, MPC, MPF, MPW, NJ, CON)
  DIMENSION ROTFF(99,30), ROTO(99), SC(30), ROS(30), SBW(30), SBF(30), ROB
1(30), ROTF(99,30), DMCB(30), DMCT(30), DMBW(30), DMWB(30), DMBF(30),
2DMFB(30), AA(30), BB(30), CC(30), DD(30), EE(30), FF(30), GG(30), HH(30), P
3A(30)
  REAL KC, MPC(30), MPF(30), MPW(30)
  DO 174 I=1, MAX
    IF(I .GT. 1) GO TO 164
    DO 163 K=1, NS
      ROTFF(I,K)=0.0
163 CONTINUE
164 N=I
    IF(N .EQ. 1) GO TO 165
    N=N-1
165 SC(NS+1)=0.0
    ROS(NS+1)=ROS(NS)
    ROTFF(N,NS+1)=ROTF(N,NS)
    MPC(NS+1)=500.0
    DMCB(NS+1)=0.0
    DMCT(NS+1)=0.0
    IF(NJ .EQ. 1) GO TO 10
    IF(ABS(DMCB(1)) .GE. MPC(1)) GO TO 20
    IF(ABS(DMCT(1)) .GE. MPC(1)) GO TO 11
10 ROTO(1)=(6.0*SC(1)*ROS(1)-2.0*SC(1)*ROTF(N,1))/(4.0*SC(1)+KC)
    GO TO 20
11 ROTO(1)=(3.0*SC(1)*ROS(1)-0.5*DMCT(1))/(3.0*SC(1)+KC)
20 DO 170 J=1, NS
    IF(NJ .EQ. 1) GO TO 21
    IF(ABS(DMBW(J)) .GE. MPW(J)) GO TO 30
    IF(ABS(DMWB(J)) .GE. MPW(J)) GO TO 40
21 AA(J)=SBW(J)*(6.0*ROB(J)-2.0*ROTF(M,J))
    EE(J)=4.0*SBW(J)
    GO TO 50
30 AA(J)=-DMBW(J)
    EE(J)=0.0
    GO TO 50
40 AA(J)=3.0*SBW(J)*ROB(J)-0.5*DMWB(J)
    EE(J)=3.0*SBW(J)
50 IF(NJ .EQ. 1) GO TO 51
    IF(ABS(DMBF(J)) .GE. MPF(J)) GO TO 60
    IF(ABS(DMFB(J)) .GE. MPF(J)) GO TO 70
51 BB(J)=0.0
    FF(J)=6.0*SBF(J)
    GO TO 80
60 BB(J)=-DMBF(J)
    FF(J)=0.0
    GO TO 80
70 BB(J)=-0.5*DMFB(J)
    FF(J)=3.0*SBF(J)

```

```

80 IF(NJ .EQ. 1) GO TO 81
   IF (ABS(DMCT(J)) .GE. MPC(J)) GO TO 90
   IF (ABS(DMCB(J)) .GE. MPC(J)) GO TO 100
81 IF(J .EQ. 1) GO TO 82
   CC(J)=SC(J)*(6.0*RDS(J)-2.0*ROTFF(I,J-1))
   GO TO 83
82 CC(J)=SC(J)*(6.0*RDS(J)-2.0*ROTFF(I))
83 GG(J)=4.0*SC(J)
   GO TO 110
90 CC(J)=-DMCT(J)
   GG(J)=0.0
   GO TO 110
100 CC(J)=3.0*SC(J)*RDS(J)-0.5*DMCB(J)
   GG(J)=3.0*SC(J)
110 IF(NJ .EQ. 1) GO TO 111
   IF(ABS(DMCB(J+1)) .GE. MPC(J+1)) GO TO 120
   IF(ABS(DMCT(J+1)) .GE. MPC(J+1)) GO TO 130
111 DD(J)=SC(J+1)*(6.0*RDS(J+1)-2.0*ROTFF(N,J+1))
   HH(J)=4.0*SC(J+1)
   GO TO 140
120 DD(J)=-DMCB(J+1)
   HH(J)=0.0
   GO TO 140
130 DD(J)=3.0*SC(J+1)*RDS(J+1)-0.5*DMCT(J+1)
   HH(J)=3.0*SC(J+1)
140 BA(J)=EE(J)+FF(J)+GG(J)+HH(J)
   IF(ABS(BA(J)) .LT. 0.0001) GO TO 170
   ROTFF(I,J)=(AA(J)+BB(J)+CC(J)+DD(J))/BA(J)
170 CONTINUE
171 ITER=I
   IF(ITER .EQ. 1) GO TO 174
   IF(ABS(DMCB(1)) .GE. MPC(1)) GO TO 176
   IF(ABS((ROTO(I)-ROTO(I-1))/ROTO(I)) .GT. CON ) GO TO 173
176 DO 172 K=1,NS
   IF(ABS(BA(K)) .LE. 0.0001) GO TO 172
   IF(ABS((ROTFF(I,K)-ROTFF(I-1,K))/ROTFF(I,K)) .GT. CON ) GO TO 173
172 CONTINUE
   RETURN
173 IF(I .EQ. MAX) GO TO 175
174 CONTINUE
175 WRITE(6,181) N,MMM
181 FORMAT(10X,'CYCLE NO.=',I3,2X,'TO',I3,7X,'CONVERGENCE (CALCULATION
   1 ON FRAME) WAS NOT ENOUGH'/)
   RETURN
   END

```

C  
C  
C  
C  
C

## OUTPUT STATEMENTS FOR FRAME FORCES AND DEFORMATIONS

```

SUBROUTINE ROFA (ROTFF,SHEC,FOC,DMCB,DMCT,ROTO,NS,NCYCLE,ITER,MMM
1)
  DIMENSION ROTFF(99,30),SHEC(30),FOC(30),ROTO(30),DMCB(30),DMCT(30)
  WRITE(6,371)
371  FORMAT(50X,28HRESULTS OF FRAME ANALYSIS///)
  WRITE(6,372) MMM,NCYCLE
372  FORMAT(10X,'CYCLE NO.   MMM=',I3,2X,'NCYCLE=',I3///)
  WRITE(6,200)
200  FORMAT(10X,7HCOLUMNS//)
  WRITE(6,373)
373  FORMAT(10X,10HFLOOR NO./,3X,19HJOINT ROTATION(RAD),3X,18HBOTTOM MO
1MENT(KIN),3X,16HTOP  MOMENT(KIN),3X,10HSHEAR(KIP),3X,10HFORCE(KIP)
2)
  WRITE(6,374)
374  FORMAT(10X,9HSTORY NO.//)
  WRITE(6,375)ROTO(ITER)
375  FORMAT(12X,4HBASE,10X,E13.6/)
  DO 377 K =1,NS
    WRITE(6,378)K,ROTFF(ITER,K),DMCB(K),DMCT(K),SHEC(K),FOC(K)
378  FORMAT(13X,I3,10X,E13.6,8X,F14.2,6X,F14.2,4X,F10.2,3X,F10.2/)
377  CONTINUE
814  WRITE(6,386)
386  FORMAT(1HK)
  WRITE(6,201)
201  FORMAT(//10X,5HBEAMS//)
  WRITE(6,380)
380  FORMAT(10X,9HFLOOR NO.,3X,16HMOMENT IN WALL,3X,16HMOMENT IN WA
1LL,3X,16HMOMENT AT COLUMN,3X,16HMOMENT AT ROLLER,3X,14HSHEAR AT
2THE,3X,14HSHEAR AT THE)
  WRITE(6,381)
381  FORMAT(22X,16HSIDE BEAM AT THE,3X,16HSIDE BEAM AT THE,3X,16HEND OF
1 THE BEAM,3X,16HEND OF THE BEAM,3X,14HENDS OF WALL,3X,14HENDS
2 OF BEAM)
  WRITE(6,382)
382  FORMAT(22X,16HCOLUMN END(K-IN),3X,16HWALL END (K-IN),3X,16HON RO
1LLER(K-IN),3X,16HON ROLLER(K-IN),3X,14HSIDE BEAM(KIP),3X,14HON RO
2LLER(KIP)///)
  RETURN

```

C  
C  
C

END

C  
C  
C  
C  
C

## OUTPUT STATEMENTS FOR SHEAR WALL FORCES AND DEFORMATIONS

```

      SUBROUTINE SR3 (BMOMF,TMOMF,ROTB,NS,F11,FOC,SHEAR,ROTF,DEFF,CROTF,
1CDEFF,MMMM)
      DIMENSION F11(30),FOC(30),SHEAR(30),ROTF(99,30),DEFF(99,30),
1CROTF(99,30),CDEFF(99,30),BMOMF(30),TMOMF(30)
      WRITE(6,55)
55  FORMAT(39X,52HSHEAR WALL ANALYSIS AND FINAL SLOPES AND DEFLECTIONS
1////)
      WRITE(6,312)
312 FORMAT(3X,10HFLOOR NO./,3X,15HWALL FORCE(KIP),3X,16HFRAME FORCE(KI
1P),3X,15HWALL SHEAR(KIP),9X,17HWALL MOMENT(K-IN),9X,10HSLOPE(RAD),
23X,14HDEFLECTION(IN))
      WRITE(6,401)
401 FORMAT(3X,9HSTORY NO.,62X,6HBOTTOM,13X,3HTOP//)
      WRITE(6,20)ROTB
20  FORMAT(5X,4HBASE,93X,E13.6/)
      DO 400 K=1,NS
      WRITE(6,313) K,F11(K),FOC(K),SHEAR(K),BMOMF(K),TMOMF(K),ROTF(1,K),
1DEFF(1,K)
313 FORMAT(6X,13,7X,F8.2,11X,F8.2,9X,F10.2,5X,F14.2,3X,F14.2,4X,E13.6,
13X,E13.6/)
400  CONTINUE
      WRITE(6,404)
404  FORMAT(1HK,50X,31HCHECK ON SLOPES AND DEFLECTIONS//)
      WRITE(6,405)
405  FORMAT(5X,9HFLOOR NO.,5X,10HSLOPE(RAD),4X,14HDEFLECTION(IN)//)
      DO 402 N=1,NS
      WRITE(6,403) N,CROTF(MMMM,N),CDEFF(MMMM,N)
403  FORMAT(8X,13,7X,E13.6,4X,E13.6/)
402  CONTINUE
      RETURN
      END

```

IF COMPILATION \*\*\*\*\*

C  
C  
C  
C  
C  
C

IN SUBROUTINE SR1 FORMATION OF PLASTIC HINGE IN A MEMBER OF  
THE FRAME IS DETECTED

403  
C  
C

SUBROUTINE SR1 (DMFB,DMBF,DMBW,DMWB,DMCT,DMCB,MOMFB,MOMBF,MOMBW,MMWB,MMCT,MMCB,NS,M3,MPF,MPW,MPC)  
DIMENSION DMFB(30),DMBF(30),DMBW(30),DMWB(30),DMCT(30),DMCB(30)  
REAL MOMFB(30),MOMBF(30),MOMBW(30),MOMWB(30),MMCT(30),  
MMCB(30),MPF(30),MPW(30),MPC(30)  
M3=0

DO 403 K=1,NS  
DMFB(K)=MOMFB(K)  
DMBF(K)=MOMBF(K)  
DMBW(K)=MOMBW(K)  
DMWB(K)=MOMWB(K)  
DMCT(K)=MMCT(K)  
DMCB(K)=MMCB(K)

403 CONTINUE

C  
C

DO 610 K=1,NS  
WRITE(6,633)

633 FORMAT(1HK)  
IF((ABS(DMCB(K))).LT.MPC(K))GO TO 616  
M3=M3+1

WRITE(6,617)K,DMCB(K)  
617 FORMAT(10X,50HHINGE AT BOTTOM POINT OF COLUMN IN STORY NO.,I  
13,5X,40HMOMENT AT BOTTOM POINT OF COLUMN =,F14.2,5H K-IN/)  
IF(DMCB(K).LT. 0.0) GO TO 10  
DMCB(K)=MPC(K)+0.0001  
GO TO 616

10 DMCB(K)=-MPC(K)-0.0001  
616 IF((ABS(DMCT(K))).LT.MPC(K))GO TO 602  
M3=M3+1  
WRITE(6,618)K,DMCT(K)

618 FORMAT(10X,50HHINGE AT TOP POINT OF COLUMN IN STORY NO.,I  
13,5X,40HMOMENT AT TOP POINT OF COLUMN =,F14.2,5H K-IN/)  
IF(DMCT(K).LT. 0.0) GO TO 20  
DMCT(K)=MPC(K)+0.0001  
GO TO 602

20 DMCT(K)=-MPC(K)-0.0001  
602 IF((ABS(DMFB(K))).LT.MPF(K))GO TO 604  
M3=M3+1  
WRITE(6,603)K,DMFB(K)

603 FORMAT(10X,50HHINGE AT ROLLER END OF BEAM ON ROLLER OF FLOOR NO.,I  
13,5X,40HMOMENT AT ROLLER END OF BEAM ON ROLLER =,F14.2,5H K-IN/)  
IF(DMFB(K).LT. 0.0) GO TO 30  
DMFB(K)=MPF(K)+0.0001  
GO TO 604

30 DMFB(K)=-MPF(K)-0.0001  
604 IF((ABS(DMBF(K))).LT.MPF(K))GO TO 606  
M3=M3+1  
WRITE(6,605)K,DMBF(K)

605 FORMAT(10X,50HHINGE AT COLUMN END OF BEAM ON ROLLER OF FLOOR NO.,I  
13,5X,40HMOMENT AT COLUMN END OF BEAM ON ROLLER =,F14.2,5H K-IN/)  
IF(DMBF(K).LT. 0.0) GO TO 40

```

      DMBF(K)=MPF(K)+0.0001
      GO TO 606
    40 DMBF(K)=-MPF(K)-0.0001
  606 IF((ABS(DMBW(K))).LT.MPW(K))GO TO 608
      M3=M3+1
      WRITE(6,607)K,DMBW(K)
  607 FORMAT(10X,50HHINGE AT COLUMN END OF WALL SIDE BEAM OF FLOOR NO.,I
    13,5X,40HMOMENT AT COLUMN END OF WALL SIDE BEAM =,F14.2,5H K-IN/)
      IF(DMBW(K) .LT. 0.0) GO TO 50
      DMBW(K)=MPW(K)+0.0001
      GO TO 608
    50 DMBW(K)=-MPW(K)-0.0001
  608 IF((ABS(DMWB(K))).LT.MPW(K))GO TO 610
      M3=M3+1
      WRITE(6,609)K,DMWB(K)
  609 FORMAT(10X,50HHINGE AT WALL END OF WALL SIDE BEAM OF FLOOR NO.,I
    13,5X,40HMOMENT AT WALL END OF WALL SIDE BEAM =,F14.2,5H K-IN/)
      IF(DMWB(K) .LT. 0.0) GO TO 60
      DMWB(K)=MPW(K)+0.0001
      GO TO 610
    60 DMWB(K)=-MPW(K)-0.0001
  610 CONTINUE
      RETURN
      END

```

## APPENDIX E

### DESIGN EXAMPLE

#### E.1 Introduction

The behavior of a 24 story structure has been studied in detail in Chapter IV. The plan view of the structure is shown in Fig. 4.1. A three step design method for coupled shear wall-frame structures has been proposed (40). This appendix presents the design of the 24 story structure using the method.

The member sizes of a typical bent (Fig. 4.2a) are those listed in Table 4.1. However, the strength and stiffness of the wall is varied in order to attain the required ultimate load and a reasonable deflection at the working load level. A uniform wind pressure of 20 psf has been assumed to act on the structure. The factored total vertical loads on each story of the building are listed in Table 4.2.

#### E.2 Design Steps

(a) In Ref. (39), the bent shown in Fig. 4.2a has been designed as a braced frame for gravity load, using a load factor of 1.70. Hence, the sizes listed in Table 4.1 are taken as the preliminary member sizes for each bent of the structure.

(b) The entire structure is then lumped into the analytical

model described in Chapter III. The wall-to-column stiffness ratio,  $K_r$ , of the shear wall has been selected as 50. However, the structure has been analyzed with  $M_r$  ratios of both 4 and 5. In this appendix, the adequacy of the design has been checked only at the 5th and 24th stories of the structure. The shear-deformation curves for these stories are plotted in Figs. E.1 and E.2 respectively. In Fig. E.1, the 5th story shear,  $V_5$ , is plotted versus the sway rotation of this story,  $\rho_5$ . At this level, the applied shear is 585 kips at the working load level and the factored load is 760 kips ( $1.3 \times 585$ ) as shown by the dashed lines in Fig. E.1. The ultimate loads of both example structures are higher than the factored load (760 kips). Therefore, the structure having  $K_r = 50$  and  $M_r = 4$  is adequate. In addition to the ultimate load criterion, the sway rotation at the working load level (585 kips) must be satisfactory. A value of 0.003 is selected as a limit for the sway rotation if the  $P\Delta$  effect is not included in the analysis. In this case a greater sway rotation might still be satisfactory. At the 5th story, the sway rotation corresponding to the working level is 0.002 which is well within the selected limit.

Figure E.2 plots the 24th story shear,  $V_{24}$ , versus the sway rotation of this story,  $\rho_{24}$ . In this case, the applied shear at working load level is 14.8 kips and the corresponding factored load is 19.4 kips as shown by the dashed horizontal lines in Fig. E.2. Again, the ultimate load capacity is satisfactory for both

structures. The sway rotation corresponding to the working load is approximately .0034 which is above the selected limit. If desired, the sway rotation can be reduced by modifying the frame members or the shear wall near the top portion of the structure.

(c) The results shown in Fig. E.1 and E.2 are based on the analysis of the lumped model (Fig. 3.1) which represents the entire structure. Hence, a check should be performed to determine whether the assumed resistance can, in fact, be delivered by the six steel rigid frames in the structure.

In Fig. E.3, the frame shear at the 5th story,  $V_5$ , has been plotted versus the sway rotation at this story,  $\rho_5$ . The solid curve represents the required frame resistance, obtained from the lumped model analysis of the structure with  $K_r = 50$  and  $M_r = 4$ , while the dashed line represents the delivered resistance of the six steel rigid frames, as predicted by the subassemblage analysis.

In the subassemblage method (27), it is assumed that the  $P\Delta$  shear on the corresponding tributary area is resisted by the frame bents. However, in the actual coupled shear wall-frame structure, the  $P\Delta$  shear is shared by the frames and shear wall. In order to account for the actual distribution, the total axial load acting on the frames is reduced by a factor,  $\beta$ , which is the ratio of the shears developed in the frame to the total applied shears (including the  $P\Delta$  shear). The resulting axial load as obtained above is then applied on the subassemblages. However, the plastic moment capacities of the

columns in the subassemblages are based on the axial loads computed from the plan areas tributary to each column. The dashed curve in Fig. E.3 is the shear-deformation response of the 5th story frame bents obtained from the modified subassemblage method. For the 5th story, since the difference between the delivered and required frame resistance is very small as shown in Fig. E.3, the member sizes in Table 4.1 are considered adequate.

Figure E.4 plots the frame shear at the 24th story,  $V_{24}$ , versus the sway rotation of this story,  $\rho_{24}$ . The shears developed in this story are relatively high on account of the 'whipping action' which occurs in the upper stories of coupled shear wall-frame structures. Hence, it is important to check the member sizes of the frame bents in this region. The PA shear in the 24th story is very small and in fact, negligible. However, the procedure described above was used to compute the shear resistance of the frames as shown in Fig. E.4.

In Fig. E.4, the dashed line represents the delivered resistance as obtained from the modified subassemblage analysis, using the member sizes listed in Table 4.1. In this case, the delivered resistance is lower than the required resistance up to a sway rotation of 0.008 radians, although the difference is not significant. However, if desired, the delivered resistance can be increased by modifying the member sizes of the 24th story. The broken curve in Fig. E.4 represents the delivered resistance corresponding to a new set of girders: 16B26, 12B14 and 16WF50 at the 24th level. In this

case, the delivered resistance is increased, although it is still slightly lower than the required resistance up to a sway rotation of approximately 0.006 radians.

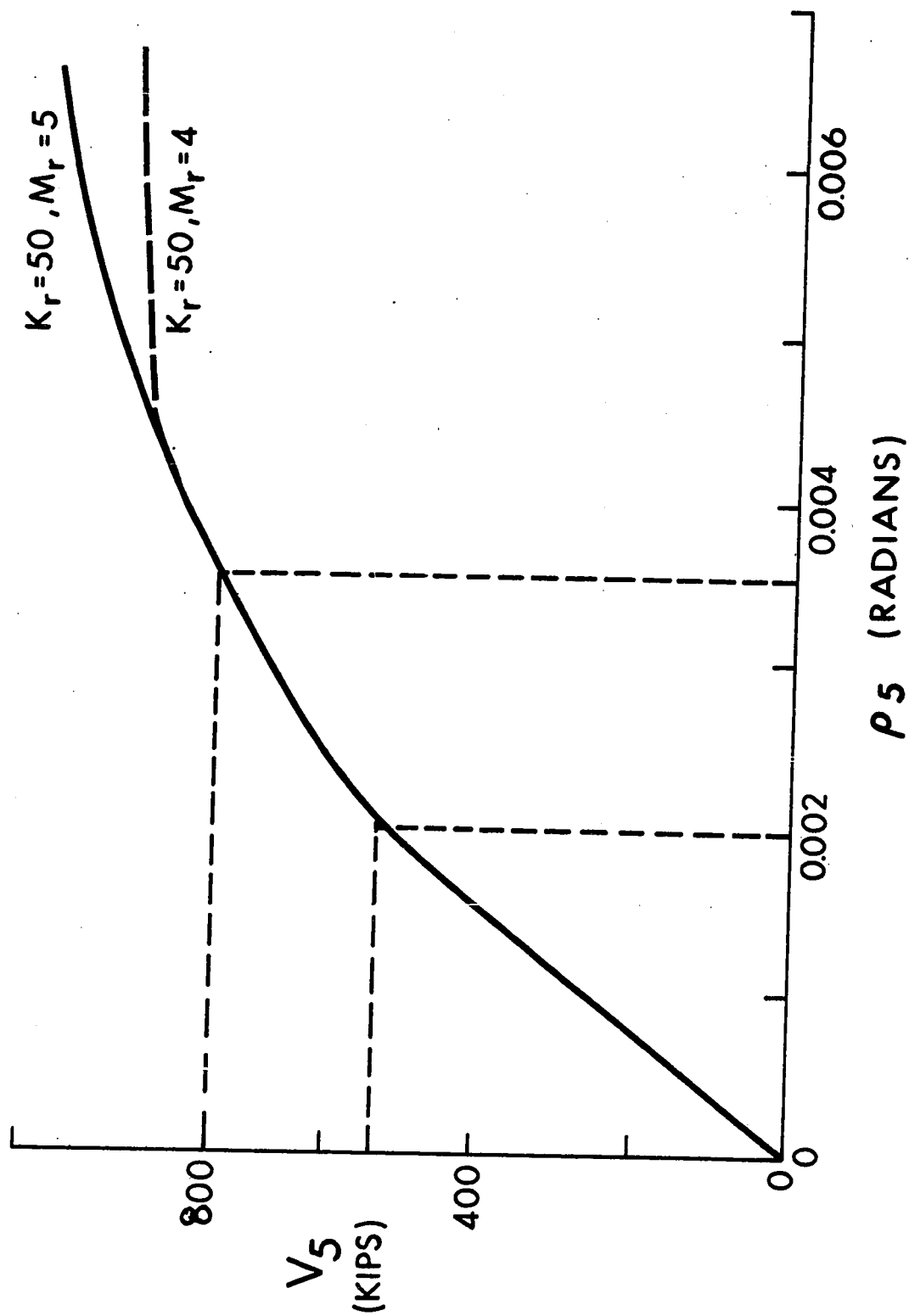


FIG. E.1 STRUCTURE LOAD-DEFLECTION RELATIONSHIPS - 5th STORY

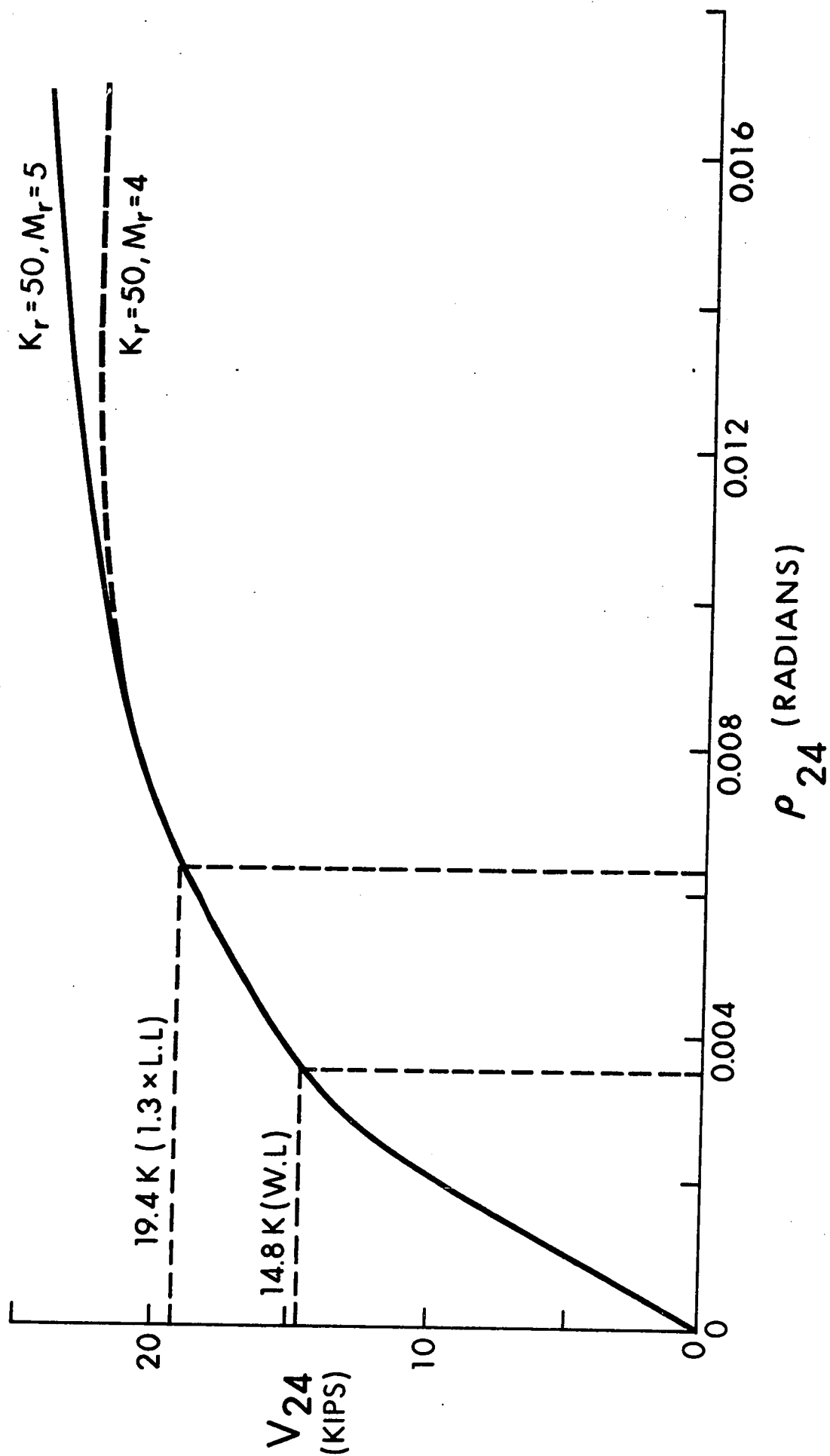


FIG. E.2 STRUCTURE LOAD-DEFLECTION RELATIONSHIPS - 24th STORY

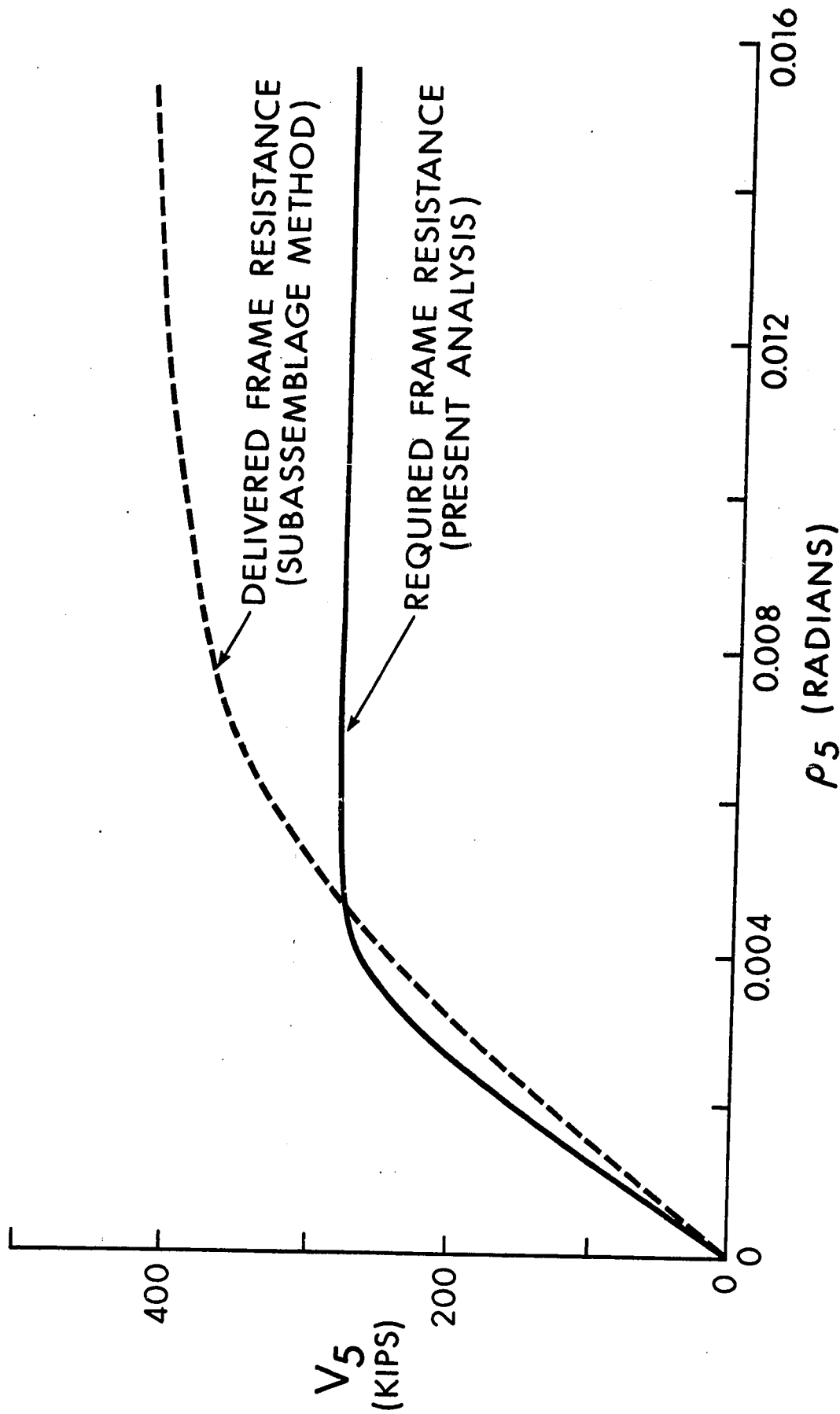


FIG. E.3 FRAME LOAD-DEFORMATION RELATIONSHIPS - 5th STORY

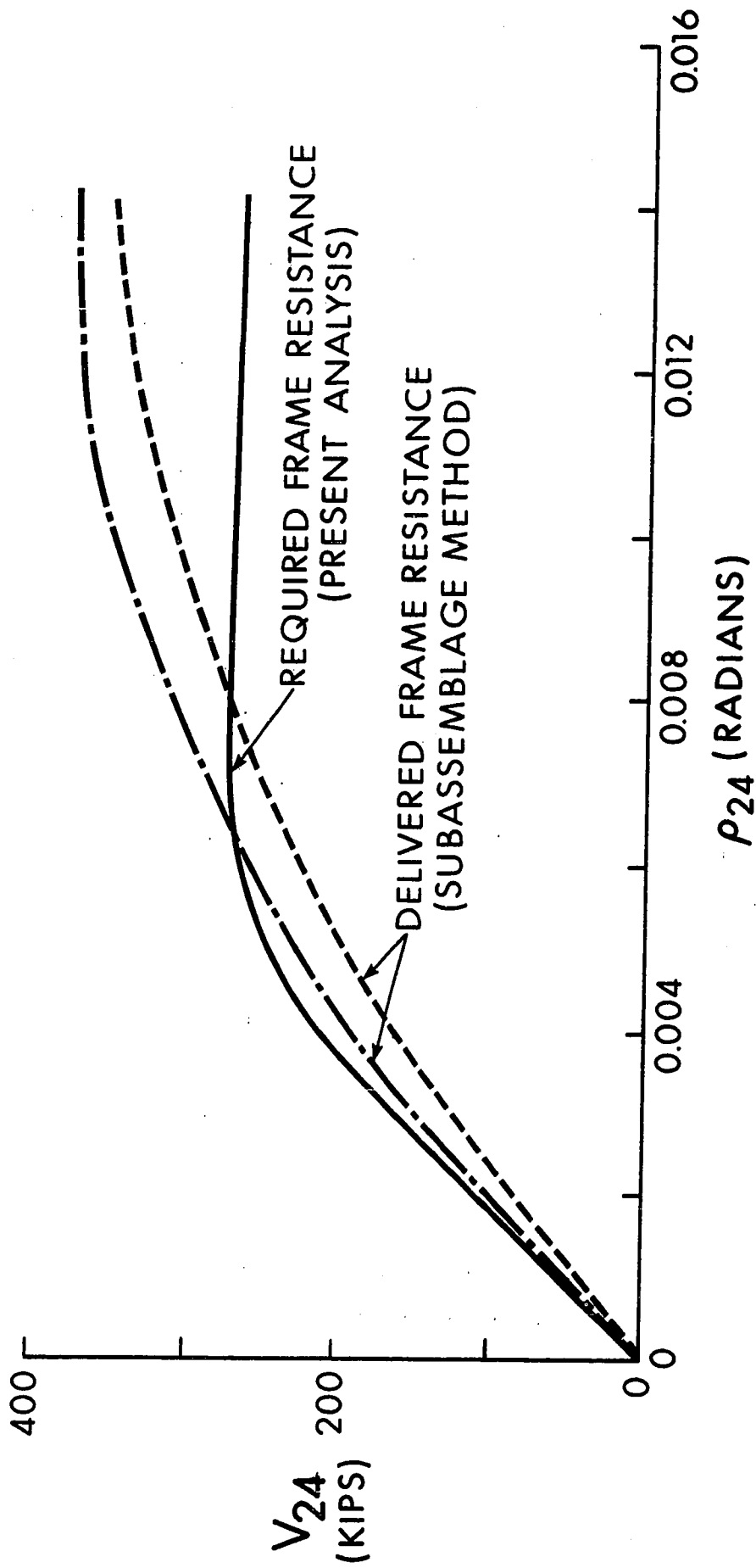


FIG. E.4 FRAME LOAD-DEFORMATION RELATIONSHIPS - 24th STORY

## APPENDIX F

### MATERIAL PROPERTIES

#### F.1 Introduction

This appendix presents the results of tests performed to determine the material properties of three wide-flange shapes used in Test Frames A, B and C; 5WF18.9, 4M13 and 5WF16. In addition, the results of tests on standard concrete cylinders and reinforcing bars used in the shear walls of the above specimens are presented.

#### F.2 Wide-Flange Shapes

The method of sectioning (48) was used to determine the residual strain distribution for each of the wide-flange shapes. The strips used for residual strain measurements were then milled to the shape of standard tensile specimens and tested in a hydraulic testing machine.

##### F.2.1 Residual Stresses

Longitudinal strips were obtained by slicing short sections of the specimen. The change in the strain before and after slicing the longitudinal strips free is taken as the residual strain. The details of the measurement procedure are given in Reference 49 .

In Table F.1, the location of each numbered coupon in the cross-section is shown as well as the resulting residual stress dis-

tribution. The numbers given represent the magnitude of the residual stress at the center of the corresponding strip. The residual stress distributions for the 5WF18.9 and 4M13 sections are typical for rotarized members (50). The distribution for the 5WF16 section is typical for a member which has been rolled and allowed to cool without cold working.

### F.2.2 Tensile Test Results

Flat tensile specimens were tested in a hydraulic testing machine. The results of the tensile tests are also given in Table F.1. In this table,  $\sigma_y$  represents the yield stress;  $\epsilon_y$ , the yield strain;  $\epsilon_{st}$ , the strain-hardening modulus and  $\sigma_u$ , the ultimate stress. The stress level of the plastic plateau (static) has been denoted by  $\sigma_y$ . However, where no plastic plateau existed,  $\sigma_y$  denotes the yield strength at 0.2% offset. The stress-strain curves are given in Reference 49 .

### F.3 Concrete

The concrete mix proportion for the fabrication of the shear wall was 1:2.8:1.9. Type III, high early strength Portland Cement was used with 3/8-in. maximum size pea gravel as coarse aggregate. The slump was approximately 4 inches. Three batches were required to cast each shear wall. Six standard control cylinders were made for each batch and tests on the cylinders were performed in accordance with ASTM C39 specifications. Four cylinders were tested in compression and the remaining two were used in the split

cylinder tensile test. In Table F.2, the average strengths obtained from the cylinders taken from each batch are listed.

#### F.4 Reinforcing Steel

Intermediate grade reinforcing bars, with the deformations conforming to ASTM A305 specification were used in the shear walls. Tension tests were performed on three specimens on each of No. 3, No. 4, No. 5, and No. 6 bars. The average yield strength and ultimate strength for these bar sizes are listed in Table F.3.

TABLE F.1 MECHANICAL PROPERTIES OF STRUCTURAL STEEL

F4

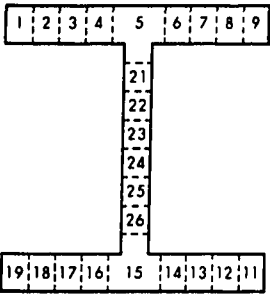
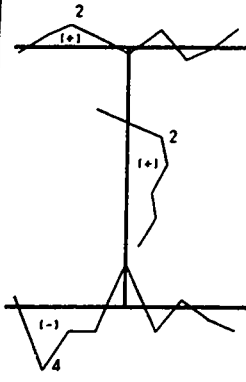
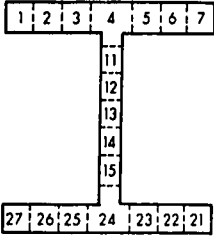
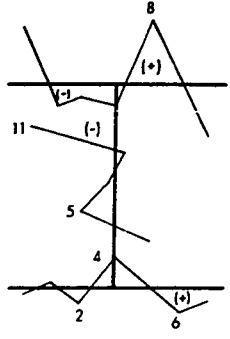
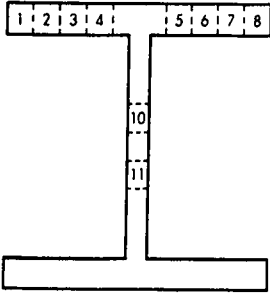
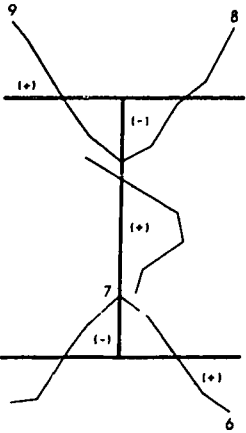
SECTION	Coupon	$\sigma_y$ (ksi)	$\epsilon_y$ (in/in)	$\epsilon_{st}$ (in/in)	$E_{st}$ (ksi)	$\sigma_u$ (ksi)	Residual Stresses ksi ( Tension - )
<b>5 W18.9</b> 	1	43.2	0.00146	0.00146	815	68.2	
	2	40.6	0.00137	0.00137	825	68.2	
	3	36.6	0.00123	0.00200	800	67.2	
	4	33.9	0.00115	0.00400	835	66.4	
	6	34.5	0.00117	0.00420	800	65.5	
	7	37.2	0.00125	0.00220	820	66.7	
	8	40.5	0.00137	0.00137	805	67.4	
	9	44.0	0.00149	0.00149	700	66.5	
	11	44.4	0.00150	0.00150	720	67.5	
	12	41.6	0.00141	0.00141	775	66.8	
	13	38.4	0.00130	0.00130	845	66.1	
	14	34.6	0.00117	0.00430	795	65.4	
	16	33.6	0.00114	0.00470	740	65.6	
	17	38.4	0.00130	0.00130	880	66.3	
	18	41.9	0.00141	0.00141	840	67.9	
	19	44.2	0.00149	0.00149	800	68.7	
	21	46.3	0.00156	0.00156	680	66.5	
	22	42.2	0.00143	0.00143	785	63.1	
	23	40.1	0.00135	0.00135	715	63.1	
	24	44.0	0.00149	0.00149	705	63.2	
	25	46.3	0.00156	0.00156	720	64.4	
	26	57.1	0.00193	0.00193	545	66.5	
<b>4M13</b> 	1	43.3	0.00146	0.0035	510	67.5	
	2	41.2	0.00139	0.0027	560	67.3	
	3	40.1	0.00135	0.0092	580	67.0	
	5	40.9	0.00138	0.0041	700	68.8	
	6	43.3	0.00146	0.0058	510	67.5	
	7	47.7	0.00161	0.0080	490	68.7	
	11	-	-	-	560	77.6	
	12	51.6	0.00174	0.0038	500	71.9	
	13	47.2	0.00159	0.0136	500	70.0	
	14	49.5	0.00167	0.0024	500	71.6	
	15	53.1	0.00179	-	615	73.6	
	21	43.1	0.00145	0.0066	565	69.9	
	22	42.1	0.00142	0.0086	630	69.3	
	23	42.4	0.00143	0.0104	510	69.6	
	25	40.1	0.00135	0.0108	610	67.7	
	26	40.0	0.00135	0.0070	620	66.4	
	27	39.3	0.00133	0.0064	630	65.7	
<b>5 W16</b> 	1	39.6	0.00134	0.0254	368	59.6	
	2	39.8	0.00135	0.0220	410	59.5	
	3	39.2	0.00132	0.0254	370	59.7	
	4	38.1	0.00129	0.0220	480	59.9	
	5	39.2	0.00132	0.0240	400	60.3	
	6	37.1	0.00125	0.0194	500	59.8	
	7	36.9	0.00125	0.0196	470	59.8	
	8	38.1	0.00129	0.0180	410	60.3	
	10	38.9	0.00131	0.0174	520	60.7	
	11	39.2	0.00132	0.0230	440	60.7	

TABLE F.2 CONCRETE STRENGTH

Frame	Batch No.	Compressive Strength (psi)	Tensile Strength (psi)
A	1	4210	673
	2	4380	503
	3	4520	648
B	1	4110	520
	2	4400	560
	3	4030	526
C	1	4140	475
	2	4030	506
	3	4240	540

TABLE F.3 PROPERTIES OF REINFORCEMENT

Bar Size	Yield Strength (ksi)	Ultimate Strength (ksi)
No. 3	59.0	87.8
No. 4	55.5	84.3
No. 5	51.5	81.0
No. 6	50.6	80.2